miRNAs in the kidney and their role in podocyte (dys)function

DISSERTATION ZUR ERLANGUNG DES
DOKTORGRADES DER NATURWISSENSCHAFTEN (DR. RER. NAT.)
DER FAKULTÄT FÜR BIOLOGIE UND VORKLINISCHE MEDIZIN
DER UNIVERSITÄT REGENSBURG

vorgelegt von
Susanne Baumgarten

aus
Ingolstadt

im Jahr
2015

Das Promotionsgesuch wurde eingereicht am:

18.09.2015

Die Arbeit wurde angeleitet von:

Prof. Dr. Ralph Witzgall

Unterschrift:

Susanne Baumgarten

I TABLE OF CONTENT

II List of figures

III List of tables

1 INTRODUCTION

1.1 Non-coding small RNAs

In the last two decades, a vast amount of evidence was discovered that RNA is not only functional as a messenger between DNA and protein, but also plays a crucial role in regulation of genome organization and gene expression (reviewed in Morris & Mattick 2014). The ENCODE (Encyclopedia of DNA elements) project identified 80% of the human genome to serve a biochemical purpose (Pennisi 2012), e.g. providing a binding site for transcription factors. In total, 76% of the human genome is transcribed to RNA, while only 3% of the whole genome codes for a total of 20,687 proteins (Pennisi 2012). In addition, 11,224 pseudogenes, 8,800 small RNA molecules and 9,600 long RNA molecules were found to be encoded in the genome (Pennisi 2012). Many classes of non-protein coding RNAs have been identified to operate on several regulatory levels in eukaryotic as well as in prokaryotic cells, adding new levels of complexity to the regulatory network in living cells. The regulation of gene expression on a post-transcriptional level is the mechanism best described for miRNA (microRNA) dependent regulation (Carthew & Sontheimer 2009). Non-coding RNAs are also able to mediate epigenetic regulation, as small RNAs as well as long non-coding RNAs can recruit histones, DNA methyltransferases and chromatin modifying complexes (reviewed by Holoch & Moazed, 2015).

This work focuses on one specific, highly conserved class of non-coding RNAs, the miRNAs, and their role in post-transcriptional regulation of protein coding transcripts in mammalian kidneys. miRNAs have already been identified to be involved in many important signaling processes in mammalian cells, e.g. the regulation of somatic stem cell proliferation and differentiation (reviewed by Shenoy & Blelloch 2014) or the modulation of autophagy and apoptosis (reviewed by Su et al. 2015). Since miRNAs are important for the homeostasis of physiological conditions in cells, dysregulation of their levels was proposed to be involved in genesis and progression of a broad variety of diseases. They play an important role in the progression of different cancers (reviewed by e.g. Hata & Lieberman 2015, Melo & Esteller 2011, Jansson & Lund 2012, Volinia et al. 2010), but also in other diseases like Alzheimer's disease (Codoceno et al. 2015, Feminella et al. 2015) or diabetes (reviewed by Guay et al. 2011) and diabetic nephropathy (reviewed by Kato & Natarajan 2015). miRNAs have been proposed as potential activators of diseases, biomarkers (reviewed by Wang et al. 2015A) and therapy targets.

1.1.1 Biogenesis and function of miRNAs in mammalian cells

miRNAs are small, non-coding RNA molecules with a length of 19-25 nt (nucleotides) that are processed in mammalian cells from endogenously generated transcripts. They play an exclusively regulatory role in cells, functioning as guide molecules in post-transcriptional gene silencing by base pairing with their target, leading to its silencing or degradation (Kim 2005). It has been estimated that up to 60% of human protein coding genes are regulated by miRNAs (Friedman et al. 2009). For many miRNAs, the sequence of the mature miRNA molecules as well as the genomic organization of the precursor transcripts is highly conserved between different species, especially between mammalian species like human and mouse.

miRNA precursor molecules

The primary miRNA transcript, the pri-miRNA, consists of a hairpin with an imperfectly paired stem of ca. 33 nucleotides and flanking sequences that extend on both the 5'-end and the 3'-end from the hairpin structure (Carthew & Sontheimer 2009). Transcription of miRNAs is typically performed by RNA polymerase II, and the primary transcripts are capped and polyadenylated (Kim 2005). miRNA transcripts synthesized by RNA polymerase III have also been described (Dieci et al. 2007). miRNAs can be categorized according to their genomic locations: exonic miRNAs are processed from their own, non-coding primary transcript that contains one or more hairpin structures, while intronic miRNA hairpins are derived from the introns of a protein coding or non-protein coding transcript (Kim 2005). A transcript containing several miRNA hairpins is called a miRNA cluster (chapter 1.1.2).

In the first pri-miRNA processing step (Fig. 1.1), occurring in the nuclei of mammalian cells, the stem loop structure is cleaved by the enzyme Drosha, releasing the miRNA precursor, the pre-miRNA (Kim 2005). Drosha, a member of the RNAse III family, and its cofactor DGCR8 (DiGeorge syndrome critical region gene 8), which is important for miRNA maturation, are called the microprocessor complex (Denli et al. 2004, Nguyen et al. 2015).

An alternative miRNA maturation pathway uses splicing to form transcripts that mimic the structural features of pre-miRNAs, the so-called "mirtrons", which also can enter the miRNA processing pathway after the Drosha processing step (Carthew & Sontheimer 2009).

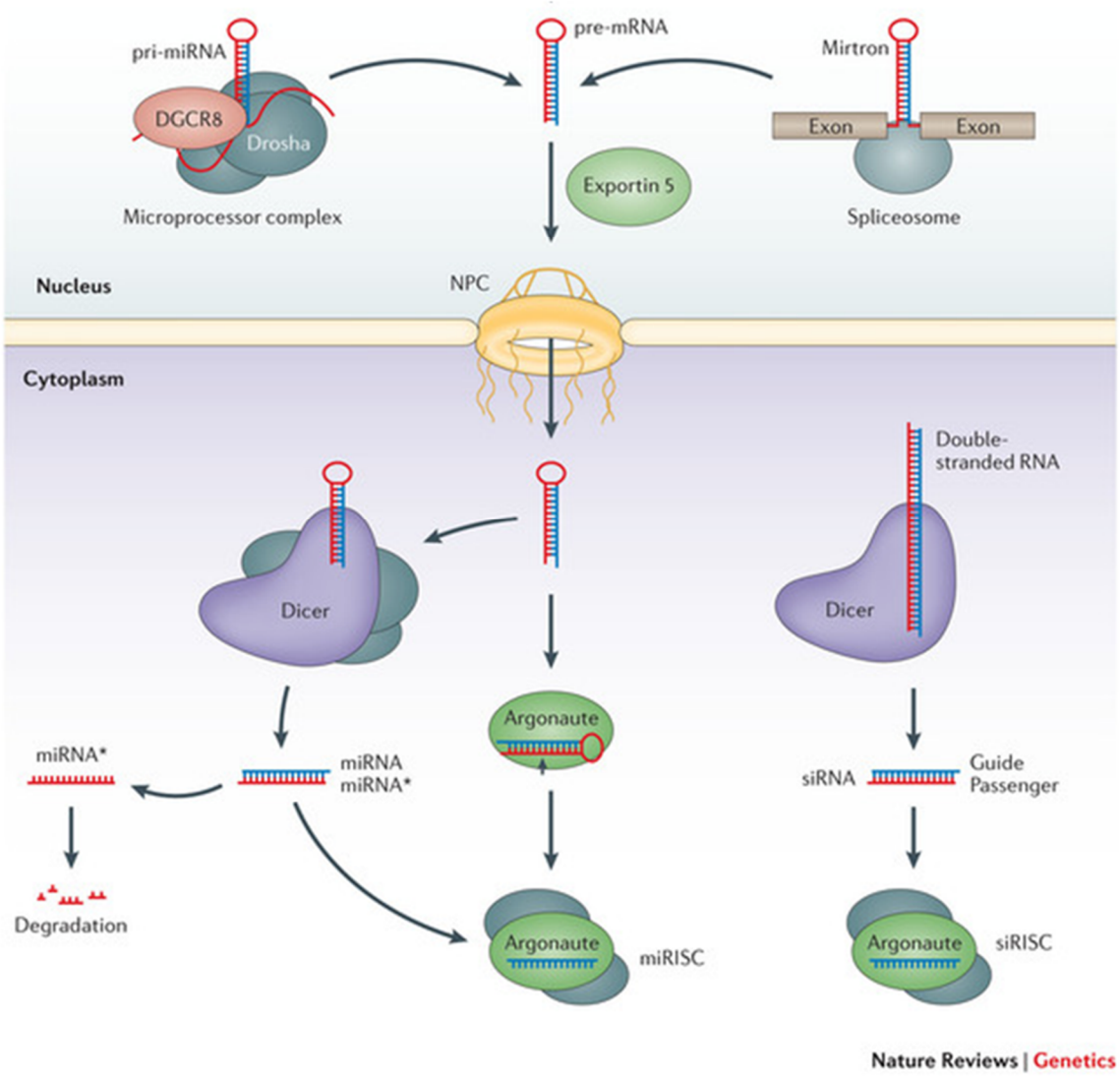

Fig. 1.1: Pathways leading to functional RISCs; after transcription and processing by Drosha and Dicer, the mature miRNAs are bound by Ago proteins, forming the RISCs (Meister 2013, modified); Abbreviations: DGCR8: DiGeorge syndrome critical region gene 8; NPC: nuclear pore complex; RISC: RNA induced silencing complex

miRNA maturation

After the pre-miRNA is exported out of the nucleus by XPO-5 (Exportin-5) and released from the transport complex in an energy dependent manner (Ha & Kim 2014), the second processing step is carried out by the conserved enzyme Dicer (Fig. 1.1), a member of the RNase III family (Kim 2005). It excises the terminal loop from the hairpin creating a mature miRNA duplex with a length of approximately 22 nucleotides (Carthew & Sontheimer 2009). Products of Dicer processing possess phosphates at the 5'-end and overhangs of two nucleotides at the 3'-end (Meister & Tuschl 2004) and can be loaded into the RISCs (RNA induced silencing complexes).

RISC complex formation

Mammalian cells possess four argonaute proteins, Ago1-4, which are all able to bind mature miRNAs to form RISCs. However, only Ago2 has a retained catalytic activity by a functional catalytic triad, while the other three Ago proteins might be partially redundant (Meister 2013). It has been shown that the different Ago proteins bind different subpopulations of miRNAs (Burroughs et al. 2011). The binding to the different Ago proteins seems to be influenced by the length of the miRNA. The Ago1 and Ago3 bound miRNAs often contain 23 to 24 nucleotides and may possess non-templated additions of mostly one nucleotide at their 3'-end (Dueck et al. 2012).

After Dicer processing, the mature miRNA is loaded into the Ago protein. The transfer of the double strand to the Ago protein is mediated by Hsp90 (Heat shock protein 90) in humans. By conformational changes of the Ago protein, its N domain is driven between the two duplex strands, leading to duplex opening and further unwinding (Meister 2013). How unwinding occurs in detail, and whether additional factors are needed, is not fully understood yet. After unwinding of the duplex, the strand with the less stably paired 5'-end is preferentially loaded into Ago proteins (Meister 2013). The passenger strand, often marked with a "*", is removed and can be degraded, but may also be a functional miRNA itself. As an example, both mature miRNAs from the mir-9 precursor regulate the tumor suppressor CAMTA1 (Calmodulin binding transcription activator 1; Schraivogel et al. 2011).

Dicer is an enzyme with a broad range of possible substrates, e.g. it is able to generate small RNAs with a length of 22 nucleotides from a 70 nucleotide stem loop precursor (Kim 2005). Thus, also other double stranded precursor molecules can be processed by Dicer and loaded into Ago proteins, e.g. siRNAs (small interfering RNA).

Posttranscriptional regulation of gene expression by miRNAs

The miRNAs function as a guide for the Ago proteins to mRNAs, directing the RISC to binding sites which are often located in the 3'-UTR of the target genes (Meister 2013). miRNA binding in the coding region of genes also has been reported (reviewed by Brümmer & Hausser 2014; Gebeshuber et al. 2013). Perfectly paired miRNA-target duplexes can be cleaved by the catalytically active Ago2 protein (Meister 2013). In mammals, miRNAs usually bind to partially complementary sites, while the "seed region", the nucleotides on position 2 to 7 or 8 of the miRNA, is often fully paired and essential for interaction (Meister 2013).

The binding of a miRNA guided RISC to a target mRNA can lead to its translational silencing as well as its degradation, with the mRNA destabilization being the main contributor to regulation in animal cell cultures (Jonas & Izaurralde 2015). Mammals possess three GW (Glycine-tryptophan repeat containing) proteins, called TNRC6A-C (Trinucleotide repeat containing 6 A-C), that can bind to Ago proteins, PAN3 (Poly (A) specific ribonuclease subunit 3) and NOT9 (also: RQCD1: Required for cell differentiation1 homolog) via their tryptophan residues (Jonas & Izaurralde 2015). Via PAN3 and NOT9, the deadenylating complexes PAN2-PAN3 and CCR4-NOT are recruited to the regulated transcript, leading to its deadenylation, decapping and degradation via the cellular 5'-to-3' mRNA decay pathway (reviewed by Jonas & Izaurralde 2015).

Non canonical miRNA processing

Two parallel studies identified a mature miRNA whose levels were not affected by Dicer loss of function, but reduced in mutant zebrafish and mice lacking enzymatic activity of Ago2 (Cifuentes et al. 2010, Cheloufi et al. 2010). Dicer requires a double strand of > 19 nucleotides for miRNA maturation from a canonical precursor (Fig. 1.2 A). A mature miRNA, miR-451-5p, is encoded in a conserved 42 nucleotide hairpin precursor with a stem of only 17 nucleotides (Fig. 1.2 B). This short hairpin can be directly bound by Ago2 and cleaved at the opposite strand (Fig. 1.2 C).

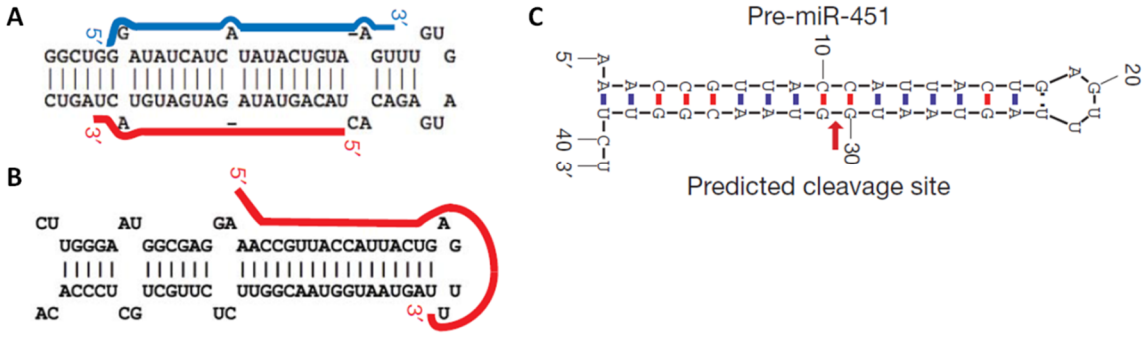

Fig. 1.2: Non-canonical miRNA precursors (A) Canonical hairpin precursor mir-144 coding for two mature miRNAs, miR-144-5p (blue) and miR-144-3p (red); (B) mir-451 hairpin precursor with shortened stem only coding for one mature miRNA, miR-451-5p (red); (C) mir-451 hairpin with predicted Ago2 cleavage site on the opposite strand (Cheloufi et al. 2010, modified)

The mir-451 pre-miRNA seems only to be bound by the only catalytically active argonaute protein, Ago2, and artificial precursors mimicking the pre-mir-451 structure will be bound and processed by Ago2 (Dueck et al. 2012). PARN (Poly (A) specific ribonuclease) could be identified as the enzyme responsible for 3'-5' exonucleolytic trimming of Ago2 cleaved pre-mir-451 (Yoda et al. 2013).

Regulation miRNA expression and maturation

By guiding the RISCs to the 3'-UTRs of target genes, miRNAs function as gene expression regulators. Vice versa, since miRNAs are generated from primary transcripts produced by RNA polymerase II or III, their expression can be regulated by transcription factors. Many miRNAs have been shown to be regulated by transcription factors like p73 and p63 (Tumor proteins P73 and P63), who have been identified as activators of miR-200 family upregulation (Knouf et al. 2012). The transcription factor Lmx1b (LIM homeobox transcription factor 1 beta) has been found to form a regulatory circuit with miR-135a-2 in brain (Anderegg et al. 2013). A feedback loop between the miR-200 family and the transcription factors ZEB1 and ZEB2 (Zinc finger E-box binding homeobox 1 and 2), controlling EMT and MET (Epithelial–mesenchymal and Mesenchymal–epithelial transition), has also been discovered (Hill et al. 2013). It was reported that the miR-709 directly regulates miRNA-15a/16-1 biogenesis on a posttranscriptional level, hinting at a possible miRNA hierarchy system (Tang et al. 2012).

Additionally, processing of miRNAs can be regulated on every stage, i.e. nuclear procession, export from the nucleus, cytoplasmic procession and loading into the Ago complex as well as the structure of the miRNA itself, e.g. by tailing (reviewed by Ha & Kim 2014). miRNA binding to human Ago proteins can also be strongly reduced by Ago phosphorylation (Rüdel et al. 2011).

1.1.2 Classification of identified miRNAs

All miRNAs identified from different organisms are registered in the online database miRBase (http://www.mirbase.org; Kozomara & Griffiths-Jones 2014; Kozomara & Griffiths-Jones 2011; Griffiths-Jones et al. 2008; Griffiths-Jones et al. 2006; Griffiths-Jones 2004). Until September 2015, 1881 miRNA precursors and 2588 mature miRNAs had been identified in human. In mouse, 1193 miRNA precursors and 1915 mature miRNAs had been identified. In the database TarBase v7.0 (Vlachos et al. 2014), more than 65,000 interactions of miRNAs and genes identified by high-throughput approaches or specific experiments had been indexed until September 2015. A database for miRNA involvement in diseases, miR2Disease (Jiang et al. 2009), listed 349 miRNAs to be involved in 163 diseases in September 2015.

Nomenclature of miRNAs

With the exception of the first two miRNAs discovered in *C. elegans*, lin-4 (Lee et al. 1993) and let-7 (Reinhart et al. 2000), miRNA precursors are numbered chronological according to their discovery. To indicate the precursor, the "r" in mir is not capitalized, e.g. mir-191. A prefix indicates the specimen the miRNA was found in (e.g. hsa for *homo sapiens*, mmu for *mus*

musculus, rno for *rattus norvegicus*). If the precursor is evolutionary conserved, the number will be the same in the different organisms, e.g. hsa-mir-22 and mmu-mir-22. To indicate that a precursor possesses two different loci in the genome, the precursor is numbered, e.g. hsa-mir-24-1 and hsa-mir-24-2. The two mature miRNAs that originate from a common precursor are indicated with a suffix describing the arm of the precursor they are derived from, e.g. miR-9-5p and miR-9-3p. According to the old nomenclature, the miRNA with the lower expression level is sometimes marked with a star, e.g. miR-9*. When the sequence of two miRNAs is very similar and the sequence of the seed region, the positions 2 to 7 or 8, is identical, the miRNAs are grouped into one family, e.g. miR-23a-3p and miR-23b-3p. However, the division into families is not very consistent, as e.g. the miRNAs mir-141, mir-200a, mir-200b, mir-200c and mir-429 belong to the same family, while there is a single base mismatch in the seed regions of miR-200a-3p and miR-200b-3p.

miRNA clusters

A miRNA cluster is a group of miRNA hairpin precursors that are processed from one common primary transcript yielding several mature miRNAs. One cluster that has been studied intensively is the miR-17~92 cluster, a genomic fragment of 786 base pairs containing 6 hairpin precursors (He et al. 2005, Hayashita et al. 2005). A common role of miRNAs organized in a cluster could be proven when overexpression of the miR-17~92 cluster enhanced tumor growth in a mouse B-cell lymphoma model (He et al. 2005) as well as lung cancer cell growth (Hayashita et al. 2005). As a second example, the five members of the mir-200 family are organized in two genomic clusters, pointing to a common role of miRNAs that are encoded near to each other in the genome. The miR-200 family is involved in kidney fibrosis and diabetic nephropathy by regulation of the EMT and the EndMT (Endothelial mesenchymal transition) (Srivastava et al. 2013). Additionally, a feedback loop between the ZEB transcription factors and the miR-200 family was identified to be an important player in the progression of cancer (Brabletz & Brabletz 2010). The two mir-23~27~24 clusters, one harboring the precursors mir-23a, mir-27a and mir-24-2 and the other containing mir-23b, mir-27b and mir-24-1, have been shown to be important for cardiovascular disorders, as they are involved in angiogenesis, endothelial apoptosis in cardiac ischemia and retinal vascular development (reviewed by Bang et al. 2011). A cooperative function of the encoded miRNAs was proposed, since the functional analysis revealed similar distributions of enriched genes (Liang et al. 2014). Additionally, the cooperative function of miRNAs organized in 20 different clusters in regulating several cell signaling pathways involved in cervical cancer has recently been reviewed (Servin-González et al. 2015).

1.2 The mammalian kidney

1.2.1 The anatomy of the mammalian kidney

The kidneys are an organ serving several important roles in the mammalian organism. Their main tasks are filtration of the blood to remove waste products from the organism, maintenance of homeostasis of electrolytes and thus, regulation of the blood pressure. The hilum, the place where the renal artery enters the kidney and the renal vein as well as the ureter leave the kidney, is located on the concave side of the bean-shaped organs. The two major segments of the kidney are the outer cortex and the inner medulla. Contrary to the murine kidney (unilobar kidney), the parenchyma of the human kidney is divided into several pyramids by projections of the renal cortex towards the center. The tip of each pyramid opens out into the calyxes that merge into the renal pelvis.

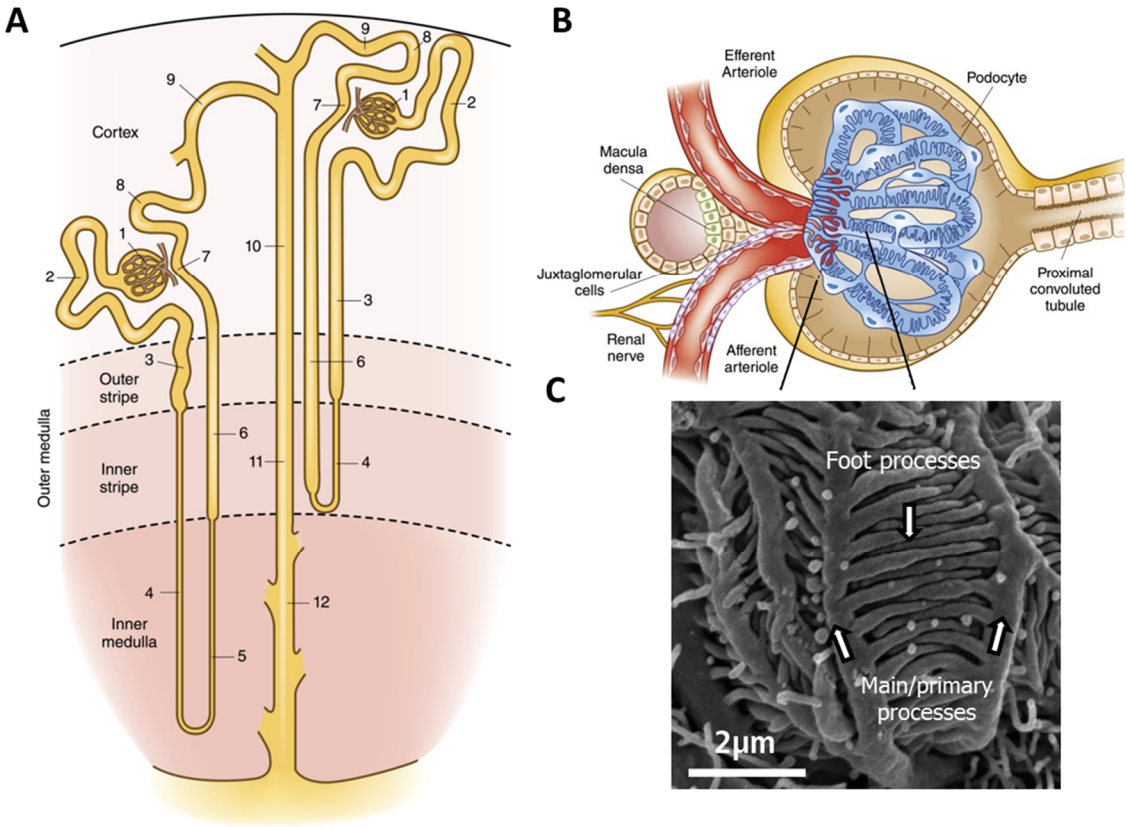

Fig. 1.3: Microscopic anatomy of the mammalian kidney (A) Nephrons spanning the cortex and medulla of a mammalian kidney: 1 glomerulus; 2 proximal convoluted tubule; 3 proximal straight tubule; 4 descending thin limb; 5 ascending thin limb; 6 thick ascending limb; 7 macula densa; 8 distal convoluted tubule; 9 connecting tubule; 10 cortical collecting duct; 11 outer medullary collecting duct; 12 inner medullary collecting duct (Mount 2014) (B) Schematic representation of a glomerulus with the podocytes covering the capillary convolute (Pollak et al. 2014, modified); (C) Scanning electron micrographs of the interdigitating processes of adjacent podocytes covering the glomerular capillaries. Micrographs by C. Niemann & H. Schmidt, Institute for Molecular & Cellular Anatomy, University of Regensburg

The functional units of the kidney are the nephrons. They span the cortex and the medulla of the kidney and consist of a glomerulus, where the initial filtration of the blood takes place, and an adjacent tubular system in which the primary urine is concentrated (Fig. 1.3 A).

1.2.2 The glomerulus and the renal filtration barrier

The mammalian glomerulus contains a capillary convolute, which is covered by highly specialized epithelial cells, the podocytes (Fig. 1.3 B, C). In the glomerulus, the primary urine is filtered from the blood into the Bowman's space, from where it flows of into the tubular system. The inner part of the glomerulus consists of three main cell types: the endothelial cells lining the capillaries, the podocytes and the stabilizing mesangial cells, smooth muscle cells intercalated into the capillary convolute (Fig. 1.4 A). In addition, the Bowman's space surrounding the capillary convolute is lined with the PECs (Parietal epithelial cells). In-between their interdigitating foot processes, the podocytes build up the slit diaphragm, a delicate protein structure crucial for blood filtration. The renal filtration barrier consists of three components: The slit diaphragms, i.e. complex protein structures built by two neighboring podocytes in-between their interdigitating foot processes (Fig. 1.4 B), the glomerular basement membrane between the endothelial cells and the podocytes and the fenestrated endothelium of the capillaries.

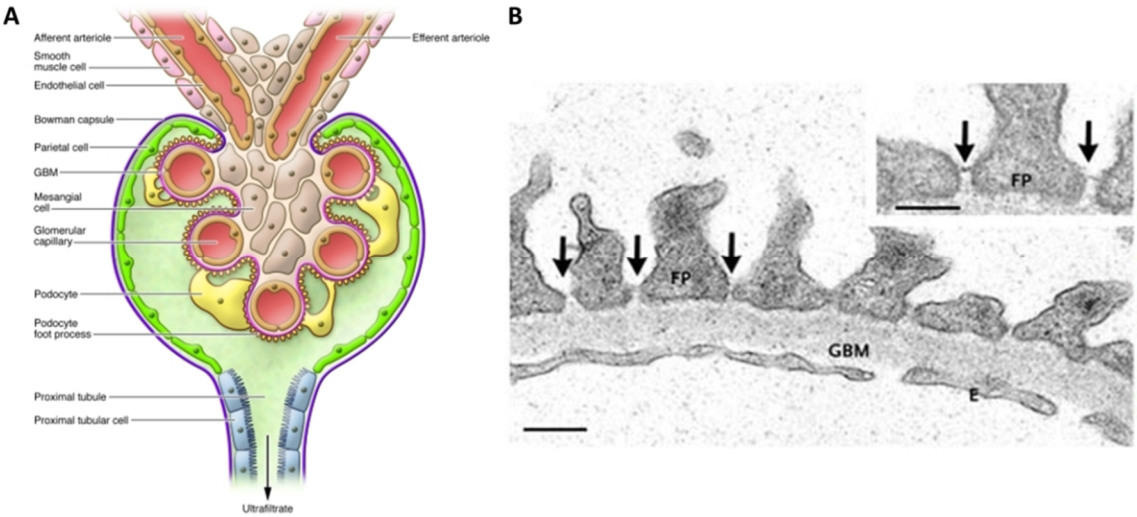

Fig. 1.4: Microscopic anatomy of the filtration barrier (A) the glomerular capillaries are covered by the podocytes which form contacts to each other with their interdigitating foot processes; the capillary convolute is stabilized by mesangial cells; from the Bowman's space bordered by the PECs, the primary urine is conducted towards the tubular system starting with the proximal tubule (Pozzi & Zent, 2012); (B) Electron micrograph of the glomerular filtration barrier: interdigitating processes of adjacent podocytes with linking slit diaphragms (arrows), the glomerular basement membrane and the fenestrated capillary endothelium (Tryggvason et al. 2006, modified); Abbreviations: FP: foot process; GBM: glomerular basement membrane; E: fenestrated endothelium; scale bar: 250 nm

In the last years, putative podocyte regeneration has been discussed. Different sources of progenitor cells, like parietal epithelial cells or cells of the renin lineage have been proposed (reviewed by Grahammer et al. 2013). PECs have been shown to play a role in podocyte regeneration in young mice from postnatal day ten (Appel et al. 2009) up to 28 days of age (Eng et al. 2015). No regeneration could be found in older mice from five weeks to 18 months of age (Berger et al. 2014), a finding that might be explained by the fact that progenitor cells are believed to be active in postnatal mice for one to two weeks (Rinkevich et al. 2014). Limited podocyte renewal from PECs was observed after diphtheria toxin induced podocyte injury, but not under physiological conditions (Wanner et al. 2014). Furthermore, miR-193a-5p was identified to play a role in modulating the phenotype and marker expression of cultured PECs towards a podocyte phenotype (Kietzmann et al. 2014).

1.2.3 Models for working with podocytes

To be able to investigate podocytes in cell culture, immortalized cell lines derived from isolated human and murine podocytes have been established previously (Saleem et al. 2002, Schiwek et al. 2004). The human as well as the murine cell line are proliferating at 33°C and can be differentiated by culturing at 37°C or 38°C, respectively.

Human podocyte cell line

Human podocytes were derived by biopsy from a three year old child (Saleem et al. 2002). By transfection with a retroviral construct coding for the SV40 large T antigen, primary podocytes were immortalized to form a cell culture line: the hPCL (Human podocyte cell line).

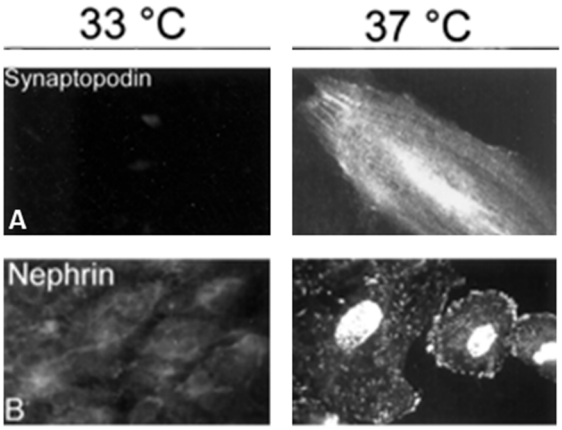

Fig. 1.5: Immunofluorescence of immortalized human podocytes; differential expression of Synaptopodin (top) and Nephrin (bottom) in proliferating (left) and differentiated (right) immortalized human podocytes (Saleem et al. 2002, modified)

When cultured at 33°C, the proliferating cells only show a low expression of synaptopodin and nephrin. After differentiation at 37°C for two weeks, expression of synaptopodin as well as

nephrin could be detected by immunofluorescence (Fig. 1.5). In the proliferating cells, PCNA (Proliferating cell nuclear antigen), a marker of cell proliferation, and CyclinA, a regulator of cell cycle progression, are expressed at high levels, but absent in the differentiated cells. Vice versa, p27 (Cyclin-Dependent Kinase Inhibitor 1B), a cell cycle inhibitor, and CyclinD1, a driver of G1/S phase (Gap 1 phase /Synthesis phase) transition, are absent in the proliferating cells but expressed in the differentiated cells.

Murine podocyte cell line

Murine podocytes were isolated from kidneys of the "Immorto-Mouse" (Charles River, St. Louis, MO, USA) by letting them grow out from isolated glomeruli (Schiwek et al. 2004). These mice carry a temperature sensitive mutant of the SV40 large T antigen under the control of the interferon-γ–inducible H-2K^b promoter. The mPCLs (Murine podocyte cell line) differentiate when cultured at 38°C for two weeks. Expression of the podocyte marker proteins nephrin and Cd2ap (CD2 associated protein) could be demonstrated by Northern Blotting, while expression of WT1 (Wilms tumor protein 1), Lmx1b, Neph1 (Kin of IRRE-like protein 1), Cd2ap, podocalyxin and other marker proteins was shown by RT-PCR (Reverse transcription polymerase chain reaction). By immunofluorescence microscopy, localization of Cd2ap and synaptopodin to the actin cytoskeleton at the cell-cell contacts was shown.

Cell culture of glomeruli isolated from mice

Glomeruli isolated from mice by magnetic bead perfusion (Takemoto et al. 2002) can be cultured in standard cell culture media for several days after isolation from mice (personal communication: M. Kubitza). From the seeded glomeruli, glomerular cells including podocytes grow out on the cell culture flask surface and can be used for experiments. However, the cells dedifferentiate and loose the typical podocyte architecture and marker protein expression within some days.

Freshly isolated murine podocytes

Using a double-fluorescent Cre reporter mouse (Muzumdar et al. 2007) crossed with a mouse with podocyte specific Cre expression (Möller et al. 2003), a mouse harboring podocytes marked by green fluorescence can be generated. By isolation of the glomeruli followed by additional digestion steps, a single cell suspension can be obtained from which the podocytes can be isolated by FACS (Fluorescent activated cell sorting) (Boerries et al. 2013). This method yields a pure podocyte sample. On the downside, the sorted podocytes do not adhere any more to cell culture substrates and thus cannot be cultured further (personal communication: T. Burghardt).

1.3 The role of miRNAs in podocyte integrity

1.3.1 miRNA expression profiles of the mammalian kidney

In several studies, miRNAs were isolated from different tissues in order to identify organ or cell type enriched miRNAs. In the first examination of nine different mouse tissues, highly enriched miRNAs for some of the tissues were identified (Lagos-Quintana et al. 2002). In order to obtain a mammalian miRNA expression atlas, more than 250 small RNA libraries from 26 different organ systems and cell types of human and rodent were sequenced, including total kidney from human as well as mouse (Landgraf et al. 2007). A study sequencing miRNAs isolated from kidney, ovaries and testis of adult mice as well as from the mesonephros, kidneys, ovaries and testis form the embryonic days E11, E12 and E13 revealed the miRNA profiles of these organs to vary during embryogenesis, hinting that miRNAs play an important role for development of murine urinary and reproductive systems (Aguilar et al. 2010).

1.3.2 Podocyte specific knockout of miRNA processing enzymes

In 2008, three parallel studies showed the importance of miRNAs for podocyte development and function (Harvey et al. 2008, Ho et al. 2008, Shi et al. 2008). Mice that expressed the Cre recombinase under the control of the podocyte specific *NPHS2* promoter (Möller et al. 2003) were crossed with mice in which the exons 20 and 21, part of the second RNase III domain of the miRNA processing enzyme Dicer, are flanked by *loxP* (Locus of X-over P1) sites (Harfe et al. 2005), the Cre recombinase recognition sites. This lead to a conditional, podocyte specific Dicer knockout. The affected mice developed proteinuria two to five weeks after birth, leading to end-stage renal disease and death. During progression of disease, several glomerular abnormalities like foot process effacement, crescent formation, wrinkling and split areas of the glomerular basement membrane were observed. In the podocytes of the affected kidneys, the expression of synaptopodin, ezrin (Harvey et al. 2008), podocin (Shi et al. 2008) and nephrin (Ho et al. 2008) was reduced in the knockout podocytes, while expression of α-actinin-4 (Harvey et al. 2008) and WT1 (Harvey et al. 2008, Ho et al. 2008) remained unchanged. It was shown by *in situ* hybridization directed against mature miRNAs, that miR-30a-5p expression in podocytes is lost in the Dicer knockout animals compared to the control animals, whereas the expression of the endothelial miR-126-3p and the mesangial miR-145-5p is not affected by the knockout (Harvey et al. 2008), thus identifying one mature miRNA highly enriched in podocytes. Vice versa, gene expression profiling of glomeruli isolated from Dicer knockout and control mice revealed an

enrichment of mRNAs with possible binding sites of the miR-30 family in the knockout glomeruli, pointing to a possible role of this miRNA family in podocytes (Shi et al. 2008).

In a different study, mice expressing the Cre recombinase under the control of the podocyte specific *NPHS2* promoter (Möller et al. 2003) where crossed with mice possessing *loxP* sites on either side of exon 9 of the miRNA processing enzyme Drosha (Chong et al. 2008), leading to a conditional, podocyte specific Drosha knockout (Zhdanova et al. 2011). At about two to three weeks of age, mice affected by this knockout developed proteinuria that progressed to renal failure and death within four to eight weeks of age. The mice showed podocyte foot process effacement as a first pathologic sign, later leading to extensive collapsing glomerulopathy, pseudo crescent formation and sclerosis. This was accompanied by the loss of synaptopodin, WT1, nephrin and podocin expression, resembling the phenotype of the Dicer knockout mice, with the exception of WT1 expression which remained normal in the Dicer knockout mice. To determine if miRNAs are not only required for podocyte development, but also podocyte function, an inducible Tet-On (Tetracycline-controlled transcriptional activation) system was used in the same study to specifically delete Drosha at later time points. Mice showed proteinuria around two weeks after beginning of the doxycycline treatment. By histological examination, a phenotype very similar to the phenotype observed in the conditional Drosha knockout mice was revealed. Thus, this study showed that miRNAs are not only important for podocyte development, but also for maintenance of the podocyte filtration barrier in adult kidneys.

1.3.3 Profiles from murine podocytes

In 2013, expression profiles from murine podocytes were obtained (Boerries et al. 2013). The transcriptome as well as proteome of podocytes isolated freshly from double fluorescent Cre reporter mice was analyzed. Together with transcripts and proteins enriched in podocytes, a list of 35 miRNAs expressed in murine podocytes and non-podocyte glomerular cells was published that are in high congruence with the data of the present work (Tab. 5.5).

1.3.4 Known miRNA functions in the glomeruli and podocytes

Many studies tried to identify miRNAs important for kidney function. Profiling studies have been performed from patients, animal models and cultured podocytes cell lines under different conditions to identify miRNAs with altered expression levels (reviewed by Chandrasekaran et al. 2012, Kato et al. 2012). For some miRNAs expressed in mammalian kidney, not only expression data, but functional roles were identified. For instance, miR-26a-5p levels were found to be

lowered in swine and human post stenotic kidneys (Zhu et al. 2015) as well as in human patients with lupus nephritis or IgA nephropathy (Ichii et al. 2014). Recently, miR-26a-5p was identified to target CTGF (Connective tissues growth factor), connecting the downregulation of miR-26a-5p to diabetic nephropathy progression in mouse models and humans (Koga et al. 2015). In another study, enhanced nephrin acetylation with attenuated renal damage was reported in miR-155-5p double knockout mice suffering from hyperglycemia induced nephropathy (Lin et al. 2014). Distinct targets have only been identified for some miRNAs in glomeruli and kidneys so far. It was reported that miR-135a-5p regulates TRPC1 (Transient receptor potential cation channel, subfamily C, member 1) during renal injury promoting renal fibrosis (He et al. 2014B). Under high glucose conditions, miR-93-5p regulates VEGF (Vascular endothelial growth factor) *in vitro* and *in vivo* (Long et al. 2010) and miR-195-5p promotes apoptosis in mouse podocytes by regulating BCL2 (B-cell lymphoma 2) activity (Chen et al. 2011). By downregulation of SOCS1 (Suppressor of cytokine signaling 1), miR-150-5p promotes renal fibrosis (Zhou et al. 2013). In immortalized cultured podocytes under mechanical stress and streptozotocin induced diabetic rats, miR-124-3p was reported as a putative regulator of Itga3 (Integrin alpha 3) (Li et al. 2013A, Li et al. 2013B)

miR-17~92 cluster

The polycistronic miR-17~92 cluster contains 6 miRNA hairpin precursors and has firstly been identified to be a potential oncogene (He et al. 2005) which enhances cell proliferation and is highly expressed in lung cancers (Hayashita et al. 2005). The expression of this cluster is upregulated in mouse models for polycystic kidney disease, while inactivation of this cluster in these mouse models retards kidney cyst growth (Patel et al. 2013). Deletion of this cluster in nephron progenitor cells impairs cell proliferation and reduces the number of developing nephrons during kidney development (Marrone et al. 2014). Postnatally, the affected mice developed signs of kidney disease including albuminuria, podocyte foot process effacement and glomerulosclerosis, underlining the importance of the cluster for kidney development.

miR-21-5p

miR-21-5p has been shown to play an important role in the progression of fibrosis (for review see Patel & Noureddine 2012) as well as in the pathogenesis of acute kidney injury (for review see Li et al. 2013C). In a study using mir-21 knockout mice and mice treated with miR-21-5p antisense oligonucleotides, miR-21-5p was shown to promote fibrosis of the kidney by silencing metabolic pathways (Chau et al. 2012). In a different study using a mouse model for Alport nephropathy, miR-21-5p silencing resulted in a milder kidney disease (Gomez et al. 2015). On the other hand, it was shown that miR-21-5p can also ameliorate glomerular injury induced by

TGF-β1 (Transforming growth factor beta 1) and hyperglycemia through repression of proapoptotic signals (Lai et al. 2015). These studies indicate that this miRNA may play different roles and that a tightly controlled physiological level is necessary for healthy kidney function.

miR-29 family

The miR-29 family, expressed in the glomeruli of mice, has been shown to play an important role in the regulation of kidney fibrosis. It was reported that miR-29b-3p regulates several collagens and related genes in Dahl salt sensitive rats (Liu et al. 2010A). By intravenous injection of LNA-antisense molecules into SS-13^{BN} rats, expression of several collagen genes in the renal cortex as well as in the medulla was upregulated. Furthermore, down regulation of these genes by miR-29b-3p was proven by luciferase assays.

miR-29c-3p was found to be a signature miRNA under high glucose conditions in diabetic *db/db* mice (mice with deficient leptin receptor activity, Long et al. 2011). It was proven by luciferase assays to target Spry1 (Sprouty homolog 1) which is an inhibitor of RhoA (Ras homolog family member A) and Rho kinase activation. Knockdown of miR-29c-3p by intraperitoneal injection of antisense oligonucleotides into *db/db* mice led to reduced matrix accumulation and reduced apoptosis in the murine glomeruli.

In another study, wild-type mice showed a reduced expression of miR-29 family and development of progressive renal fibrosis after induction of unilateral ureteral obstructive nephropathy, whereas Smad3 (Smad family member 3) knockout mice had an increased expression of the miR-29 family along with the absence of fibrosis (Qin et al. 2011). *In vitro*, overexpression of miR-29b-3p inhibited, but knockdown of miR-29 family enhanced TGF-β1-induced expression of collagens I and III in renal tubular cells. Delivery of miR-29b-3p blocked progressive renal fibrosis, making it a downstream inhibitor of TGF-β/Smad3-mediated fibrosis.

Furthermore, it was reported by a different group that expression of TGF-β1 reduces the expression of the whole miR-29 family, thus enhancing the expression of proteins of the extracellular matrix (Wang et al. 2012). Ectopic expression of the miR-29 family repressed the expression of collagen I and collagen IV. Additionally, low miR-29 family levels in three different models of renal fibrosis were found.

Recently, it was shown that miR-29a-3p levels are lowered in glomeruli from mice with streptozotocin induced hyperglycemia (Lin et al. 2014). Transgenic overexpression of miR-29a-3p in these diabetic mice improved nephrin levels, podocyte viability and renal function while

reducing glomerular fibrosis and inflammation reaction compared to wild-type diabetic mice. Overexpression of miR-29a-3p restored the acetylation of nephrin by modulation of HDAC4 (Histone deacetylase 4), thus ameliorating hyperglycemia induced podocyte dysfunction.

Taken together, maintenance of healthy miR-29 family levels seems to play an important role in the prevention of fibrosis and the maintenance of glomerular structure.

miR-30 family

miR-30a-5p was firstly identified to be an important podocyte miRNA in the podocyte specific Dicer knockout mice, when it was shown that targets with possible miR-30a-5p binding sites are upregulated after the knockout (Shi et al. 2008). Additionally, *in situ* hybridization showed the absence of this mature miRNA in glomeruli after the podocyte specific Dicer knockout (Harvey et al. 2008). It was shown that miR-30a-5p knockdown in the developing *Xenopus* pronephros phenocopies the defects caused by a pronephric Dicer knockdown, indicating that miR-30a-5p plays an important role in pronephros development (Agrawal et al. 2009). Additionally, a major transcriptional regulator during kidney development, Xlim1/Lhx1 (Lim homeobox 1), was shown to be targeted by miR-30a-5p. In contrast to wildtype mice, miR-30 family expression was lowered in albumin/TGF-β transgenic mice who suffered from podocyte apoptosis and glomerulosclerosis (Shi et al. 2013). *In vitro*, TGF-β is able to downregulate the miR-30 family in wildtype and Smad3 deficient, but not Smad2 (Smad family member 2) or Smad2/Smad3 deficient cultured podocytes. TGF-β induced apoptosis could be hindered by lentiviral overexpression of miR-30d-5p. Taken together, these results hint that loss of miR-30 family signaling is a specific mechanism of TGF-β signaling during glomerulosclerosis.

Later it was reported that downregulation of miRNA-30 facilitates podocyte injury (Wu et al. 2014). Podocyte cytoskeletal damage and apoptosis after treatment of cells with TGF-β and PAN (Puromycin amino-glycoside) were ameliorated by exogenous miR-30 expression and aggravated by miR-30 knockdown. It was found that the miR-30 family exerts this protective role by direct inhibition of Notch1 (Notch homolog 1, translocation-associated) and the transcription factor p53 (Tumor protein P53). Similar results were shown in rats, when PAN treatment lead to a downregulation of podocyte miR-30s and podocyte damage, while exogenous overexpression of miR-30a-5p ameliorated this phenotype. Additionally, glucocorticoid treatment maintained the miR-30 expression levels in TGF-β and PAN stressed cultured podocytes (Wu et al. 2014).

In another study, miR-30a-5p was identified to be upregulated in murine injured podocytes, while the inhibition of miR-30a-5p prevented PAN induced podocyte apoptosis (Xie et al. 2015).

miR-193a-5p

In 2013, it was shown that FSGS (Focal segmental glomerulosclerosis) can be induced by an upregulation of miR-193a-5p, a miRNA that can downregulate the podocyte transcription factor WT1 (Gebeshuber et al. 2013). A transgenic mouse with an inducible miR-193a-5p overexpression under the CMV (Cytomegalovirus) promoter showed a severe kidney phenotype with foot process effacement after two weeks and focal sclerosis after four weeks of induction. WT1, a transcription factor regulating several genes important for maintenance of normal podocytes structure and function, was shown to be targeted by miR-193a-5p, as a predicted miR-193a-5p binding site at the end of the coding region of the WT1 transcript was confirmed as functional. miR-193a-5p upregulation in samples from patients suffering from focal segmental glomerulosclerosis was suggested to be a new pathogenic mechanism for genesis of this disease.

miR-193a-5p was also shown to play a crucial role in the transdifferention of PECs towards a podocyte phenotype (Kietzmann et al. 2014). PECs express miR-193a-5p in high levels. A stable knockdown of this miRNA in immortalized human PECs leads to a shift towards a podocyte-like morphology, expression of podocyte marker proteins like WT1, podocalyxin, synaptopodin, α-actinin-4 and nephrin, and a simultaneous decrease of PEC markers. In a mouse model for rapid progressive glomerulosclerosis, the nephrotoxic nephritis, the formation of interglomerular crescent could be ameliorated by injection of miR-193a-5p-antisense oligonucleotides, again linking miR-193a-5p overexpression to progression of glomerulosclerosis.

1.4 Identification of miRNA targets in podocytes

The podocyte specific *Dicer* knockout mice as well as the inducible podocyte specific *Drosha* knockout mice displayed foot process effacement of the affected podocytes as well as loss of some of the podocyte specific marker proteins (Harvey et al. 2008, Ho et al. 2008, Shi et al. 2008, Zhdanova et al. 2011). Thus, miRNAs play an important role not only in the development, but also in the maintenance of podocyte ultrastructure. The structural proteins themselves as well as the signaling processes needed to maintain the slit diaphragms or the link of the slit diaphragm proteins to the actin cytoskeleton might by targets of miRNA dependent regulation.

1.4.1 Proteins important for podocyte structure and function

Podocytes are highly specialized cells with a unique cytoarchitecture. A lot of proteins have been identified to be important for podocyte integrity. The slit diaphragm, a highly specialized extracellular structure, is built up between the interdigitating foot processes of two neighboring podocytes (Fig. 1.2 C, chapter 1.2.1) by nephrin and the members of the NEPH family. By several adapter proteins, like e.g. podocin, CD2AP, NCK1 and NCK2 (Non-catalytic region of tyrosine kinase adaptor protein 1/2) and the aPKC-PAR3-PAR6 (atypical protein kinase C - Partitioning defective 3 homolog - Partitioning defective 6 homolog) complex, it is linked to the actin cytoskeleton.

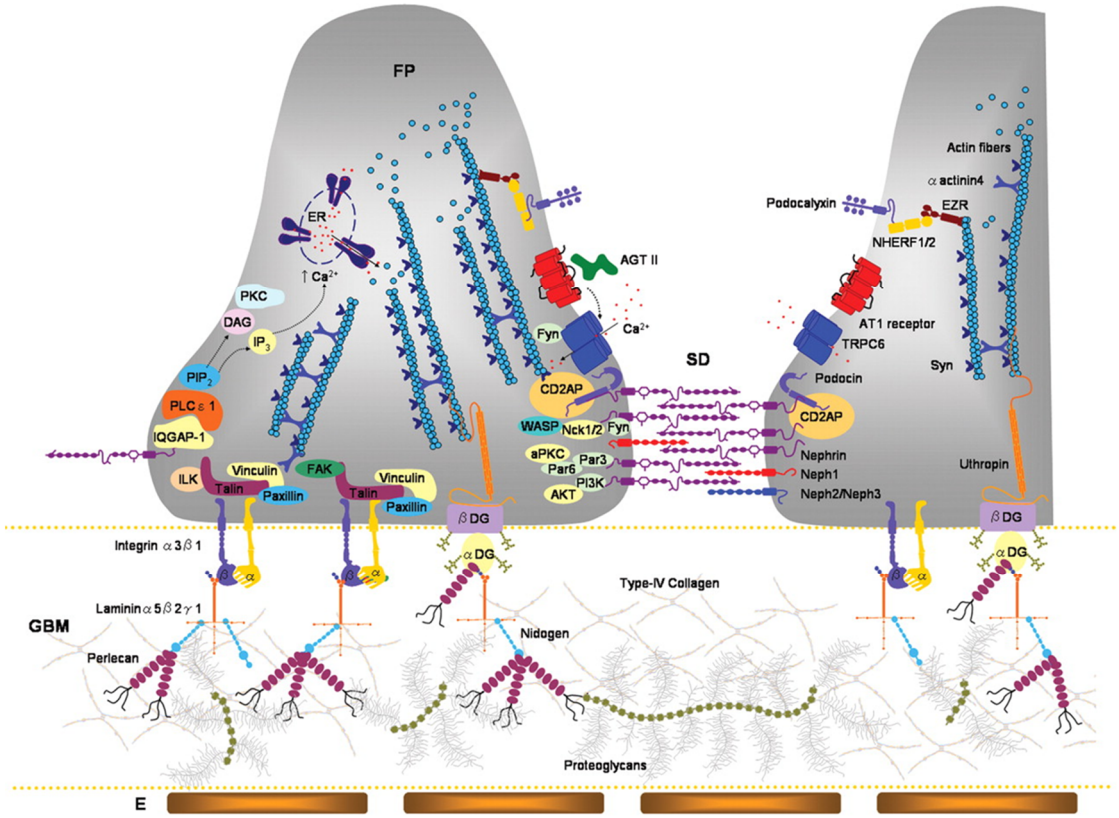

Fig. 1.6: The podocyte slit diaphragm and podocyte-matrix interactions; Cross section of two neighboring foot processes and their slit diaphragm (SD): depiction of proteins forming the slit diaphragm and linking the podocytes to the GBM (glomerular basement membrane), maintaining foot process structure and function (Machuca et al. 2009, modified); Abbreviations: AGTII: Angiotensin 2, aPKC: Atypical protein kinase C, AT1 receptor: Angiotensin II receptor type 1, CD2AP: CD2 associated protein, DAG: Diacylglycerol, DG: Dystroglycan, EF: Fenestrated endothelium, ER: Endoplasmic reticulum, EZR: Ezrin, FAK: Focal adhesion kinase, FP: Foot-process, GBM: Glomerular basement membrane, IP3: Inositol triphosphate, IQGAP-1: IQ motif containing GTPase activating protein, ILK: Integrin-linked kinase, Nck1/2: Non-catalytic region of tyrosine kinase adaptor protein 1/2, NHERF1/2: Sodium-hydrogen antiporter 3 regulator 1/2, Par3: Partitioning defective 3 homolog, Par6: Partitioning defective 6 homolog, PI3K: Phosphatidylinositol-4,5-bisphosphate 3-kinase, PIP2: Phosphatidylinositol 4,5-bisphosphate, PLCε1: Phospholipase C epsilon 1, SD: slit diaphragm, Synpo: Synaptopodin, TRPC6: Transient receptor potential cation channel, subfamily C, member 6, WASP: Wiskott-Aldrich syndrome protein

The podocyte cytoskeleton and its links to the slit diaphragm as well as to the glomerular basement membrane (Fig. 1.6) play an important role for maintenance of the delicate podocyte structure, making it a key component of podocyte function (reviewed in Welsh & Saleem, 2012). Many mutations in genes coding for slit diaphragm proteins and the regulatory network have been identified to be mutated in patients with kidney diseases (reviewed by Machuca et al. 2009). The slit diaphragm components as well as the cell matrix contacts of the podocytes are linked to the actin cytoskeleton via numerous protein interactions and signaling pathways (Fig. 1.7, reviewed in Faul et al. 2007). The proteins involved in the maintenance of the slit diaphragm as well as their interaction partners important for regulation and signaling might be targets of miRNA dependent regulation. The main slit diaphragm component, nephrin, has been shown to interact with several structural proteins like podocin, Neph1-3, CD2AP, synaptopodin and NCK2 (Fig. 1.6, left), ultimately linking the slit diaphragm to the actin cytoskeleton. Three small GTPases, CDC42 (Cell division control protein 42 homolog), RAC1 (Ras-related C3 botulinum toxin substrate 1) and RHOA (Ras homolog gene family, member A) have been shown to play an important role in mediating the interplay between the slit diaphragm and the actin cytoskeleton (Welsh & Saleem, 2012). Additionally, the podocyte actin cytoskeleton is linked to the glomerular basement membrane via several adaptor proteins and regulators (Fig. 1.7, right). Mutations in proteins involved in cell-matrix adhesion are known to be responsible for the genesis of several kidney diseases (reviewed in Sachs & Sonnenberg, 2013).

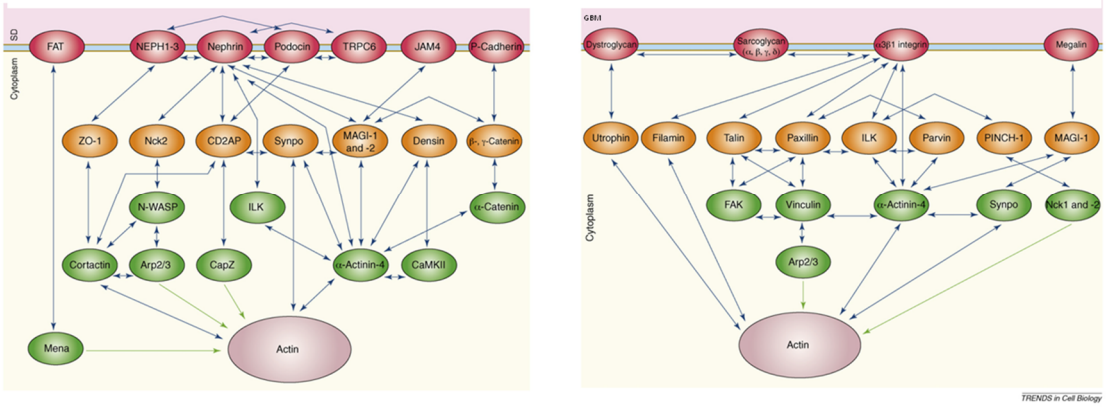

Fig. 1.7: Links between the actin cytoskeleton and the slit diaphragm proteins (left) and the cell-matrix adhesions in podocytes (right) (Faul et al. 2007, modified); Abbreviations: Arp2/3: Arp2/3 complex, CaMKII: Ca^{2+}/calmodulin-dependent protein kinase, CapZ: Capping protein (actin filament) muscle Z-line, CD2AP: CD2 associated protein, FAK: Focal adhesion kinase, ILK: Integrin-linked kinase, JAM4: Junctional cell adhesion molecule 4, MAGI-1/2: Membrane-associated guanylate kinase, WW and PDZ domain-containing protein 1/2, NCK1/2: Non-catalytic region of tyrosine kinase adaptor protein 1/2, N-Wasp: Neural Wiskott-Aldrich syndrome protein, PINCH-1: Particularly interesting new cysteine-histidine-rich protein, Synpo: Synaptopodin, TRPC6: Transient receptor potential cation channel, subfamily C, member 6, ZO-1: Zonula occludens 1

Nephrin

Nephrin, transcribed from the *NPHS1* gene, is the main component of the slit diaphragm and was identified in 1998 to be mutated in patients suffering from the congenital nephrotic syndrome of the Finnish type (Kestilä et al. 1998). It is a transmembrane protein of the immunoglobulin family that consists of a large extracellular portion with eight IgG-like domains, a single fibronectin type 4 motif and a cytoplasmic domain with eight tyrosine phosphorylation sites (Welsh & Saleem 2012). Nephrin is known to interact with CD2AP (see below) as well as with IQGAP (IQ motif containing GTPase activating protein), a protein that can regulate the small GTPases CDC42 and RAC1, which are both important for actin cytoskeleton reorganization (Brandt & Grosse 2007). Additionally, it is a potential key regulator of actin dynamics via recruitment of the actin related Arp2/3 complex and/or formin dependent actin polymerization machineries (Brandt & Grosse 2007). Nephrin is also known to regulate the phosphoinositide-3-OH kinase – protein kinase B pathway, which is important for nephrin mediated actin reorganization in podocytes (Welsh & Saleem 2012).

Podocin

Podocin, a 42 kDa integral membrane protein transcribed from the *NPHS2* gene is exclusively expressed in developing and mature podocytes and was firstly described in 2000 (Boute et al. 2000). It was shown to be localized to the slit diaphragm, interacting with nephrin and CD2AP (Schwarz et al. 2001). Podocin has a hairpin like structure with both the N- and the C-terminus facing the cytosolic side of the slit diaphragm (Welsh & Saleem 2012). It organizes complexes containing the ion channel TRPC6 (Transient receptor potential cation channel, subfamily C, member 6), who is known to be a sensor of mechanically and osmotically induced membrane stretch, giving the slit diaphragm the ability to act as a mechanosensor (Huber et al. 2007). Podocin might also serve as a scaffold protein, linking tight junction proteins to the cytoskeleton (Shono et al 2007).

Neph1

The protein Neph1, also known as Kirrel1 (Kin of IRRE like protein 1), is structurally related to nephrin and belongs to a family of three closely related proteins, Neph1-3, which all share a binding motif for podocin (Sellin et al. 2002). Neph1 knockout mice suffer from extreme proteinuria and die shortly after birth (Donoviel et al. 2001). Neph1 localizes to the slit diaphragms in rat kidneys (Barletta et al. 2003). Hetero dimerization of nephrin and Neph1 (Barletta et al. 2003, Gerke et al. 2003) as well as homodimeric interaction of nephrin and Neph1 (Gerke et al. 2003) were observed in cell culture. The direct interaction of nephrin and Neph1

was proven by co-immunoprecipitation from murine glomerular lysates (Liu et al. 2003). ZO-1 (Zonula occludens 1), a tight-junction associated protein known to be localized to the slit diaphragms in podocytes, was shown to bind to the PDZ domain (Protein domain found in PSD95, Dlg1 and ZO-1) of Neph1 (Huber et al. 2003B). Neph1 is phosphorylated by the kinase FYN (see below) which results in the recruitment of the adaptor protein Grb2 (Growth factor receptor-bound protein 2), an event important for Neph1 induced actin polymerization (Garg et al. 2007). By juxtaposing GRB2 and NCK1/2, the Neph1-nephrin complex augments the efficiency of actin polymerization (Garg et al. 2007). Phosphorylation dependent binding of Neph1 to Grb2 also modulates ERK (Extracellular-signal-regulated kinase) signaling (Harita et al. 2008). The Neph1-Nephrin complex binds polarity proteins, Par3, Par6 and aPKC, via the PDZ domain of Par3 and conserved carboxyl terminal residues in Neph1 and nephrin to regulate podocyte cell polarity (Hartleben et al. 2008).

Expression of Neph2 was detected at the slit diaphragms of murine podocytes (Gerke et al. 2005). It was shown to interact with nephrin *in vivo*, but failed to interact with Neph1. Neph3 has been shown to homodimerize and heterodimerize with Nephrin as well as Neph1, with nephrin and Neph1 or Neph3 trans-interactions promoting cell contacts in cell culture experiments (Heikkilä et al. 2011).

CD2AP

The protein CD2AP was firstly identified as an adapter protein important for the formation of a specialized junction between T cells and antigen presenting cells (Dustin et al. 1998). Surprisingly, global knockout mice demonstrated a compromised immune function, but died at six to seven weeks of age due to renal failure (Shih et al. 1999). The Cd2ap deficient mice exhibits defects in epithelial foot processes accompanied by extra cellular matrix deposition (Shih et al. 1999), underlining the importance of CD2AP for the organization of the renal filtration barrier. CD2AP is localized to the slit diaphragm in murine glomeruli and could be co-immunoprecipitated with nephrin using differentiated cells from an immortalized murine podocyte cell line (Shih et al. 2001). CD2AP has been shown to directly interact with the actin cytoskeleton (Lehtonen et al. 2002). It also interacts with the actin binding proteins CapZ, cortactin (linking it to the actin cytoskeleton regulating Arp2/3 complex) and synaptopodin (Faul et al. 2007). Furthermore, Nephrin and CD2AP associate with PI3K (Phosphoinositide 3-OH kinase) and stimulate AKT (Protein kinase B)–dependent signaling (Huber et al. 2003A).

Synaptopodin

Synaptopodin is a proline-rich actin-associated protein expressed in differentiated podocytes (Mundel et al. 1997). The fine structure and function of murine podocytes seems unaffected in synaptopodin knockout mice (Deller et al. 2003), but the animals display impaired recovery from protamine sulfate induced foot process effacement and LPS (lipopolysaccharide)-induced nephrotic syndrome (Asanuma et al. 2005). Synaptopodin was shown to interact with the tight junction protein MAGI-1 (Membrane-associated guanylate kinase, WW and PDZ domain-containing protein 1), and both synaptopodin and α-actinin-4 localize to the tight junctions when expressed in cell culture (Patrie et al. 2002). Synaptopodin is a regulator of RHOA signaling and cell migration in podocytes, inducing stress fibers by competitive blocking of Smurf1 (E3 ubiquitin-protein ligase) -mediated ubiquitination of RHOA (Asanuma et al. 2006). It can also inhibit filopodia formation by blocking CDC42 signaling (Yanagida-Asanuma et al. 2007). Therefore, it is an important regulator of actin dynamics in podocytes.

a-Actinin-4

The structural proteins of the α-actinin family are four closely related proteins that were originally described as actin-crosslinking proteins (Otey & Carpen 2004). They are present in multiple subcellular regions, including cell-cell and cell-matrix contacts, cellular protrusions, lamellipodia and stress fibers, link the cytoskeleton to transmembrane proteins and serve as a scaffold connecting the cytoskeleton to diverse signaling pathways (Otey & Carpen 2004). Knockout mice as well as mice carrying a mutation in their *Actn4* gene known from human patients with familial focal segmental glomerulosclerosis developed collapsing glomerulopathy (Henderson et al. 2008). The structural protein α-actinin-4 is also required for podocyte adhesion (Dandapani et al. 2007) and its actin bundling activity is regulated by synaptopodin (Asanuma et al. 2005).

The tyrosine kinase FYN

The Src (SRC proto-oncogene, non-receptor tyrosine kinase) family tyrosine kinase Fyn binds to and phosphorylates nephrin, the main slit diaphragm component (Verma et al. 2003). The phosphorylation of nephrin is a prerequisite for the recruitment of Nck adapter proteins which leads to the assembly of actin filaments (Verma et al. 2006). Fyn also phosphorylates the slit diaphragm component Neph1, thus modulating the binding to Grb2 (Harita et al. 2008). Since Nephrin phosphorylation triggers Ca^{2+} signaling by recruitment and activation of PLCG1, (Phospholipase C, gamma 1; Harita et al. 2009), Fyn plays an important role in podocyte signaling.

NCK1 and NCK2

NCK1 and NCK2 are two closely related adapter proteins that couple phosphotyrosine signals to polypeptides that regulate the actin cytoskeleton (Bladt et al. 2003). They are functionally redundant in the sense that mice deficient for either one of the proteins are viable, but double knockout mice die at embryonic day 9.5 (Bladt et al. 2003). The Nck adapter proteins control actin polymerization through their activation of N-WASP (Neuronal Wiskott–Aldrich syndrome protein) and WASP (Wiskott–Aldrich syndrome protein) (Tomasevic et al. 2007). Both are key players in regulating the actin cytoskeleton via the ARP2/3 complex (Tomasevic et al. 2007). The phosphorylation of the slit diaphragm protein nephrin by the kinase Fyn leads to recruitment of the Nck adapter protein via the SH2-SH3 (Src homology 2/3) domain, resulting in the Nck-dependent assembly of actin filaments (Verma et al. 2006). After phosphorylation, the YDxV (Tyrosine – aspartic acid – x – valine) domains in the cytoplasmic tail of nephrin represent binding motifs for the SH2 domains of Nck2 proteins (Jones et al. 2006). Since the interaction between the Nck proteins and nephrin is crucial for actin reorganization, podocyte specific deletion of *Nck1* and *Nck2* leads to foot process deformations and congenital nephrotic syndrome in mice (Jones et al. 2006). Additionally, an inducible podocyte specific deletion of both Nck proteins in adult mice leads to proteinuria, glomerulosclerosis and foot process effacement with loss of slit diaphragms in the affected animals (Jones et al. 2009). Binding of Nck to nephrin leads to recruitment and phosphorylation of PAK (p21 activated kinases), activating the enzyme and leading to actin remodeling (Zhu et al. 2010). The members of the PAK family of serine/threonine kinases are also targets of the Rho family of small GTPases, RAC1 and CDC42, and act as regulators of actin dynamics (Welsh & Saleem 2012).

LMX1B

LMX1B is a transcription factor important for maintenance of podocyte architecture in adult kidneys (Burghardt et al. 2013), comprising two LIM domains (LIM1, LIM2; domain discovered in Lin11, Isl-1, Mec-3) that mediate protein-protein interactions and one homeodomain responsible for DNA binding. Mutations in the *LMX1B* gene cause the nail-patella syndrome (Dreyer et al. 1998, McIntosh et al. 1998, Vollrath et al. 1998). This autosomal-dominant hereditary disease with an incidence of approximately 1:50,000 is characterized by dysplastic nails, absent or hypo plastic kneecaps and chronic nephropathy (Sweeney et al. 2003). In ~40% of patients, nephrologic symptoms develop over the course of several decades (Witzgall 2008). Cd2ap and podocin mRNA and protein levels were lowered in *Lmx1b* knockout mice, and binding of LMX1B to the promoters of *CD2AP* and *NPHS2* (podocin) could be shown *in vitro* (Miner et al.

2002). Microarray studies of glomeruli isolated from inducible podocyte specific *Lmx1b* knockout mice showed significant increase of several actin associated proteins, like Abra (Actin-binding Rho activating protein) and Arl4c (ADP-ribosylation factor-like 4C) (Burghardt et al. 2013). Chromatin immunoprecipitation *in vivo* showed that LMX1B binds to FLAT (Far linked AT rich elements) elements in the promoter regions of ABRA and ARL4C (Burghardt et al. 2013). It has also been described to regulate podocin expression together with the transcription factor FoxC (He et al. 2014A). Lmx1b also plays an important role during the development of the embryonic central nervous system. It is regulated by an auto regulatory feedback loop with miR-135a2, thus modulating Wnt1/Wnt signaling (Proto-oncogene protein Wnt-1/Wnt) (Anderegg et al. 2013).

1.4.2 Manipulation of miRNA levels in cell culture and animal models

To study the effect of altered miRNA levels in cell culture and *in vivo*, several techniques to elevate or lower miRNA levels have been established.

miRNA overexpression

Elevated miRNA levels in cells can be achieved by overproducing either the pri-miRNA, pre-miRNA, a short hairpin RNA precursor coding for the desired miRNA or a precursor with a shortened stemloop structure for Dicer independent processing mimicking miR-451-5p maturation.

One system of generating miRNA overexpression constructs is the pSuper system (oligoengine) originally designed for shRNA (short hairpin RNA) expression (Brummelkamp et al. 2002). In this system, the future precursor is annealed from two oligonucleotides and cloned directly into the backbone. The system was expanded further, now also offering inducible overexpression vectors (pSuperior constructs) containing selection markers or resistance genes, like GFP (Green fluorescent protein) expression or puromycin resistance.

The pSuper system has been used for miRNA overexpression in the present work.

Antisense oligonucleotides

Antisense oligonucleotides can be used to downregulate endogenous miRNA levels by binding irreversible to their targets. Oligonucleotides with a miRNA antisense sequence and a modified, non-degradable backbone, like 2'-O-methylation of the ribose (Meister et al. 2004) or the 2'-O-methylation of the ribose and a phosphorothioate backbone, the so called "antagomirs" (Krützfeldt et al. 2005) have been developed. Both techniques have been applied successfully in cell culture or mouse model, respectively (Meister et al. 2004, Krützfeldt et al. 2005).

Another example for antisense oligonucleotides are the so-called *Vivo-Morpholinos* (GeneTools), single stranded oligonucleotides of usually 25 nucleotides that can be used for a transient miRNA knockdown. They bind to their complementary target sequences through standard nucleic acid base-pairing. To prevent their degradation by the cellular machinery, they possess a modified backbone, in which the ribose ring is substituted by a morpholine ring and the anionic phosphodiester bonds are replaced by an uncharged phosphorodiamidate group. At the 3'-end, they possess an octaguanidinium residue which facilitates their transport through the cellular plasma membrane (Fig. 1.8). Entering and functioning of *Vivo-Morpholinos* in cultured cells and their delivery to several murine tissues including the small intestine, colon, stomach, liver and kidney after intravenous injection could be detected (Morcos et al. 2008). In this study, their functionality in different tissues of mice was demonstrated using a test system were a splicing error is corrected by *Vivo-Morpholino* binding.

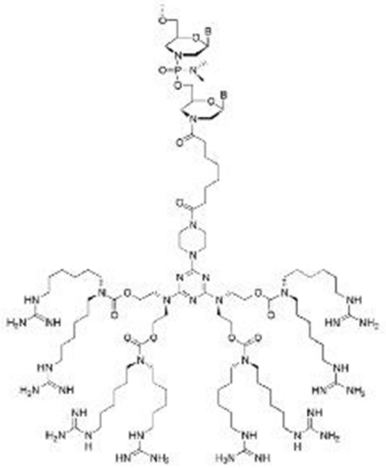

Fig. 1.8: Chemical structure of a vivo-Morpholino; the molecule consists of a oligonucleotide with a modified backbone (top) and a octaguanidinium residue (bottom) linked by a linker

In the present work, *Vivo-Morpholinos* were used for a short term treatment of mice, knocking down two mature miRNAs expressed in podocytes.

The sponge method

Another method for miRNA knockdown are the so called "sponges" (Ebert et al. 2007), competitive inhibitor transcripts containing multiple binding sites for a mature miRNA of interest. They consist of a destabilized GFP gene and a 3'-UTR with several possible binding sites with perfect sequence complementary except for a "bulge" at the positions 9 - 12 (Fig. 1.8 C). When expressed in a cell, the sponge transcripts bind RISCs containing distinct miRNAs or miRNAs of a certain family, rescuing the original target of these miRNAs from regulation (Fig. 1.8 A, B).

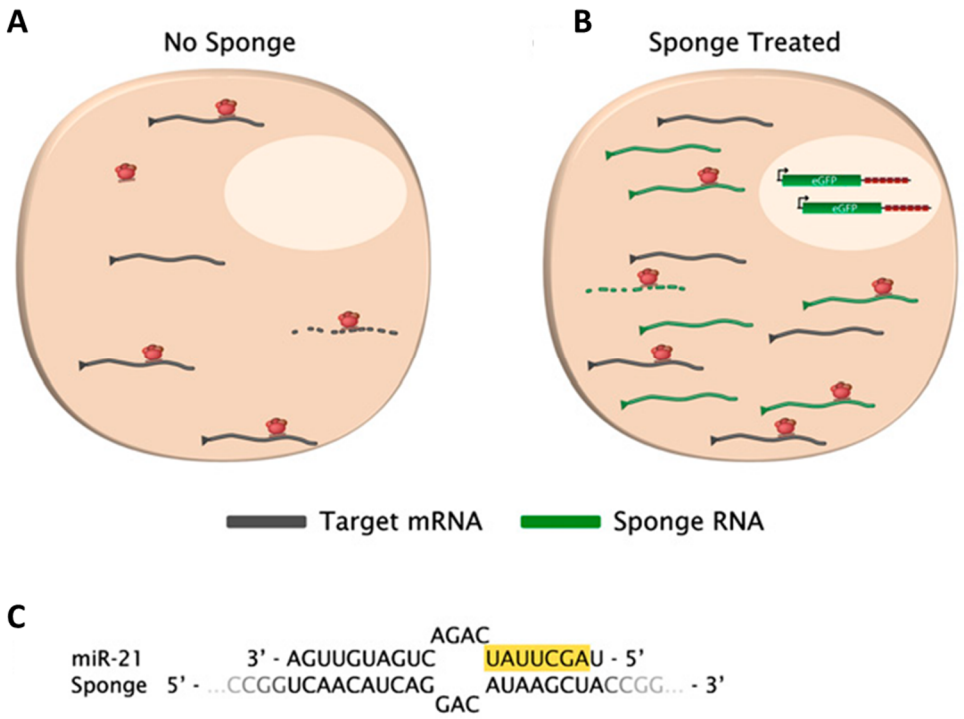

Fig. 1.9: Principle of sponge functionality; (A) In the absence of a sponge, the RISC (red) binds to its target genes, leading to transcript degradation (dotted line); (B) By sponge expression, RISCs are sequestered and target expression is rescued; (C) miR-21 binding to a complementary sponge via a bulged binding site (Ebert & Sharp, 2010B)

Since a perfect match of the sequences is not required for a physiological miRNA-target binding in cells, and since members of a miRNA family possess very similar sequences, a sponge can downregulate a whole miRNA family. A broad variety of sponges have been developed targeting lots of different miRNA families and have been applied for transient and stable knockdown of miRNA levels in cell culture (reviewed by Ebert & Sharp 2010B). They have also been used for *in vivo* studies, e.g. for the knockdown of the miR-183/96/182 cluster, which is known to be highly expressed in photoreceptor cells (Zhu et al. 2011). Fertilized mouse eggs were injected with a construct harboring five binding sites for each of the mature miRNAs, engineering a transgenic sponge mouse (Zhu et al. 2011). Another sponge mouse with a transgenic expression of a sponge directed against the miR-29 family was developed to investigate immune responses (Ma et al. 2011). Several examples for natural sponges have been discovered until now (reviewed by Ebert & Sharp 2010A). The *Herpesvirus saimiri* expresses a small non-coding RNAs with a miR-27a-3p binding site that can downregulate this miRNA in the host organism (Cazalla et al. 2010). A circular RNA expressed in human and mouse brain containing more than 70 conserved miR-7-5p binding sites (ciRS-7, circular RNA sponge for miR-7) and a testis specific circular RNA (Sry, sex-determining region Y) containing 16 putative miR-138-5p binding sites have been proven to be functional (Hansen et al. 2013).

In the present work, sponges were designed and tested for miRNA families that are expressed in high levels in podocytes.

TALEN mediated genome editing

TALE (Transcription activator-like effector) nucleases can be used for directed genomic knockout of protein coding genes as well as for miRNA knockout. They comprise a non-specific DNA-cleaving nuclease, *Fok*I, originally derived from *Flavobakterium okeanokoites,* fused to a sequence specific DNA binding domain (Joung & Sander 2013).

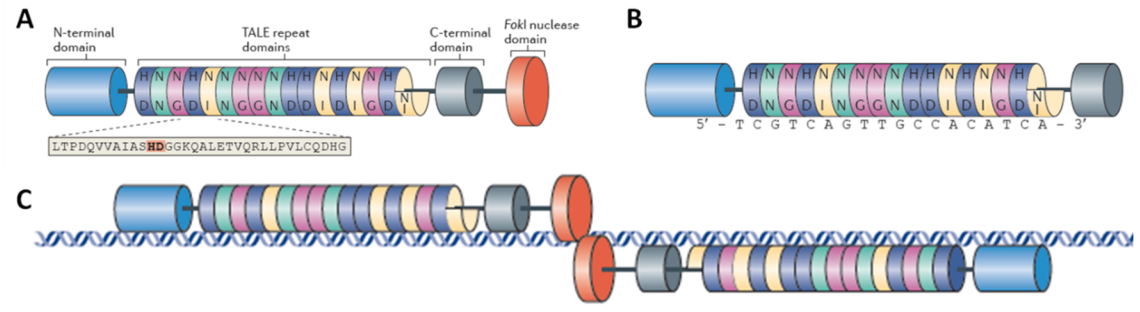

Fig. 1.10: Overview of TALE array nucleases; (A) TALEN consisting of a n-terminal domain, the sequence specific TALE array, the c-terminal domain and a *Fok*I nuclease domain; (B) TALEN bound to a specific target sequence; (C) TALEN pair leading to a directed double strand break (Joung & Sander 2013, modified)

The DNA-binding array consists of TALEs, which are proteins secreted by *Xanthomonas spp*. to alter gene transcription in host plant cells. The protein array forms a super helix around the DNA double strand, the positions 12 and 13 positioned in the major groove of the DNA (Fig. 1.9). The amino acids at these two positions determine the selectivity of the TALE array (Tab. 1.1).

Tab. 1.1: List of amino acid combinations in TALE array monomers that bind specifically to DNA bases

Amino acid combination at positions 12 & 13	Recognized base
Asn - Asn	guanine
Asn - Ile	adenine
His - Asp	cytosine
Asn - Gly	thymine

With a pair of TALENs, both containing a sequence specific array and one part of the dimeric or heterodimeric *Fok*I nuclease, a double strand break in the DNA can be induced. It has been shown that a heterodimeric split of the FokI nuclease enhances its activity (Doyon et al. 2011). The cellular repair mechanisms NHEJ (Non homologous end-joining) and HDR (Homology directed repair) can both be used for directed genomic engineering (Joung & Sander 2013). NHEJ normally leads to deletions of several bases or insertions, causing a frame shift in coding genes.

It has been shown that knockout of different target genes in *Xenopus* embryos can lead to a wide variety of deletions and insertions (Lei et al. 2012). By offering a donor template to the cells for HDR, desired sequence alterations or marker sequences for mutated clone identification can be inserted. Identification of knockout clones by PCR detection of the integrated donor cassette has been demonstrated (Uhde-Stone et al. 2014). The TALEN technology has been applied successfully for directed gene knockout in a broad variety of organisms until now (reviewed by Sun & Zhao 2013). By microinjection of TALEN RNA into one cell stage of embryo and transfer to pseudo pregnant mice, mice with mutations in the genomic loci of mir-146a, mir-10a and mir-10b were generated (Takada et al. 2013). A library of TALEN plasmids for miRNA knockout in human cell was engineered (Kim et al. 2013). A total of 540 pairs of TALENs for 274 miRNA loci for specific miRNA knockout were designed. The plasmids coding for these TALENs can be obtained via http://www.talenlibrary.net/.

In the present work, a TALEN pair directed against the human mir-30a locus was used to generate a miRNA knockout cell line, to establish this technique investigate effects of miRNA loss on cells.

Tab. 1.2: Overview of methods for miRNA level manipulation

Method	Direction/location of manipulation		Regulatory target
miRNA overexpression	upregulation of	cytoplasmic levels	one specific mature sequence (and opposite strand)
Knockdown by "sponges"	knockdown of	cytoplasmic levels	family of miRNAs
Knockdown by antisense oligonucleotides	knockdown of	cytoplasmic levels	one specific mature sequence
Knockout by TALENs	knockout on	genomic level	one specific locus (off-target effects possible)
Knockout by CRISPR/Cas9	knockout on	genomic level	one specific locus (off-target effects possible)

Recently, an alternative genomic knockout method, the CRISPR/Cas9 (Clustered regularly interspaced short palindromic repeats/CRISPR associated protein 9) system, based on a bacterial and archaeal immune response system, has been developed (Jinek et al. 2012). The Cas9 protein, a nuclease able to induce double strand breaks, can be guided to the target site by a chimeric guide RNA. The advantages and disadvantages of the different systems for the present work will be discussed in chapter 5.4.

1.4.3 Methods for miRNA-mRNA pair identification

In the last years, several techniques have been developed to identify and characterize specific regulatory miRNA-mRNA interactions.

In silico *predictions*

Since miRNAs bind to their targets in a sequence dependent manner, many algorithms have been developed to predict putative binding sites for miRNAs in transcripts. The platform miRWalk and its update miRWalk2 use eight (DIANAmT, miRanda, miRDB, RNAhybrid, PICTAR4, PICTAR5, PITA, RNA22 and Targetscan) or 12 (miRWalk, Microt4, miRanda, mirbridge, miRDB, miRMap, miRNAMap, Pictar2, PITA, RNA22, RNAhybrid and Targetscan) different prediction algorithms, respectively, to generate sorted lists of possible interaction partners (Dweep et al. 2011). Since total sequence complementary is not required for binding of mammalian miRNAs and mismatches are tolerated outside the miRNA seed sequence under physiological conditions (Carthew & Sontheimer 2009), the predictions yield long lists of putative regulatory pairs. Using *in silico* predictions, putative pairs of miRNAs expressed in podocytes and mRNAs coding for proteins important for podocyte structure and function were predicted.

Argonaute immunoprecipitation (Ago-IP)

Target mRNAs bound and silenced by miRNA mediated RISC binding can be identified by performing an immunoprecipitation of the argonaute proteins (Beitzinger et al. 2007). With this technique, the Ago bound target mRNAs can be purified and identified, e.g. by qPCR (quantitative polymerase chain reaction), Northern Blotting or microarray analyses.

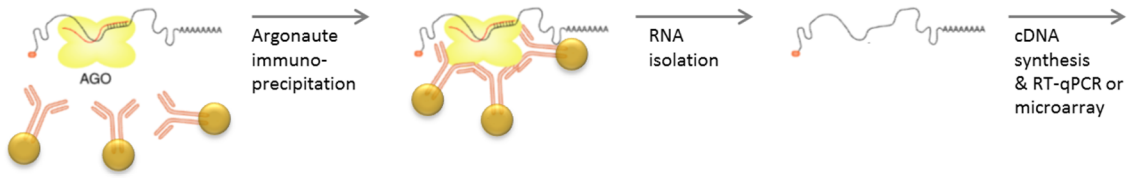

Fig. 1.11: Principle of Ago-IP experiment; The RISCs are bound by magnetic beads coupled Ago specific antibodies; after clean-up of the complexes by magnetic extraction, the RNA is isolated by protein degradation and further analyzed (Long et al. 2012, modified)

To increase the yield of a protein-RNA complex immunoprecipitation, the complexes can be crosslinked with UV (Ultra violet) light. These CLIP (Cross-linking and immunoprecipitation) protocols (Ule et al. 2003) can be combined with Ago-IP (Jaskiewicz et al. 2012). In addition, the isolated RNAs can be further analyzed by high-throughput sequencing, the HITS-CLIP (High-throughput sequencing of RNA isolated by crosslinking immunoprecipitation; Licatalosi et al. 2008).

In the present work, miRNA regulated mRNAs were isolated by Ago-IP using hPCLs, mPCLs and freshly isolated murine podocytes.

Luciferase reporter assays

The susceptibility of a 3‘-UTR for regulation by miRNAs can be tested by luciferase assays, e.g. with the pMir-REPORT system (Ambion, modified G. Meister). The 3’-UTR of a putative target gene is cloned behind a luciferase gene, which is located on the same plasmid as an untargeted renilla luciferase serving as internal control (Fig. 1.11 A). The expression level of luciferase protein, which can be measured with the help of a chemo luminescence producing reaction, is dependent on the characteristics of the 3’-UTR. By overexpression of the assumed miRNA binding partner and/or mutation of the supposed binding site, the levels of luciferase are affected and the functionality of a predicted miRNA-mRNA binding pair can be tested in cell culture (Fig. 1.11 B).

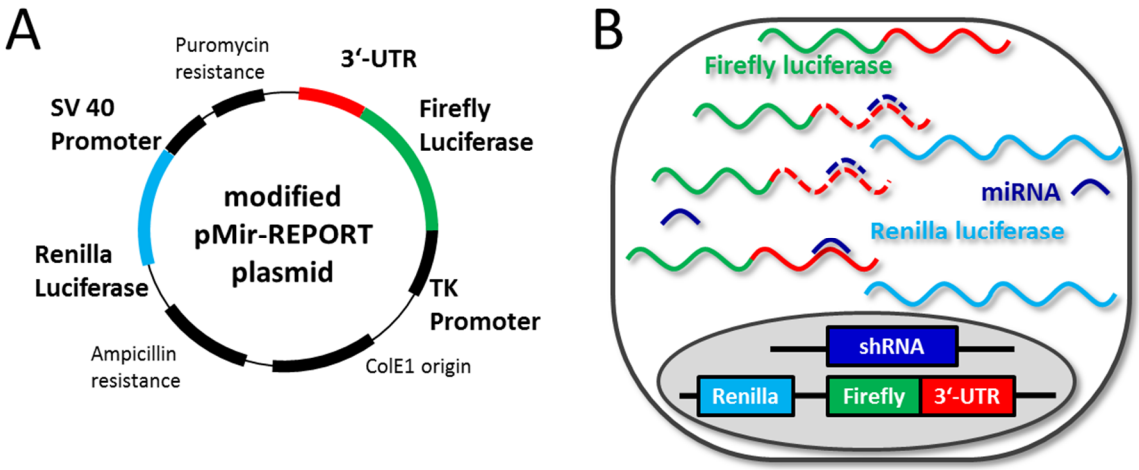

Fig. 1.12: Principle of miRNA binding Luciferase Assay; (A) Plasmid coding for firefly luciferase containing 3’-UTR of a putative target gene and untargeted renilla luciferase as control; (B) Situation in cell for luciferase assay: cotransfection of cells with luciferase reporter plasmid and miRNA overexpression plasmid; if binding of the miRNA to the 3’-UTR occurs, the firefly level is downregulated

By cotransfection of luciferase reporter constructs and miRNA overexpression constructs into cells, binding of predicted regulatory pairs of miRNAs and mRNAs were analyzed in the present work.

2 AIMS OF THIS WORK

Due to the improvement of sequencing techniques in the last decade, thousands of miRNAs have been identified to be expressed in tissues and organs of many species. From different studies working with mice harboring a podocyte specific knockout for miRNA processing enzymes (Harvey et al. 2008, Ho et al. 2008, Shi et al. 2008, Zhdanova et al. 2011), it is known that miRNAs are important for development as well as for maintenance of podocyte structure and function. However, little is known yet about the precise roles of distinct miRNAs in maintenance of podocyte structure and function and their respective target mRNAs. Since the complex cytoarchitecture of the podocyte foot processes is lost in the Dicer and Drosha knockout mice, the proteins building up and stabilizing the slit diaphragms in-between the foot processes might be targets for miRNA dependent regulation.

The aims of the present work were the identification of the podocyte miRNAs essential for the maintenance of the slit diaphragm in healthy podocytes and their regulatory miRNA-mRNA pairs in order to elucidate the processes leading to podocyte injury and foot process effacement after dysregulation of miRNA levels as seen in the Dicer and Drosha knockout mice.

Many earlier studies as well as the initial experiments of the present work used isolated glomeruli, samples consisting of three different cell types. Thus, the first goal of the present work was the generation of a podocyte specific reporter mouse using the double fluorescent Cre reporter mouse (Muzumdar et al. 2007) to isolate a clean podocyte population from the glomerular sample. To elucidate the role miRNAs play in adult podocytes, two strategies were applied. An overview of the miRNAs expressed in mammalian podocytes was generated by *deep sequencing* profiles. Putative miRNA-mRNA pairs between miRNAs enriched in podocytes and targets known to be important for podocyte structure and function were generated by *in silico* predictions. To validate these predicted mRNA targets, Ago-IP combined with qPCR detection of predicted targets and luciferase assays for the identification of binding sites were performed. In a second approach, miRNA regulated mRNAs in podocytes were identified by Ago-IP using freshly isolated murine podocytes followed by a focused microarray detection of the RISC bound targets. Additionally, different techniques for miRNA level manipulation were applied *in vivo* and in cell culture for functional analyses of specific miRNAs.

It is known that miRNA expression can be regulated by transcription factors. The role of the transcription factor Lmx1b, known to be important for podocyte function, in the regulation of miRNA levels in podocytes was investigated.

3 MATERIALS AND METHODS

3.1 Materials

3.1.1 Equipment and consumables

Instruments

Equipment	Source
Agarose gel electrophoresis chamber "Owl EasyCast B2"	Thermo Scientific
Autoclave "2540 ML"	Tuttnauer
Autoclave "5050 ELV"	Tuttnauer
Blotting Chamber "Trans-Blotr SD Semi-Dry"	BioRad
Blotting Chamber "Tank Blot SE 600"	Hoefer
Centrifuge "Hitachi himac CT15RE"	VWR
Centrifuge "Multifuge 3 L-R"	Hereaus
Centrifuge "Pico"	Hereaus
Chemiluminescence system "Fusion Fx7"	Vilber Lourmat
CO_2 incubator for cell culture	Binder
Electroporator "Gene Pulser Xcell Electroporation System"	Bio-Rad
Fluorescence microscope "Axioskop HBO-50"	Carl Zeiss
Fluorescence microscope camera "AxioCam MRC"	Carl Zeiss
Freezers -20°C	Privileg
Freezers -80°C "Herafreeze"	Heraeus
Gel Documentation System "GelDoc XR+"	BioRad
Gel electrophoresis cell "Mini Protean 3"	BioRad
Glassware (bottles, flasks, beakers)	Schott; VWR
Hybridization oven "HB-1000" and "OV3"	UVP; Biometra
Ice machine	Ziegra
Imaging system "FLA-5000"	Fujifilm
Incubator	Heraeus
Laboratory pH Meter "CG 842"	SCHOTT Gerte GmbH
Laminar flow bench "Lamin Air HA 2448 GS"	Heraeus
Liquid nitrogen container "ARPEGE TP 170"	Air Liquide Medical GmbH
Luminometer "Mithras LB480"	Berthold
Magnetic collector "IMagnet"	BD Bioscience
Magnetic Stirrer "MR3001"	Heidolph
Neubauer counting chamber (depth 0.1 mm)	Marienfeld
pH electrode "SenTix60"	WTW
Phosphor screen "BAS-IP MS 2025"	Fujifilm
Photometer "NanoDrop"	ThermoScientific
Pipettes	Brand; Gilson
Power Supply "PS608"	life technologies
Power Supply "Standard Power Pack 25"	Biometra
qPCR Cycler "LightCycler 480 II"	Roche
Refrigerators	SEG, privileg
Repetitive pipette "HandyStep electronic"	Brand

Rotating wheel for Eppendorf-tubes	Workshop of University
Screen eraser for phosphor screens	Raytest
Sequencer "HiSeq 1000"	Illumina
Shaking incubator "Kelvitron t"	Infors
Shaking plate "Duomax 1030"	Heidolph
Thermal cycler "MyCycler"	Bio-Rad
Thermoshaker	Hartenstein
UV/Vis Spectrophotometer "Evolution201"	ThermoScientific
Vortexer "Vortex-Genie2"	Scientific Industries
Water deionizer "Seralpur Pro 90 CN"	Seral
Weighing scale "BL 1500 S"	Sartorius
Weighing scale "Kern 770"	Kern & Sohn GmbH

Consumables

Consumables	Source
96-well white non-binding plate for luciferase assay	Greiner bio-one
96-well light cycler plate PP	Sarstedt
96-well light cycler plate PP sealing tape	Sarstedt
Autoclave tape	Brand
Bottle top filter for sterile filtration (45µm)	Sarstedt
Cell culture dishes (P3, P6, P10, P15)	Sarstedt
Cell culture flasks (25 cm^2, 75 cm^2)	Sarstedt
Cell culture plates (12 well, 24 well)	Sarstedt
Cell scraper 39 cm	Sarstedt
Cell strainer 100 µm	BD Falcon/Corning
Chromotography paper	Whatman
Cuvette for electroporation (Gene Pulser)	Bio-Rad
CryoPure tubes 1.8 ml	Sarstedt
Filter paper for dialysis	Millipore
Filters for sterile filtration (20 µm, 45 µm)	Sarstedt
Glass Pasteur pipettes	VWR
HyBond Membrane	GE Healthcare
Hypodermic needles	Braun
Microscope cover glass 15 mm	R. Langenbrinck
Microscope slides	R. Langenbrinck
Nitrile gloves	Kimtech
PCR cups 0.2 ml	Sarstedt
Parafilm	Pechiney Plastic
Pipette tips	Sarstedt
Pipette tips with filter (RNAse free)	Sarstedt
Polystyrene cuvettes for spectrophotometer	Sarstedt
Roundbottom tube with cell strainer for FACS	BD Falcon
Tubes (15 ml, 50 ml)	Sarstedt
PVDF transfer membrane (0.45 µm)	Millipore
Reaction tubes (1.5 ml, 2 ml)	Sarstedt
Scalpels	Hartenstein
Serological pipettes (1, 2, 5, 10, 25 ml)	Sarstedt
Syringes	Brown
Task wipes	Kimtech

3.1.2 Chemicals and reagents

Chemicals

Chemical	Source
Acetic acid, glacial	Sigma
Agarose (NEEO quality, ultra quality)	Roth
Ampicillin (Sodium-salt)	Roth
APS (Ammoniumpersulfate)	Fluka
ATP (Adenosine triphosphate; 100 mM)	ThermoScientific
ATP powder for luciferase assay substrate	PJK
Beads, Protein G coupled	invitrogen by lifetechnologies
Beads, tosylactivated	invitrogen by lifetechnologies
Boric acid	Merck
BSA (Bovine serum albumin)	Roth
Bromphenol blue	Sigma
β-mercaptoethanol	Merck
Chloroforme	Merck
Coelenterazine, 1000x, for luciferase assay	PJK
CoenzymeA for luciferase assay	PJK
Coomassie Brilliant Blue R-250	Roth
D-Luciferin for luciferase assay	PJK
DABCO (1,4-Diazabicyclo[2.2.2]octan)	Roth
DAPI (4′,6-Diamidin-2-phenylindol)	Sigma
DEPC (Diethylpyrocarbonate)	Roth
DMSO (Dimethylsulfoxide)	Sigma
dNTPs (Deoxynucleotide triphosphates)	Fermentas
Doxycyclin hyclate	Applichem
DTT (1,4-Dithio-DL-threitol)	Roth
EDC (1-Ethyl-3-(3-dimethylaminopropyl)carbodiimid	Roth
Ethanol	Sigma
Ethidium bromide	Sigma
Formamide deionized	Roth
Ficoll 400	Serva
HEPES(4-(2-hydroxyethyl)-1-piperazineethanesulfonic acid)	Roth
Hydrochloric acid	Fluka
Hydrogen peroxide, 30%	FisherChemical
Isopropanole	Merck
G-418-sulfate	Invitrogen
Glucose	Merck
Glycerol	Roth
Glycine	FisherChemical
Glycogen	Peqlab
Kanamycin sulfate	Applichem
Magnesiumchloride ($MgCl_2$*$6H_2O$)	Merck
Magnesiumsulfate	Merck
Methanol	Roth
Methimidazole	Roth
Narcoren	Merial
Nonidet P-40	Applichem
PEI (Polyethylenimine)	Polysciences Inc.

PFA (Paraformaldehyde)	Merck
PVP (Polyvinylpyrrolidone)	Merck
Propidiumiodide	Applichem
Potassium chloride	Merck
Potassiumdihydrogenphosphate	Merck
Rabbit IgG	Sigma
Puromycine	PAA
SDS (Sodium dodecylsulfate)	Serva
Skim milk powder	Sucofin
Sodium acetate	Roth
Sodium azide	Merck
Sodium citrate*2H_2O	Merck
Sodium chloride	Merck
Sodium EDTA	Roth
Sodium fluoride	Merck
Sodiumdihydrogenphosphate *2H_2O	Roth
di-Sodiummonohydrogenphosphate *12H_2O	Merck
Sodiumhydroxide solution (1M)	Merck
Sodiumhydroxide pellets	Merck
Sucrose	Merck
TEMED (Tetramethylethylenediamine)	Roth
Tricine	Roth
Tris base	Sigma
Triton-X-100	Roth
Tween 20	Roth

All standard chemicals not listed in the above table were purchased at Merck, Roth or Sigma.

Premixed chemicals and solutions

Premixed chemicals and solutions	Source
30% Acrylamide/0.8% Bisacrylamide solution	Serva
Acid Phenol	Roth
ATP [γ-32P] (radioactively labeled, stabilized (SRP-501))	Hartmann Analytics
CollagenI (for coverslip coating)	Sigma
DMEM (Dulbecco's modified Eagle's medium) high glucose	Sigma
EDTA solution (pH=8.0, RNAse free)	Ambion
FCS (Fetal calf serum)	PAN Biotech
Glycogen [35µg/µl]	Peqlab
HBSS (Hank's balanced salt solution) premix powder	Sigma
Horse serum	PAA
Immersol 518F for Microscope	Carl Zeiss
ITS-G (100x Insulin-Transferrin-Selenium)	life technologies
LB-Medium (Lennox) mix	Roth
LB-Agar (Lennox) mix for plates	Roth
Passive lysis buffer for Luciferase Assay	Promega
PeqFECT	Peqlab
qPCR Mastermix: Sensifast Sybr No-Rox	Bioline
qPCR Mastermix: LightCycler480 Sybr Green I	Roche
Roti Aqua-Phenol	Roth
Roti-Quant	Roth

RNAse away	Molecular BioProducts
RPMI medium 1640 with L-Glutamine	Sigma
SuperSignal West Pico for WesternBlots	ThermoScientific
Trifast	Peqlab
TRIS buffer: pH=8.0, RNAse free	gibco by life technologies
Trypsin	Sigma-Aldrich
TurboFECT	ThermoScientific
Western Lightning-ECL Enhanced Luminol Reagent	Perkin Elmer
Western Lightning-ECL Oxidizing Reagent	Perkin Elmer
Urea gel system: Ultra pure sequagel system	National diagnostics

3.1.3 Kits, enzymes and markers

DNA Work

Kit Name	Source
GeneJET Plasmid Miniprep Kit	Thermo Scientific
QIAGEN Plasmid Midi Kit	QIAGEN
Qiaquick Gel Extraction Kit	QIAGEN
Qiaquick Nucleotide Removal Kit	QIAGEN

RNA Work

Kit Name	Source
DNAse I Kit	QIAGEN
iScript DNA Synthesis Kit	Bio-Rad
miRNeasy mini Kit	QIAGEN
miRVana miRNA Isolation Kit	life technologies
RNase free DNAse Set	QIAGEN
RNeasy micro Kit	QIAGEN

Enzymes

DNA modifying enzymes and buffers	Source
Alkaline Phosphatase	Roche
DNase I	Applichem
Phusion High-Fidelity DNA Polymerase	NEB (New England Biolabs)
Phusion HF 5x reaction buffer	NEB (New England Biolabs)
***Pfu* DNA Polymerase**	Fermentas
T4 DNA Ligase	Fermentas
T4 DNA Ligase 10x reaction buffer	Fermentas
T4 DNA Ligase	NEB (New England Biolabs)
T4 DNA Ligase 10x reaction buffer	NEB (New England Biolabs)
T4 PNK (Polynucleotide Kinase)	NEB (New England Biolabs)
T4 PNK (Polynucleotide Kinase) 10x reaction buffer	NEB (New England Biolabs)
***Taq* DNA Polymerase**	NEB (New England Biolabs)
Thermopol 10x buffer	NEB (New England Biolabs)

Restriction enzymes and buffers	Source
***Apa*I**	NEB (New England Biolabs)
***Bgl*II**	Fermentas
CutSmart 10x reaction buffer	NEB (New England Biolabs)
***Eco*RI-HF**	NEB (New England Biolabs)
***Hind*III-HF**	NEB (New England Biolabs)
Orange buffer 10x reaction buffer	Fermentas
***Sac*I-HF**	NEB (New England Biolabs)
***Spe*I-HF**	NEB (New England Biolabs)
***Xho*I**	NEB (New England Biolabs)

RNA modifying enzymes	Source
EPAP (E.coli poly-A polymerase)	Ambion

Protein modifying enzymes	Source
Pronase E from Streptomyces griseus	Sigma
Proteinase K	Merck
Collagenase Type II	Worthington

Markers

Markers	Source
2-log DNA Marker (100 - 10000 bp)	NEB (New England Biolabs)
microRNA MArker	NEB (New England Biolabs)
PageRuler Prestained Protein Ladder	ThermoScientific

3.1.5 Cells and plasmids

Cells

Cell line/Bacterial strain		Source
HEK293T	human embryonic kidney cells	ATCC
hPCL	human podocyte cell line, AB 8/13	Saleem et al. 2002
mPCL	murine podocyte cell line, E11	Schiwek et al. 2004
DH5α	*E. coli* strain	DSMZ
TOP10	*E. coli* strain	life technologies

Plasmids

Plasmid	Resistance	Source
CMV-d2eGFP-empty	ampicillin	Addgene, Ebert et al. 2007
CMV-d2eGFP-21 „pSponge“	ampicillin	Addgene, Ebert et al. 2007
Human-hsa-mir-30a_5'TALEN L1	ampicillin	www.talenlibrary.net (Kim et al 2013)
Human-hsa-mir-30a_5'TALEN R1	ampicillin	www.talenlibrary.net (Kim et al 2013)
pMir-Report (modified)	ampicillin	Ambion, modified (G. Meister)
(changed promoter CMV→TK; Renilla luciferase on same plasmid**)**		
pSuper (modified resistance)	kanamycin	oligoengine, modified (G. Meister)
pWE2	ampicillin, neomycin	ATCC, Cockett et al. 1997
pWE3	ampicillin, puromycin	ATCC, Cockett et al. 1997

3.1.6 Software

Programs

Program	Company
AIDA Image Analyzer v4.27	Raytest
Bio1D	Vilber Lourmat
Chromas Lite 2.1.1	Technelysium Pty Ltd
FileMaker Pro 6	FileMaker, Inc.
Fusion version 15.18	Vilber Lourmat
Image Reader FLA-5000 V2.0	Fujifilm
ImageJ 1.46r	National Institutes of Health
ImageLab V5.2	BioRad
LightCycler 480 1.5.0	Roche
Microsoft Excel	Microsoft
Microsoft Powerpoint	Microsoft
Microsoft Word	Microsoft
NanoDrop 2000/2000c	ThermoScientific
Snapgene Viewer 2.7.3	GSL Biotech, LL
Thermo Insight 1.4.40	ThermoScientific
ZEN (blue edition)	Carl Zeiss MicroImaging

Internet databases and online programs

Name of database	Internet address
ensembl	www.ensembl.org (Cunningham et al. 2015)
miR2Disease	www.mir2disease.org/ (Jiang et al. 2009)
mirbase	www.mirbase.org (Kozomara & Griffiths-Jones 2014; Kozomara & Griffiths-Jones 2011; Griffiths-Jones et al. 2008; Griffiths-Jones et al. 2006; Griffiths-Jones 2004)
Pubmed	www.ncbi.nlm.nih.gov/pubmed
smirnaDB	www.mirz.unibas.ch/cloningprofiles (Hausser et al. 2009)
UCSC genome browser	https://genome.ucsc.edu (Kent et al. 2002)
TarBase v7.0	http://diana.imis.athena-innovation.gr/DianaTools/ (Vlachos et al. 2014)
Name of program	**Internet address**
BLAST	www.ncbi.nlm.nih.gov/BLAST
Primer3	http://primer3.ut.ee (Koressaar et al. 2007, Untegasser et al. 2012)
miRWalk	http://www.umm.uni-heidelberg.de/apps/zmf/mirwalk (Dweep et al. 2011)
miRWalk2	http://zmf.umm.uni-heidelberg.de/apps/zmf/mirwalk2/index.html (Dweep et al. 2011)

3.1.7 Prepared solutions and buffers

50x Denhardt's solution:	1%	Ficoll 400
	1%	PVP
	1%	BSA
	in H_2O	
10x DNA loading dye:	50%	glycerol
	0.25%	Bromphenolblue
	20 mM	EDTA
	in H_2O	

LB-Agar plates (Lennox):	35 g in 1 l H_2O	premixed powder
LB-Medium (Lennox):	20 g in 1 l H_2O	premixed powder
10x PBS buffer:	137 mM 2.7 mM 10 mM 2 mM in H_2O, adjusted to pH=7.4	NaCl KCl Na_2HPO_4 KH_2PO_4
20x SSC buffer:	3 M 300 mM in H_2O, adjusted to pH=7.0 with HCl	NaCl Na_3Citrat
10% SDS solution:	347 mM in H_2O	SDS
50xTAE buffer:	2 M 100 mM in H_2O, adjusted to pH = 8.0 with acetic acid	Tris EDTA
10x TBE buffer:	890 mM 890 mM 20 mM in H_2O	Tris base Boric acid EDTA

Prepared buffers and solutions for protein gel electrophoresis

4x Lower Tris buffer:	1.5 M Tris, pH = 8.8 0.4% SDS in H_2O	
4x Upper Tris buffer:	0.5 M Tris, pH=6.8 0.4% SDS in H_2O	
10% acrylamide separating gel solution:	30% Acrylamide/0.8% Bisacrylamide 4x Lower Tris buffer H_2O 10% APS in H_2O TEMED	7.2 ml 4.5 ml 6.3 ml 50 µl 10 µl
Stacking gel solution:	30% Acrylamide/0.8% Bisacrylamide 4x Upper Tris Buffer H_2O 10% APS in H_2O TEMED	1.3 ml 2.5 ml 6.1 ml 50 µl 10 µl

1x SDS gel running buffer:	0.19 M	glycine
	25 mM	Tris-Cl
	3.5 mM	SDS
	in H_2O	
5x Laemmli sample buffer:	60 mM	Tris-Cl pH 6.8
	2%	SDS
	10%	glycerol
	5%	β-mercaptoethanol
	0.01%	bromophenol blue
	in H_2O	
Coomassie blue staining solution:	3 mM	Coomassie Brilliant Blue R-250
	45%	methanol
	10%	acetic acid
	in H_2O	
Coomassie blue destaining solution:	45%	methanol
	10%	acetic acid
	in H_2O	

3.1.8 External services

All oligonucleotides used in this work were synthesized by Metabion, Planegg/Steinkirchen. The sponge sequences were ordered as genes in a plasmid from Geneart, Regensburg.

3.2 Cell Culture Work

3.2.1 General handling of cells

Cell cultures are maintained in a CO_2-incubator at 95% relative humidity and 5% CO_2. To avoid contamination, all cell culture work is performed under sterile conditions in a laminar flow bench. All solutions to be used are bought sterile, autoclaved at 121°C or sterile filtered. All plastic ware used in cell culture is bought sterile or autoclaved at 121°C.

3.2.2 Culturing of cells

Human podocyte cell line

The hPCL (human podocyte cell line) "8/13" was originally established in the lab of P. Mundel (Saleem et al. 2002). The cells are cultivated in RPMI 1640 medium with 5% FCS (Fetal calf serum) and 1x ITS-G (Insulin-Transferrin-Selenium) under permissive conditions at 33°C and 5% CO_2. The medium is changed every two to three days. After growing to ca. 80% confluency, cells are detached with trypsin every four to five days and subcultured at 1:5 - 1:6. For

differentiation, the cells are seeded at 7200 cells/cm^2. The cells are shifted to a higher temperature of 37°C 24 h after seeding, and the growth medium is changed every two to three days. Cells used for immunostaining are cultured on collagen I coated glass slides.

Murine podocyte cell line

The mPCL (murine podocyte cell line) "E11" was originally established in the lab of K. Endlich (Schiwek et al. 2004). The cells are cultivated in RPMI 1640 medium with 5% FCS under permissive conditions at 33°C and 5% CO_2. The medium is changed every two to three days. After growing to ca. 80% confluency, cells are detached with trypsin every four to five days and subcultured at 1:5 - 1:6.

HEK293T cells

The HEK293T cells are cultured in DMEM medium with 5% FCS at 37°C and 5% CO_2. The medium is changed every two to three days. After growing to ca. 80% confluency, cells are detached with trypsin every four to five days and subcultured at 1:10 – 1:20.

3.2.3 Freezing and thawing of cells

Freezing of cells

For freezing, cells are grown in a T75 flask to 80 - 90% confluency. The cells are once washed with 1x PBS and afterwards incubated with 1 ml of trypsin for 5 min at 33°C or 37°C, respectively. The cells are resuspended in growth medium (RPMI 1640 or DMEM with 10% FCS) and centrifuged (300 *xg*, 5 min, 4°C). The cell pellet is resuspended in 3 ml freezing medium (FCS containing 10% DMSO (Dimethyl sulfoxide)) and separated into three cryovials. The cells are slowly frozen down to - 80°C and short term stored at - 80°C, long term stored in liquid nitrogen.

Thawing of cells

The cryovial containing the frozen cells is thawed and rapidly brought to room temperature. The cell suspension is diluted in 10 ml of growth medium (RPMI 1640 or DMEM with 10% FCS) and centrifuged (300 *xg*, 5 min, 4°C). After resuspending the cell pellet in growth medium, the cells are seeded in two to three T25 flasks at different densities. The cells recovering the fastest are used for future subculturing.

3.2.4 Harvesting of cells

For RNA preparation, proliferating cells are harvested 24 h after seeding, whereas differentiated cells are harvested 14 days after the temperature shift to 37°C. Cells are washed twice with ice-cold 1x PBS and scraped from the plate. The cell suspension is centrifuged (350 *xg*, 10 min, 4°C). The cell pellet is then shock-frosted in liquid nitrogen and stored at - 80°C.

3.2.5 Immunostaining of cells

All steps of the staining protocol are carried out at room temperature (RT). Prior to staining, proliferating and differentiated hPCLs are washed twice with 1x PBS. Cells are fixed with 4% PFA (Paraformaldehyde) for 8 min and washed three times with 1x PBS. After permeabilization with 0.05% Triton-X-100 in 1x PBS for 30 min, cells are blocked for 30 min with 5% horse serum in 1x PBS. Cells are incubated with the primary antibody diluted in 5% horse serum in 1x PBS according to the following table for 2 h. After washing three times for 5 min with 1x PBS, cells are incubated with the secondary antibody diluted according to the following table in 5% horse serum in 1x PBS for 30 min. After washing three times with 1x PBS, nuclei are DAPI (4', 6-Diamidin-2-phenylindol) stained by incubation with DAPI working solution (β = 0.17 µg/ml) for 5 min. After washing with 1x PBS three times for 5 min, cells are mounted on glass slides. Cells are analyzed by fluorescence microscopy with a 40x oil objective. Samples only treated with the secondary antibodies served as controls.

Tab. 3.1: Antibodies used in immunofluorescence staining

Primary antibody		**Dilution**
α -Nephrin	from guinea pig (BP5030, Acris)	1 : 100
α -α–Actinin-4	from rabbit (0042-05, Immunoglobe)	1 : 200
α -Synaptopodin	from rabbit (SC-50459, Santa Cruz	1 : 200
Secondary antibody		**Dilution**
Alexa Fluor 488 α -guinea pig	from goat (A11073, Molecular Probes)	1 : 200
Alexa Fluor 488 α-rabbit	from goat (A11008, invitrogen)	1 : 200

3.3 Mouse Work

3.3.1 Used and generated mouse lines

The mice are kept in the animal lab of the University of Regensburg with unlimited access to drinking water and complete food in a 12 h day/night cycle. Mice are mated from the age of twelve weeks, pups are separated from the mothers between 21 - 28 days of age.

mT/mG x P2.5 Cre

To generate a mouse strain with sortable podocytes, a mouse in which the expression of the Cre recombinase was placed under the regulation of a 2.5 kb fragment of the human *NPHS2* (podocin) promoter (Möller et al. 2003) is crossed with a double fluorescent Cre reporter mouse containing the *mT/mG* cassette (Muzumdar et al. 2007). This mouse expresses membrane-targeted tandem dimer Tomato (mT) in all cells without Cre expression and monomeric green fluorescent protein (mG) after Cre mediated excision of the Tomato cassette in Cre expressing cells. This allows FACS (Fluorescent activated cell sorting) analysis of the green fluorescent podocytes isolated from murine glomeruli.

P2.5 rtTA x LC1 x Lmx1b flox

For isolation of *Lmx1b* knockout glomeruli, inducible, podocyte specific *Lmx1b* knockout mice (Burghardt et al. 2013) are used. In these mice, two *loxP* sites are inserted in the *Lmx1b* gene upstream of exon 4 and downstream of exon 6, respectively. The Cre recombinase is controlled by the TetOn system, a promoter activated by rtTA (reverse tetracycline transactivator). rtTA is placed under the control of the podocyte specific P2.5 promoter that contains a 2.5 kb fragment of the promoter of the human *NPHS2* gene. Animals not harboring the Cre recombinase gene are used as control animals.

mT/mG x P2.5 rtTA x LC1 x Lmx1b flox

A mouse harboring all genes for a doxycycline inducible, podocyte specific *Lmx1b* knockout (Burghardt et al. 2013) is crossed with a double fluorescent Cre reporter mouse containing the mT/mG cassette (Muzumdar et al. 2007). The generated mouse expresses membrane-targeted tandem dimer Tomato (mT) in all cells and wildtype Lmx1b in podocytes prior to Cre mediated excision. By induction of podocyte specific Cre expression through administration of doxycycline, the tomato cassette as well as the DNA binding domain of *Lmx1b* is excised from the genome. This yields *Lmx1b* knockout podocytes expressing monomeric GFP, allowing FACS analysis of the green fluorescent *Lmx1b* knockout podocytes isolated from murine glomeruli. Animals with wildtype *Lmx1b* genes not harboring the *loxP* sites for Cre recombinase recognition are used as control animals.

3.3.2 Genotyping of animals

All laboratory animals are genotyped by PCR using genomic DNA isolated from tail biopsies.

Isolation of genomic DNA of laboratory animals

Tail buffer:	100 mM	TRIS buffer (pH = 8.0)
	5 mM	EDTA
	200 mM	NaCl
	0.2%	SDS
	in H_2O	

Tail biopsies of laboratory animals are digested in 700 µl of tail buffer with 7 µl Proteinase K solution (20 mg/ml) overnight at 50°C under rotation. The next day, the sample is vortexed and centrifuged (16,000 *xg*, 30 min, 4°C). The supernatant is mixed with 700 µl of isopropanol and the precipitated DNA is transferred to 600 µl of ethanol and pelleted by centrifugation (16,000 *xg*, 15 min, 4°C). After removal of the supernatant, the DNA pellet is dried at 37°C for 30 min and dissolved overnight at 50°C in 50 µl water under rotation.

Genotyping of laboratory animals

Genotypes of animals are determined by PCR using isolated DNA. Dependent on the primer pair, PCR is performed with different primers and annealing temperatures (Tab. 3.2) according to the following standard protocol using the *Taq* polymerase.

Standard reaction mix for genotyping PCR:

Thermopol 10x reaction buffer:	2.5 µl
Primers (10 µM):	0.5 µl (each)
dNTPs (10 mM each):	0.5 µl
Taq Polymerase:	0.5 µl
Mouse DNA solution (100 ng/µl):	2.5 µl
ad 25 µl with H_2O	

Standard PCR protocol for genotyping:

95°C	5 min	
95°C	1 min	⎫
58–63°C	1 min	⎬ 35 cycles
68°C	1 min	⎭
68°C	5 min	

The PCR products from the genotyping PCRs are analyzed for size by agarose gel electrophoresis. 2-3 g of agarose is suspended in 100 ml of 1xTAE buffer and heated in a microwave until the solution is clear. After adding 50 µl of a 1 mg/ml ethidium bromide solution, the gel is cast in a tray with a comb were it solidifies. For each sample, 9 µl of the PCR reaction mixture is mixed with one part 10x DNA loading dye. The samples and 10 µl of 2-log DNA marker are loaded into the wells. Gel electrophoresis is performed in 1x TAE buffer at 140 V for 60 min. The results are recorded with the GelDocXR+ system (BioRad).

Tab. 3.2: PCR Primer for mouse genotyping; mut: length of PCR product from animals harboring the mutation; wt: length of PCR product from wildtype animals; pos: length of PCR product for animals harboring the transgene

Primer name	Sequence	PCR product	Annealing temperature
mT/mG forward	CTCTGCTGCCTCCTGGCTTCT	wt: 330 bp	63°C
mT/mG reverse1	CGAGGCGGATCACAAGCAATA	mut: 250 bp	
mT/mG reverse2	TCAATGGGCGGGGGTCGTT		
Cre forward	TGGACATGTTCAGGGATCGC	pos: 613 bp	60°C
Cre reverse	TCAGCTACACCAGAGACGGA		
rtTA forward	CCCACTTCTGAGACAAGC	pos: 188 bp	58°C
rtTA reverse	GGTCAAAGTCGTCAAGGG		
Lmx1b flox forward	AGGCTCCATCCATTCTTCTC	wt: 220 bp	59°C
Lmx1b flox reverse	CCACAATAAGCAAGAGGCAC	mut: 330 bp	

3.3.3 Induction of *Lmx1b* knockout in the mouse model

For the inducible *Lmx1b* knockout, *mT/mG x P2.5rtTA x LC1 x LMX1b-flox* or *P2.5rtTA x LC1 x LMX1b-flox* mice receive drinking water containing 2 mg/ml doxycycline, a structural analog of tetracycline, and 50 mg/ml sucrose for 9 days. To analyze for proteinuria, the laboratory animals are placed in metabolic cages on the 8th day of induction to collect urine samples. Glomeruli or podocytes are only isolated from knockout animals showing proteinuria and control animals not showing proteinuria.

Check for proteinuria in laboratory animals

For protein separation, 10% acrylamide gels are cast using the Mini Protean 3 gel system (BioRad). The separating gel is cast firstly and covered with a thin layer of water to achieve a smooth surface. After 60 min of polymerization, the excessive water is removed, the stacking gel is cast and a comb is inserted into the stacking gel. After polymerization for 45 min, the gel is inserted into the gel chamber and pre-run at 250 V for 30 min. As samples, 1 µl of spot urine is mixed with H_2O and 5x Laemmli sample buffer and heated to 95°C for 5 min. As control samples, 1, 3 and 10 µg of BSA (Bovine serum albumin) are diluted in H_2O and treated like the mouse urine samples. The samples are loaded on the gel together with 3 µl of prestained protein marker. After applying 150 V for 5 min to allow the samples to enter the gel, the voltage is increased to 250 V for 30 min. For staining, the gel is placed in Coomassie staining solution and shaken slowly (15 min, RT). For destaining, the gel is placed in Coomassie blue destaining

solution shaking slowly at room temperature. The destaining solution is changed every 15-20 min until the BSA control samples are all clearly visible.

3.3.4 Isolation of glomeruli and tubules from mice

The mouse glomeruli are isolated from laboratory animals by magnetic beads perfusion. The isolation protocol used is a modification of a protocol published by Takemoto et al. (2002). Mice are anesthetized by intraperitoneal injection of Narcoren (0.12–0.16 mg/g bodyweight) in two to three doses. 40 ml of magnetic bead suspension containing $2x10^6$ beads/ml in 1x PBS, are injected with a syringe into the left ventricle. The abdominal aorta is opened and the bead solution is perfused at a constant pressure of 60 mmHg. After removal of the renal capsule, the kidney is cut into small pieces with a scalpel, subsequently resuspended in collagenase A digestion solution (1 mg/ml in 1x PBS) and digested for 30 min at 37°C. The sample is pushed through a 100 µm cell strainer and the glomeruli are isolated from the filtrate with a magnetic collector. The isolated glomeruli are washed 8 - 10 times with 1x PBS to get rid of the tubular fragments. The washing fractions 3 - 6 are collected and centrifuged (450 *xg*, 10 min, 4°C) to pellet the tubular fragments that serve as a control cell population in the experiments. The clean glomerular fraction and the tubular fraction are shock frozen in liquid nitrogen and stored at -80°C.

3.3.5 Isolation of podocytes and endothelial/mesangial cells from mice

The mouse podocytes are isolated from laboratory animals by magnetic beads perfusion. The isolation protocol used is a modification of a protocol published by Boerries et al. (2013).

Preparation of perfusion solutions

HBSS (Hank's buffered salt solution) is prepared by solving 9.7 g of premixed salt solution powder per 1 l of H_2O. The buffer is adjusted to pH = 7.4, sterile filtered and stored at 4°C.

HBSS buffer:	1.26 mM	$CaCl_2$
	5.37 mM	KCl
	0.44 mM	KH_2PO_4
	0.138 M	NaCl
	0.33 mM	Na_2HPO_4
	0.81 mM	$MgSO_4$
	5.55 mM	D-Glucose
Bead solution:	$2*10^6$ /ml	Tosylactivated magnetic beads in HBSS buffer

The beads are washed three times with HBSS before being diluted to the working concentration.

Bead solution with enzymes:	$2*10^6$ /ml	Tosylactivated magnetic beads
	1 mg/ml	Collagenase Type II
	1 mg/ml	Pronase E
	100 U/ml	DNase I
	in HBSS buffer	
Digestion solution:	1 mg/ml	Collagenase Type II
	1 mg/ml	Pronase E
	100 U/ml	DNase I
	in HBSS buffer	

Isolation of glomeruli

Mice are anesthetized by intraperitoneal injection of Narcoren (0.12 – 0.16 mg/g bodyweight) in two to three doses. The kidneys with their adjacent blood vessels are dissected from the mice and perfused *ex vivo* through the arteria renalis with 1 ml HBSS buffer, 4 ml bead solution and 1 ml bead solution with enzymes per kidney. The capsule is removed and the kidney is minced into small pieces using a scalpel, subsequently suspended in 2 ml digestion solution and digested at 37°C for 10 min on a shaking rotator plate in an incubator. The digest is filtered through a 100 µm cell strainer and pelleted by centrifugation (450 *xg*, 5 min, 4°C). The pellet is resuspended in HBSS buffer and transferred to 2 ml cups. The glomeruli are collected using a magnetic collector. The collected glomeruli are washed with HBSS buffer four to six times until the supernatant is void of tubular fragments.

Single cell preparation

The isolated glomeruli are resuspended in 2 ml of digestion solution, and incubated for 45 min at 37°C in and thermomixer shaking at 1400 rpm. Samples are treated during incubation as follows:

5 min: pipetted up and down through glass pipet

10 min: vortexed and pipetted up and down through glass pipet

15 min: sheared through a 27G needle

20 min: vortexed and pipetted up and down through glass pipet

25 min: pipetted up and down through glass pipet

30 min: vortexed and pipetted through a 200 µl pipet tip put on a 1000 µl pipet tip

35 min: pipetted up and down through glass pipet

40 min: vortexed and pipetted through a 200 µl pipet tip put on a 1000 µl pipet tip

45 min: sheared through a 27G needle

Detachment of the green fluorescent podocytes and some red fluorescent endothelial or mesangial cells is observed after 45 min by fluorescence microscopy.

Preparation of FACS samples

The samples are put on the magnet again to get rid of beads and glomerular structures void of podocytes. The supernatants are pooled and sieved through a 40 µm pore size filter. The single cells are collected from the suspension by centrifugation (450 *xg*, 5 min, 4°C) and resuspended in 475 µl of 1x PBS containing 0.2% FCS. Afterwards, 25 µl propidium iodide solution (β = 1 mg/ml) is added to the cell suspension to stain non-viable cells.

3.3.6 FACS analysis of isolated podocytes

FACS analysis is performed by Jaqueline Igl (Department for Internal Medicine III: Hematology and Internal Oncology, University Hospital Regensburg, Regensburg) using a cell sorter (BD FACSAria IIu sorter, BD Biosciences). Propidium iodide positive cells are discarded, viable green and red fluorescent cells are collected. The sorted cells are pelleted by centrifugation (450 *xg*, 10 min, 4°C). The supernatant is discarded and the dry cell pellets are either shock frozen in liquid nitrogen and stored at -80°C or directly used for RNA preparation (A. Dueck, Department of Biochemistry I, University of Regensburg).

3.4 RNA Work

3.4.1 General handling of RNA samples

To avoid degradation of RNA during preparation, water, solutions and buffers to be used in RNA preparation are treated with DEPC (Diethylpyrocarbonate, 1 ml/l) overnight followed by autoclaving at 121°C. TRIS buffer (1 M; pH = 8.0), and EDTA solution (0.5 M, pH = 8.0) are purchased RNase free. Glassware used for RNA preparation is heated to 200°C for 3 h. Plastic ware is treated with RNAse Away and rinsed with DEPC-H_2O (DEPC treated water) afterwards.

3.4.2 RNA isolation and quantification

For further analysis, RNA samples were isolated from cultured cells and freshly isolated murine cells.

RNA isolation for Northern Blotting

For Northern Blotting, RNA is isolated from cells stored at -80°C according to the TriFast protocol (peqlab). Up to five million cells are resuspended and lysed in 1 ml TriFast solution and incubated (5 min, RT). After addition of 0.2 ml chloroform, the tube is shaken by hand for 15 s and afterwards incubated (5 min, RT). After centrifugation (12,000 *xg*, 5 min, RT), the upper aqueous phase is transferred to a new cup and mixed with 0.5 ml isopropanol. For RNA precipitation, 1 µl of glycogen (β = 35 µg/µl) is added and RNA is precipitated overnight at -20°C. The next day, RNA is pelleted by centrifugation (12,000 *xg*, 15 min, 4°C). The pellet is washed twice with 75% ethanol in DEPC-H_2O and centrifuged (12,000 *xg*, 10 min, 4°C). After drying the pellet (30 min, 37°C), it is dissolved in 20 – 50 µl DEPC-H_2O. The RNA solution is stored at -80°C. Its concentration is measured using a NanoDrop photometer.

Isolation of miRNAs for qPCR

For qPCR, RNA is isolated from cells frozen at -80°C with the miRVana Kit (Ambion) according to the manufacturer's protocol. Shortly, the cell pellet is resuspended and lysed in 600 µl lysis/binding buffer, vortexed and the lysate is incubated with 60 µl of miRNA homogenate additive on ice for 10 min. After addition of 600 µl acid Phenol:Chloroform-mixture and vortexing for 1 min, the sample is centrifuged (12,000 *xg*, 5 min, RT). The upper aqueous phase is mixed with ethanol in a new cup and the mixture is then passed through the first filter cartridge. The eluate is mixed with 533 µl ethanol and passed to a second filter cartridge. Both cartridges containing the long and small RNA fraction are then washed three times with 700 µl or 500 µl of the washing buffers 1 and 2/3, respectively, by centrifugation (16,000 *xg*, 1 min, RT). After spin drying of the filter for 1 min, the bound RNA is eluted from the filter cartridges with 100 µl DEPC-H_2O preheated to 95°C. The RNA solution is stored at -80°C and the concentration is measured using a NanoDrop photometer.

Isolation of long RNAs for qPCR

For qPCR, the long RNA fraction (see above) is concentrated and cleaned using the miRNeasy kit (Qiagen) combined with the DNase I kit (Qiagen) using a modified protocol. Shortly, the aqueous RNA solution is mixed with the double amount of ethanol and passed through a spin column. After washing the membrane once with RWT buffer, the sample is incubated on column with DNAse I in RDD buffer for 1 h at 28°C. Three washing steps with 350 µl RWT buffer of 500 µl RPE buffer, respectively, are followed by spin drying the column for 1 min. The long RNAs are eluted with 30 µl DEPC-H_2O. The RNA solution is stored at -80°C. The concentration of RNA solutions is measured with a NanoDrop photometer.

3.4.3 Gel electrophoresis and Northern Blotting

Gel solution per gel:	Urea concentrate	4.8 ml
	Urea diluent	4.2 ml
	Urea buffer	2.0 ml
	APS (10% in DEPC-H_2O)	80 µl
	TEMED	8 µl
Crosslinking solution:	Methylimidazole	61.25 µl
	1 M HCl	75 µl
	EDC	0.18825 g
	in 6 ml DEPC-H_2O	
Prehybridization buffer:	20x SSC in DEPC-H_2O	15 ml
	Na_2HPO_4 solution, pH = 7.2, in DEPC-H_2O	1.2 ml
	10% SDS in DEPC-H_2O	42 ml
	50x Denhardt's solution in DEPC-H_2O	1.2 ml
Blot washing solution 1:	5x SSC buffer	
	1% SDS	
	in DEPC-H_2O	
Blot washing solution 2:	1x SSC buffer	
	1% SDS	
	in DEPC-H_2O	

Gel preparation

miRNAs are separated on 12% denaturing urea polyacrylamide gels cast with premixed solutions from the Ultra pure sequagel system. Urea concentrate, urea diluent and gel buffer are mixed according to the manufacturer's protocol (see above). After addition of 160 µl 10% APS (Ammonium persulfate) in DEPC-H_2O and 16 µl TEMED (Tetramethylethylenediamine), gels are cast using the Mini Protean3 gel chambers (BioRad). Gels are left for polymerization for 45 min and prerun in 1x TBE buffer in DEPC-H_2O at 250 V for 45 min.

Sample and marker preparation

For each lane, the desired amount of isolated RNA is diluted with DEPC-H_2O to a total sample volume of 20 – 30 µl. The sample is mixed with the same amount of RNA loading dye comprising formamide with 0.1% bromphenolblue and preheated to 65°C for 5 min. Additionally, 3 µl of the microRNA marker are diluted with 17 µl of DEPC-H_2O and mixed with 20 µl of RNA loading dye.

Gel Run and Blotting of miRNAs

After rinsing the gel pockets, the samples are loaded on the gel and separated at 250 V for 45 min. The RNA is then blotted semidry in water from the gel onto a Hybond membrane at 20 V

for 30 min in a Semi-Dry blotting chamber. From bottom to top, the stack consists of 3 layers of chromatography paper, the membrane, the gel, and another 3 layers of chromatography paper.

Crosslinking of miRNAs to the membrane

The microRNA marker is crosslinked to the membrane by exposure to UV light (λ = 312 nm) for 3 min. Afterwards, the other RNAs were crosslinked to the membrane by immersion with the crosslinking solution for 1.5 h at 50°C.

Preparation of Northern Blot probes

The oligonucleotides (Tab. 3.3) are labeled using γ-P32-ATP by addition of a radioactive phosphate to the 5'-end of the oligonucleotides by the T4-PNK (Polynucleotide kinase).

Probe labeling mix:	Marker	U6	miRNAs
DNA probe	5 µl (20 ng/µl)	1 µl (20 mM)	1 µl (20 mM)
T4-PNK	1 µl	1 µl	1 µl
10x PNK buffer	2 µl	2 µl	2 µl
γ-P32-ATP	1 µl	1 µl	6 µl
DEPC-H_2O	11 µl	15 µl	10 µl

The probe labeling mix is incubated at 37°C for 45 min and denatured at 65°C for 10 min. The labeled probes are cleaned with the Qiaquick nucleotide removal kit (Qiagen) according to the manufacturer's protocol. Shortly, the labeling mixtures are diluted in 200 µl of PNI buffer and passed through a spin column by centrifugation (3,380 *xg*, 1 min, RT). The column is washed two times with 500 µl of PE buffer and afterwards spun dry by centrifugation (16,000 *xg*, 1 min, RT). The labeled probe is eluted from the spin column with 100 µl of DEPC-H_2O.

Tab. 3.3: Sequences of probes used for snRNA U6 and miRNA detection in Northern Blotting

Small RNA to be detected	Northern Blotting probe sequence
hsa/mmu-U6	GCC ATG CTA AAT CTT CTC TGT AT
hsa/mmu-miR-10a-5p	CAC AAA TCC GGA TCT ACA GGG TA
hsa/mmu-miR-10b-5p	CAC AAA TTC GGT TCT ACA GGG TA
hsa/mmu-miR-19b-3p	TCA GTT TTG CAT GGA TTT GCA CA
hsa/mmu-miR-22-3p	GTT CTT CAA CTG GCA GCT T
hsa/mmu-miR-23a-3p	GGA AAT CCC TGG CAA TGT GAT
hsa/mmu-miR-23b-3p	GGT AAT CCC TGG CAA TGT GAT
hsa/mmu-miR-24-3p	CTG TTC CTG CTG AAC TGA GCC A
hsa/mmu-miR-26a-5p	AGC CTA TCC TGG ATT ACT TGA A
hsa/mmu-miR-27a-3p	GCG GAA CTT AGC CAC TGT GAA
hsa/mmu-miR-27b-3p	GCA GAA CTT AGC CAC TGT
hsa/mmu-miR-29a-3p	TAA CCG ATT TCA GAT GGT GCT A
hsa/mmu-miR-29c-3p	TAA CCG ATT TCA AAT GGT GCT A
hsa/mmu-miR-30a-5p	CTT CCA GTC GAG GAT GTT TAC A
hsa/mmu-miR-30a-3p	GCT GCA AAC ATC CGA CTG AAA G

Small RNA to be detected	Northern Blotting probe sequence
hsa/mmu-miR-92a-3p	CAG GCC GGG ACA AGT GCA ATA
hsa/mmu-miR-99a-5p	CAC AAG ATC GGA TCT ACG GGT T
hsa/mmu-miR-107-3p	TGA TAG CCC TGT ACA ATG CTG CT
hsa/mmu-miR-130a-3p	ATG CCC TTT TAA CAT TGC AC
hsa/mmu-miR-146b-5p	AGC CTA TGG AAT TCA GTT CTC A
hsa/mmu-miR-148a-3p	ACA AAG TTC TGT AGT GCA CTG A
hsa/mmu-miR-196b-5p	CCC AAC AAC AGG AAA CTA CCT A
hsa-miR-424-3p	ATA GCA GCG CCT CAC GTT TTG
hsa-miR-503-5p	CAG AAC TGT TCC CGC TGC TA
hsa/mmu-miR-542-3p	TTT CAG TTA TCA ATC TGT CAC A

Prehybridization and hybridization of the blot

After crosslinking, the membrane is cut according to the regions that are to be hybridized with the different probes. The marker lane is separated from the sample lanes. The sample lanes are cut to separate the locations of the snRNA (small nuclear RNA) U6 and the mature miRNA signals. The parts of the blot are prehybridized in hybridization buffer for 1 h at 50°C. Afterwards, the labeled probes eluted in DEPC-H_2O are added to the hybridization buffers. The blots are hybridized slowly shaking at 50°C overnight.

Washing of the blots and developing of signals

The next day, blots are washed twice for 10 min with blot washing solution 1 and once for 10 min with blot washing solution 2. The blots are afterwards covered in plastic film. A storage phosphor screen is exposed to the radioactive signals of the blots and developed with an image reader. The time of exposure was 2 h for the U6 signal and the marker signal. For the miRNA signals, the exposure time was 9 - 10 days for the northern blots with RNA isolated from murine glomeruli and tubules and from HEK293T cells and 14 days for the northern blots with RNA isolated from hPCLs. The intensity of the signals was measured with the Bio1D program (Vilber Lourmat).

3.4.4 Quantitative real-time PCR (qPCR)

cDNA preparation for miRNA qPCR

To generate templates long enough for qPCR from isolated miRNAs, a miRNA elongation protocol (Hurteau et al. 2006) is used. In the first step, the miRNA is elongated by addition of a poly-A-tail by the EPAP (Ambion). Afterwards, an adapter primer consisting of a poly-T-sequence and a universal sequence is annealed to the poly-A-tail. Before cDNA synthesis, the reaction mix is split into the sample and a nonRT control sample, in which everything but the reverse

transcriptase is added. The poly-A-poly-T-double strand is then used as a starting point for cDNA generation with the iScript Select cDNA synthesis kit (BioRad). All synthesis steps are performed in a PCR cycler.

miRNA elongation reaction mix:

Isolated small RNAs	0.2-0.5 µg
5x EPAP buffer	4 µl
$MnCl_2$ (25 mM)	2 µl
ATP (10 mM)	2 µl
EPAP	0.8 µl
ad 20 µl with DEPC-H_2O	

The miRNA elongation reaction mix is incubated for Poly-A-tail synthesis at 37°C for 60 min. Afterwards, the reaction mix is denatured at 65°C for 15 min and rapidly cooled to 4°C.

Poly-A-tail annealing reaction mix:

miRNA elongation reaction mix	20 µl
Universal adapter primer	1 µl

The Poly-A-tail annealing reaction mix is heated to 65°C for 5 min and afterwards cooled down 1°C/min until the sample reaches 4°C.

cDNA synthesis reaction mix:

Poly-A-tail reaction mix	18 µl
iScript select 5x reaction mix	5 µl
iScript reverse transcriptase	1.25 µl
DEPC-H_2O	0.75 µl

NonRT control synthesis reaction mix:

Poly-A-tail reaction mix	3 µl
iScript select 5x reaction mix	1.25 µl
DEPC-H_2O	0.75 µl

After incubating the cDNA synthesis reaction mix at 25°C for 5 min, the cDNA synthesis is performed by incubation at 42°C for 60 min. After denaturation of the reaction mix at 85°C for 5 min, it is rapidly cooled to 4°C.

cDNA preparation for long RNA qPCR

The concentration of RNA solutions is measured with a NanoDrop photometer. cDNA from isolated long RNA species is synthesized with the iScript Select cDNA synthesis kit (BioRad) according to the following protocol. After incubating the cDNA synthesis protocol at 25°C for 5 min, the cDNA synthesis is performed by incubation at 42°C for 60 min. After denaturation of the reaction mix at 85°C for 5 min, it is rapidly cooled to 4°C. The cDNA synthesis is performed in a PCR cycler (BioRad).

cDNA synthesis reaction mix:	cDNA sample	nonRT control
Isolated long RNA	<1 µg	<1 µg
iScript select 5x reaction mix	4 µl	4 µl
random primer mix	2 µl	2 µl
iScript reverse transcriptase	1 µl	-----
DEPC-H_2O	3 µl	4 µl

RT-qPCR

For relative quantification by qPCR, the cDNAs reverse transcribed from short or long RNA is prediluted 1:5 to 1:10 depending on the amount of RNA used. Samples to be compared are diluted equally. The qPCR analyses are performed in a LightCycler480II in 96 well plates.

qPCR reaction mix:		
	cDNA sample	2 µl
	Primer forward	1 µl
	Primer reverse	1 µl
	H_2O	6 µl
	qPCR Mastermix	10 µl

Standard program for qPCR:

95°C	7 min	
95°C	10 s	⎫
55–62°C	10 s	⎬ 55 cycles
68°C	10 s	⎭
95°C	5 s	
40°C	1 min	⎫ melting curve
+2.2°C/min until 97°C		⎭
→ 4°C/∞		

The relative quantification of cDNAs synthetized from mRNAs (Tab. 3.4) is performed at 60°C. Most miRNAs (Tab. 3.5) are analyzed with an annealing temperature of 62°C, while relative quantification of miR-146b-5p and miR-322-3p is performed with an annealing temperature of 55°C, and relative quantification of miR-130a-3p, miR-148a-3p and miR-542-3p is performed with an annealing temperature of 59°C. The melting curves in all wells are monitored to exclude the synthesis of more than one product. For every RNA sample isolated, a non-RT control is treated like the cDNA sample. Only samples where the non-RT control does not yield a product are used for relative quantification. In every relative quantification run, the efficiencies of all primer pairs used are measured with the help of dilution standard curves from the used cDNAs. The relative quantification of the unknown samples is performed using the efficiencies measured in the same run with the LightCycler software, version 1.5.0.39. As internal standards for relative quantification, snRNA U6 is used for relative quantification of small RNAs and LaminA/C is used as an internal standard for relative quantification of long RNAs.

Tab. 3.4: Primer for detection of long transcripts in human (h) and murine (m) samples by qPCR

Primer name	Sequence
hCD2AP-Forw	TGG AGC TGA AAG TGG GAG T
hCD2AP-Rev	TTG AGG GAA ACA GTC CCA AC
mCd2ap-Forw	AAC TCA CAA CGC TCA GGA GGA
mCd2ap-Rev	TGT GCA ACT GAT CCG GGA
mCD31-Forw	AGC CAG TAG CAT CAT GGT CA
mCD31-Rev	AGC AGG ACA GGT CCA ACA AC
hE2F1-Forw	GGT CCC TGA GCT GTT CTT CT
hE2F1-Rev	CTT CCC TCA CTT TCC CAA TA
mE2F1-Forw	GCA CGA TCC ATA CCC TCT GT
mE2F1-Rev	CAA CAT CCT TCC CAT TTT GG
hFYN-Forw	GAA CGC CCC ACT TTT GAG TA
hFYN-Rev	GGC CTT ACA GGT TTT CAC CA
mFyn-Forw	TCT GCG ATC AGC AAA CAT TC
mFyn-Rev	CTT CAA TCA ACC GAG CCA AT
hLamin-Forw	CTC GTC GTC CTC AAC CAC AGT
hLamin-Rev	TGC GTA CGG CTC TCA TCA ACT
mLamin-Forw	TGA CTT GGT GTG GAA GGC G
mLamin-Rev	CAG TGG AGT TGA TGA GAG CGG
mLmx1b-Forw	GAG CAA AGA TGA AGA AGC TGG C
mLmx1b-Rev	GGC CAC GAT CTG CTG CTG
hNCK2-Forw	ACC GCA TCT ACG ACC TCA AC
hNCK2-Rev	CAC CAG GGA CAA CTC ATC CT
mNck2-Forw	CAA GGT GTC CTC AGA CAG CA
mNck2-Rev	TTG GCA CGC AGT TAC AAG AG
hNEPH1-Forw	CTT TGG CCT AGG GAC ATG AA
hNEPH1-Rev	TGC AGA CAA CAG AGG GAC TG
mNeph1-Forw	GGA GGG TGC AAC ATT CAG TT
mNeph1-Rev	TGT GGC CTC TGT CTT CTG TG
hNephrin-Forw	CAC TCA GAG CTC CAC GGT CA
hNephrin-Rev	GAG CGG TAA TAC GGC TCT GC
hNOTCH1-Forw	ATG ACC AGT GGC TAC GTG TG
hNOTCH1-Rev	ATA CAC GTG CCC TGG TTC AG
hPodocin-Forw	CTC CCA GCA ACA GAA CTC AGG
hPodocin-Rev	GTG GCT CAA CAG GTT TGG AAG
mPodocin-Forw	GCG AGC GAC CAG AGG AAG
mPodocin-Rev	GAG GCG AGG ACA AGA AGC C

Tab. 3.5: Primers for miRNA detection by qPCR

Primer name	Sequence
URT-Adapter	AAC GAG ACG ACG ACA GAC TTT TTT TTT TTT TTT
Universal reverse primer	AAC GAG ACG ACG ACA GAC TTT
cxcr4-control	TGT TAG CTT TCT GAA AAC TT
snRNA-U6 Forward	CGC TTC GGC AGC ACA TAT AC
snRNA-U6 Reverse	TTC ACG AAT TTG CGT GTC AT
hsa/mmu-miR-10a-5p	CCC TGT AGA TCC GAA TTT GTG
hsa/mmu-miR-21-5p	AGC TTA TCA GAC TGA TGT TGA
hsa/mmu-miR-22-3p	AAG CTG CCA GTT GAA GAA C
hsa/mmu-miR-23a-3p	ATC ACA TTG CCA GGG ATT TC
hsa/mmu-miR-24-3p	GGC TCA GTT CAG CAG GAA CA
hsa/mmu-miR-26a-5p	TTC AAG TAA TCC AGG ATA GGC
hsa/mmu-miR-27a-3p	TTC ACA GTG GCT AAG TTC C
hsa/mmu-miR-29a-3p	AGC ACC ATC TGA AAT CGG TTA
hsa/mmu-miR-30a-5p	TGT AAA CAT CCT CGA CTG GAA G
hsa/mmu-miR-30b-5p	TGT AAA CAT CCT ACA CTC AGC
hsa/mmu-miR-30c-5p	TGT AAA CAT CCT ACA CTC TCA GC
hsa/mmu-miR-30e-5p	TGT AAA CAT CCT TGA CTG GAA G
hsa/mmu-miR-92a-3p	GCA CTT GTC CCG GCC TGT
hsa/mmu-miR-99a-5p	AAC CCG TAG ATC CGA TCT TGT

Primer name	Sequence
hsa/mmu-miR-107-3p	AGC AGC ATT GTA CAG GGC TA
hsa/mmu-miR-126-3p	TCG TAC CGT GAG TAA TAA TGC
hsa/mmu-miR-127-3p	CGG ATC CGT CTG AGC TTG
hsa/mmu-miR-130a-3p	AGT GCA ATG TTA AAA GGG CAT
hsa/mmu-miR-143-3p	TGA GAT GAA GCA CTG TAG C
hsa/mmu-miR-145-5p	GTC CAG TTT TCC CAG GAA TC
hsa/mmu-miR-146b-5p	GAA CTG AAT TCC ATA GGC T
hsa/mmu-miR-148a-3p	TCA GTG CAC TAC AGA ACT TT
hsa/mmu-miR-191-5p	AAC GGA ATC CCA AAA GCA G
hsa/mmu-miR-192-5p	CTG ACC TAT GAA TTG ACA GC
hsa/mmu-miR-200a-3p	AAC ACT GTC TGG TAA CGA TGT
hsa/mmu-miR-200b-3p	AAT ACT GCC TGG TAA TGA TGA
hsa/mmu-miR-200c-3p	ATA CTG CCG GGT AAT GAT GG
hsa/mmu-miR-203-3p	GTG AAA TGT TTA GGA CCA CT
hsa/mmu-miR-210-3p	CTG TGC GTG TGA CAG CGG
mmu-miR-322-3p	ACA TGA AGC GCT GCA ACA
mmu-miR-351-5p	AGG AGC CCT TTG AGC CTG
hsa/mmu-miR-429-3p	TAA TAC TGT CTG GTA ATG C
mmu-miR-503-3p	TAG CAG CGG GAA CAG TAC TG
hsa/mmu-miR-542-3p	TGT GAC AGA TTG ATA ACT GAA A
hsa/mmu-miR-1839-5p	AAG GTA GAT AGA ACA GGT CTT G

3.5 *In silico* predictions of putative miRNA-mRNA pairs

For *in silico* predictions of putative miRNA-mRNA pairs, the free online prediction programs miRWalk and miRWalk2 are used. In addition to being a prediction algorithm itself, miRWalk also uses eight additional programs (DIANAmT, miRanda, miRDB, RNAhybrid, PICTAR4, PICTAR5, PITA, RNA22 and Targetscan), to generate a list showing the number of programs that predict a certain interaction. miRWalk2 is the succeeding program that is able to compare the prediction results of twelve programs (miRWalk, Microt4, miRanda, mirbridge, miRDB, miRMap, miRNAMap, Pictar2, PITA, RNA22, RNAhybrid and Targetscan). Since prediction of possible targets yields enormous lists of possible protein targets, the predictions are done the other way round, predicting miRNAs that are able to bind to a specific 3'-UTR. The miRNA lists are searched for the candidate miRNAs and sorted according to the number of programs predicting a certain interaction.

3.6 Argonaute Immunoprecipitation (Ago-IP)

To identify the transcript regulated by miRNAs in vivo, argonaute immunoprecipitation (Ago-IP) is used to isolate the RISCs including the regulatory miRNAs as well as the regulated mRNAs. For the immunoprecipitation from human cells, a monoclonal antibody directed against the human

Ago2 protein is used (Rüdel et al. 2008). As control, an unrelated monoclonal antibody directed against the complement system protein RmC from rat is used (Dueck et al. 2012). For the immunoprecipitation from murine cells, a commercially available antibody directed against the murine Ago2 is used (Tab. 3.6). An unspecific IgG isolated from rabbit served as a control.

Cell lysis buffer:	0.5%	Nonidet P40
	150 mM	KCl
	25 mM	Tris (pH = 7.5)
	2 mM	EDTA
	1 mM	NaF
IP washing buffer:	0.1%	Nonidet P40
	300 mM	NaCl
	50 mM	Tris (pH = 7.5)
	5 mM	$MgCl_2$
Digestion buffer:	300 mM	NaCl
	200 mM	Tris (pH = 7.5)
	25 mM	EDTA
	2%	SDS

Tab. 3.6: Antibodies used in Ago immunoprecipitation

Antibody for Ago2-IP and Western Blot		Amount of antibody per experiment
α-Ago2 human (11A9)	G. Meister Department of Biochemistry I, University of Regensburg; Rüdel et al. 2008	1 ml hybridoma supernatant
α-RMC rat (control)	G. Meister, Department of Biochemistry I, University of Regensburg; Dueck et al. 2012	1 ml hybridoma supernatant
α-Ago2 murine	Wako (clone 2D4)	16 µg
rabbit IgG	Sigma-Aldrich	16 µg
α-Mouse-IgG	Sigma-Aldrich (HRP conjugated)	Dilution 1:20,000

3.6.1 Western Blotting detection of Argonaute2

Preparation of antibody-coupled beads

Magnetic Protein G-coupled beads are vortexed on the fastest level for 1 min. For each sample, 80 µl of the suspension are transferred to a new cup and washed three times with 1x PBS. The beads are mixed with the α-Ago2 antibody solutions or the control antibody solutions (Tab. 3.6). The beads/antibody mixtures are incubated at 4°C overnight on a rotating wheel.

Cell lysis

The cell pellets are resuspended in 1 ml of cell lysis buffer per 25 million cells by pipetting up and down. After 5 s of vortexing on the highest level, the lysates are incubated at 4°C on a rotating wheel for 15 min, followed by centrifugation (17,000 *xg*, 45 min, 4°C). The supernatant is used for further experiments.

Protein quantification

The protein mass concentration of the supernatant is measured with the Bradford method. In order to prepare a calibration curve, solutions of BSA in cell lysis buffer ranging from 0 µg/µl to 5 µg/µl are prepared. From each calibration solution and each sample, 1 µl is mixed with 1 ml Roti-Quant solution in a plastic cuvette. After incubation (10 min, RT), the ratio of absorbances at 595 nm and 450 nm is calculated for each sample. Unknown sample concentrations are calculated using the calibration curve.

Protein gel electrophoresis

For protein separation, 10% acrylamide gels are cast with the Protean 3 system. The separating gel is cast firstly and covered with a thin layer of water to achieve a smooth surface. After 60 min of polymerization, the excessive water is removed, the stacking gel is cast and a comb is inserted into the stacking gel. After polymerization for 45 min, the gel is inserted into the gel chamber and pre-run at 250 V for 30 min. Four parts of sample are mixed with one part 5x Laemmli sample buffer and heated to 95°C for 5 min. Together with 3 µl of prestained protein marker, the samples are loaded on the gel. After applying 150 V for 5 min to allow the samples to enter the gel, the voltage is increased to 250 V for 30 min.

Western Blotting of proteins

After being separated by polyacrylamide gel electrophoresis, the proteins are transferred to a 0.45 µm PVDF-membrane using three different protocols.

Semi-dry blot transfer buffer:	25 mM	Tris
	192 mM	Glycine
	20%	methanol
	0.02%	SDS
	in H_2O	
Tank blot transfer buffer:	50 mM	Tris
	384 mM	Glycine
	20%	methanol
	0.01%	SDS
	in H_2O	

For semi-dry blotting, the PVDF membrane is first soaked in 100% methanol for 1 min. The membrane as well as six pieces of chromatography papers is soaked in semi-dry blot transfer buffer. On the bottom of a Trans-Blot Semi-Dry system, a stack of from bottom to top three layers of chromatography paper, the membrane, the gel, and another three layers of

chromatography papers is built up. The blotting chamber is closed and the proteins are transferred onto the membrane by applying 22 V for 1.5 h.

For tank blotting, the PVDF membrane is first soaked in 100% methanol for 1 min. The membrane as well as six pieces of chromatography papers is soaked in tank blot transfer buffer. A stack of from bottom to top three layers of chromatography paper, the membrane, the gel, and another three layers of chromatography papers is built up on the middle tray of the Tank Blotting chamber. The chamber is then filled up with tank blot transfer buffer and the proteins are transferred to the membrane either using 1 A for 3 h or 20 V for 18 h.

Antibody detection of mAgo2

Blocking solution:	5% Skim milk powder 0.1% Tween-20 in 1x PBS buffer
Washing solution:	0.1% Tween-20 in 1x PBS buffer

After blotting, the membrane is blocked by incubation in blocking solution (30 min, RT). After washing the membrane three times with washing solution (each 10 min, RT), and once with 1x PBS, the blot is incubated overnight at 4°C in blocking solution containing the first antibody, α-mAgo2, diluted 1:500. The next day, the blot is washed three times with washing solution and incubated with the second antibody, diluted 1:20,000 (30 min, RT). After washing the blot three times with washing solution (each 10 min, RT), and once with 1x PBS, the blot is developed with the Western Lightning Chemoluminiscence Reagent or the SuperSignal West Pico Chemiluminescent Substrate. In both cases, the luminol solution and the oxidation reagent are mixed in equal amounts and the membrane is incubated with the mixture according to the respective protocols. The signal from the membrane is recorded with the chemoluminescence system Fusion Fx7.

3.6.2 Argonaute Immunoprecipitation using hPCLs and mPCLs

Preparation of antibody-coupled beads

Magnetic Protein G-coupled beads are vortexed on the fastest level for 1 min. For each sample, 80 µl of the suspension are transferred to a new cup and washed three times with 1x PBS. The beads are mixed with the antibody solutions (Tab. 3.6). The beads/antibody mixtures are incubated at 4°C overnight on a rotating wheel.

Cell lysis

The cell pellets are resuspended in 1 ml of cell lysis buffer per 25 million cells by pipetting up and down. After 5 s of vortexing on the highest level, the lysates are incubated at 4°C on a rotating wheel for 15 min, followed by centrifugation (17,000 *xg*, 45 min, 4°C).

As input control, 200 µl of the supernatant are taken and the rest of the supernatant is split in half. One sample is incubated with the α-Ago2 coupled beads, whereas the other half is incubated with the control beads for 4 h at 4°C on a rotating wheel.

Preparation of input RNA sample

For RNA isolation, the input sample is mixed with an equivalent volume of TriFast (peqlab) and incubated for 5 min at room temperature. After addition of 40 µl of chloroform, the samples are shaken by hand for 15 s, incubated for 5 min at room temperature and centrifuged (12,000 *xg*, 15 min, 4°C). The RNA extraction from the upper, aqueous phase is performed with the miRNeasy Kit (Qiagen) using a modified protocol. Shortly, the upper phase is mixed with 1.5 volumes of pure ethanol. The mixture is passed through an RNeasy spin column by centrifugation (13,000 *xg*, 15 s, RT). After washing once with RWT buffer, the column is incubated with 10 µl DNase I in 70 µl RDD buffer for 1 h at 28°C for DNA digestion. Afterwards, the column is once washed with buffer RWT and twice with buffer RPE by centrifugation (17,000 *xg*, 1 min, RT). After dry centrifugation (17,000 *xg*, 2 min, RT), the RNA is eluted from the column with 30 µl DEPC-H_2O and stored at -80°C.

Preparation of IP-RNA samples

After 4 h of incubation with the protein lysate, the magnetic beads of both samples are washed four times with the IP washing buffer by placing the tube at the magnet and removing the supernatant. Afterwards, the beads are incubated in 250 µl Protease K buffer containing 2 µl of 20 mg/ml Proteinase K solution for 15 min at 65°C. 300 µl of acid phenol is added and the mixture is centrifuged (12,000 *xg*, 10 min, 4°C). The RNA extraction from the upper, aqueous phase is done with the miRNeasy Kit using a modified protocol. Shortly, the upper phase is mixed with 1.5 volumes of pure ethanol. The mixture is passed through an RNeasy spin column by centrifugation (13,000 *xg*, 15 s, RT). After washing once with RWT buffer, the column is incubated with 10 µl DNase I in 70 µl RDD buffer for 1 h at 28°C for DNA digestion. Afterwards, the column is once washed with buffer RWT and twice with buffer RPE by centrifugation (17,000 *xg*, 1 min, RT). After dry centrifugation (17,000 *xg*, 2 min, RT), the RNA is eluted from the column with 30 µl DEPC-H_2O and stored at -80°C.

cDNA synthesis

cDNA from isolated long RNA species (≥ 200 nt) from the input sample, Ago2 sample and control antibody sample is synthesized with the iScript Select cDNA synthesis kit (BioRad) according to the following protocol.

cDNA synthesis mixture:	cDNA sample	non-RT control
RNA solution	25 µl	5 µl
iScript 5x reaction mix	8 µl	1.6 µl
random primer solution	4 µl	0.8 µl
iScript reverse transcriptase	2 µl	-----
DEPC-H_2O	1 µl	0.6 µl

After incubating the cDNA synthesis protocol at 25°C for 5 min, the cDNA synthesis is performed by incubation at 42°C for 60 min. After denaturation of the reaction mix at 85°C for 5 min, it is cooled rapidly to 4°C. The cDNA synthesis is performed in a PCR cycler (BioRad).

qPCR of samples isolated from Ago2

The qPCR analyses are performed in duplicates for every potential target and the positive control.

qPCR reaction mix:	
qPCR Mastermix	10 µl
Primer 1 (10 µM)	1 µl
Primer 2 (10 µM)	1 µl
cDNA sample/ nonRT control	2 µl
H_2O	6 µl

Calculation of the cp value of each sample is done with the LightCycler software, version 1.5.0.39. Enrichment of target in the α-Ago2 sample from the input is calculated using Excel. Cp values of the samples isolated from the control antibodies serve as background control. The nonRT control sample is checked for DNA contamination and only experiments with a clean nonRT control are evaluated.

3.6.3 Argonaute Immunoprecipitation using murine podocytes

Preparation of antibody-coupled beads

Magnetic Protein G-coupled beads are vortexed on the fastest level for 1 min. For each sample, 80 µl of the suspension are transferred to a new cup and washed three times with DEPC treated 1x PBS. For each sample, 16 µg of antibody (Tab. 3.6) are diluted in 200 µl 1x PBS containing 0.01% Nonidet P40 and the beads/antibody mixtures are incubated at 4°C overnight on a rotating wheel.

Cell lysis

The cell pellets are resuspended in 1 ml of cell lysis buffer per sample by pipetting up and down. After 5 s of vortexing on the highest level, the lysates are incubated at 4°C on a rotating wheel for 15 min, followed by centrifugation (17,000 *xg*, 45 min, 4°C). A small sample for Bradford quantification (chapter 3.6.1) is taken from the supernatant, the rest of the supernatant is mixed with the rabbit IgG coupled beads (see next paragraph) and incubated at 4°C for 1 h on a rotating wheel.

Sample incubation with clearance beads

After coupling overnight, the beads coupled with the control antibody are washed twice with cell lysis buffer. Afterwards, they are mixed with the supernatant after centrifugation and incubated at 4°C for 1 h on a rotating wheel.

Sample incubation with Argonaute specific beads

After coupling overnight, the beads coupled with the α-Ago2 antibody are washed twice with cell lysis buffer. Afterwards, they are mixed with the supernatant after clearance and incubated at 4°C for 4 h on a rotating wheel.

RNA isolation from beads after IP

After immunoprecipitation, the magnetic beads are washed with washing buffer four times. Afterwards, 2 µl of Proteinase-K solution (20 mg/ml) in 250 µl digestion buffer is added and the beads are incubated for digestion for 15 min at 65°C. After addition of 300 µl acid phenol and vortexing, the samples are centrifuged (12,000 *xg*, 10 min, 4°C). The upper phase is mixed with 500 µl ethanol and the RNA is then purified with the miRNeasy micro Kit (Qiagen) using a modified protocol. Shortly, the RNA is bound to the column by centrifugation, and washed with buffer RW1. For DNA digestion, 10µl DNase I in 70µl RDD buffer is added and the samples are incubated at 28°C for 1 h. The column is once washed with buffer RW1, once with buffer RPE and once with 80% ethanol in DEPC-H_2O. After dry centrifugation, the sample is eluted from the column with 14 µl DEPC-H_2O and frozen at -80°C. The samples are further analyzed by the KFB (Kompetenzzentrum **f**luoreszente Bioanalytik, Biopark, Regensburg) on a GeneChiP-Array (Mouse Transcriptome Array, Gen2.0/2.1ST, Affymetrix).

3.7 Luciferase Assay

Using luciferase assays, regulatory processes in cells can be analyzed. Cells are transfected with plasmids coding for firefly luciferase and containing putative regulatory elements. After harvesting and lysis of the cells, the amount of luciferase is measured using a chemoluminescence producing reaction. In the present work, the binding between miRNAs and the 3'-UTRs of protein coding transcript as well as the functionality of miRNA-"sponges" is investigated by luciferase assays.

3.7.1 Design and generation of Luciferase Assay constructs

Bacterial cells containing plasmids harboring the ampicillin resistance gene are cultured in LB medium and on LB agar plates containing 100 µg/ml ampicillin. Bacterial cells containing plasmids harboring the kanamycin resistance gene are cultured in LB medium and on LB agar plates containing 50 µg/ml kanamycin.

Preparation of vectors

The pMir-Report vectors coding for a targeted firefly luciferase under the control of the TK promoter and an untargeted renilla luciferase as control are obtained from the Department for Biochemistry I, University of Regensburg. The pMir-Report plasmid is digested with *Spe*I/*Sac*I yielding the pMir-Report vector for further cloning. The sponge plasmids that contain seven bulged binding sites for miR-21-5p in its 3'-UTR or the negative control that do not contain any binding sites, CMV-d2eGFP-21 and CMV-d2eGFP-empty, are obtained from Addgene. The CMV-d2eGFP-21 plasmid is digested with *Xho*I/*Apa*I yielding the pSponge vector for further sponge design.

Digestion of pMir-Report vector:

pMir-Report plasmid	<1 µg
*Spe*I-HF [20 U/µl]	0.5 µl
*Sac*I-HF [20 U/µl]	0.5 µl
CutSmart 10x buffer	2 µl
ad 20 µl H_2O	

Digestion of CMV-d2e-GFP-21 to generate sponge vector:

CMV-d2e-GFP-21 plasmid	<1 µg
*Xho*I [20 U/µl]	0.5 µl
*Apa*I [50 U/µl]	0.5 µl
CutSmart 10xbuffer	2 µl
ad 20µl H_2O	

The digestion mixes are incubated for 2 h at 37°C. After 1 h, 1 µl of alkaline phosphatase is added to each of the mixtures.

After the digestion, the vectors are cleaned via agarose gel electrophoresis using a 1% agarose gel running in 1x TAE buffer for 2 h at 120 V. The digested vector band is extracted from the gel using a scalpel and isolated using the Qiaquick Gel Extraction Kit (Qiagen). Shortly, the excised piece of gel is melted in three volumes of QG buffer by incubation for 10 min at 50°C. The mixture is then passed through a spin column (16,000 *xg*, 1 min, RT). The column is then washed twice with PE buffer (16,000 *xg*, 1 min, RT). After spin drying the column (16,000 *xg*, 2 min, RT), the DNA is eluted with 50 µl of H_2O and quantified using a NanoDrop photometer.

Preparation of inserts

The 3'-UTR inserts with wildtype sequence or mutated binding sites (chapter 3.7.2) and the insert for sponge functionality analysis (chapter 3.7.4) are purified and isolated using a 1.5% agarose gel running in 1x TAE buffer for 1 - 2 h at 140 V. The inserts are excised from the gel and isolated using the Qiaquick Gel Extraction Kit (see above). The inserts are digested using *Spe*I/*Sac*I or *Xho*I/*Apa*I afterwards.

Digestion of inserts for pMir-Report:

PCR product isolated from agarose gel	0.5-1.3 µg
*Spe*I-HF [20 U/µl]	0.5 µl
*Sac*I-HF [20 U/µl]	0.5 µl
CutSmart 10x buffer	3 µl
ad 30 µl H_2O	

Digestion of inserts for pSponge:

PCR product isolated from agarose gel	0.5-1.3 µg
*Xho*I-HF [20 U/µl]	0.5 µl
*Apa*I-HF [50 U/µl]	0.5 µl
CutSmart 10x buffer	3 µl
ad 30 µl H_2O	

The digestion mix is incubated for 2 h at 37°C. After digestion of the insert ends with *Spe*I/*Sac*I or *Xho*I/*Apa*I the inserts are purified using the Qiaquick Nucleotide Removal Kit (Qiagen). Shortly, the reaction mix is mixed with five volumes of PNI buffer and passed through a spin column (3,380 *xg*, 1 min, RT). After washing the column twice with PE buffer (16,000 *xg*, 1 min, RT), the column is spin dried (16,000 *xg*, 2 min, RT). The DNA is eluted with 50 µl of H_2O and quantified using a NanoDrop photometer.

Ligation of pMir-Report constructs and pSponge constructs

For ligation, vector and insert are mixed in a molar ratio between 1:3 and 1:5. The ligation mixture is mixed and incubated for 2 h at room temperature. Afterwards, the mixture is slowly cooled from 16°C to 4°C in a water bath overnight.

Ligation of pMir-Report and pSponge constructs:

Vectors	60 - 100 ng
Inserts	50 - 100 ng
T4-Ligase	1 µl
10x Ligase buffer	2 µl
ad 20 µl H_2O	

Electroporation

The day after ligation, the ligase is deactivated by heating the ligation mix to 65°C for 10 min. The ligation mix is dialyzed in a Petri dish filled with water on a dialysis filter paper (1 h, RT). It is then mixed with 80 µl of freshly thawed electro competent *E.coli* suspension in an electroporation cuvette and electroporated (2,500 V). The electroporated cells are immediately diluted in 500 µl LB medium and incubated in a shaking incubator for 1 h at 37°C. The cell suspension is then plated on agarose plates containing ampicillin or kanamycin for selection.

Screening for positive clones

The plates with the transformed *E.coli* cells are incubated at 37°C overnight. The next day, colonies are picked from the plates and transferred to 5 ml of LB medium containing ampicillin or kanamycin and grown overnight in a shaking incubator. The next day, the plasmids are isolated from the *E.coli* cells using the GeneJET Plasmid Miniprep Kit (Thermo Scientific). Shortly, the bacterial cells from 5 ml overnight culture are collected by centrifugation (16,000 *xg*, 1 min, RT). The pellets are resuspended in 250 µl of resuspension solution. After adding 250 µl lysis solution and 350 µl neutralization solution, the samples are centrifuged (16,000 *xg*, 5 min, RT). The supernatant is then passed through a GeneJet column (16,000 *xg*, 1 min, RT), which is then washed twice with washing solution (16,000 *xg*, 1 min, RT). After spin drying the column by centrifugation (16,000 *xg*, 1 min, RT), the DNA is eluted using 50 µl H_2O. The concentration is measured using a NanoDrop photometer. The isolated plasmids are analyzed using restriction digest or sequencing.

Plasmid isolation for cell transfection

For transfection in cell culture, larger amounts of plasmids are isolated using a Plasmid plus Midiprep Kit (Qiagen) from a 50 ml overnight culture. The bacterial cells are pelleted by

centrifugation (4,000 *xg*, 15 min, 4°C). After resuspending the pellet in 2 ml of P1 buffer, 2 ml of P2 buffer are added and the solution is incubated for 3 min. After addition of 2 ml of S3 buffer, the lysate is put in a filter cartridge and incubated for 10 min at room temperature, filtered through the cartridge and mixed with 2 ml of BB buffer. Using vacuum, the solution is then drawn through the midi spin column. The spin column is then washed with 700 µl ETR buffer and 700 µl PE buffer by centrifugation (10,000 *xg*, 1 min, RT). After spin drying the column (10,000 *xg*, 1 min, RT), the DNA is eluted using 200 µl H_2O and the concentration is measured using a NanoDrop photometer.

3.7.2 pMir-Report constructs containing 3'-UTRs of putative target genes

For the miRNA binding assays, a luciferase reporter system based on the pMir-report vector (Ambion, modified) is used. Additionally to the targeted firefly luciferase, the plasmids code for an untargeted control, a renilla luciferase, and the CMV promoter is exchanged for a TK promoter (chapter 3.1.5). The construct containing a 3'-UTR is cotransfected with a pSuper construct (oligoengine, modified) coding for a mature miRNA or a control sequence, harboring kanamycin resistance (chapter 3.1.5).

Amplification of wildtype 3'-UTRs

The wildtype target 3'-UTRs are amplified from DNA extracted from hPCL cells with primers containing restriction sites for *Spe*I and *Sac*I, respectively (Tab. 3.7).

Tab. 3.7: Primers for PCR amplification of 3'-UTR fragments from genomic hPCL DNA

Primer name	Sequence
pMIR-Report-hCD2AP_3'UTR_SpeI_F	CAT TGC CAA ATT ACT AGT GAA TGT ATA GTT CA
pMIR-Report-hCD2AP_3'UTR_SacI_R	GAG AGA AGC GAG CTC TTA AAT ACA GCA C
pMIR-Report-hFYN_3'UTR_SpeI_F	GTG AAA ACT AGT AAG GCC CG
pMIR-Report-hFYN_3'UTR_SacI_R	GCA ATG AGC TCC AAA TGT AAA ATG CTC TCT T
pMIR-Report-hNCK2_3'UTR_SpeI_F	GAG AAG CAC TAG TTC GTC AGG GC
pMIR-Report-hNCK2_3'UTR_SacI_R	GCA ATG AGC TCA TGT GCC ATC TCA AGA CGT
pMIR-Report-hNEPH1_3'UTR_SpeI_F	CAC TCG GAC TAG TGC CAG CGA
pMIR-Report-hNEPH1_3'UTR_SacI_R	GCA ATG AGC TCC CCT GTT CGC TCC CTT CTG C

The 3'-UTRs of FYN and NCK2 are amplified using an annealing temperature of 54°C, while the primers amplifying the CD2AP and the NEPH1 3'-UTR are annealed at 57°C or 59°C, respectively.

PCR amplification of target 3'-UTRs:

Thermopol 10x reaction buffer	2.5 µl
Primers (10 µM)	0.5 µl (each)
dNTPs (10 mM each)	0.5 µl
Taq polymerase	0.5 µl
Pfu polymerase:	0.1 µl
DNA from hPCLs	ca. 100 ng
ad 25 µl with H_2O	

Standard program for Luciferase insert PCR:

95°C	5 min	
95°C	1 min	⎫
54–59°C	1 min	⎬ 35 cycles
68°C	3 min	⎭
68°C	10 min	

The PCR products are purified and isolated by agarose gel electrophoresis (see above).

Amplification of point-mutated 3'-UTRs

For luciferase assay, constructs containing 3'-UTRs with point mutated putative binding sites are designed. To destroy the putative binding sites for the miRNA seed regions, the positions 2, 4 and 6 are mutated. For the CD2AP construct containing a mutated miR-30a-e-5p binding site, the 3'-UTR amplification PCR is performed with a reverse primer harboring a mutated miR-30a-e-5p binding site (Tab. 3.8) according to the same protocol as the wildtype 3'-UTRs. For the constructs containing a mutated binding site in the middle of the 3'-UTR, two PCRs are performed with one of the flanking forward or reverse primers from above combined with a reverse or forward primer harboring the mutated binding site (Tab. 3.8). The two PCR products are purified and isolated using a 1.5% agarose gel running in 1x TAE buffer for 1 h at 140 V and mixed in the molar ratio of 1:1.

First PCR for 3'-UTR fragment generation:

Phusion 5x HF-buffer	5 µl
Primers (10 µM)	1 µl (each)
dNTPs (10 mM each)	1 µl
Phusion polymerase	0.25 µl
DNA from hPCLs	ca. 100 ng
ad 25 µl with H_2O	

Program for first PCR for 3'-UTR parts generation:

95°C	5min	
95°C	30s	⎫
57–60°C	1min	⎬ 35 cycles
72°C	1min	⎭
72°C	5min	

The first PCR is performed using an annealing temperature of 57°C for the CD2AP_Δ92a/b-3p fragments and an annealing temperature of 60°C for the Neph1_Δ29a-c-3p fragments.

Tab. 3.8: Primers for binding site mutations in 3'-UTRs

Primer Name	Sequence
hCD2AP_Δ30a-e-5p_R	GAG AAG CGA GCT CTT AAA TAC AGC ACC TCT TAT CAA GTT AGT GAA GTA
hCD2AP_Δ92a/b-3p_F	GCT GTA GCA ATA AAA TGA CCA AGT CCT AAG ACT TGA
hCD2AP_Δ92a/b-3p_R	TTA TTA AAT CAA GTC TTA GGA CTT GGT CA
hNEPH1_Δ29a-c-3p_F	CAC CCC GTC CCG AGG ATG TTA CGC TGT
hNEPH1_Δ29a-c-3p_R	CTG GGG CAT GCA CAG CGT AAC ATC

The two products are annealed heating them up to 98°C for 5 min, incubating the mixture for 10 min at 70°C and then either by slowly cooling of the mixture from 70°C to 25°C (-1°C/min) (CD2AP_Δ92a/b-3p) or a rapid cooling from 68°C to 4°C (Neph1_Δ29a-c-3p). The fill-up reaction mix is incubated for 15 min at 72°C.

Fill-up reaction after the annealing

Annealing mix	16.5 µl
Phusion 5x HF-buffer	2.5 µl
dNTPs (10 mM each)	1 µl
Phusion polymerase	0.3 µl
ad 25 µl H_2O	

After filling up the cross-annealed products, the inserts are amplified by a second PCR using both flanking primers. The second PCR is performed with an annealing temperature of 57°C for the CD2AP_Δ92a/b-3p 3'-UTR and an annealing temperature of 60°C for the Neph1_Δ29a-c-3p 3'-UTR.

Second PCR for full length 3'-UTRs generation:

Fill-up reaction mix	25 µl
Flanking primers	1 µl each
Phusion 5x HF-buffer	0.5 µl
ad 30 µl with H_2O	

Program for second PCR for full length 3'-UTRs generation:

95°C	5 min	
95°C	30 s	⎫
57–60°C	1 min	⎬ 35 cycles
72°C	1 min	⎭
72°C	5 min	

3.7.3 pSuper constructs for miRNA overexpression

The inserts for the miRNA overexpression constructs are designed according to the pSuper manual. After phosphorylation, oligonucleotides containing the hairpin precursor of the mature miRNA sequence, are annealed, thus forming overhangs at both ends corresponding to the restriction sites of the vector backbone.

Oligo phosphorylation mixture:

Oligonucleotide (10 µM)	2 µl
T4 PNK 10x buffer	2 µl
ATP (100 mM)	0.2 µl
T4 PNK	1 µl
ad 20 µl H_2O	

The oligo phosphorylation mixture is incubated at 37°C for 45 min. The two fitting single strands (Tab. 3.9) are mixed in a molar ratio of 1:1 and annealed by heating the mixture to 95°C for 10 min, incubating them at 70°C for 10 min and cooling from 70°C to 25°C (-1°C/min). Afterwards, they are isolated by gel electrophoresis.

Tab. 3.9: Precursor-oligonucleotides for annealing and cloning into pSuper overexpression vector

Name of annealed oligo	Sequence of annealed oligo
pSuper_control_Forw	GAT CCC CTG TTA GCT TTC TGA AAA CTT TTC AAG AGA AAG TTT TCA GAA AGC TAA CAT TTT TA
pSuper_control_Rev	AGC TTA AAA ATG TTA GCT TTC TGA AAA CTT TCT CTT GAA AAG TTT TCA GAA AGC TAA CAG GG
pSuper_23b-3p_Forw	GAT CCC CAT CAC ATT GCC AGG GAT TAC CTT CAA GAG AGG TAA TCC CTG GCA ATG TGA TTT TTT A
pSuper_23b-3p_Rev	AGC TTA AAA AAT CAC ATT GCC AGG GAT TAC CTC TCT TGA AGG TAA TCC CTG GCA ATG TGA TGG G
pSuper_27b-3p_Forw	GAT CCC CTT CAC AGT GGC TAA GTT CTG CTT CAA GAG AGC AGA ACT TAG CCA CTG TGA ATT TTT A
pSuper_27b-3p_Rev	AGC TTA AAA ATT CAC AGT GGC TAA GTT CTG CTC TCT TGA AGC AGA ACT TAG CCA CTG TGA AGG G
pSuper_29a-3p_Forw	GAT CCC CTA GCA CCA TCT GAA ATC GGT TAT TCA AGA GAT AAC CGA TTT CAG ATG GTG CTA TTT TTA
pSuper_29a-3p_Rev	AGC TTA AAA ATA GCA CCA TCT GAA ATC GGT TAT CTC TTG AAT AAC CGA TTT CAG ATG GTG CTA GGG
pSuper_30a-3p_Forw	GAT CCC CTG TAA ACA TCC TCG ACT GGA AGT TCA AGA GAC TTC CAG TCG AGG ATG TTT ACA TTT TTA
pSuper_30a-3p_Rev	AGC TTA AAA ATG TAA ACA TCC TCG ACT GGA AGT CTC TTG AAC TTC CAG TCG AGG ATG TTT ACA GGG
pSuper_92a-3p_Forw	GAT CCC CTA TTG CAC TTG TCC CGG CCT GTT TCA AGA GAA CAG GCC GGG ACA AGT GCA ATA TTT TTA
pSuper_92a-3p_Rev	AGC TTA AAA ATA TTG CAC TTG TCC CGG CCT GTT CTC TTG AAA CAG GCC GGG ACA AGT GCA ATA GGG
pSuper_130a-3p_Forw	GAT CCC CCA GTG CAA TGT TAA AAG GGC ATT TCA AGA GAA TGC CCT TTT AAC ATT GCA CTG TTT TTA
pSuper_130a-3p_Rev	AGC TTA AAA ACA GTG CAA TGT TAA AAG GGC ATT CTC TTG AAA TGC CCT TTT AAC ATT GCA CTG GGG

Name of annealed oligo	Sequence of annealed oligo
pSuper_146b-5p_Forw	GAT CCC CTG AGA ACT GAA TTC CAT AGG CTT TCA AGA GAA GCC TAT GGA ATT CAG TTC TCA TTT TTA
pSuper_146b-5p_Rev	AGC TTA AAA ATG AGA ACT GAA TTC CAT AGG CTT CTC TTG AAA GCC TAT GGA ATT CAG TTC TCA GGG

First digestion of pSuper plasmids:

pSuper Plasmid	5 µg
*Bgl*II [10 U/µl]	1 µl
10x buffer orange	2 µl
ad 20 µl H_2O	

The first digestion mix is incubated at 37°C for 1 h. The vector is purified using a 1% agarose gel running in 1x TAE buffer for 1 h at 140 V and a subsequent gel extraction (see above).

Second digestion of pSuper plasmids:

pSuper Plasmid/*Bgl*II	29 µl
*Hind*III-HF [20 U/µl]	1 µl
10x buffer CutSmart	4 µl
Alkaline Phosphatase	1 µl
ad 40µl H_2O	

The second digestion mix is incubated at 37°C for 1 h. The vector is purified using the Qiaquick nucleotide removal kit (see above).

Ligation of pSuper constructs:

pSuper vector	80 ng
Annealed insert mixture	1 µl
T4 Ligase 10x buffer	1.5 µl
T4 Ligase (Fermentas)	1 µl
ad 15 µl H_2O	

The ligation mixture is mixed and incubated for 2 h at room temperature. Afterwards, the mixture is slowly cooled from 16°C to 4°C in a water bath overnight.

3.7.4 Constructs for sponge functionality Luciferase Assay

Sponge insert harboring seven bulged binding sites for miRNAs and miRNA families of interest containing 7 bulged binding sites for mature miRNAs are designed and subsequently ordered at Geneart (Regensburg).

For the design of a negative control mock sponge, a sequence from the trimethylamine methyltransferase, a gene from the archaeal organism *Methanosarcina mazei* is taken and mutated until no similarity to mammalian sequences is found anymore in BLAST analyses.

miR-23a/b-3p sponge sequence (bulged) (169 nt):
5`**CTCGAG**GGAAATCCCCCGAATGTGAT**CCG**GGAAATCCCCCGAATGTGAT**CAT**GGAAATCCCCCGAATGTG
AT**CGC**GGAAATCCCCCGAATGTGAT**TCA**GGAAATCCCCCGAATGTGAT**GTG**GGAAATCCCCCGAATGTGAT**A**
AGGAAATCCCCCGAATGTGAT**GGGCCC** **3'**

miR-24-3p sponge sequence (bulged) (176 nt):
5`**CTCGAG**CTGTTCCTGCCTTCTGAGCCA**CCG**CTGTTCCTGCCTTCTGAGCCA**CAT**CTGTTCCTGCCTTCTG
AGCCA**CGC**CTGTTCCTGCCTTCTGAGCCA**TCA**CTGTTCCTGCCTTCTGAGCCA**GTG**CTGTTCCTGCCTTCTG
AGCCA**AA**CTGTTCCTGCCTTCTGAGCCA**GGGCCC** **3'**

miR-27a/b-3p sponge sequence (bulged) (169 nt):
5`**CTCGAG**GCGGAACTTCGGACTGTGAA**CCG**GCGGAACTTCGGACTGTGAA**CAT**GCGGAACTTCGGACTGTG
AA**CGC**GCGGAACTTCGGACTGTGAA**TCA**GCGGAACTTCGGACTGTGAA**GTG**GCGGAACTTCGGACTGTGAA**A**
AGCGGAACTTCGGACTGTGAA**GGGCCC** 3`

miR-29a-c-3p sponge sequence (bulged) (176 nt):
5`**CTCGAG**TAACCGATTTTCTTGGTGCTA**CCG**TAACCGATTTTCTTGGTGCTA**CAT**TAACCGATTTTCTTGG
TGCTA**CGC**TAACCGATTTTCTTGGTGCTA**TCA**TAACCGATTTTCTTGGTGCTA**GTG**TAACCGATTTTCTTGG
TGCTA**AA**TAACCGATTTTCTTGGTGCTA**GGGCCC** 3`

miR-92a/b-3p sponge sequence (bulged) (169 nt):
5`**CTCGAG**CAGGCCGGGGTTGTGCAATA**CCG**CAGGCCGGGGTTGTGCAATA**CAT**CAGGCCGGGGTTGTGCAA
TA**CGC**CAGGCCGGGGTTGTGCAATA**TCA**CAGGCCGGGGTTGTGCAATA**GTG**CAGGCCGGGGTTGTGCAATA**A**
ACAGGCCGGGGTTGTGCAATA**GGGCCC** 3`

mock sponge sequence (169 nt):
5`**CTCGAG**AGCAACTTCCGCGACGGAGC**CCG**AGCAACTTCCGCGACGGAGC**CAT**AGCAACTTCCGCGACGGA
GC**CGC**AGCAACTTCCGCGACGGAGC**GCA**AGCAACTTCCGCGACGGAGC**GTG**AGCAACTTCCGCGACGGAGC**A**
AAGCAACTTCCGCGACGGAGC**GGGCCC** 3`

Fig. 3.1: Sequences of sponge inserts; black: miRNA binding sites; red: *Xho*I restriction sites; green: *Apa*I restriction sites; blue: linkers between miRNA binding sites

Generation of pSponge insert for sponge assay

The sponge inserts (see above) are digested with *Xho*I/*Apa*I from the pMA plasmids they were delivered in and ligated into the pSponge vector (chapter 3.7.1). Positive clones are identified by restriction digestion and sequencing.

Generation of pMir-report insert for sponge assay

The sponge inserts for pMir-Report vector are amplified by PCR using primers containing *Spe*I or *Sac*I restriction sites (Tab. 3.10).

PCR for sponge insert amplification

10x *Pfu* reaction buffer	5 µl
Primers (10 µM)	1 µl (each)
dNTPs (10 mM each)	1 µl
Pfu-Polymerase	0.5 µl
sponge plasmid	ca. 50 ng
ad 25 µl with H_2O	

Program for sponge insert amplification PCR:

95°C	5 min	
95°C	30 s	⎫
58°C	1 min	⎬ 35 cycles
72°C	1 min	⎭
72°C	5 min	

Tab. 3.10: Primer for PCR amplification of sponge sequences for cloning into pMir-Report vector

Primer name	Sequence
pMir-Report-sponge21-SpeI-F	CGC CTC GAG ACT AGT CCG GTC AAC
pMir-Report-sponge21-SacI-R	TTA AAC GGG CCC GAG CTC GCG ATC C
pMir-Report-sponge23-SpeI-F	CAA TCA ACT AGT GGG AAA TCC
pMir-Report-sponge23-SacI-R	TAA GAG GTA CCG AGC TCA TCA C
pMir-Report-sponge24-SpeI-F	GGC CGC ATC AAC ACT AGT CTC GAG
pMir-Report-sponge24-SacI-R	ACT CGA GAT GAT TGA GCT CTG G
pMir-Report-sponge27-SpeI-F	CAT GAG CTA CTA GTG GCG GAA CTT
pMir-Report-sponge27-SacI-R	AGA TGA TTG AGC TCT TCA CAG TC
pMir-Report-sponge29-SpeI-F	GAG CCA GGG CCC AAT CAT CTA GT
pMir-Report-sponge29-SacI-R	GGT ACC GAG CTC TAG CAC CAA G
pMir-Report-sponge92-SpeI-F	TAG GCG CGC CAT GAA CTA GTC GAG
pMir-Report-sponge92-SacI-R	ATG ATT GAG CTC TAT TGC ACA AC

3.7.5 Luciferase Assay procedure

To investigate the regulation of mRNAs by miRNAs that are predicted in the *in silico* predictions and to access sponge functionality, luciferase assays are performed in cell culture.

Transfection of cells for luciferase assay

For the miRNA-mRNA binding assay, HEK293T cells are seeded in 24 well plates at a density of 50,000 cells per well 24 h before transfection. Per well, 200 ng luciferase plasmid and 300 ng pSuper miRNA overexpression plasmid are mixed in 100 µl of DMEM medium. After addition of 2 µl of peqFECT or Turbofect transfection reagent, the mix is incubated at room temperature for 20 min and then added to the wells. For each condition, three biological replicates are transfected.

To test sponge functionality, hPCLs are seeded in 24 well plates at a density of 10,000 cells per well 24 h before transfection. Per well, 200 ng luciferase reporter plasmid and 300 ng pSponge plasmid are mixed in 100 µl of RPMI 1640 medium. After addition of 2.4 µl of PEI (Polyethylenimine, 1 mg/ml in H_2O), the mix is incubated at room temperature for 20 min. The medium is removed from the cells and they are incubated with the transfection mix. After 6 h, the transfection mix is removed and normal medium is added to the cells. For each condition, three biological replicates are transfected.

Luciferase assay substrate

To measure the amount of expressed luciferase in the transfected cells, buffers containing the substrates for firefly luciferase and renilla luciferase are prepared for measurement.

Firefly luciferase substrate:

470 µM	D-Luciferin
530 µM	ATP
270 µM	Coenzyme A
20 mM	Tricine
5.34 mM	$MgSO_4$
0.1 mM	EDTA
in H_2O	

The buffer is first prepared without D-Luciferin. After adjusting to pH = 8.0, D-Luciferin is added. The substrate solution is then sterile filtered, aliquoted and stored at -80°C. Prior to luciferase assay, 33.3 µl 1 M DTT solution per ml substrate is added.

Renilla luciferase substrate:

2.2 mM	EDTA
0.22 M	K_xPO_4, pH = 5.1 (from 1 M stock)
0.44 mg/ml	BSA
1.1 M	NaCl
1.3 mM	NaN_3
in H_2O	

After adjusting to pH = 5.0, the buffer is sterile filtered, aliquoted and stored at -20°C. Prior to luciferase assay, 1 µl of 1000x coelenterazine per ml substrate is added.

Harvesting of cells for luciferase assay

24 h after transfection, the cells are washed once with cold 1x PBS and lysed with 1x passive lysis buffer (promega). After 15 min of shaking at room temperature, the lysates are collected and centrifuged (16,000 *xg*, 10 min, 4°C). The supernatant is frozen at -80°C.

Measuring luciferase assays

To test for miRNA-mRNA binding, 3 µl of the HEK293T lysate mixed with 22 µl water are pipetted in 96 well plates. To test for sponge functionality, 10 µl of the hPCL lysate mixed with 15 µl water are pipetted in 96 well plates. For each biological replicate, three technical replica are measured. The luminescence is measured using a luminometer (Berthold). In each well, 20 µl of the firefly luciferase substrate are injected and firefly luciferase luminescence intensity is measured after a delay of 3 s. Afterwards, 20 µl of the renilla luciferase substrate are injected in each well and renilla luciferase luminescence intensity is measured after a delay of 3 s. For analysis, the

background of non-transfected cells is measured and deducted from the measured values. Afterwards, the ratio of firefly luciferase luminescence intensity to renilla luciferase luminescence intensity is calculated.

3.8 miRNA knockout techniques *in vivo* and in cell culture

To investigate the effect of lowered miRNA levels *in vivo* and in cell culture, two different methods for miRNA level manipulation, the *Vivo-Morpholinos* and the miRNA sponges, were tested.

3.8.1 miRNA level manipulation by *Vivo-Morpholinos*

For a short-term knockdown of miRNAs in the kidney, male eight weeks old C57/bl6 (C57black6) mice weighting 20 - 25 g receive three injections of *Vivo-Morpholino* solutions directed against certain miRNAs or a control *Vivo-Morpholino*, respectively. The first injection is performed by Prof. Frank Schweda (Institute for Physiology, University of Regensburg). In the first injection, 5 nmol of antisense *Vivo-Morpholinos* diluted in 200 µl 1x PBS is injected directly into the renal aorta of left kidney. The aorta and vein are clamped for 15 min to enhance the retention time of *Vivo-Morpholinos* in the kidney. The second and third injection after 24 h and 48 h, respectively, are performed by Andrea Schreiber. In the second and third injection, 25 nmol of *Vivo-Morpholinos* are injected by retro orbital injection. After 48 h, urine of the animals is collected in metabolic cages for 16 h and checked for proteinuria.

3.8.2 miRNA knockout by TALEN constructs

The plasmids coding for a TALE nuclease pair directed against the human genomic locus of miR-30a-5p are derived from www.talenlibrary.net (Kim et al. 2013). Clones of HEK293T cells are generated by cotransfection with plasmids coding for antibiotic resistance, pWE2 (G418 resistance, ATCC) and pWE3 (puromycin resistance, ATCC).

In total, $0.5*10^6$ HEK293T cells are seeded 24 h before transfection in a T25 flask. Cells are transfected with 3 µg of TALEN-L1, 3 µg TALEN-R1 and 0.6 µg of pWE2 or pWE3 plasmid. The plasmids are previously mixed with 13.2 µl peqFECT in 1 ml DMEM medium not containing any serum and incubated for 20 min. 24 h after transfection, the cells are trypsinized and seeded in three different densities. For selection, G418 (200 µg/mL) or puromycin (1 µg/mL) is added to the growing medium. After selection for nine to twelve days, clones are picked and further

cultivated separately in 12- or 24- well plates and expanded for DNA and RNA preparation in P10 cell culture dishes. Over the whole time, the cells are cultured in media containing G418 or puromycin.

The RNA is isolated and analyzed by Northern Blotting and qPCR according to the protocols in chapter 3.4. For genome analysis, the DNA is isolated according to the TriFast protocol (chapter 3.4.2). Shortly, the lower organic phase is mixed with 0.5 ml of 100% ethanol after removal of the RNA. After incubation (2 min, RT), the sample is centrifuged (18,700 *xg*, 15 min, 4°C). The DNA pellet is washed twice with 1 ml of sodium citrate in 10% ethanol. Every washing step consists of an incubation step (15 min, RT) and a centrifugation step (18,700 *xg*, 15 min, 4°C). The pellet is then washed twice with 2 mL of 75% ethanol, each washing step consisting of an incubation step (15 min, RT) and a centrifugation step (18,700 *xg*, 15 min, 4°C). After drying the pellet at 37°C for 15 min, the DNA is resuspended 100 µl of 8 mM NaOH solution. The DNA solution is brought to pH = 8.4 with 0.66 µl of 1 M HEPES-buffer.

The genomic locus of the mir-30a precursor is amplified using isolated genomic DNA from the putative knockout cell clones (Tab. 3.11). The PCR products are purified and isolated by agarose gel electrophoresis and sequenced.

Reaction mix for genomic locus PCR:

Thermopol 10x reaction buffer	5 µl
Primers (10 µM)	2 µl (each)
dNTPs (10 mM each)	2 µl
Taq-Polymerase (5 U/µl)	2 µl
HEK293T clone DNA	500 ng
ad 50 µl with H_2O	

PCR protocol for genomic locus PCR:

95°C	1 min	
95°C	30 s	⎫
60°C	1 min	⎬ 35 cycles
68°C	1 min	⎭
68°C	1 min	

Tab. 3.11: Primer for amplification of the human genomic locus of mir-30a

Primer name	Sequence
hsa-genloc-30a-F	ACA GAA TCG TTG CCT GCA
hsa-genloc-30a-R	GCA GAA AGG GCA GGA CAA AA

4 RESULTS

4.1 Characterization of human podocyte cell line

To investigate podocytes in cell culture, immortalized cell lines derived from isolated human podocytes had been established (Saleem et al. 2002). These cells proliferate at 33°C and differentiate when cultured at 37°C for two weeks.

4.1.1 Immunostaining for podocyte proteins in hPCLs

To characterize the hPCLs (human podocyte cell line), proliferating and differentiated podocytes were stained with antibodies against proteins expressed in podocytes (chapter 3.2.5): the podocyte marker protein nephrin, the structural proteins synaptopodin and α-actinin-4.

With all three antibodies (α-nephrin, α-synaptopodin, α-α-actinin-4), distinct differences in the staining could be detected. Proliferating hPCLs stained with the α-nephrin antibody showed only a weak staining around the nucleus (Fig. 4.1 A, B). Differentiated hPCLs showed localization of the protein to the cellular membrane, either in a punctual distribution (Fig. 4.1 C, D) or in a linear distribution along the cellular membrane (Fig. 4.1 E, F). Proliferating hPCLs stained with the α-synaptopodin antibody showed nuclear staining of the cells with very weak staining of the cellular periphery (Fig. 4.2, A, B). In differentiated hPCLs, numerous fine lines run through the cytoplasm (Fig. 4.2, C-F), indicating that synaptopodin is localized to the actin cytoskeleton in the differentiated podocytes. Proliferating cells stained with the α-α-actinin-4 antibody show staining in lines throughout the cell (Fig. 4.3, A, B), arguing for an actin localization of α-actinin-4 in proliferating hPCLs. In differentiated hPCLs, the protein relocates to "spikes" at the cellular membrane together with some punctual spots in the periphery of the cells (Fig. 4.3, C-F).

Taken together, all three proteins are expressed in distinct patterns in proliferating hPCLs compared to differentiated hPCLs. All of them show a relocalization after differentiation, arguing for structural and thus metabolic and functional differences between the proliferating and the differentiated state.

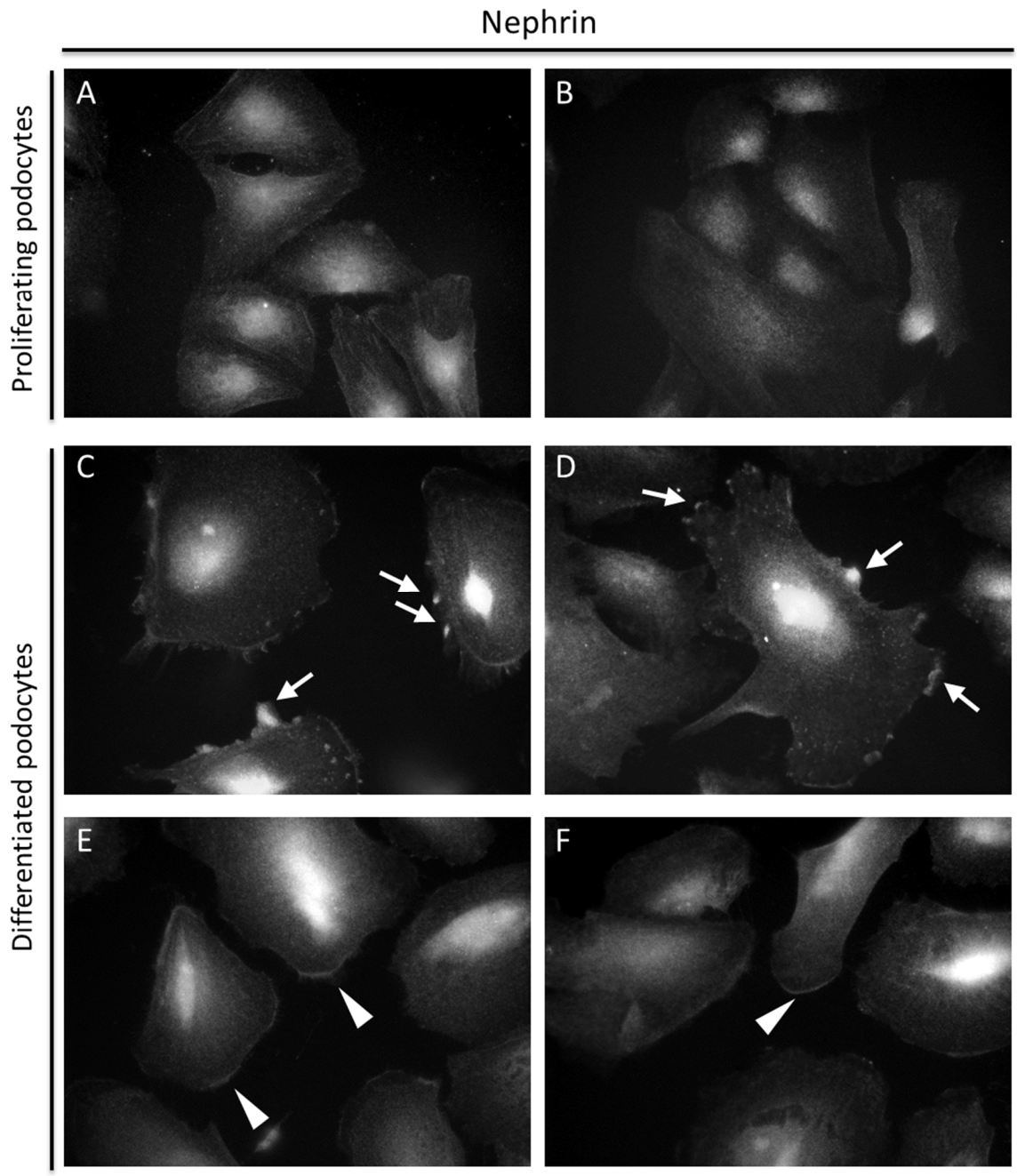

Fig. 4.1: Immunostaining of proliferating and differentiated hPCLs with α-Nephrin antibody; (A, B) Proliferating human podocytes stained with α-Nephrin antibody showing weak, non-localized perinuclear staining; (C-F) Differentiated human podocytes stained with α-Nephrin antibody; cells show nephrin localization at the plasma membrane of the cells, either as distinct punctual accumulation (arrows: C, D) or as line shaped accumulation along the plasma membrane (arrowheads: E, F) of the cells

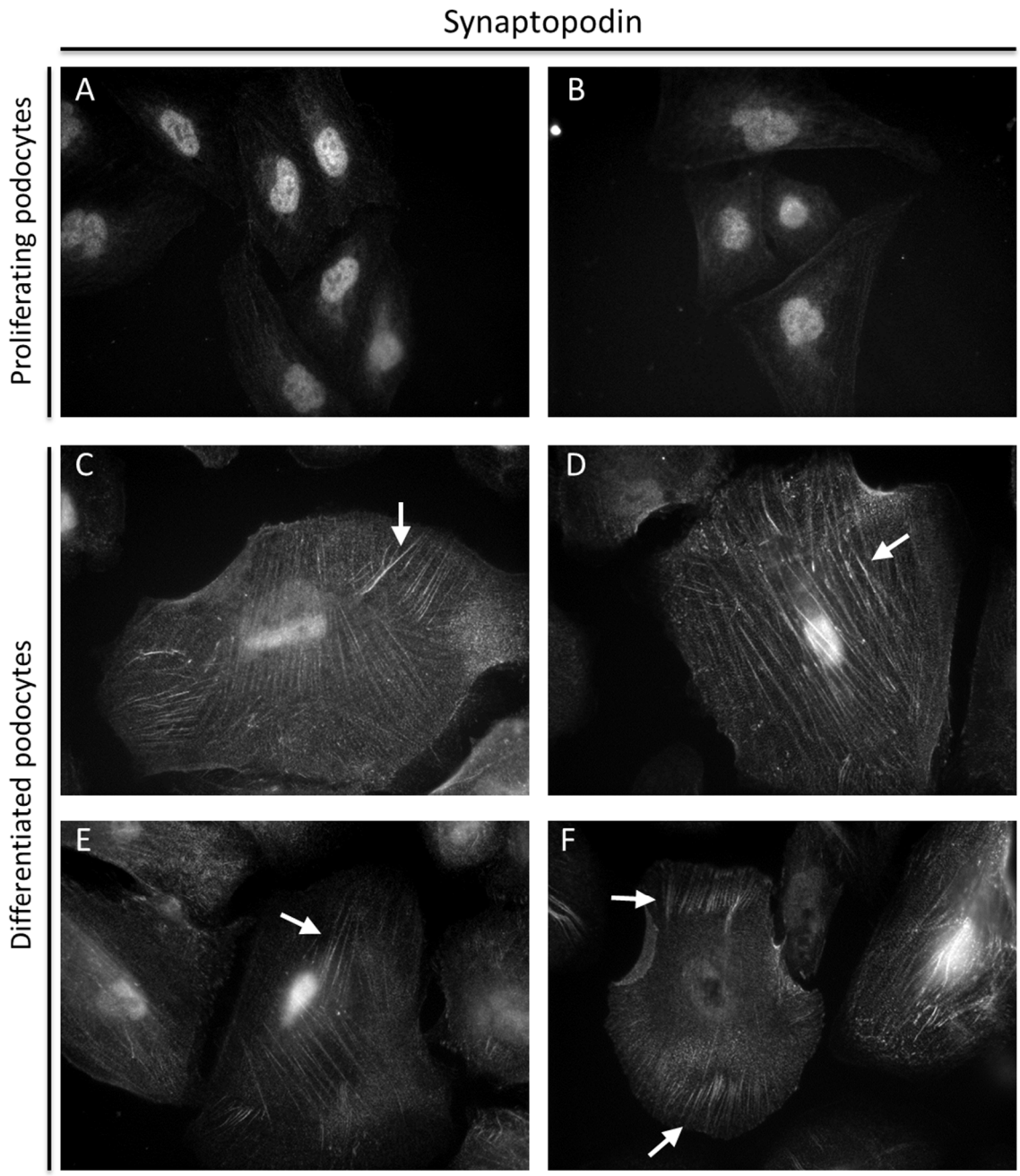

Fig. 4.2: Immunostaining of proliferating and differentiated hPCLs with α-Synaptopodin antibody; (A,B) Proliferating human podocytes stained with α-Synaptopodin antibody show nuclear staining of the cells with a very weak cytoplasmic staining; (C-F) Differentiated hPCL cells stained with α-Synaptopodin antibody; cells show Synaptopodin localization in fine lines throughout the whole cell body (arrows), indicating actin association of the protein

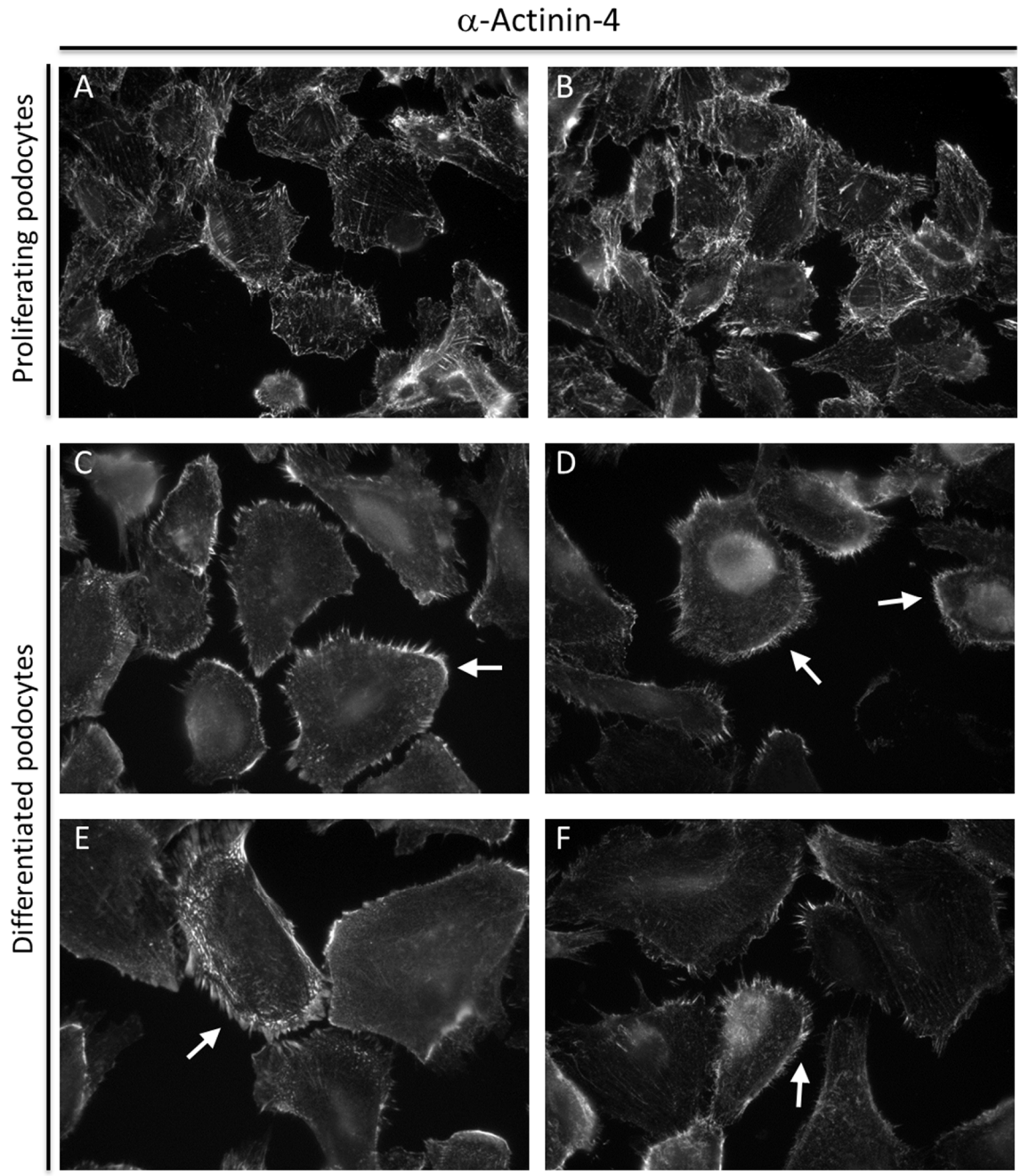

Fig. 4.3: Immunostaining of proliferating and differentiated hPCLs with α–α-actinin-4 antibody; (A,B) Proliferating human podocytes stained with α–α-actinin-4 antibody show α-actinin-4 localization in lines throughout the cell, indicating actin association of the protein; (C-F) Differentiated human podocytes stained with α–α-actinin-4 antibody show an altered α-actinin-4 localization, with relocation of the protein into "spikes" at the cell cortex (arrows)

4.1.2 Northern Blotting of miRNAs expressed in human podocyte cell line

By Northern Blotting (see chapter 3.4.3), hPCLs were tested for expression of miRNAs that were found to be expressed in murine glomeruli (chapter 4.2) and murine podocytes (chapter 4.3). For each of the candidate miRNAs, expression in proliferating and differentiated cells was investigated.

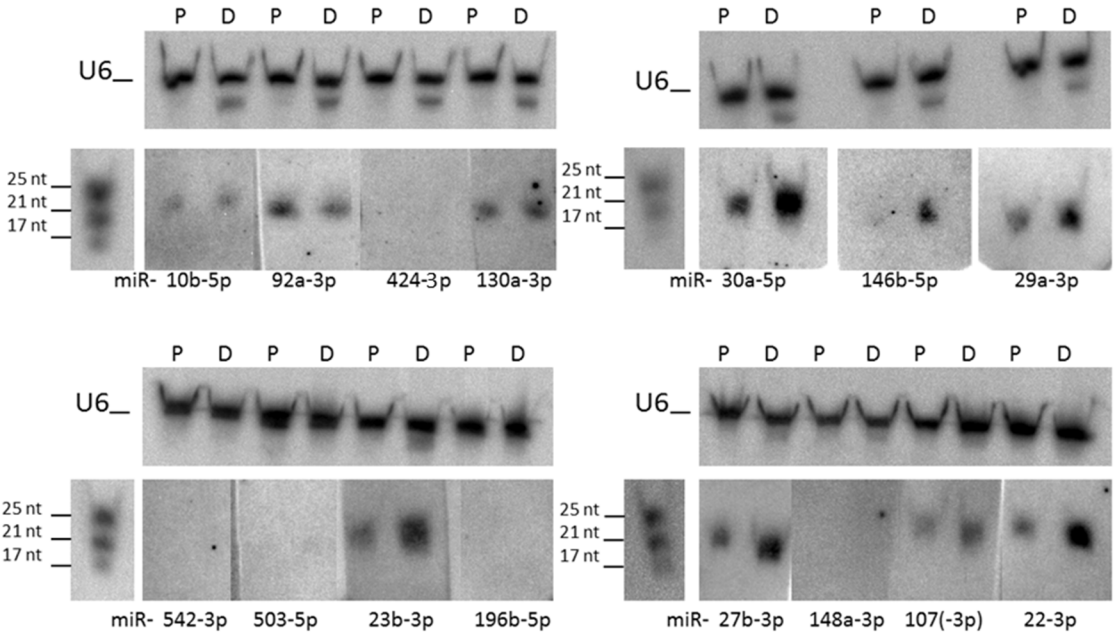

Fig. 4.4: Northern Blotting of candidate miRNAs isolated from proliferating and differentiated cells; detection of miRNA expression in 15 µg of total RNA isolated from proliferating (P) and differentiated (D) hPCLs; detection of internal standard (snRNA U6) and mature miRNAs

The intensity of the signals was measured with the Bio1D program (Vilber Lourmat). The expression ratio of the mature miRNAs was calculated for all candidate miRNAs with the U6 signals serving as an internal standard (Tab. 4.1).

Tab. 4.1: Relative expression of mature miRNAs in proliferating and differentiated hPCLs

Mature miRNA	Diff:Prolif ratio
miR-10b-5p	0.5 : 1
miR-92a-3p	0.6 : 1
miR-130a-3p	1.4 : 1
miR-30a-5p	1.4 : 1
miR-146b-5p	2.5 : 1
miR-29a-3p	1.0 : 1
miR-23b-3p	2.2 : 1
miR-22-3p	2.3 : 1
miR-107(-3p)	1.3 : 1
miR-27b-3p	2.3 : 1

The mature miRNAs miR-10b-5p, miR-92a-3p, miR-130a-3p, miR-mir-30a-5p, miR-146b-5p, miR-29a-3p, miR-23b-3p, miR-22-3p, miR-107 and miR-27b-3p were expressed in the proliferating as well as in the differentiated human podocyte cell line (Fig. 4.4). miR-10b-5p and miR-92a-3p showed a reduction of expression after differentiation, while eight miRNAs were expressed at higher levels in the differentiated hPCLs. miR-148a-3p, miR-196b-5p, miR-424-5p, miR-542-3p and miR-503-5p could neither be detected in the proliferating nor in the differentiated cells.

4.2 miRNA expression in murine glomeruli and tubules

4.2.1 *Deep sequencing* profiles

For miRNA expression analyses, glomeruli and tubules were isolated from six female 12 week old C57bl/6 mice (see chapter 3.3.6). RNA extraction and library preparation was performed by A. Dueck (Department of Biochemistry I, University of Regensburg). One *deep sequencing* profile was generated from the total RNA preparation, while the second profile was generated from the small RNA fraction enriched by gel electrophoresis. The RNA samples were sequenced on a HiSeq1000 sequencer (Illumina). The annotation of the sequenced libraries to the known miRNA sequences (miRBase Version 18) was performed by N. Eichner (Department of Biochemistry I, University of Regensburg).

From the total RNA isolated, a glomerular library containing 5.38 million reads and a tubular library containing 3.78 million reads were generated. From the enriched small RNA fraction, a glomerular library of 4.44 million reads and a tubular library of 5.71 million reads were generated (Tab. 10.1). In total, 260 mature miRNA sequences have been identified to be expressed more than 5 ppm reads in at least one of the libraries. A total of 69 miRNAs were glomerular enriched according to both profiles, while 27 mature miRNAs were detected to be glomerular enriched in one of the profiles and equally expressed in the other profile. In addition, 84 miRNAs were equally expressed in glomeruli and tubules, while 62 miRNAs were tubular enriched and 18 miRNAs were tubular enriched in one of the profiles and equally expressed in the other profile.

4.2.2 miRNA library validation by Northern Blotting and qPCR

The miRNA profiles obtained from murine glomeruli and tubules were validated by Northern Blotting and qPCR.

Northern Blotting of miRNAs from murine glomeruli and tubules

For miRNA expression analyses by Northern Blotting (Fig.4.5), RNA was extracted from glomeruli and tubules isolated from six female 12 week old C57bl/6 mice with the TriFast protocol (chapter 3.4.2). Four candidate miRNAs, expressed in murine glomeruli and tubules according to the *deep sequencing* profiles, were chosen to be validated. Two candidates, miR-10a-5p and miR-99a-5p were expected to be equally expressed in glomeruli and tubules, whereas miR-27b-3p was enriched in glomeruli. miR-26a-5p was equally expressed in the *deep-sequencing* profile from total RNA and slightly glomerular enriched in the profile from the small RNA fraction.

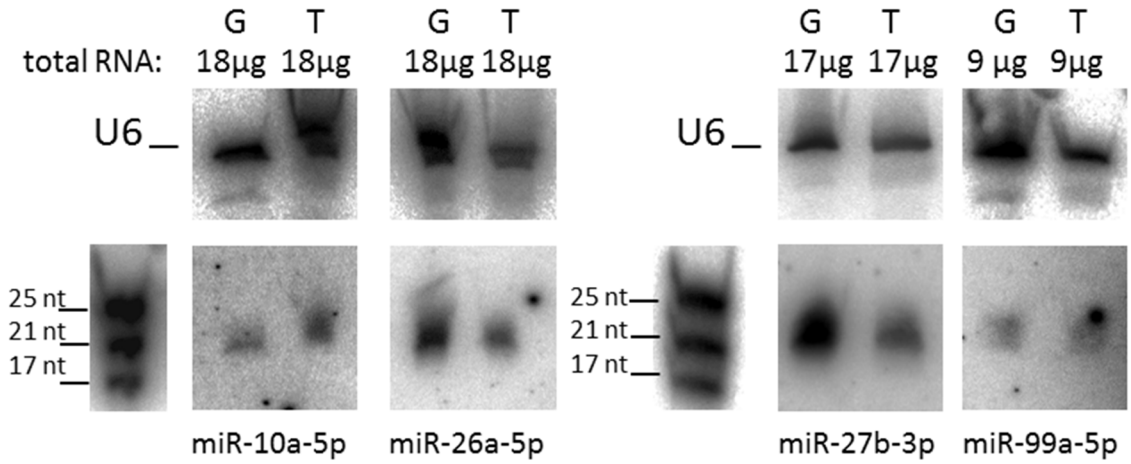

Fig. 4.5: Northern Blotting of mature miRNAs in total RNA isolated from murine glomeruli (G) and tubules (T); Detection of internal standard (snRNA U6) and the mature miRNAs

The intensity of the signals was measured with the Bio1D program (Vilber Lourmat). The expression ratio of the mature miRNAs was calculated for all candidate miRNAs using the U6 signals as an internal standard. The results were compared to the miRNA enrichment according to the *deep sequencing* profiles (Tab. 4.2).

Tab. 4.2: Relative expression of mature miRNAs in murine glomeruli and tubules; quantification of Northern Blotting results

miRNA	**Glom:Tub ratio in deep sequencing**		**Glom:Tub ratio in**
	small RNA	total RNA	**Northern Blotting**
miR-10a-5p	1.2 : 1	1.1 : 1	0.7 : 1
miR-26a-5p	2.8 : 1	1.4 : 1	0.9 : 1
miR-27b-3p	4.7 : 1	4.8 : 1	2.0 : 1
miR-99a-5p	0.7 : 1	0.9 : 1	0.9 : 1

All four mature miRNAs, miR-10a-5p, miR-26a-5p, miR-27b-3p and miR-99a-5p could be detected in total RNA isolated from murine glomeruli as well as in total RNA isolated from

murine tubules (Fig. 4.5). For miR-10a-5p, miR-26a-5p and miR-99a-5p, the equal expression in glomeruli and tubules could be validated. For miR-27b-3p, the glomerular enrichment could be validated.

qPCR of miRNAs from murine glomeruli and tubules

To validate expression of a subset of miRNAs, glomeruli and tubules were isolated from six female 12 week old C57bl/6 mice. From the isolated small RNA fractions, cDNA was reverse transcribed. The relative enrichment of miRNAs in the glomeruli compared to tubules was calculated and compared to the result from the *deep sequencing* profile. The snRNA U6 served as an internal control. Since qPCR with normal DNA primers cannot distinguish between miRNAs that differ only by one base, enrichment results were treated as total enrichment of whole miRNA families. The qPCR was performed on a LightCycler 480II (Roche). The results were gathered and analyzed with the LightCycler 480 1.5.0 software (Roche).

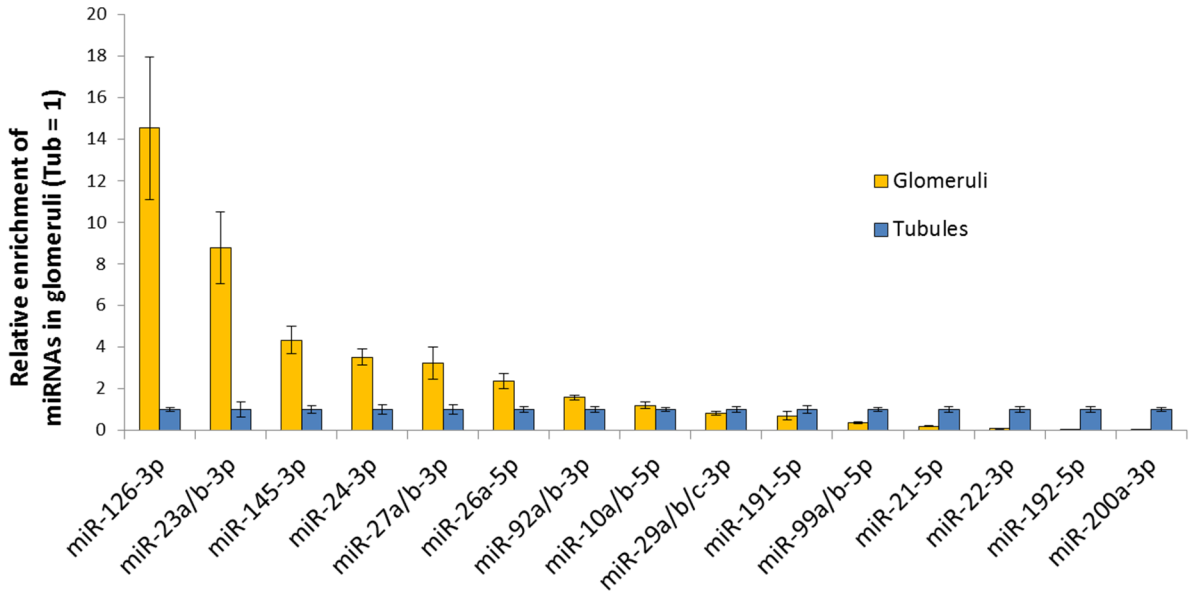

Fig. 4.6: Relative enrichment of miRNAs in murine glomeruli compared to tubular expression; internal standard: snRNA U6

Expression ratio between glomeruli and tubules were investigated by qPCR for five miRNAs or miRNA families enriched in glomeruli (miR-126-3p, miR-23a/b-3p, miR-145-5p, miR-24-3p and miR-27a/b-3p), five miRNAs or miRNA families supposed to be equally expressed in glomeruli and tubules (miR-26a/b-5p, miR-92a/b-3p, miR-10a/b-5p, miR-29a/b/c-3p and miR-191-5p) and five miRNAs or miRNA families that were enriched in tubules according to *the deep sequencing* profiles (miR-99a/b-5p, miR-21-5p, miR-22-3p, miR-192-5p and miR-200a-3p). All mature miRNAs could be detected in both of the samples (Fig. 4.6).

Tab. 4.3: Glomerular enrichment of miRNAs; comparison of qPCR experiment and miRNA enrichment in the previously obtained deep sequencing *profiles*

Glom/Tub miRNA ratio		miR-126-3p	miR-23a/b-3p	miR-145-5p	miR-24-3p	miR-27a/b-3p	miR-26a/b-5p	miR-92a/b-3p	miR-10a/b-5p	miR-29a/b/c-3p	miR-191-5p	miR-99a/b-5p	miR-21-5p	miR-22-3p	miR-192-5p	miR-200b-3p
qPCR		14.5	8.8	4.3	3.5	3.2	2.4	1.6	1.2	0.8	0.7	0.3	0.2	0.1	0.03	0.02
sequencing	total RNA	10.0	7.2/ 7.7	11.3	6.2	5.6/ 4.7	2.8/ 1.4	2.2/ 0.9	1.1/ 1.2	1.7/ 1.3/ 2.0	0.9	0.7/ 1.7	0.3	0.6	0.04	0.04
deep profiles	small RNA	16.6	1.7/ 1.7	3.1	2.8	3.8/ 4.8	1.5/ 0.6	1.1/ 0.9	1.2/ 1.3	1.7/ 0.5/ 1.6	0.9	0.9/ 2.0	0.1	0.7	0.04	0.03

The results of the qPCR analysis were compared to the results from the deep sequencing profiles (Tab. 4.3). miR-126-3p, miR-145-5p, miR-24-3p and miR-27a/b-3p showed a clear glomerular enrichment in both *deep sequencing* profiles as well as in the qPCR. Both miR-23a-3p and miR-23b-3p were glomerular enriched in the *deep sequencing* profile from total RNA, but not in the *deep sequencing* from enriched small RNAs. Glomerular enrichment of this miRNA family could be shown by qPCR. miR-26a/b-5p was slightly glomerular enriched in the qPCR analysis, while the results from the *deep sequencing* analyses differ from profile to profile and for both family members. For miR-92a/b-3p, miR-10a/b-5p, miR-29a/b/c-3p and miR-191-5p, equal expression between glomeruli and tubules was found in the *deep sequencing* profiles as well as in the qPCR analysis. miR-21-5p, miR-192-5p and miR-200a-5p were all found to be tubular enriched in qPCR, confirming the results from both *deep sequencing* profiles. miR-99a/b-5p and miR-22-3p both showed equal expression in the *deep sequencing* profiles but tubular enrichment in the qPCR analysis.

Taken together, expression of the candidate miRNAs and miRNA families could be validated in glomeruli and tubules. The enrichment from the *deep sequencing* profiles could be validated for eleven of 15 miRNAs. For miR-23a/b-3p family, the qPCR result matches one of the *deep sequencing* profiles. For miR-26a/b-5p, the qPCR result can be explained by the fact that miR-26a-5p, which is glomerular enriched in the profile obtained from total RNA, is higher expressed than miR-26b-5p. For miR-99a/b-3p and miR-22-3p, enrichment in the qPCR analyses does not fit the result from the *deep sequencing* profiles.

4.3 Differential miRNA expression in the different glomerular cell types

The mammalian glomeruli consist of the three main cell type, the podocytes, the mesangial and the endothelial cells (Fig. 4.7 A), meaning that a miRNA expressed in the glomeruli is not necessarily a miRNA important for podocyte structure and function.

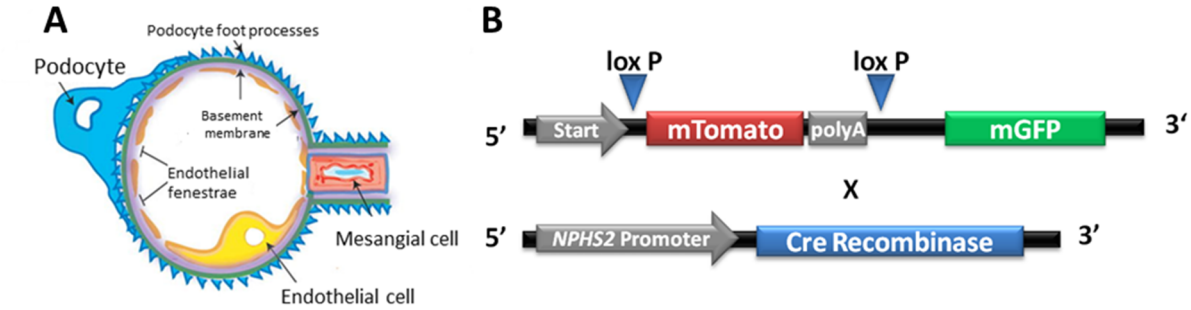

Fig. 4.7: Cell populations in mammalian glomeruli; (A) Representation of the localization of the three main cell types in the mammalian glomerulus (Aitsebaomo et al. 2008, modified) (B) Genomic organization of the mTmG x P2.5Cre mouse

A double fluorescent Cre reporter mouse crossed with a mouse expressing podocyte specific Cre recombinase under the control of the *NPHS2* promotor was used for podocyte isolation (Fig. 4.7 B). The mTomato gene in these mice is flanked by *loxP* sites, the Cre recombinase recognition sites. In cells expressing Cre recombinase, the Tomato cassette is cut out and the mGFP cassette is transcribed, leading to green fluorescent cells while the rest of the animal cell show red fluorescence.

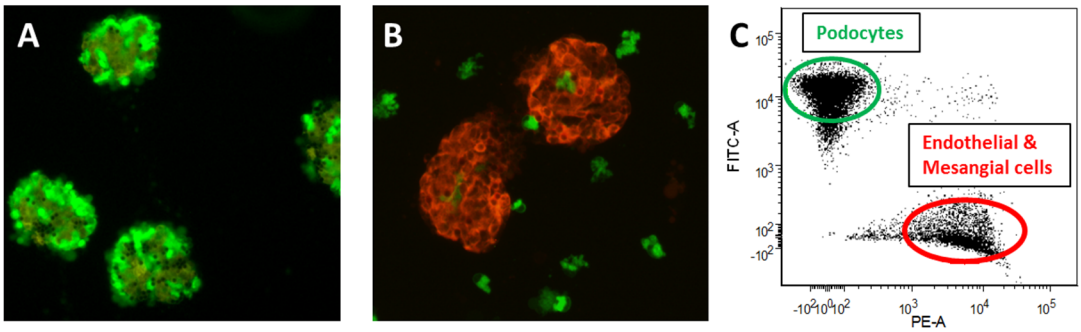

Fig. 4.8: Double fluorescent glomeruli from mTmG x P2.5Cre mice; (A) freshly isolated glomeruli consisting of green podocytes and red endothelial and mesangial cells; (B) After second digestion, the green podocytes are detached from the glomerular structure; (C) The green and red fluorescent cell populations are separated by FACS analysis

Glomeruli consisting of green and red fluorescent cells were isolated from male mTmG x P2.5Cre mice of 12 - 30 weeks of age (Fig. 4.8 A). After the second digestion step (chapter 3.3.6), the green fluorescent podocytes were detached from the glomerular structure (Fig. 4.8 B). The cell suspension consisting of green and red fluorescent cells could be sorted by FACS (Fig. 4.8 C).

4.3.1 Confirmation of cell populations

To check for identity of the sorted green and red fluorescent cell population, the "green cells" and the "red cells", qPCR was performed against cell type specific miRNAs. In the podocyte specific Dicer knockout mouse, it was shown by *in situ* hybridization that the Dicer knockout leads to a strong miR-30a-5p reduction in the mouse glomeruli, whereas the expression levels of miR-126-3p and miR-145-5p seem to be unaffected (Harvey et al. 2008). miR-126-3p seemed to be a miRNA predominantly expressed in the endothelium, while miR-145-5p seemed to be mesangially expressed. The strong enrichment of miR-30a-5p in the podocytes as well as the endothelial and mesangial expression, respectively, of miR-126-3p and miR-145-5p could be validated by qPCR (Fig. 4.9 left). Furthermore, it could be shown that the podocyte-specific transcription factor Lmx1b and the podocyte-specific slit diaphragm component podocin were highly enriched in the green cell population. Both enrichments were measured to be higher than 20-fold over the expression levels in the red cell population (Fig. 4.9 right). The residual expression of these two markers in the red cell population can be explained by a small population of podocytes still expressing the mTomato gene, meaning that the Cre recombinase mediated "switch" from red to green fluorescence did not work in these cells. Additionally, expression of the endothelial marker CD31 (Newman et al. 1990) could only be detected in the red cell population, proving the presence of endothelial cells in the mixed red cell population. Taken together, these results confirm that the green cell population consists of podocytes, while the red population is a mixture of endothelial cells, mesangial cells and some residual podocytes.

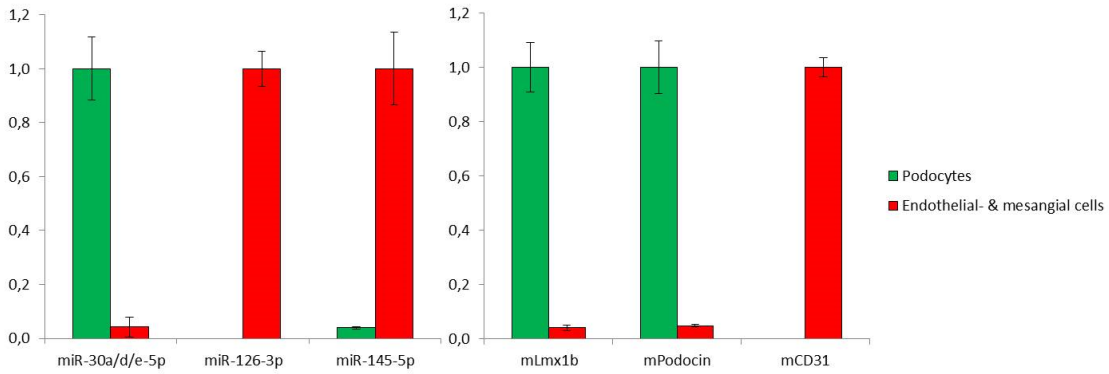

Fig. 4.9: Identification of cell types in glomerular cell population; cell type specific expression of mature miRNAs (left) and protein coding genes (right) in the green and red cell populations

4.3.2 *Deep-sequencing* profiles

Two independent miRNA *deep sequencing* profiles from green and red fluorescent cells were generated from around 150,000 green fluorescent podocytes and 150,000 red fluorescent mesangial and endothelial cells or around 100,000 green fluorescent podocytes and 100,000 red

fluorescent mesangial and endothelial cells. The samples were each isolated from six 12 to 14 weeks old male mTmG x P2.5Cre mice.

Tab. 4.4: Podocyte enriched miRNAs; enrichment according to two deep sequencing profiles derived from freshly isolated murine podocytes and the red fluorescent cell population

miRNAs	podocytes vs. red fluorescent cells									
	1st profile					2nd profile				
	Red Cells reads	Red Cells ‰	Podocytes reads	Podocytes ‰	Ratio (Pc/ Red C.)	Red Cells reads	Red Cells ‰	Podocytes reads	Podocytes ‰	Ratio (Pc/ Red C.)
mmu-let-7e-3p	81	0.02	214	0.04	2.65	79	0.01	211	0.04	2.76
mmu-miR-23b-3p	8,916	1.68	20,360	3.84	2.29	7,866	1.46	22,111	4.25	2.90
mmu-miR-24-1-5p	27	0.01	60	0.01	2.23	27	0.01	113	0.02	4.32
mmu-miR-27b-5p	339	0.06	847	0.16	2.51	279	0.05	760	0.15	2.81
mmu-miR-30a-3p	17,250	3.24	60,898	11.48	3.54	23,919	4.45	92,817	17.83	4.01
mmu-miR-30a-5p	221,539	41.63	1,080,588	203.78	4.90	110,666	20.60	738,560	141.87	6.89
mmu-miR-30b-3p	195	0.04	623	0.12	3.21	237	0.04	946	0.18	4.12
mmu-miR-30b-5p	2,663	0.50	8,906	1.68	3.36	3,197	0.59	10,086	1.94	3.26
mmu-miR-30c-2-3p	4,969	0.93	19,948	3.76	4.03	5,423	1.01	24,398	4.69	4.64
mmu-miR-30c-5p	11,104	2.09	36,253	6.84	3.28	14,980	2.79	58,989	11.33	4.06
mmu-miR-30d-3p	114	0.02	355	0.07	3.13	70	0.01	282	0.05	4.16
mmu-miR-30d-5p	27,942	5.25	146,004	27.53	5.24	24,399	4.54	127,730	24.54	5.40
mmu-miR-99a-3p	64	0.01	495	0.09	7.76	33	0.01	169	0.03	5.29
mmu-miR-99a-5p	134	0.03	795	0.15	5.95	182	0.03	485	0.09	2.75
mmu-miR-107-3p	530	0.10	2,513	0.47	4.76	788	0.15	3,170	0.61	4.15
mmu-miR-125b-2-3p	70	0.01	436	0.08	6.25	59	0.01	248	0.05	4.34
mmu-miR-125b-5p	333	0.06	952	0.18	2.87	642	0.12	1,273	0.24	2.05
mmu-miR-130a-3p	994	0.19	4,660	0.88	4.70	998	0.19	3,059	0.59	3.16
mmu-miR-146b-5p	542	0.10	13,295	2.51	24.62	455	0.08	7,755	1.49	17.59
mmu-miR-148a-3p	1,376	0.26	6,333	1.19	4.62	2,292	0.43	5,082	0.98	2.29
mmu-miR-149-5p	24	0.00	310	0.06	12.96	61	0.01	448	0.09	7.58
mmu-miR-196b-5p	908	0.17	4,904	0.92	5.42	1,396	0.26	9,553	1.83	7.06
mmu-miR-210-3p	199	0.04	1,595	0.30	8.04	166	0.03	856	0.16	5.32
mmu-miR-322-3p	1,810	0.34	14,940	2.82	8.28	3,093	0.58	13,469	2.59	4.49
mmu-miR-330-3p	25	0.00	222	0.04	8.91	23	0.00	120	0.02	5.39
mmu-miR-330-5p	37	0.01	306	0.06	8.30	21	0.00	112	0.02	5.50
mmu-miR-340-5p	1,281	0.24	3,535	0.67	2.77	925	0.17	3,263	0.63	3.64
mmu-miR-351-3p	3	0.00	54	0.01	18.06	15	0.00	46	0.01	3.17
mmu-miR-351-5p	1,332	0.25	8,439	1.59	6.36	1,400	0.26	5,192	1.00	3.83
mmu-miR-450a-5p	272	0.05	962	0.18	3.55	378	0.07	1,000	0.19	2.73
mmu-miR-450b-5p	64	0.01	334	0.06	5.24	64	0.01	296	0.06	4.77
mmu-miR-503-3p	38	0.01	152	0.03	4.01	50	0.01	197	0.04	4.07
mmu-miR-503-5p	591	0.11	2,677	0.50	4.55	713	0.13	1,832	0.35	2.65
mmu-miR-542-3p	550	0.10	1,829	0.34	3.34	626	0.12	3,334	0.64	5.50
mmu-miR-574-3p	369	0.07	1,473	0.28	4.01	725	0.13	2,017	0.39	2.87
mmu-miR-615-3p	21	0.00	167	0.03	7.98	45	0.01	134	0.03	3.07
mmu-miR-652-3p	315	0.06	878	0.17	2.80	278	0.05	847	0.16	3.14
mmu-miR-873a-5p			170	0.03		1	0.00	80	0.02	82.57

RNA extraction and library preparation was performed by A. Dueck and N. Eichner (Department of Biochemistry I, University of Regensburg). For both profiles, the small RNAs were enriched by gel electrophoresis. The RNA samples were sequenced on a HiSeq1000 sequencer (Illumina). The annotation of the sequenced libraries to the known miRNA sequences (miRBase Version 19) was performed by N. Eichner (Department of Biochemistry I, University of Regensburg).

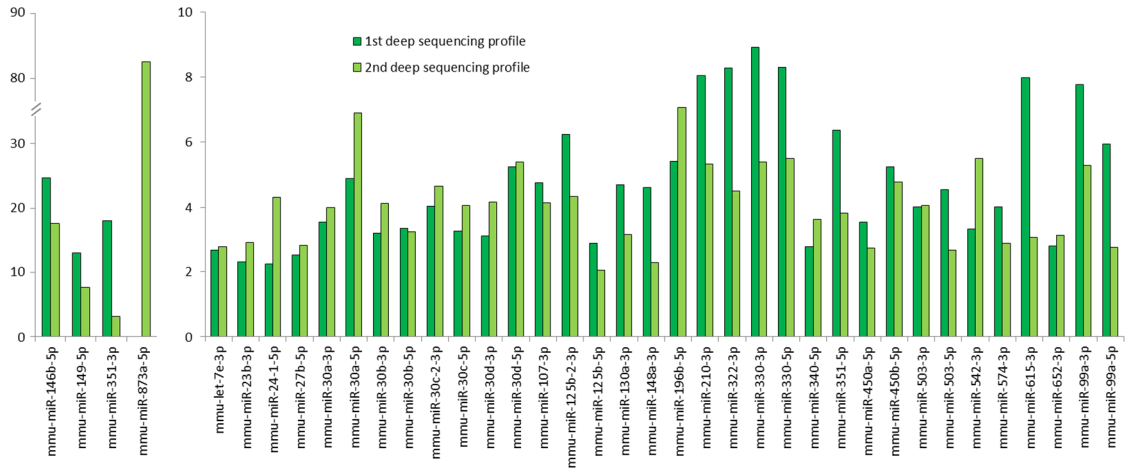

Fig. 4.10: miRNAs enriched in podocytes; miRNAs showing a more than two fold enrichment in podocytes compared to the red fluorescent cell population in two deep sequencing profiles; Left: miRNAs showing more than ten-fold enrichment in one of the profiles; right: miRNAs showing less than ten-fold enrichment in both profiles

The two *deep sequencing* profiles, consisting of 4.19 million reads from podocytes and 4.02 million reads from the red fluorescent cell population and 4.45 million reads from podocytes and 3.88 million reads from the red fluorescent cell population showed a very good result overlap (Tab. 10.2). A total of 38 miRNAs were enriched more than two-fold in the podocytes compared to the red fluorescent cell population in both profiles (Tab. 4.4, Fig. 4.10). Four mature miRNAs were only detected as podocyte enriched in one profile. As mmu-miR-873a-5p was not detected in the red fluorescent cell population in the first profile, a ratio could not be calculated. In total, 69 miRNAs were equally expressed in both cell populations according to the profiles, while 93 miRNAs were enriched in the red fluorescent cell population both times. One miRNA was enriched in podocytes in one profile but enriched in the red cell population in the other profile. A total of 42 miRNAs were found to be enriched in one of the profiles while being equally expressed in the other profile and 47 miRNAs were only detected in one of the profiles.

Surprisingly, only ten miRNAs that had earlier been identified as glomerular enriched could be identified as podocyte enriched miRNAs. Seven miRNAs were equally expressed in the glomerular cell populations, while the majority of 36 mature miRNAs, was enriched in the endothelial and mesangial cells, with some of them hardly expressed in podocytes.

4.3.3 Profile validation by qPCR

To validate the *deep sequencing* profiles, a subset of 23 miRNAs expressed in the murine podocytes and the endothelial and mesangial cells was analyzed for relative enrichment by qPCR. For validation, the small RNA fraction was isolated from 700,000 podocytes and 330,000 endothelial and mesangial cells from six female 14 week old mTmGxP2.5Cre mice. Equal amounts of RNA were reverse transcribed to cDNA. The relative enrichment of miRNAs in the podocytes compared to the endothelial and mesangial cells was calculated and compared to the result from the *deep sequencing* profiles. The snRNA U6 served as an internal control. Since qPCR with normal DNA primers cannot distinguish between miRNAs that differ only by one base, enrichment results were treated as total enrichment of whole miRNA families. The qPCR was performed on a LightCycler 480II (Roche). The results were gathered and analyzed with the LightCycler 480 1.5.0 software (Roche).

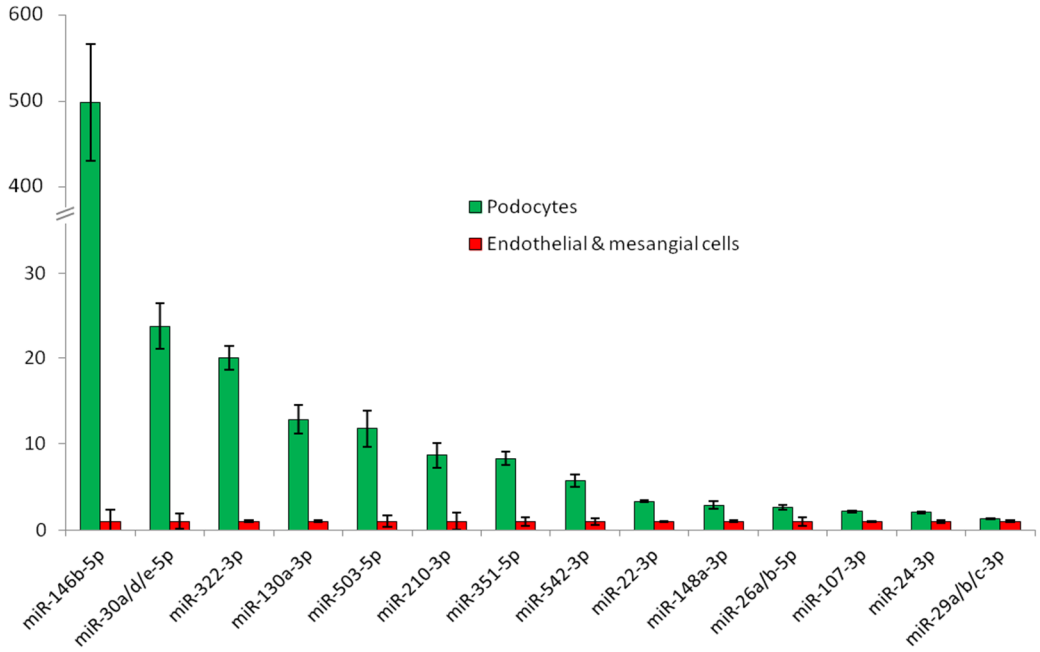

Fig. 4.11: qPCR quantification of mature miRNAs enriched in podocytes; relative expression in the murine podocytes (green) and the red fluorescent cell population (red) was calculated (expression in red fluorescent cell population = 1)

For ten miRNAs that were podocyte enriched in both *deep sequencing* profiles, miR-146b-5p, miR-30a/d/e-5p, miR-322-3p, miR-130a-3p, miR-503-5p, miR-210-3p, miR-351-5p, miR-542-3p, miR-148a-3p and miR-107-3p, podocyte enrichment could be confirmed by qPCR (Fig. 4.11, Tab. 4.5). miR-22-3p which was podocyte enriched in one of the profiles, and miR-26a/b-5p, where only one family member was podocyte enriched in one of the *deep sequencing* profiles, were podocyte enriched in the qPCR analysis. miR-24-3p was equally expressed according to both

deep sequencing profiles, but podocyte enriched in the qPCR. The miR-29a/b/c-3p family was equally expressed in both profiles as well as in the qPCR.

Tab. 4.5: Enrichment of mature miRNAs in podocytes; enrichment according to qPCR analyses and two deep sequencing *profiles in green fluorescent podocytes compared to red fluorescent endothelial and mesangial cells*

Podocyte/ endothelial & mesangial cells miRNA ratio		miR-146b-5p	miR-30a/d/e-5p	miR-322-3p	miR-130a-3p	miR-503-5p	miR-210-3p	miR-351-5p	miR-542-3p	miR-22-3p	miR-148a-3p	miR-26a/b-5p	miR-107-3p	miR-24-3p	miR-29a/b/c-3p
	qPCR	499	23.8	20.0	12.9	11.8	8.7	8.3	5.7	3.3	2.9	2.6	2.1	2.0	1.3
Deep sequencing profiles	First profile	24.6	4.9/ 5.2/ 1.4	8.3	4.7	4.6	8.1	6.4	3.3	2.7	4.6	1.5/ 0.8	4.8	1.3	1.4/ 1.3/ 0.8
	Second profile	17.6	6.9/ 5.4/ 1.2	4.5	3.2	2.7	5.3	3.8	5.5	1.9	2.3	2.1/ 1.3	4.1	1.5	2.0/ 1.1/ 0.8

Relative expression was also validated for miRNAs that were enriched in the red cell population according to the *deep sequencing* profiles (Fig. 4.12, Tab. 4.6). In the miR-27a/b-3p family, one miRNA was equally expressed and one family member was enriched in the red fluorescent cell population according to the profiles. The total result from the qPCR showed it to be equally expressed. miR-23a-3p was enriched in the red fluorescent cell population while miR-23b-3p was enriched in the podocytes according to both *deep sequencing* profiles. In total, the miR-23a/b-3p family was enriched in the red fluorescent cell population in the qPCR.

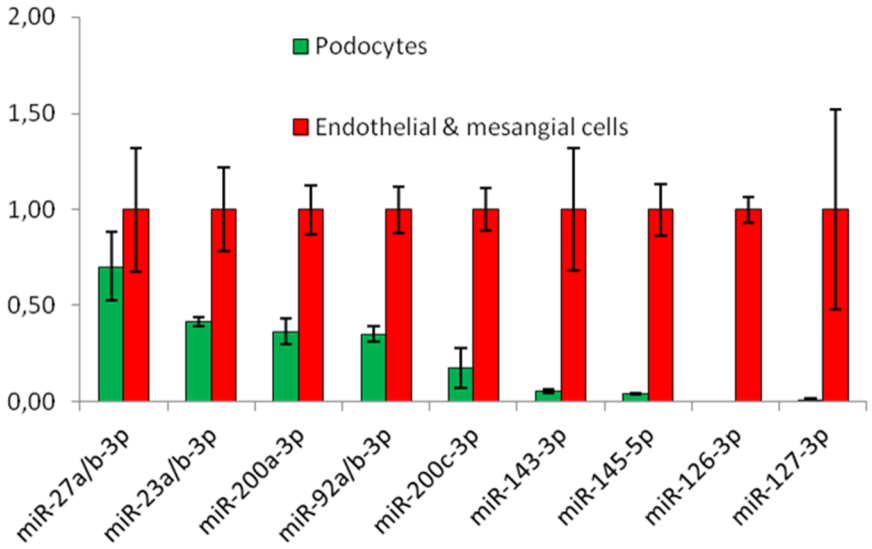

Fig. 4.12: qPCR quantification of mature miRNAs enriched in the red fluorescent cell population; relative expression in the murine podocytes (green) and the red fluorescent cell population (red) was calculated (expression in red fluorescent cell population = 1)

Tab. 4.6: Enrichment of mature miRNAs in "red fluorescent cell population"; enrichment according to qPCR analyses and two deep sequencing *profiles in green fluorescent podocytes compared to the red fluorescent cell population*

Podocyte/ endothelial & mesangial cells miRNA ratio		miR-27a/b-3p	miR-23a/b-3p	miR-200a-3p	miR-92a/b-3p	miR-200c-3p	miR-143-3p	miR-145-5p	miR-126-3p	miR-127-3p
qPCR		0.7	0.4	0.4	0.4	0.1	0.1	0.04	0.000	0.001
Deep sequencing profiles	First profile	0.2/ 1.5	0.2/ 2.3	0.02	0.4/ 2.6	0.003	0.06	------	0.001	0.000
	Second profile	0.3/ 1.7	0.3/ 2.9	0.01	0.4/ 0.4	0.004	0.04	0.08	0.001	0.001

For six miRNAs, miR-200a-3p, miR-200c-3p, miR-143-3p, miR-145-5p, miR-126-3p and miR-127-3p, enrichment in the red fluorescent cell population could be validated by qPCR. According to both *deep sequencing* profiles, miR-92a-3p is expressed in much higher amount than miR-92b-3p (> 100 in podocytes and > 300 in the red fluorescent cell population). This explains why the qPCR result is mainly influenced by miR-92a-3p. In total, podocyte enrichment could be validated for ten miRNAs or miRNA families. One miRNA family was equally expressed in both profiles as well as in the qPCR analyses, while seven miRNAs could be validated as enriched in the red fluorescent cell population.

4.4 miRNA target prediction by different *in silico* tools

In this work, the main focus lies on the specific interactions between the mRNAs coding for proteins important for maintenance of podocyte structure and function and the miRNAs that are enriched or highly expressed in podocytes.

Initial screening for putative miRNA targets using miRWalk

The first *in silico* predictions were performed using miRWalk, a prediction algorithm itself that also assesses the prediction results of seven other prediction programs (DIANAmT, miRanda, miRDB, RNAhybrid, PICTAR4, PICTAR5, PITA, RNA22 and Targetscan). The human 3'-UTRs of mRNAs coding for proteins important for podocyte structure and function were analyzed for binding sites of miRNAs enriched or highly expressed in podocytes. Only miRNAs that were

predicted as possible regulators by at least half of the programs, N ≥ 4, were considered hits (Tab. 4.7). When members of a miRNA family received different numbers of hits, the number for the family member with the highest score is given in the table.

Tab. 4.7: Podocyte miRNAs target prediction using miRWalk; podocyte candidate miRNAs predicted to target mRNAs coding for proteins important for podocyte structure and functions (chapter 1.4.1); in column "hits", the number of different programs predicting a certain interaction is given

Potential target	miRNA	hits (max. = 8)
ACTN4 – α-Actinin-4	no hits meeting the criteria	
ACTR2 – Actin related protein 2 (member of ARP2/3 complex)	hsa-miR-23a/b-3p	6
	hsa-miR-107	6
	hsa-miR-22-3p	5
	hsa-miR-27a/b-3p	5
	hsa-miR-340-5p	5
	hsa-miR-450b-5p	5
	hsa-miR-503-5p	5
CD2AP – CD2 associated protein	hsa-miR-26a/b-5p	6
	hsa-miR-27a/b-3p	6
	hsa-miR-30a-e-5p	6
	hsa-miR-92a/b-3p	6
	hsa-miR-340-5p	6
	hsa-miR-130a-3p	5
	hsa-miR-450b-5p	5
	hsa-miR-503-5p	5
	hsa-miR-107	4
CDC42 – Cell division control protein 42 homolog	hsa-miR-29a-c-3p	6
	hsa-miR-27a/b-3p	5
	hsa-miR-92a/b-3p	4
	hsa-miR-107	4
CLIC5 – Chloride intracellular channel protein 5	hsa-miR-26a/b-5p	4
	hsa-miR-340-5p	4
EZR - Ezrin	hsa-miR-27a/b-3p	7
	hsa-miR-22-3p	6
	hsa-miR-23a/b-3p	5
	hsa-miR-148a-3p	5
	hsa-miR-450b-5p	5
	hsa-miR-107	4
	hsa-miR-130a-3p	4
FAT1 - Protocadherin Fat 1	hsa-miR-26a/b-5p	4
FYN – Proto-oncogene tyrosinkinase Fyn	hsa-miR-27a/b-3p	5
GRB2 – Growth factor receptor-bound protein 2	hsa-miR-27a/b-3p	8
	hsa-miR-10a/b-5p	5
	hsa-miR-22-3p	5
	hsa-miR-149-5p	5
	hsa-miR-450b-5p	5
	hsa-miR-107	4
	hsa-miR-146b-3p	4

Potential target	miRNA	hits (max. = 8)
IQGAP1 – Ras GTPase-activating-like protein IQGAP1	hsa-miR-107	6
	hsa-miR-146b-5p	6
	hsa-miR-24-3p	5
	hsa-miR-30a-e-5p	5
	hsa-miR-340-5p	5
	hsa-miR-542-5p	5
LMX1B – LIM homeobox transcription factor 1-beta	hsa-miR-210-3p	5
	hsa-miR-149-5p	4
NCK1 - Non-catalytic region of tyrosine kinase adaptor protein 1	hsa-miR-542-3p	6
	hsa-miR-340-5p	5
NCK2 - Non-catalytic region of tyrosine kinase adaptor protein 2	hsa-miR-30a-e-5p	4
	hsa-miR-92a/b-3p	4
	hsa-miR-340-5p	4
	hsa-miR-450b-5p	4
NEPH1 (KIRREL) - Kin of IRRE-like protein 1	hsa-miR-29a-c-3p	6
	hsa-miR-10a/b-5p	5
	hsa-miR-107	5
	hsa-miR-149-5p	4
NEPH3 (KIRREL2) - Kin of IRRE-like protein 1	hsa-miR-149-5p	4
NOSTRIN - Nitric oxide synthase trafficking	hsa-miR-196b-5p	4
NPHS1 – Nephrin	hsa-miR-107	5
NPHS2 – Podocin	hsa-miR-450b-5p	5
	hsa-miR-542-3p	5
PARD3 - Partitioning defective 3 homolog	no hits meeting the criteria	
PARD6A - Partitioning defective 6 homolog alpha	no hits meeting the criteria	
PARD6B - Partitioning defective 6 homolog beta	hsa-miR-23a/b-3p	6
	hsa-miR-27a/b-3p	6
	hsa-miR-10a/b-5p	5
	hsa-miR-92a/b-3p	5
	hsa-miR-146b-5p	5
	hsa-miR-340-5p	5
	hsa-miR-503-5p	5
	hsa-miR-542-3p	5
	hsa-miR-196b-5p	4
PODXL - Podocalyxin	Hsa-miR-149-5p	5
	hsa-miR-22-3p	4
	hsa-miR-107	4
	hsa-miR-148a-3p	4
	hsa-miR-340-5p	4
RAC1 - Ras-related C3 botulinum toxin substrate 1	hsa-miR-542-3p	5
	hsa-miR-146b-5p	4
	hsa-miR-148a-3p	4
	hsa-miR-340-5p	4
	hsa-miR-450b-5p	4
	hsa-miR-574-3p	4
RHOA - Ras homolog gene family, member A	hsa-miR-340-5p	6
	hsa-miR-146b-5p	4
TLN1 – Talin-1	hsa-miR-196b-5p	4
	hsa-miR-503-5p	4
TRPC6 - Transient receptor potential cation channel, subfamily C, member 6	hsa-miR-10a/b-5p	6
	hsa-miR-29a-c-3p	6
	hsa-miR-30a-e-5p	6
	hsa-miR-26a/b-5p	5

Potential target	miRNA	hits (max. = 8)
	hsa-miR-340-5p	5
	hsa-miR-23a/b-3p	4
VEGFA - Vascular endothelial growth factor A	hsa-miR-29a-c-3p	7
	hsa-miR-24-3p	6
	hsa-miR-107	6
	hsa-miR-503-5p	5
	hsa-miR-23a/b-3p	4
WASL - Neural Wiskott-Aldrich syndrome protein	hsa-miR-130a-3p	7
	hsa-miR-92a/b-3p	6
	hsa-miR-148a-3p	6
	hsa-miR-23a/b-3p	5
	hsa-miR-27a/b-3p	5
	hsa-miR-30a-e-5p	5
	hsa-miR-196b-5p	5
	hsa-miR-340-5p	5
	hsa-miR-10a/b-5p	4
	hsa-miR-107	4
	hsa-miR-503-5p	4
WT1 - Wilms tumor protein	hsa-miR-503-5p	6
	hsa-miR-23a/b-3p	5
	hsa-miR-340-5p	5

To narrow down the candidate set, proteins that are important for the slit diaphragm predicted to be targeted by miRNAs expressed in podocytes in sufficiently high levels were chosen as a first candidate set. A group of four putative target proteins, CD2AP, Fyn, Nck2, Neph1, all known to directly interact with nephrin, the main protein of the slit diaphragm, was selected for the first further studies. *In silico* predictions for these four candidates were refined using miRWalk2, a prediction platform that compares the results of 12 different prediction algorithms, miRWalk, Micro4t, miRanda, mirbridge, miRDB, miRMap, miRNAMAp, Pictar2, PITA, RNA22, RNAhybrid and Targetscan (Tab. 4.8 – 4.15). Additionally, the alignment analysis of the human and murine 3'-UTRs was performed to identify conserved binding sites.

CD2AP

The human and murine protein coding transcripts of CD2AP, NM_012120 and NM_009847, both possess relatively long 3'-UTRs of 3,036 and 3,377 nucleotides, respectively. For both transcripts, possible miRNA interaction partners were predicted with miRWalk2 using 12 different prediction algorithms (Tab. 4.8 and 4.9).

Tab. 4.8: miRWalk2 predictions of miRNAs targeting human CD2AP 3'-UTR; criterion: sum of predictions ≥4

Gene	Transcript number	Mature miRNA	miRWalk	Microt4	miRanda	mirbridge	miRDB	miRMap	miRNAMap	Pictar2	PITA	RNA22	RNAhybrid	Targetscan	Sum
CD2AP	NM_012120	hsa-miR-92a-3p	1	1	1	0	1	1	0	1	1	1	1	1	10
CD2AP	NM_012120	hsa-miR-92b-3p	0	1	1	1	1	1	0	1	1	1	1	1	10
CD2AP	NM_012120	hsa-miR-27b-3p	0	1	1	0	1	1	0	1	1	1	1	1	9
CD2AP	NM_012120	hsa-miR-450b-5p	1	1	1	0	1	1	0	1	1	0	1	1	9
CD2AP	NM_012120	hsa-miR-27a-3p	0	1	1	0	1	1	0	1	1	1	1	1	9
CD2AP	NM_012120	hsa-miR-30b-5p	1	1	1	0	0	1	0	0	1	1	1	1	8
CD2AP	NM_012120	hsa-miR-30e-5p	1	1	1	0	0	1	0	0	1	1	1	1	8
CD2AP	NM_012120	hsa-miR-30c-5p	1	1	1	0	0	1	0	0	1	1	1	1	8
CD2AP	NM_012120	hsa-miR-340-5p	1	1	1	0	1	1	0	0	1	0	1	1	8
CD2AP	NM_012120	hsa-miR-30a-5p	1	1	1	0	0	1	0	0	1	1	1	1	8
CD2AP	NM_012120	hsa-miR-503-5p	1	1	0	0	0	1	0	0	1	1	1	1	7
CD2AP	NM_012120	hsa-miR-30d-5p	1	1	1	0	0	1	0	0	1	0	1	1	7
CD2AP	NM_012120	hsa-miR-130a-3p	0	1	1	0	0	1	0	0	1	0	1	1	6
CD2AP	NM_012120	hsa-miR-107	1	1	0	0	0	1	0	0	1	1	1	0	6
CD2AP	NM_012120	hsa-miR-29b-3p	0	1	0	0	0	1	0	0	1	1	1	0	5
CD2AP	NM_012120	hsa-miR-29c-3p	0	1	0	0	0	1	0	0	1	1	1	0	5
CD2AP	NM_012120	hsa-miR-450a-5p	0	0	1	0	0	1	0	0	1	0	1	1	5
CD2AP	NM_012120	hsa-miR-29a-3p	0	1	0	0	0	1	0	0	1	1	1	0	5
CD2AP	NM_012120	hsa-miR-30e-3p	0	0	1	0	0	1	0	0	0	0	1	1	4
CD2AP	NM_012120	hsa-miR-23b-3p	0	1	0	0	0	0	0	0	1	1	1	0	4
CD2AP	NM_012120	hsa-miR-30d-3p	0	0	1	0	0	1	0	0	0	0	1	1	4
CD2AP	NM_012120	hsa-miR-30a-3p	0	0	1	0	0	1	0	0	0	0	1	1	4
CD2AP	NM_012120	hsa-miR-23a-3p	0	1	0	0	0	0	0	0	1	1	1	0	4

Equivalent predictions were performed for the murine 3'-UTR of Cd2ap.

Tab. 4.9: miRWalk2 predictions of miRNAs targeting murine Cd2ap 3'-UTR; criterion: sum of predictions ≥4

Gene	Transcript number	Mature miRNA	miRWalk	Microt4	miRanda	mirbridge	miRDB	miRMap	miRNAMap	Pictar2	PITA	RNA22	RNAhybrid	Targetscan	Sum
Cd2ap	NM_009847	mmu-miR-92a-3p	1	1	1	0	1	1	0	0	1	1	1	1	9
Cd2ap	NM_009847	mmu-miR-92b-3p	1	1	1	0	1	1	0	0	1	1	1	1	9
Cd2ap	NM_009847	mmu-miR-27a-3p	1	1	1	0	1	1	0	0	1	0	1	1	8
Cd2ap	NM_009847	mmu-miR-27b-3p	1	1	1	0	1	1	0	0	1	0	1	1	8
Cd2ap	NM_009847	mmu-miR-340-5p	1	1	1	0	0	1	0	0	1	0	1	1	7
Cd2ap	NM_009847	mmu-miR-542-3p	1	0	0	0	0	1	0	0	1	1	1	1	6
Cd2ap	NM_009847	mmu-miR-503-5p	1	1	0	0	0	1	0	0	1	0	1	1	6
Cd2ap	NM_009847	mmu-miR-107-3p	1	1	0	0	0	1	0	0	1	1	1	0	6
Cd2ap	NM_009847	mmu-miR-29b-3p	1	1	0	0	0	1	0	0	1	1	1	0	6
Cd2ap	NM_009847	mmu-miR-30f	1	0	1	0	0	1	0	0	0	0	1	1	5
Cd2ap	NM_009847	mmu-miR-29a-3p	0	1	0	0	0	1	0	0	1	1	1	0	5
Cd2ap	NM_009847	mmu-miR-23a-3p	1	1	0	0	0	1	0	0	1	0	1	0	5
Cd2ap	NM_009847	mmu-miR-30c-2-3p	1	0	0	0	0	1	0	0	0	1	1	1	5
Cd2ap	NM_009847	mmu-miR-450b-5p	1	0	0	0	0	1	0	0	1	1	1	0	5
Cd2ap	NM_009847	mmu-miR-23b-3p	1	1	0	0	0	1	0	0	1	0	1	0	5
Cd2ap	NM_009847	mmu-miR-29c-3p	1	1	0	0	0	1	0	0	1	0	1	0	5
Cd2ap	NM_009847	mmu-miR-30a-5p	1	1	0	0	0	0	0	0	1	0	1	0	4
Cd2ap	NM_009847	mmu-miR-30e-5p	1	1	0	0	0	0	0	0	1	0	1	0	4
Cd2ap	NM_009847	mmu-miR-30b-3p	1	0	0	0	0	1	0	0	0	1	1	0	4
Cd2ap	NM_009847	mmu-miR-196b-5p	0	0	0	0	0	1	0	0	1	1	1	0	4
Cd2ap	NM_009847	mmu-miR-30b-5p	1	1	0	0	0	0	0	0	1	0	1	0	4
Cd2ap	NM_009847	mmu-miR-30c-1-3p	0	0	0	0	0	1	0	0	0	1	1	1	4
Cd2ap	NM_009847	mmu-miR-30c-5p	1	1	0	0	0	0	0	0	1	0	1	0	4
Cd2ap	NM_009847	mmu-miR-30d-5p	1	1	0	0	0	0	0	0	1	0	1	0	4
Cd2ap	NM_009847	mmu-miR-130b-3p	1	0	0	0	0	0	0	0	1	1	1	0	4
Cd2ap	NM_009847	mmu-miR-322-3p	1	0	0	0	0	1	0	0	1	0	1	0	4

Only the 3'-end of the 3'-UTRs of the human and the murine transcript show a good interspecies alignment. The region was especially analyzed for conserved miRNA binding sites (Fig. 4.13).

```
Murine  2683  ACAGCATTGAATCTGTCATTGCCAAATTATTAGTGAATGTATAGTTCAGATTTGCTAGTC  2742
              |||||||  |||||  |||||||||||||||||||||||||||||||||    | || ||
Human   2259  ACAGCATGGAATC--TCATTGCCAAATTATTAGTGAATGTATAGTTCAG----G-TATTC  2311

Murine  2743  TTTGA-A-ACACAGCACTCCTAAGTTTCT-AACAGGATTCCAATGTTATTTTGGTGTGTT  2799
              |||||  | ||||||  | ||  | |  |||||  ||   | |||  || |||||||||   | ||||
Human   2312  TTTGAGACACACAGTA-TCATTAATTTCTGAATTGTATTTCAGTGTTATTTT--T-TGTT  2367

Murine  2800  TGTGACCACTAAGCTTGCT-TCTTACTATAAAGGTATTACCT-CTATACAACTGTACAGG  2857
              |||||||||||||||  ||  |||||  ||  ||||  |  ||||||  |||  |  ||  ||  |  |
Human   2368  TGTGACCACTAAGCTT-CTGTCTTAATACAAAGCTGTTACCTTCTACAGAA-TTTA-A-G  2423

Murine  2858  ACTTCACAGAAAATCAGAAGATGCAGAGAGAGTGGGCCCGGTCTTAACAG-AG-GACTC-  2914
               |  |  |  ||  |   |  |  ||||  |  |||  |  |    ||||   ||   ||||||  ||   ||||
Human   2424  TC-TGA-AG-ATGT-A-AAGA-G-AGA-ACA---GGCCTTGT-GTAACAGAAGATACTCT  2471

Murine  2915  --CTTACACTCCTAACTGTGATCACAGACAAGAAAT-ACCTTCCGAAGTGCTCTGTAGAt  2971
                 |||  |||||  |||||||||||||||  ||  ||  |  |   |||  |||||||||  ||||
Human   2472  TTTTTATGCTCCTTACTGTGATCACAGA-AA-AATTAAAAATCC-AAGTGCTCTCTAGA-  2527

Murine  2972  tttttGATGAATGTTTTATGCTTGCATTTAAACTTGAAATGTATGAGCAGAATGAGACA  3031
              |||  |||||  ||  ||||||||||||||||||||||||||||||||||||||||||||||
Human   2528  TTTGTTGATAAACATTTTATGCTTGCATTTAAACTTGAAATGTATGAGCAGAATGAGACA  2587

Murine  3032  ATCT-TTACAATCAGAATTGAGAAGTGTTACAATTGAATGGCCTTG---TGCTGTAGCAA  3087
              |||  |||  ||||||||  ||||||||  |||  |||  ||  |||||||   ||||||||||
Human   2588  ATCAGTTA-AATCAGAAATGAGAAGTATTATAATGTAAAGGCCTTGTTTTGCTGTAGCAA  2646

Murine  3088  TAAAATGACCAAGTGCAATGAC----TTTAATAAAATCATCTTTCAAACGTTGCTGCTAT  3143
              |||||||||||||||||||||    |||||||||||||| |||  |||  ||||||||||
Human   2647  TAAAATGACCAAGTGCAATGACTTGATTTAATAAAATCATATTTTAAAAGTTGCTGCTAT  2706

Murine  3144  TAATATTTTTAGTTAACAAAATT  3166
               |||||||||  |  ||  ||||||
Human   2707  GAATATTTTTGGCTAT-AAAATT  2728
```

Fig. 4.13: Alignment of the 3'UTRs of CD2AP transcripts from human (NM_012120) and mouse (NM_009847); predicted seed binding sites are indicated as follows: yellow: miR-27a/b-3p; red: miR-92a/b-3p; turquoise: miR-107-3p; boxed: miR-503-5p (overlapping with miR-107-3p binding site)

The possible binding site of the seed region of miR-27a/b-3p, miR-92a/b-3p, miR-107-3p and miR-503-5p are conserved between the two species (Fig. 4.13). Furthermore, the 3'-end of the human CD2AP 3'-UTR contains a miR-30a-e-5p and a miR-29a-c-3p binding site which are not conserved between human and mouse (Fig. 4.14).

```
Human  2728  TTACCCTGACTTGCTTTCAATAACTGTTACGTAATGCAGTTGATGTGTAACCTAACATTC  2788

Human  2789  CAAAAAAAAAATTGAGAGGGGGAATCTCAAAATAGTATATACTTCACTAACTTGTTTACA  2849

Human  2851  GGTGCTGTATTTAAAAGCAUGCTTCTC  2878
```

Fig.4.14: 3'-end of human 3'-UTR of CD2AP transcript (NM_012120); predicted seed binding sites are indicated as follows: yellow: miR-30a-e-5p; red: miR-29a-c-3p

The 3'-end fragment of the human 3'-UTR of CD2AP with a length of 606 bp was cloned into the luciferase reporter vector (pMir-Report, modified) for subsequent luciferase assay (chapter 4.6).

The tyrosine kinase Fyn

The longest human and murine protein coding transcripts for the tyrosine kinase Fyn, NM_002037 and NM_008054, possess a 3'-UTR of 1,407 nucleotides and 1,409 nucleotides, respectively. For both transcripts, possible miRNA interaction partners were predicted with miRWalk2 using 12 different prediction algorithms (Tab. 4.10 and 4.11).

Tab. 4.10: miRWalk2 predictions of miRNAs targeting human FYN 3'-UTR; criterion: sum of predictions ≥4

Gene	Transcript number	Mature miRNA	miRWalk	Microt4	miRanda	mirbridge	miRDB	miRMap	miRNAMap	Pictar2	PITA	RNA22	RNAhybrid	Targetscan	Sum
FYN	NM_002037	hsa-miR-146b-5p	1	1	1	0	0	1	1	0	0	0	1	1	7
FYN	NM_002037	hsa-miR-27a-3p	1	1	0	0	0	1	0	1	0	1	1	1	7
FYN	NM_002037	hsa-miR-27b-3p	1	1	0	0	0	1	0	1	0	1	1	1	7
FYN	NM_002037	hsa-miR-30e-5p	1	1	0	0	0	1	0	1	0	1	1	1	7
FYN	NM_002037	hsa-miR-130a-3p	0	1	1	0	0	1	0	0	0	1	1	1	6
FYN	NM_002037	hsa-miR-23a-3p	1	1	0	0	0	1	1	0	0	1	1	0	6
FYN	NM_002037	hsa-miR-24-3p	1	0	1	0	0	1	1	0	0	0	1	1	6
FYN	NM_002037	hsa-miR-29a-3p	1	1	0	0	0	1	0	1	0	0	1	1	6
FYN	NM_002037	hsa-miR-29b-3p	1	1	0	0	0	1	0	1	0	0	1	1	6
FYN	NM_002037	hsa-miR-29c-3p	1	1	0	0	0	1	0	1	0	0	1	1	6
FYN	NM_002037	hsa-miR-30a-5p	1	1	0	0	0	1	0	1	0	0	1	1	6
FYN	NM_002037	hsa-miR-30b-5p	1	1	0	0	0	1	0	1	0	0	1	1	6
FYN	NM_002037	hsa-miR-30c-5p	1	1	0	0	0	1	0	1	0	0	1	1	6
FYN	NM_002037	hsa-miR-30d-5p	1	1	0	0	0	1	0	1	0	0	1	1	6
FYN	NM_002037	hsa-miR-340-5p	1	1	0	0	0	1	1	0	0	0	1	1	6
FYN	NM_002037	hsa-miR-450b-5p	0	1	1	0	0	1	0	0	0	0	1	1	5
FYN	NM_002037	hsa-miR-149-5p	0	1	0	0	0	1	1	0	0	1	1	0	5
FYN	NM_002037	hsa-miR-23b-3p	1	1	0	0	0	1	1	0	0	0	1	0	5
FYN	NM_002037	hsa-miR-30a-3p	0	1	0	0	0	1	1	0	0	0	1	1	5
FYN	NM_002037	hsa-miR-503-5p	0	1	0	0	0	1	1	0	0	0	1	0	4
FYN	NM_002037	hsa-miR-23c	1	1	0	0	0	1	0	0	0	0	1	0	4
FYN	NM_002037	hsa-miR-30d-3p	0	1	0	0	0	1	0	0	0	0	1	1	4

Equivalent predictions were performed for the murine 3'-UTR of Fyn.

Tab. 4.11: miRWalk2 predictions of miRNAs targeting murine Fyn 3'-UTR; criterion: sum of predictions ≥4

Gene	Transcript number	Mature miRNA	miRWalk	Microt4	miRanda	mirbridge	miRDB	miRMap	miRNAMap	Pictar2	PITA	RNA22	RNAhybrid	Targetscan	Sum
Fyn	NM_008054	mmu-miR-27b-3p	1	0	1	0	0	1	1	0	0	0	1	1	6
Fyn	NM_008054	mmu-miR-27a-3p	1	0	1	0	0	1	0	0	0	0	1	1	5
Fyn	NM_008054	mmu-miR-30f	1	0	1	0	0	1	0	0	0	0	1	1	5
Fyn	NM_008054	mmu-miR-29a-3p	1	0	0	0	0	1	1	0	0	0	1	1	5
Fyn	NM_008054	mmu-miR-322-3p	1	0	1	0	0	1	0	0	0	0	1	1	5
Fyn	NM_008054	mmu-miR-30e-5p	1	0	0	0	0	1	0	0	0	0	1	1	4
Fyn	NM_008054	mmu-miR-30b-5p	1	0	0	0	0	1	0	0	0	0	1	1	4
Fyn	NM_008054	mmu-miR-29b-3p	1	0	0	0	0	1	0	0	0	0	1	1	4
Fyn	NM_008054	mmu-miR-29c-3p	1	0	0	0	0	1	0	0	0	0	1	1	4
Fyn	NM_008054	mmu-miR-30c-5p	1	0	0	0	0	1	0	0	0	0	1	1	4
Fyn	NM_008054	mmu-miR-30d-5p	1	0	0	0	0	1	0	0	0	0	1	1	4
Fyn	NM_008054	mmu-miR-30a-5p	1	0	0	0	0	1	0	0	0	0	1	1	4

Both 3'-UTRs show good alignment over their complete length, but not all predicted binding sites are conserved between the human and murine transcript (Fig. 4.15).

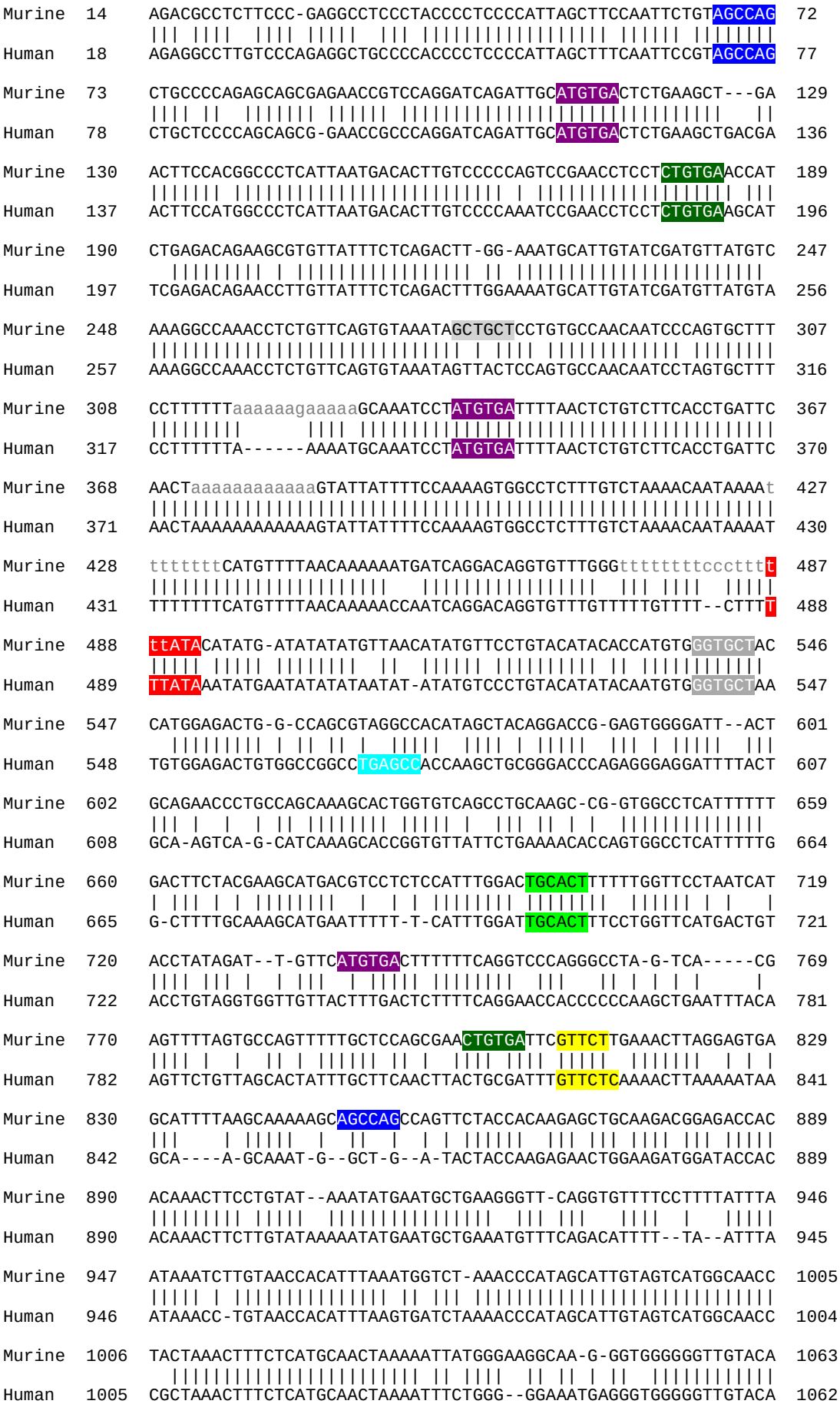
Murine 14 AGACGCCTCTTCCC-GAGGCCTCCCTACCCCTCCCCATTAGCTTCCAATTCTGTAGCCAG 72
Human 18 AGAGGCCTTGTCCCAGAGGCTGCCCCACCCCTCCCCATTAGCTTTCAATTCCGTAGCCAG 77
Murine 73 CTGCCCCAGAGCAGCGAGAACCGTCCAGGATCAGATTGCATGTGACTCTGAAGCT---GA 129
Human 78 CTGCTCCCCAGCAGCG-GAACCGCCCAGGATCAGATTGCATGTGACTCTGAAGCTGACGA 136
Murine 130 ACTTCCACGGCCCTCATTAATGACACTTGTCCCCCAGTCCGAACCTCCTCTGTGAACCAT 189
Human 137 ACTTCCATGGCCCTCATTAATGACACTTGTCCCCAAATCCGAACCTCCTCTGTGAAGCAT 196
Murine 190 CTGAGACAGAAGCGTGTTATTTCTCAGACTT-GG-AAATGCATTGTATCGATGTTATGTC 247
Human 197 TCGAGACAGAACCTTGTTATTTCTCAGACTTTGGAAAATGCATTGTATCGATGTTATGTA 256
Murine 248 AAAGGCCAAACCTCTGTTCAGTGTAAATAGCTGCTCCTGTGCCAACAATCCCAGTGCTTT 307
Human 257 AAAGGCCAAACCTCTGTTCAGTGTAAATAGTTACTCCAGTGCCAACAATCCTAGTGCTTT 316
Murine 308 CCTTTTTTaaaaaagaaaaaGCAAATCCTATGTGATTTTAACTCTGTCTTCACCTGATTC 367
Human 317 CCTTTTTTA------AAAATGCAAATCCTATGTGATTTTAACTCTGTCTTCACCTGATTC 370
Murine 368 AACTaaaaaaaaaaaaGTATTATTTTCCAAAAGTGGCCTCTTTGTCTAAAACAATAAAAt 427
Human 371 AACTAAAAAAAAAAAAGTATTATTTTCCAAAAGTGGCCTCTTTGTCTAAAACAATAAAAT 430
Murine 428 tttttttCATGTTTTAACAAAAAATGATCAGGACAGGTGTTTGGGttttttttccctttt 487
Human 431 TTTTTTTCATGTTTTAACAAAAACCAATCAGGACAGGTGTTTGTTTTTGTTTT--CTTTT 488
Murine 488 ttATACATATG-ATATATATGTTAACATATGTTCCTGTACATACACCATGTGGGTGCTAC 546
Human 489 TTATAAATATGAATATATATAATAT-ATATGTCCCTGTACATATACAATGTGGGTGCTAA 547
Murine 547 CATGGAGACTG-G-CCAGCGTAGGCCACATAGCTACAGGACCG-GAGTGGGGATT--ACT 601
Human 548 TGTGGAGACTGTGGCCGGCCTGAGCCACCAAGCTGCGGGACCCAGAGGGAGGATTTTACT 607
Murine 602 GCAGAACCCTGCCAGCAAAGCACTGGTGTCAGCCTGCAAGC-CG-GTGGCCTCATTTTTT 659
Human 608 GCA-AGTCA-G-CATCAAAGCACCGGTGTTATTCTGAAAACACCAGTGGCCTCATTTTTG 664
Murine 660 GACTTCTACGAAGCATGACGTCCTCTCCATTTGGACTGCACTTTTTTGGTTCCTAATCAT 719
Human 665 G-CTTTTGCAAAGCATGAATTTTT-T-CATTTGGATTGCACTTTCCTGGTTCATGACTGT 721
Murine 720 ACCTATAGAT--T-GTTCATGTGACTTTTTTCAGGTCCCAGGGCCTA-G-TCA-----CG 769
Human 722 ACCTGTAGGTGGTTGTTACTTTGACTCTTTTCAGGAACCACCCCCCAAGCTGAATTTACA 781
Murine 770 AGTTTTAGTGCCAGTTTTTGCTCCAGCGAACTGTGATTCGTTCTTGAAACTTAGGAGTGA 829
Human 782 AGTTCTGTTAGCACTATTTGCTTCAACTTACTGCGATTTGTTCTCAAAACTTAAAAATAA 841
Murine 830 GCATTTTAAGCAAAAAGCAGCCAGCCAGTTCTACCACAAGAGCTGCAAGACGGAGACCAC 889
Human 842 GCA----A-GCAAAT-G--GCT-G--A-TACTACCAAGAGAACTGGAAGATGGATACCAC 889
Murine 890 ACAAACTTCCTGTAT--AAATATGAATGCTGAAGGGTT-CAGGTGTTTTCCTTTTATTTA 946
Human 890 ACAAACTTCTTGTATAAAAATATGAATGCTGAAATGTTTCAGACATTTT--TA--ATTTA 945
Murine 947 ATAAATCTTGTAACCACATTTAAATGGTCT-AAACCCATAGCATTGTAGTCATGGCAACC 1005
Human 946 ATAAACC-TGTAACCACATTTAAGTGATCTAAAACCCATAGCATTGTAGTCATGGCAACC 1004
Murine 1006 TACTAAACTTTCTCATGCAACTAAAAATTATGGGAAGGCAA-G-GGTGGGGGGTTGTACA 1063
Human 1005 CGCTAAACTTTCTCATGCAACTAAAATTTCTGGG--GGAAATGAGGGTGGGGGTTGTACA 1062

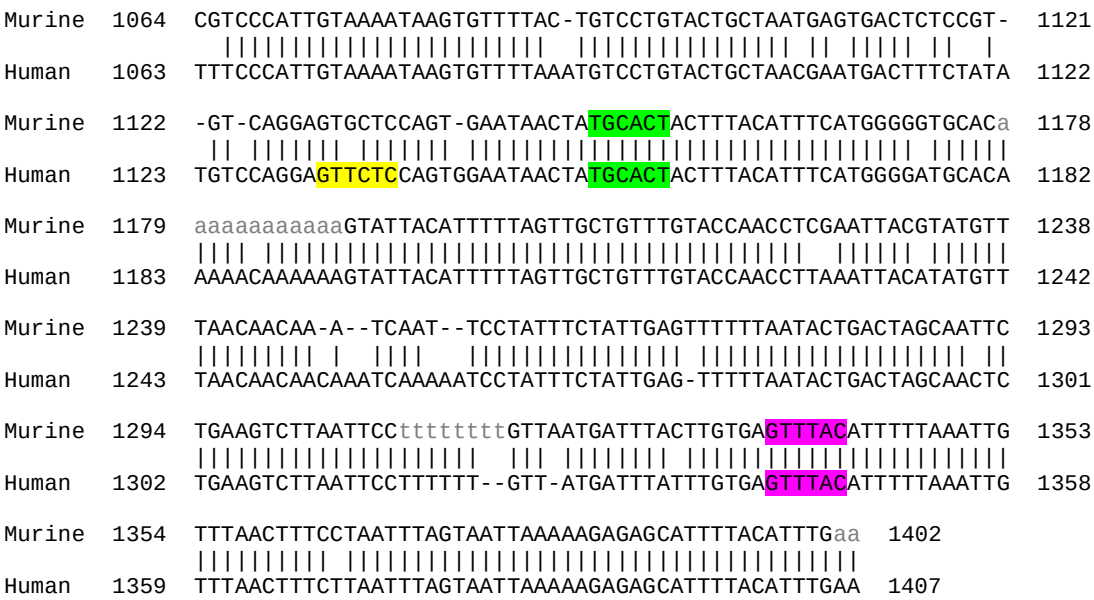

Fig. 4.15: Alignment of the 3'UTRs of longest Fyn transcripts in human (NM_002037) and mouse (NM_008054); predicted seed binding sites are indicated as follows: purple: miR-23a/b-3p; turquoise: miR-24-3p; dark green: miR-27a/b-3p; dark grey: miR-29a-c-3p; pink: miR-30a-f-5p; light green: miR-130a-3p; yellow: miR-146b-5p; blue: miR-149-5p; light grey: miR-322-3p and miR-503-5p; red: miR-340-5p

The possible binding site of the seed region of miR-30a-e-5p, miR-340-5p and two binding sites for miR-130a-3p are conserved between the two species. Additionally, two of three binding sites for miR-23a/b-3p, one of two binding sites for miR-27a/b-3p and one of two binding sites for miR-149-5p are conserved between human and mouse, while the binding site for miR-24-3p and two binding sites for miR-146b-5p are not conserved between human and mouse.

The full length 3'-UTR of the human FYN transcript length of 1,407 bp was cloned into the luciferase reporter vector (pMir-report, modified) for subsequent luciferase assay (chapter 4.6).

Nck2

The longest human and murine protein coding transcripts for Nck2, NM_003581 and NM_010879, possess a 3'-UTR of 1,098 nucleotides and 1,173 nucleotides, respectively. For both transcripts, possible miRNA interaction partners were predicted with miRWalk2 using 12 different prediction algorithms (Tab. 4.12 and 4.13).

Tab. 4.12: miRWalk2 predictions of miRNAs targeting human NCK2 3'-UTR; criterion: sum of predictions ≥4

Gene	Transcript number	Mature miRNA	miRWalk	Microt4	miRanda	mirbridge	miRDB	miRMap	miRNAMap	Pictar2	PITA	RNA22	RNAhybrid	Targetscan	Sum
NCK2	NM_003581	hsa-miR-92a-3p	1	1	0	0	0	1	0	1	0	1	1	1	7
NCK2	NM_003581	hsa-miR-92b-3p	1	1	0	0	0	1	0	1	0	1	1	1	7
NCK2	NM_003581	hsa-miR-30c-5p	1	1	0	1	0	1	0	1	0	0	1	1	7
NCK2	NM_003581	hsa-miR-30a-5p	1	1	0	0	0	1	0	1	0	0	1	1	6
NCK2	NM_003581	hsa-miR-340-5p	0	1	1	0	1	1	0	0	0	0	1	1	6
NCK2	NM_003581	hsa-miR-450b-5p	1	1	0	0	0	1	0	0	0	1	1	1	6
NCK2	NM_003581	hsa-miR-30d-5p	1	1	0	0	0	1	0	1	0	0	1	1	6
NCK2	NM_003581	hsa-miR-30b-5p	1	1	0	0	0	1	0	0	0	0	1	1	5
NCK2	NM_003581	hsa-miR-30e-5p	1	1	0	0	0	1	0	0	0	0	1	1	5
NCK2	NM_003581	hsa-miR-30c-1-3p	0	0	1	0	0	1	0	0	0	1	1	1	5
NCK2	NM_003581	hsa-miR-23a-3p	1	1	0	0	0	1	0	0	0	0	1	0	4
NCK2	NM_003581	hsa-miR-23b-3p	1	1	0	0	0	1	0	0	0	0	1	0	4
NCK2	NM_003581	hsa-miR-30c-2-3p	0	0	1	0	0	1	0	0	0	0	1	1	4
NCK2	NM_003581	hsa-miR-23c	1	1	0	0	0	1	0	0	0	0	1	0	4

Equivalent predictions were performed for the murine 3'-UTR of Nck2.

Tab. 4.13: miRWalk2 predictions of miRNAs targeting murine Nck2 3'-UTR; criterion: sum of predictions ≥4

Gene	Transcript number	Mature miRNA	miRWalk	Microt4	miRanda	mirbridge	miRDB	miRMap	miRNAMap	Pictar2	PITA	RNA22	RNAhybrid	Targetscan	Sum
Nck2	NM_010879	mmu-miR-340-5p	1	1	1	0	1	1	0	0	1	0	1	1	8
Nck2	NM_010879	mmu-miR-450b-5p	1	1	1	0	0	1	0	0	1	1	1	1	8
Nck2	NM_010879	mmu-miR-30d-5p	1	1	0	0	0	1	0	0	1	0	1	1	6
Nck2	NM_010879	mmu-miR-30a-5p	1	1	0	0	0	1	0	0	1	0	1	1	6
Nck2	NM_010879	mmu-miR-30e-5p	1	1	0	0	0	1	0	0	1	0	1	1	6
Nck2	NM_010879	mmu-miR-30b-5p	1	1	0	0	0	1	0	0	1	0	1	1	6
Nck2	NM_010879	mmu-miR-30c-5p	1	1	0	0	0	1	0	0	1	0	1	1	6
Nck2	NM_010879	mmu-miR-196b-5p	1	0	0	0	0	1	0	0	1	0	1	1	5
Nck2	NM_010879	mmu-miR-23a-3p	1	1	0	0	0	1	0	0	1	0	1	0	5
Nck2	NM_010879	mmu-miR-23b-3p	1	1	0	0	0	1	0	0	1	0	1	0	5
Nck2	NM_010879	mmu-miR-27a-3p	1	0	0	0	0	0	0	0	1	1	1	0	4
Nck2	NM_010879	mmu-miR-503-5p	0	0	0	0	0	1	0	0	1	1	1	0	4
Nck2	NM_010879	mmu-miR-27b-3p	1	0	0	0	0	0	0	0	1	1	1	0	4
Nck2	NM_010879	mmu-miR-148a-3p	0	1	0	0	0	1	0	0	1	0	1	0	4

The 3'-half of the 3'-UTRs of the full length transcripts of human and mouse show good alignment over the whole length, but not all predicted binding sites are conserved between the human and murine transcript.

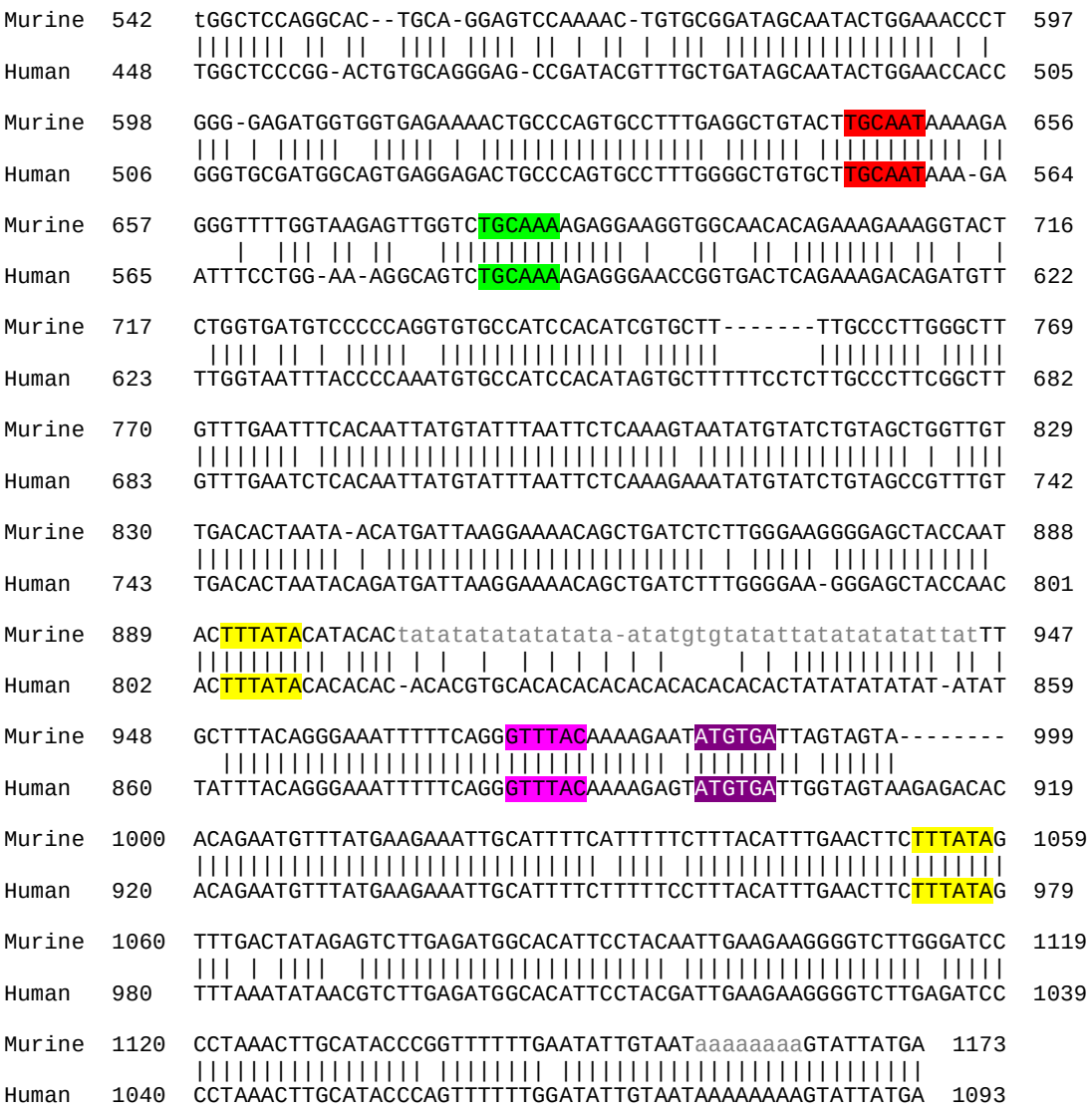

Fig. 4.16: Alignment of the 3'UTRs of longest Nck2 transcripts in human (NM_003581) and mouse (NM_010879); predicted seed binding sites are indicated as follows: purple: miR-23a/b-3p; pink: miR-30a-f-5p; red: miR-92a/b-3p; yellow: miR-340-5p; green: miR-450b-5p;

Binding sites for miR-23a/b-3p, miR-30a-e-5p, miR-340-5p and miR-450b-5p are conserved between both transcripts. A binding site for miR-92a/b-3p seems to be preserved in the sequences, but is not predicted for the murine transcript. The full length human 3'-UTR of 1,098 bp was cloned into the luciferase reporter vector (pMir-Report, modified) for subsequent luciferase assay (chapter 4.7).

Neph1

The 3'-UTR of the longest human protein coding transcript of NEPH1, also known as KIRREL, (NM_001286349) consists of 5,141 nucleotides and shows a good overlap with the 3'-UTR of the murine protein coding transcript, NM_130867. The 3'-UTR of a shorter human protein coding

transcript, NM_018240, corresponds to the first 533 nucleotides of the longer human transcript. For *in silico* predictions, the shorter human 3'-UTR was used (Tab. 4.14 and 4.15).

Tab. 4.14: miRWalk2 predictions of miRNAs targeting human NEPH1/KIRREL; criterion: sum of predictions ≥4

Gene	Transcript number	Mature miRNA	miRWalk	Microt4	miRanda	mirbridge	miRDB	miRMap	miRNAMap	Pictar2	PITA	RNA22	RNAhybrid	Targetscan	Sum
KIRREL	NM_018240	hsa-miR-29a-3p	1	1	1	0	0	1	0	1	1	1	1	1	9
KIRREL	NM_018240	hsa-miR-30c-1-3p	1	1	1	0	1	1	0	0	0	1	1	1	8
KIRREL	NM_018240	hsa-miR-29b-3p	0	1	1	0	0	1	0	1	1	1	1	1	8
KIRREL	NM_018240	hsa-miR-29c-3p	0	1	1	0	0	1	0	1	1	1	1	1	8
KIRREL	NM_018240	hsa-miR-149-5p	1	1	0	0	0	1	0	1	1	1	1	1	8
KIRREL	NM_018240	hsa-miR-30c-2-3p	1	1	1	0	0	1	0	0	0	1	1	1	7
KIRREL	NM_018240	hsa-miR-27a-3p	1	1	0	0	0	1	0	0	1	1	1	0	6
KIRREL	NM_018240	hsa-miR-107	0	1	0	0	0	1	0	0	1	1	1	1	6
KIRREL	NM_018240	hsa-miR-27b-3p	1	1	0	0	0	1	0	0	1	1	1	0	6
KIRREL	NM_018240	hsa-miR-30b-3p	0	1	1	0	0	1	0	0	0	1	1	1	6
KIRREL	NM_018240	hsa-miR-24-3p	0	1	0	0	0	1	0	0	1	1	1	0	5
KIRREL	NM_018240	hsa-miR-148a-3p	0	1	0	0	0	1	0	0	1	1	1	0	5
KIRREL	NM_018240	hsa-miR-210-3p	0	1	0	0	0	1	0	0	0	1	1	0	4
KIRREL	NM_018240	hsa-miR-450b-5p	0	1	0	0	0	1	0	0	0	1	1	0	4
KIRREL	NM_018240	hsa-miR-130a-3p	0	0	0	0	0	1	0	0	1	1	1	0	4

Equivalent predictions were performed for the murine 3'-UTR of Neph1.

Tab. 4.15: miRWalk2 predictions of miRNAs targeting murine Neph1/Kirrel; criterion: sum of predictions ≥4

Gene	Transcript number	Mature miRNA	miRWalk	Microt4	miRanda	mirbridge	miRDB	miRMap	miRNAMap	Pictar2	PITA	RNA22	RNAhybrid	Targetscan	Sum
Kirrel	NM_130867	mmu-miR-107-3p	1	0	1	0	1	1	0	0	0	0	1	1	6
Kirrel	NM_130867	mmu-miR-29b-3p	1	0	1	0	0	1	0	0	1	0	1	1	6
Kirrel	NM_130867	mmu-miR-29c-3p	1	0	1	0	0	1	0	0	1	0	1	1	6
Kirrel	NM_130867	mmu-miR-351-5p	1	0	1	0	0	1	0	0	1	0	1	1	6
Kirrel	NM_130867	mmu-miR-29a-3p	1	0	1	0	0	1	0	0	1	0	1	1	6
Kirrel	NM_130867	mmu-miR-30b-3p	1	0	1	0	0	1	0	0	0	0	1	1	5
Kirrel	NM_130867	mmu-miR-30e-5p	1	0	1	0	0	1	0	0	0	0	1	1	5
Kirrel	NM_130867	mmu-miR-23a-3p	1	0	1	0	0	1	0	0	0	0	1	1	5
Kirrel	NM_130867	mmu-miR-27b-3p	1	0	1	0	0	1	0	0	0	0	1	1	5
Kirrel	NM_130867	mmu-miR-30b-5p	1	0	1	0	0	1	0	0	0	0	1	1	5
Kirrel	NM_130867	mmu-miR-30f	1	0	1	0	0	1	0	0	0	0	1	1	5
Kirrel	NM_130867	mmu-miR-30c-1-3p	1	0	1	0	0	1	0	0	0	0	1	1	5
Kirrel	NM_130867	mmu-miR-322-3p	1	0	1	0	0	1	0	0	0	0	1	1	5
Kirrel	NM_130867	mmu-miR-340-5p	1	0	1	0	0	1	0	0	0	0	1	1	5
Kirrel	NM_130867	mmu-miR-23b-3p	1	0	1	0	0	1	0	0	0	0	1	1	5
Kirrel	NM_130867	mmu-miR-30c-2-3p	1	0	1	0	0	1	0	0	0	0	1	1	5
Kirrel	NM_130867	mmu-miR-30c-5p	1	0	1	0	0	1	0	0	0	0	1	1	5
Kirrel	NM_130867	mmu-miR-30d-3p	1	0	1	0	0	1	0	0	0	0	1	1	5
Kirrel	NM_130867	mmu-miR-30a-3p	1	0	1	0	0	1	0	0	0	0	1	1	5
Kirrel	NM_130867	mmu-miR-30d-5p	1	0	1	0	0	1	0	0	0	0	1	1	5
Kirrel	NM_130867	mmu-miR-27a-3p	1	0	1	0	0	1	0	0	0	0	1	1	5
Kirrel	NM_130867	mmu-miR-30a-5p	1	0	1	0	0	1	0	0	0	0	1	1	5
Kirrel	NM_130867	mmu-miR-30e-3p	1	0	1	0	0	1	0	0	0	0	1	1	5
Kirrel	NM_130867	mmu-miR-196b-5p	1	0	1	0	0	1	0	0	0	0	1	1	5
Kirrel	NM_130867	mmu-miR-542-3p	1	0	1	0	0	1	0	0	0	0	1	1	5
Kirrel	NM_130867	mmu-miR-149-5p	1	0	0	0	0	1	0	0	0	0	1	1	4
Kirrel	NM_130867	mmu-miR-148a-3p	1	0	0	0	0	1	0	0	0	0	1	1	4
Kirrel	NM_130867	mmu-miR-24-1-5p	1	0	0	0	0	1	0	0	0	0	1	1	4
Kirrel	NM_130867	mmu-miR-24-2-5p	1	0	0	0	0	1	0	0	0	0	1	1	4
Kirrel	NM_130867	mmu-miR-24-3p	1	0	0	0	0	1	0	0	0	0	1	1	4

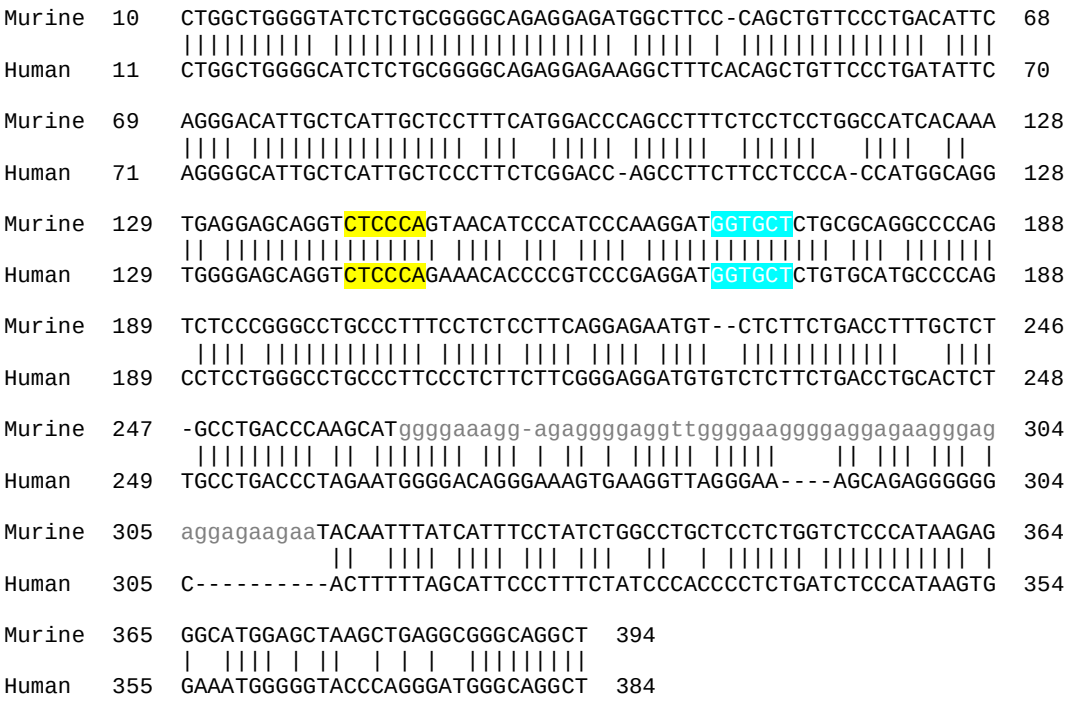

Fig. 4.17: Alignment of the 3'-UTR of Neph1 transcripts in human (NM_018240) and mouse (NM_130867); predicted binding sites; turquoise: miR-29a-c-3p; yellow: miR-30b/c-3p;

A binding site for miR-29a-c-3p as well as a minding site for miR-30b/c-3p is conserved between the human and the murine transcript. The 3'-UTR of the human protein coding transcript of NEPH1 with a length of 533 bp, NM_018240, was cloned into the luciferase reporter vector (pMir-Report, modified) for subsequent luciferase assay (chapter 4.7).

4.5 Argonaute immunoprecipitation (Ago-IP) applied for target identification

To analyze mRNAs that are targeted by miRNAs *in vivo*, Ago-IP (Argonaute immunoprecipitation) was established to isolate the regulated mRNAs from the RISCs.

4.5.1 Ago-IP using hPCLs and subsequent target detection by qPCR

The first Ago-IP was performed using proliferating human podocytes. The targets isolated by Ago-IP were identified by qPCR.

To confirm the specificity of the used primer for the predicted targets, PCR was performed with cDNA generated from RNA isolated from proliferating human podocytes. The PCR products were isolated by agarose gel electrophoresis and subsequently sequenced. For all primer pairs used, the identity of the amplified targets could be validated (Tab. 10.3).

To verify targets predicted to be regulated by miRNAs in human podocytes, three independent Ago-IP experiments were performed from proliferating hPCLs (M. Billmeier) according to 3.6.2. The Ago-IPs were performed using ca. 75 millions of proliferating hPCLs per experiment.

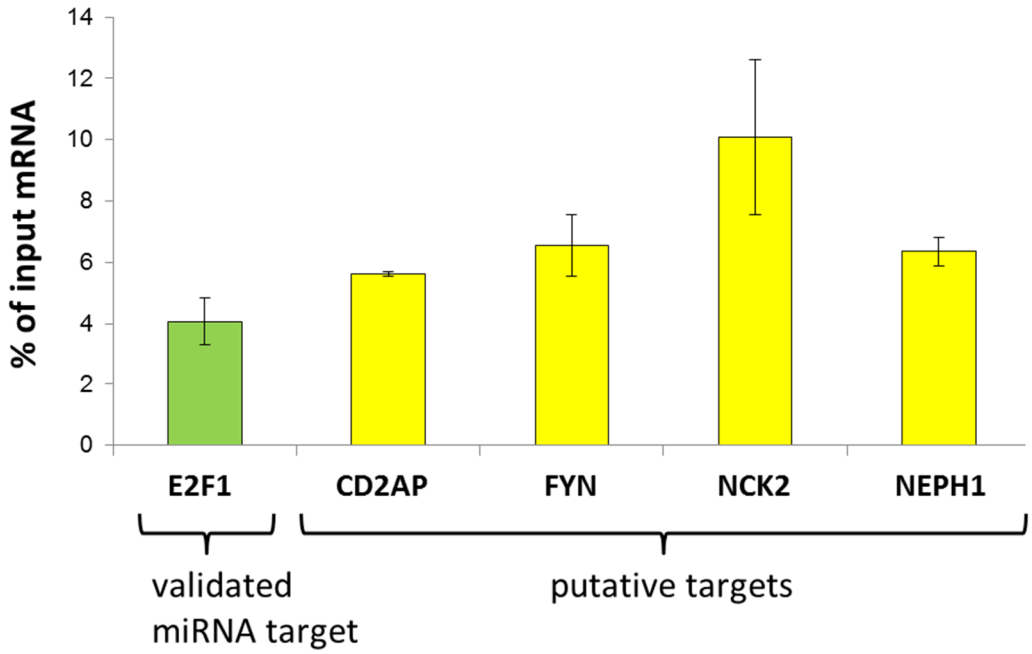

Fig. 4.18: Ago-IP from proliferating hPCLs; enrichment of transcript in the IP sample compared to the control antibody sample, enrichment referring to the input; data of 3 independent experiments

In the Ago-IP from hPCLs, the validated miRNA target E2F1 (personal communication G. Meister), a transcription factor belonging to the E2F family, could be identified to be enriched in the Ago-IP sample compared to the control antibody background. The four mRNAs predicted to be potential miRNA targets, CD2AP, FYN, NCK2 and NEPH1 could be identified to be Ago2 bound as well.

4.5.2 Ago-IP using mPCLs and subsequent target identification by qPCR

Before the Ago-IP from freshly isolated murine podocytes, preliminary experiments using the immortalized murine podocyte cell line were performed.

Testing of α-mAgo2 antibody

Before Ago-IP was performed from freshly isolated murine podocytes, the antibody was tested with lysates from proliferating mPCLs. 50 µl cell lysate (β = 3.1 µg/µl) of total protein was compared with the same amount of supernatant after Ago-IP. A faint band of ca. 100 kDa indicated a low expression of Ago2 protein in the mPCLs. As the band was not detectable in the supernatant after IP, this proved the functionality of the α-Ago2 antibody (Fig. 4.19 A). To confirm the binding of the Ago2 protein to the antibody coupled beads, the protein bound to the

beads was extracted and also investigated by Western Blotting. This time, Ago2 protein could neither be detected in 50 µl of the lysate (β = 3.4 µg/µl) nor in the supernatant after IP, but a very strong signal was detected in the sample derived from the beads, indicating that the Ago2 protein present in the lysate was bound to the beads (Fig. 4.19 B). Since Ago2 protein was hard to detect in mPCLs, mPCL lysates were compared to lysates of N2A cells, a murine brain neuroblastoma cell line known to express Ago2 protein in high amounts (N2A lysate was a kind gift of D. Hasler, Department of Biochemistry I, University of Regensburg; N2A lysis buffer: 50 mM Tris/HCl (pH = 8.0), 150 mM NaCl, 5% glycerol, 0.1% Tween20). Using 170 µg of total protein, Ago2 could be detected in high amount in the N2A cell lysate, but practically not in the mPCL lysate (Fig. 4.19 C), confirming a low level of Ago2 in mPCLs.

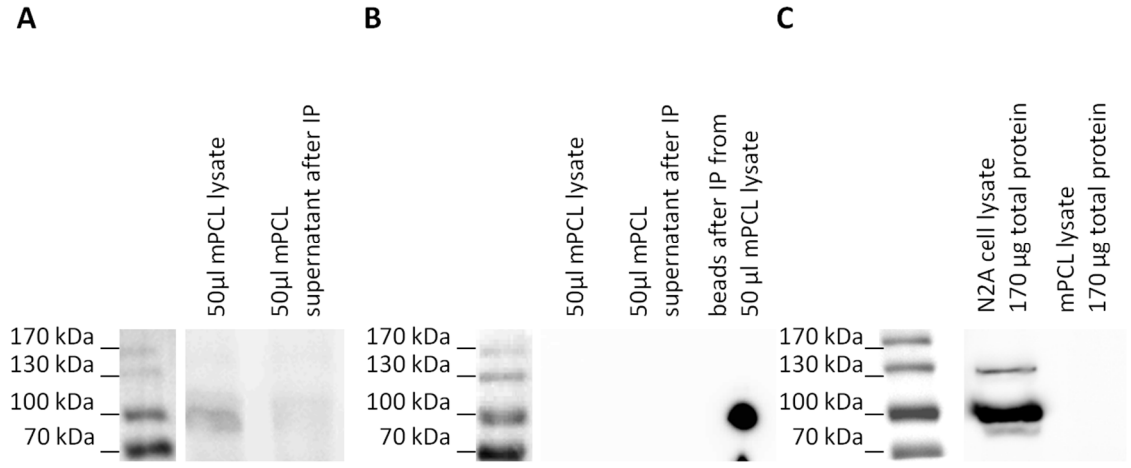

Fig. 4.19: α-Ago2 Western Blot with lysates from mPCLs and N2A cells; (A) α-Ago2 Western Blot of mPCL cell lysate before and after IP with α-Ago2 coupled beads; (50 µl mPCL lysate=155 µg total protein before IP) (B) α-Ago2 Western Blot of mPCL cell lysate before and after IP with α-Ago2 coupled beads, and α-Ago2 coupled beads after IP; (50 µl lysate=170 µg total protein before IP per lane); (C) α-Ago2 Western Blot of mPCL cell lysate and N2A cell lysate; 170 µg total protein/lane

Taken together, it could be shown that Ago2 is expressed in proliferating mPCLs (Fig. 4.17 A), but at low levels compared to N2A cells (Fig. 4.17 C). Nevertheless, it is extensively bound by the α-Ago2 coupled beads (Fig. 4.18 B), enabling extraction of RISCs from murine cells.

Ago-IP using mPCLs

The targets isolated by Ago-IP were identified by qPCR. To confirm the specificity of the used primer for the predicted targets, PCR was performed with cDNA generated from RNA isolated from proliferating mPCL cells. The PCR products were isolated by agarose gel electrophoresis and sequenced. For all primer pairs used, the identity of the amplified targets could be validated

(Tab. 10.4). Ago-IP was performed from five million proliferating mPCLs as described previously. The enrichment of the predicted targets was analyzed by subsequent qPCR (Fig. 4.20).

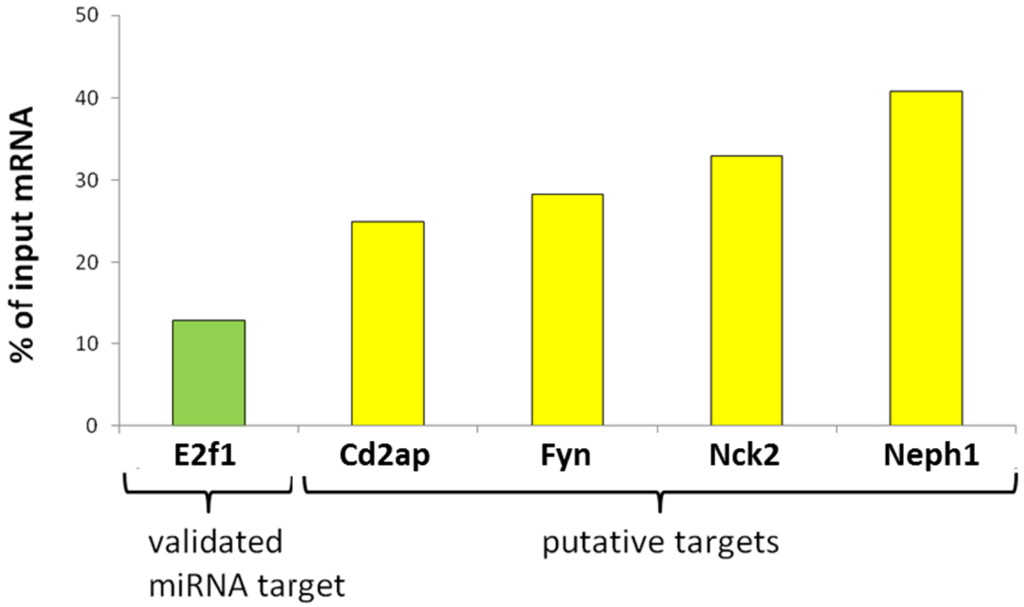

Fig. 4.20: Ago-IP from proliferating mPCLs; enrichment of possible target mRNAs in Ago-IP above control antibody background; analyses by qPCR

The Ago-IP from five million proliferating mPCLs yielded enough RNA for the qPCR analyses of five targets. The validated miRNA target E2f1 could be detected as enriched in the Ago bound sample. All four putative miRNA targets, Cd2ap, Fyn, Nck2 and Neph1 could be measured to be clearly enriched above the background, hinting them to be miRNA regulated targets in proliferating mPCLs as well.

4.5.3 Ago-IP using freshly isolated murine podocytes and analysis using microarray

For a focused approach to identify miRNA regulated targets in podocytes under physiological conditions, Ago-IP was performed using isolated green podocytes freshly isolated from double fluorescent reporter mice (*mTmG x P2.5 Cre*, chapter 4.3).

In total, 6.5 million green podocytes were isolated from 39 male *mTmGxP2.5Cre* mice aged between 16 and 30 weeks. The Ago-IP was performed according to the protocol in chapter 3.6.3. The RNA of miRNA targets in podocyte was isolated from the α-Ago2 coupled beads, while the RNA isolated from the rabbit IgG coupled beads served as a background control. The two isolated RNA samples were analyzed on a murine GeneChiP-Array (Mouse Transcriptome Array, Gen2.0/2.1ST, Affymetrix) at the Center of Excellence for Fluorescent Bioanalytics (Biopark, University of Regensburg).

The enrichment of mRNAs of transcripts in the Ago2 bound sample in relation to the sample isolated from IgG coupled beads, was calculated. In total, 425 transcripts were enriched more than 2-fold in the Ago2 bound sample, 23 of which were enriched more than 10-fold. Additionally, the enrichment of transcripts in the Ago2 bound sample generated from podocytes compared to their enrichment in the red fluorescent cell population was calculated. A total of 262 transcripts were found to be enriched more than 2-times in podocytes, with one transcript being enriched more than 10-fold in the podocyte sample. Both lists were analyzed for mRNAs coding for proteins known to be important directly for kidney structure.

Tab. 4.16: miRNA targets isolated in Ago-IP from murine podocytes; genes important for filtration function with enrichment above background ≥2 (bold); grey: enrichment factors <2

Gene Symbol	Gene Description	Annotated Gene Accession number	Fold Change	
			Podocytes α-Ago2 vs Podocytes IgG	Podocytes α-Ago2 vs "red cells" α-Ago2
Actg1	Actin, gamma, cytoplasmic 1	BC018571	**5.61**	**3.99**
Podxl	Podocalyxin-like	AK134723	**4.26**	**3.59**
Itgb1	Integrin beta 1 (fibronectin receptor beta)	AK076526	**3.55**	**2.94**
Vegfa	Vascular endothelial growth factor A	AY120866	**3.34**	**2.27**
Cd2ap	CD2-associated protein	AK045218	**2.58**	1.99
Nphs2	Nephrosis 2 homolog, podocin	AK052746	**2.51**	**2.40**
Fyn	Fyn proto-oncogene	AK156584	**2.23**	**2.34**
Actbl2	Actin, beta-like 2	AK029110	**2.20**	1.88
Itgb5	Integrin beta 5	AK087476	**2.20**	**2.35**
Wipf3	WAS/WASL interacting protein family, member 3	BC044880	1.54	**2.40**

These results represent preliminary data, as only one hybridisation was performed so far. The experiment will be repeated with independent murine samples.

4.6 Luciferase assay for confirmation of predicted miRNA-mRNA pairs

To check for possible interaction of miRNAs with the 3'-UTRs of the target genes, luciferase assays were performed. HEK293T cells were transfected with two plasmids. One plasmid, a

modified pMir-Report construct (pMir-Report modified, life technologies/G. Meister) coded for a firefly luciferase containing the 3'-UTR of the possible target genes and a renilla luciferase as an untargeted control. The second plasmid, a pSuper construct were the ampicillin resistance was exchanged for a kanamycin resistance (pSuper modified, oligoengine/G. Meister) contained a shRNA precursor for a miRNA predicted to be a possible regulator of the respective gene.

To be sure that the candidate miRNA is present in sufficient amount in the cells, luciferase assays were performed with a parallel overexpression of the miRNA of interest. The control cells were transfected with pSuper construct overexpressing the CXCR4 control sequence (Ebert et al. 2007) to provide comparable environments in both samples.

A paired student's t-test was performed using the results to identify regulative pairs of miRNAs and mRNAs. P-values were calculated over the five repetitions of each combination of target gene and miRNA compared to the respective control.

Transfection of HEK293T cells

To test for transfection efficiency, HEK293T cells were transfected using a control plasmid coding for d2eGFP (Destabilized enhanced green fluorescent protein). The transfection efficiency was controlled by fluorescence microscopy (Fig. 4.21).

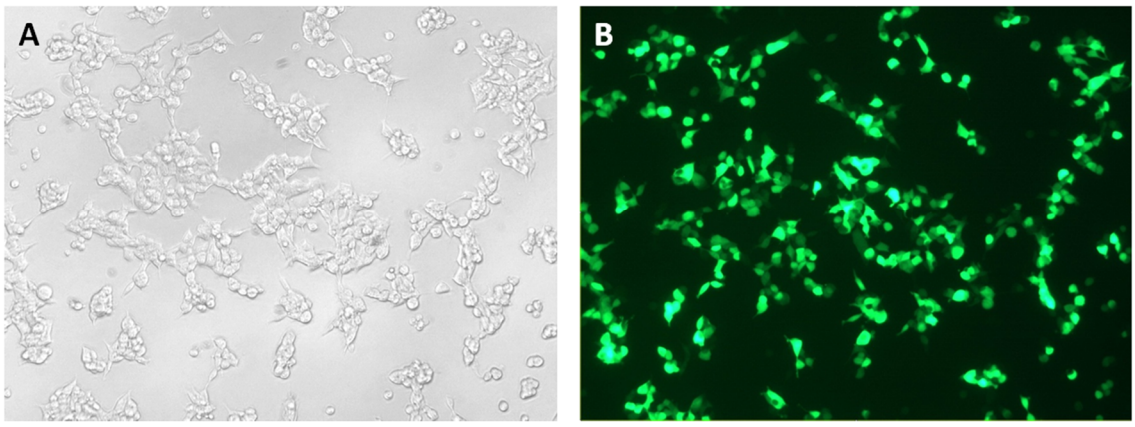

Fig 4.21: Transfection efficiency test using HEK293T cells; plasmid transfected: empty sponge control plasmid coding for d2eGFP (Ebert et al. 2007)

The control transfection showed very good and also very stable transfection efficiency. In every luciferase experiment, a transfection control with the eGFP (Enhanced green fluorescent protein) coding plasmid was performed to monitor transfection efficiencies. The high transfection rate was reproducible in every single experiment.

CD2AP

For the CD2AP luciferase assay, the c-terminal part of the 3'-UTR of the human CD2AP gene, consisting of 606 bp (chapter 4.4), was cloned into the modified pMir-Report luciferase construct. The luciferase construct was used to co-transfect HEK293T cells together with respective pSuper constructs either overexpressing the control sequence (green bars) or a functional miRNA. The overexpression of miR-27b-3p and miR-29a-3p did not seem to have an effect on the expression of the targeted luciferase, while a reduction of luminescence ratio to values between 60% and 84% (70%, 67%, 72%,84% and 60%) compared to the control conditions could be measured when cotransfecting with the pSuper construct overexpressing miR-92a-3p.

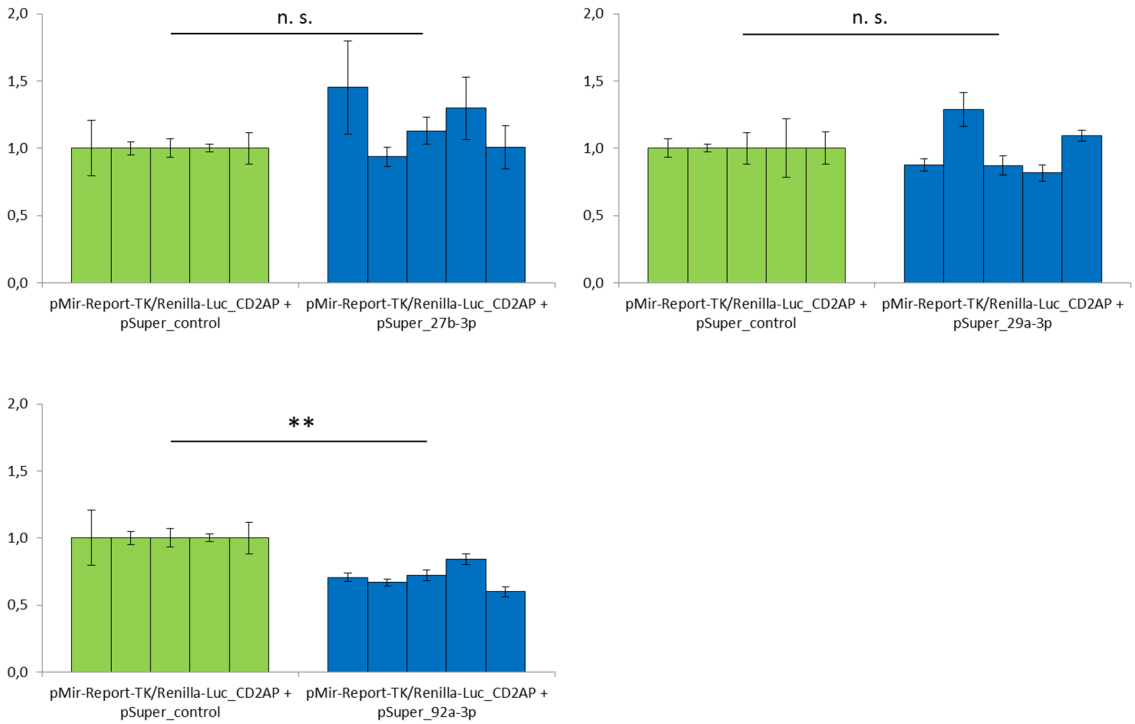

Fig. 4.22: Luciferase assay using 3'-end of human CD2AP-3'-UTR, screening for putative regulatory miRNAs: cotransfection of luciferase containing the 3'-end of the CD2AP 3'-UTR with pSuper constructs overexpressing a control sequence (green bars), miR-27b-3p, miR-29a-3p or miR-92a-3p, respectively (blue bars); n.s. not significant; **: $p < 0.01$; p-values for five repetitions of experiment compared to the control

To confirm binding of miR-92a-3p to the binding site which was predicted consistently by the prediction algorithms at the 3'-UTR positions 2,660-2,665, it was destroyed by mutating the positions 2, 4 and 6 in the binding region of the miRNA seed region. The luciferase reporter constructs containing the wildtype 3'-UTR or the 3'-UTR with the mutated binding site were cotransfected with the pSuper constructs overexpressing the control sequence or miR-92a-3p (Fig. 4.23).

The first notable result is the reduced reduction of luciferase intensity of the wildtype construct by coexpression of miR-92a-3p, showing the varying results between several experiments. Only a slight, but not significant reduction of luciferase activity could be measured (95%, 103%, 93%, 88% and 85%), while the overexpression of the control sequence or miR-92a-3p did not have an effect on the luciferase containing the 3'-UTR harboring the mutated miR-92a/b-3p binding site. In conclusion, it seems like the co-expression of miR-92a-3p has a repression effect on the luciferase containing the wildtype CD2AP 3'-UTR, but the results of different experiments differ due to the biological variability between the single experiments. The mutation of the assumed binding site has no effect on the luciferase intensity, which might prove the functionality of the predicted binding site.

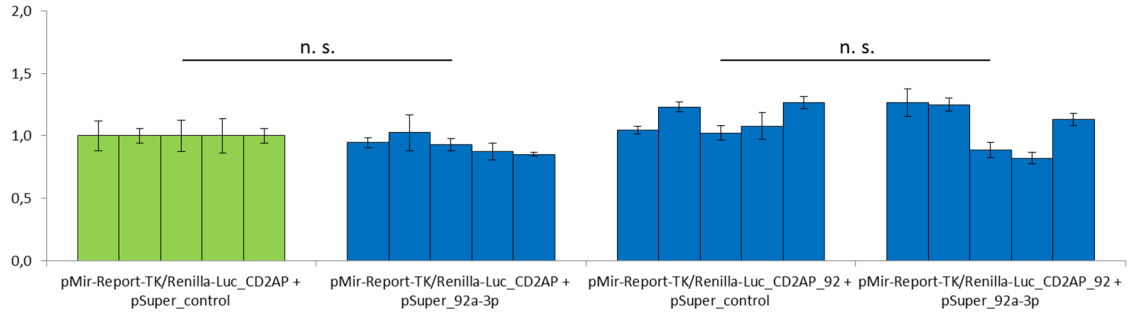

Fig. 4.23: Luciferase assay using 3'-end of human CD2AP-3'-UTR and miR-92a/b-3p: cotransfection of luciferase containing either CD2AP wildtype 3'-UTR or CD2AP 3'-UTR with mutated miR-92a-3p binding site together with pSuper constructs coding for control sequence or miR-92a-3p; n.s. not significant; p-values for five repetitions of experiment compared to the control

Additionally, miR-30a-5p was checked for targeting of CD2AP. In the predicted binding site of the seed region of miR-30a-5p in the 3'-UTR, positions 2,844-2,849, the positions 2, 4 and 6 were mutated to destroy the binding site of the seed region. The wildtype 3'-UTR construct as well as the mutated construct were used to cotransfect HEK293T cells together with either a pSuper construct overexpressing the control sequence or the mature miR-30a-5p.

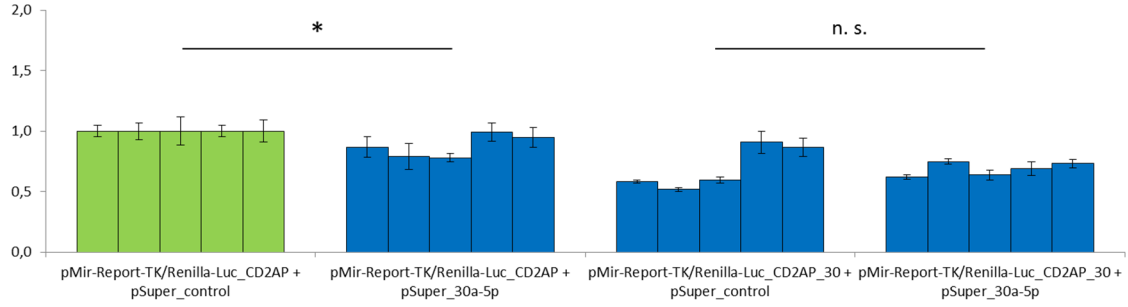

Fig. 4.24: Luciferase assay using 3'-end of human CD2AP-3'-UTR and miR-30a-e-5p; cotransfection of luciferase containing either CD2AP wildtype 3'-UTR or CD2AP 3'-UTR with mutated miR-30a-3p binding site together with pSuper constructs coding control sequence or for miR-30a-5p; n.s. not significant; *: $p < 0.05$; p-values for five repetitions of experiment compared to the control

It could be shown that an overexpression of the mature miR-30a-5p leads to a reduction of the luminescence intensity of the luciferase construct containing the wildtype 3'-UTR to values between 79% and 99% (87%, 79%, 78%, 99% and 95%) compared to the cotransfection with the pSuper construct expressing the control sequence (Fig. 4.24). When cotransfected with the mutated construct lacking the binding site, the coexpression of miR-30a-5p does not influence the intensity of the targeted luciferase compared to coexpression with the control sequence. This shows that the predicted binding site seems to be active and accessible for miR-30a-5p.

Taken together, these results hint that human CD2AP might be regulated by miR-30a-5p as well as miR-92a-3p in the cell.

FYN

For the FYN luciferase assay, the whole 3'-UTR of the longest human FYN transcript, consisting of 1407 bp (chapter 4.4), was cloned into the modified pMir-Report luciferase construct. The luciferase construct was used to co-transfect HEK293T cells together with respective pSuper constructs either overexpressing the control sequence (green bars) or a functional miRNA (blue bars) (Fig.4.25).

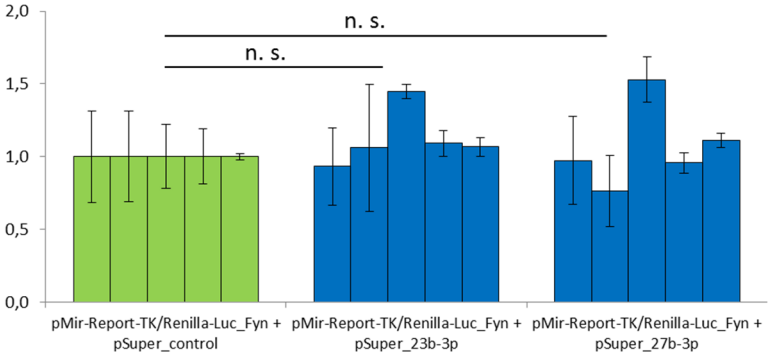

Fig. 4.25: Luciferase assay using complete human FYN-3'-UTR, screening for putative regulatory miRNAs: cotransfection of luciferase containing FYN 3'-UTR together with pSuper constructs coding for control sequence (green bars), miR-23b-3p or miR-27b-3p, respectively (blue bars); n.s. not significant; p-values for five repetitions of experiment compared to the control

The overexpression of miR-23b-3p and miR-27b-3p did not seem to have an effect on the expression of the targeted luciferase, meaning that the predicted binding sites are not functional under these conditions.

Additionally, possible targeting of miR-130a-3p and miR-146b-5p was investigated (Fig. 4.26) by coexpressing either the control sequence (green bars) or the pSuper constructs coding for the mature miRNAs (blue bars).

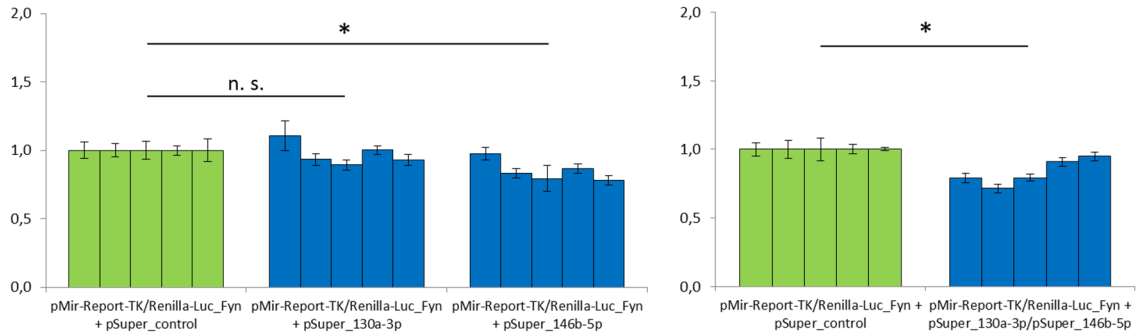

Fig. 4.26: Luciferase assay using complete human FYN-3'-UTR, screening for putative regulatory miRNAs and putative cooperative regulation: cotransfection of luciferase containing Fyn 3'-UTR with pSuper constructs coding for control sequence (green bars) or miR-130a-3p or miR-146b-5p, respectively (blue bars, left) or miR-130a-3p and miR-146b-5p (blue bars, right); n.s. not significant; *: $p < 0.05$; p-values for five repetitions of experiment compared to the control

The overexpression of miR-130a-3p did not have a reproducible effect on the expression of the targeted luciferase, while coexpression of miR-146b-5p lead to a reproducible reduction of luciferase activity to intensity values of 78% to 97% (97%, 83%, 80%, 87% and 78%) of the control intensity. This indicates a specific interaction between the human 3'-UTR of FYN and miR-146b-5p.

Since the 3'-UTR of human FYN contains two predicted binding sites for miR-130a-3p as well as for miR-146b-5p, and the two miRNAs might have a cooperative effect, the luciferase construct containing the wildtype 3'-UTR of human FYN was cotransfected with a mixture of pSuper constructs overexpressing miR-130a-3p and miR-146b-5p. The reduction caused by the cotransfection of pSuper_130a-3p and pSuper_146b-5p to values between 71% and 95% (79%, 71%, 79% 91% and 95%; Fig. 4.26 right) compared to the control sequence was similar to the reduction caused by the miR-146b-5p alone.

Taken together, FYN seems to be regulated by miR-146b-5p in human cells. The putative regulation of FYN by miR-146b-5p was further investigated using a luciferase construct harboring the FYN 3'-UTR with mutated miR-146b-5p binding sites (bachelor thesis K. Heizler). The reduction is lost when either of the miR-146b-5p binding sites is mutated. This will be further investigated with a construct with both binding sites mutated.

NCK2

For the NCK2 luciferase assay, the whole 3'-UTR of the longest human protein coding transcript, consisting of 1,098 bp (chapter 4.4), was cloned into the modified pMir-Report luciferase construct. The luciferase construct was used to co-transfect HEK293T cells together with pSuper constructs either overexpressing the control sequence (green bars) or a functional miRNA. The

overexpression of miR-23b-3p and miR-92a-3p does not have a big effect on the expression of the targeted luciferase, while miR-30a-5p causes a reduction to values between 73% and 98% (88%, 98%, 88%, 73% and 77%) compared to the control sequence. Compared to the other luciferase assays, the experiment showed higher standard deviations, making it harder to register reductions of luciferase activity (Fig. 4.27).

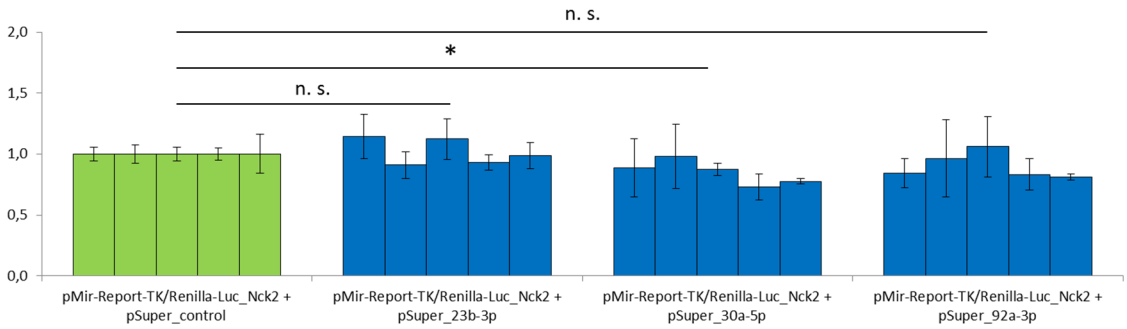

Fig. 4.27: Luciferase assay using complete human NCK2-3'-UTR, screening for putative regulatory miRNAs: cotransfection of luciferase containing Nck2 3'-UTR with pSuper constructs coding for control sequence (green bars) or miR-23b-3p, miR-30a-5p or miR-92a-3p, respectively (blue bars); n.s. not significant; *: $p < 0.05$; p-values for five repetitions of experiment compared to the control

Since coexpression of miR-30a-5p shows a reduction of luciferase intensity, a possible binding might be investigated more closely by mutating the putative binding site in the 3'-UTR.

NEPH1

For the NEPH1 luciferase assay, the 3'-UTR of the human protein coding transcript NM_018240, consisting of 533 bp (chapter 4.4), was cloned into the modified pMir-Report luciferase construct. The luciferase construct was used to co-transfect HEK293T cells together with pSuper constructs either overexpressing the control sequence (green bars) or the mature miR-29a-3p.

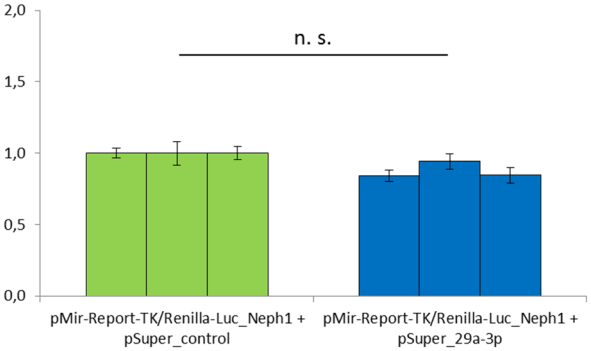

Fig. 4.28: Luciferase assay using human NEPH1-3'-UTR, investigating miR-29a-3p regulation; cotransfection of luciferase containing NEPH1 3'-UTR with pSuper construct coding for control sequence (green bars) or miR-29a-3p (blue bars); n.s. not significant; p-values for three repetitions of experiment compared to the control

Coexpression of miR-29a-3p lead to a small, but reproducible reduction of luciferase activity of luciferase containing the NEPH1 3'-UTR to values between 84% and 94% (84%, 94% and 85%) compared to the control sequence (Fig. 4.28).

The predicted miR-29a-c-3p binding site at the positions 167-172 was mutated by exchange of 3 bases at the positions 2, 4 and 6 of the predicted seed binding site. The constructs containing the wildtype 3'-UTR or the 3'-UTR with the mutated binding site were cotransfected with the pSuper constructs overexpressing the control sequence or miR-29a-3p.

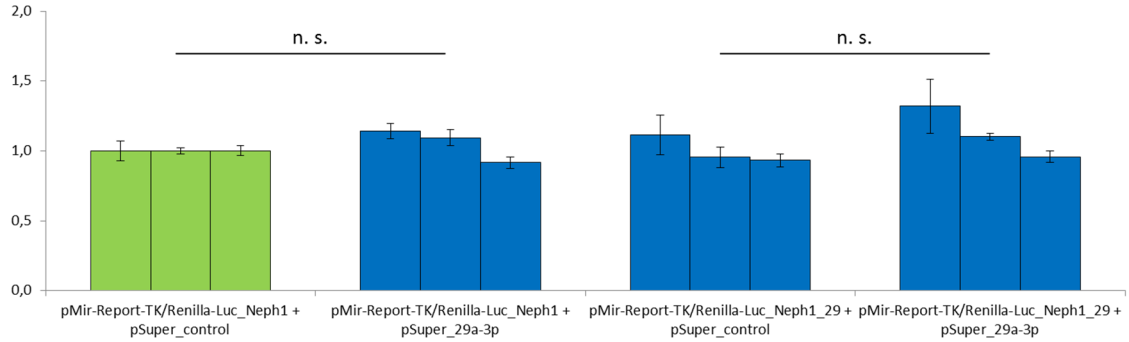

Fig. 4.29: Luciferase assay using human NEPH1 3'-UTR, investigating miR-29a-3p regulation: cotransfection of luciferase containing either NEPH1 wildtype 3'-UTR or NEPH1 3'-UTR with mutated miR-29a-3p binding site with pSuper constructs coding for control sequence or miR-29a-3p; n.s. not significant; p-values for three repetitions of experiment compared to the control

The small reduction of luciferase activity by coexpression of miR-29a-3p that was detected in earlier experiments could not be reproduced in these experiments. Furthermore, the overexpression of miR-29a-3p seemed to have no influence on the luciferase construct with the 3'-UTR containing the mutated binding sites (Fig. 4.29).

Taken together, these results suggest that if there is a regulation of Neph1 by miR-29a-3p, the effect is rather small.

4.7 Sponge constructs for miRNA knockdown

One possibility for functional analysis of mature miRNAs in cell culture and *in vivo* is the downregulation of their levels. Competitive inhibitors, so-called "sponges", were designed to target miRNA families known to be expressed in high levels in murine podocytes. The miRNA families miR-23-3p, miR-27-3p, miR-29-3p and miR-92-3p as well as the mature miRNA miR-24-3p, all highly expressed in murine podocytes, were chosen as a candidate set.

Detection of studied miRNAs in hPCLs by Northern Blotting

Since the sponge constructs were to be tested for functionality in proliferating hPCLs, expression of the target miRNAs in was checked by Northern Blotting. For each mature miRNA, 10 µg of total RNA was analyzed.

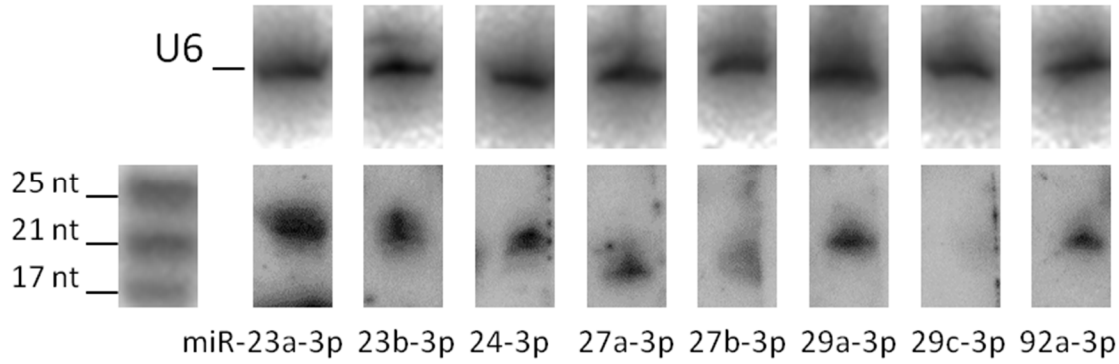

Fig. 4.30: Northern Blotting of sponge candidate miRNAs using proliferating hPCLs: detection of miRNA expression in 10 µg of total RNA isolated from proliferating hPCLs; detection of snRNA U6 as internal standard and the mature miRNAs

The expression of miR-23a-3p, miR-23b-3p, miR-24-3p, miR-27a-3p, miR-27b-3p, miR-29a-3p and miR-92a-3p in proliferating hPCLs could be validated. Interestingly, miR-29c-3p could not be detected. The sequences of mature miR-29a-3p and miR-29c-3p differ by just one base. Thus, this experiment also demonstrates the high sequence specificity in Northern Blotting.

Proof of sponge functionality by dual luciferase assay

The functionality of competitive inhibitors, the "sponges", was tested in proliferating hPCLs (cloning and measurement performed by G. Knoll). The sponges, transcripts coding for a 2 h destabilized GFP reporter gene containing seven binding sites for a specific miRNA in its 3'-UTR, were checked for functionality in dual luciferase assays. hPCLs were cotransfected using pMir-Report construct expressing firefly luciferase containing seven binding sites for a specific miRNA and untargeted renilla luciferase and a pSponge construct not harboring any binding sites or a pSponge construct containing seven fitting miRNA binding sites in its 3'-UTR. The firefly luciferase intensity was measured and normalized to intensity of the untargeted renilla luciferase. Each experiment was normalized to the conditions where an empty sponge was cotransfected. A functional sponge directed against miR-21-5p served as a positive control (Ebert et al. 2007).

By cotransfection of a matching sponge construct, the signal intensity of the targeted firefly luciferase could be rescued for the positive control miR-21-5p as well as for the candidate

miRNA families miR-23a/b-3p, miR-24-3p, miR-27/a-3p, miR-29a/b/c-3p and miR-92a/b-3p (Fig. 4.31). The sponge construct harboring binding sites for a non-functional mock sequence was not able to rescue the firefly luciferase signal intensity of the pMir-report construct for miR-24-3p, proving the miRNA-sponge binding to be functional and specific.

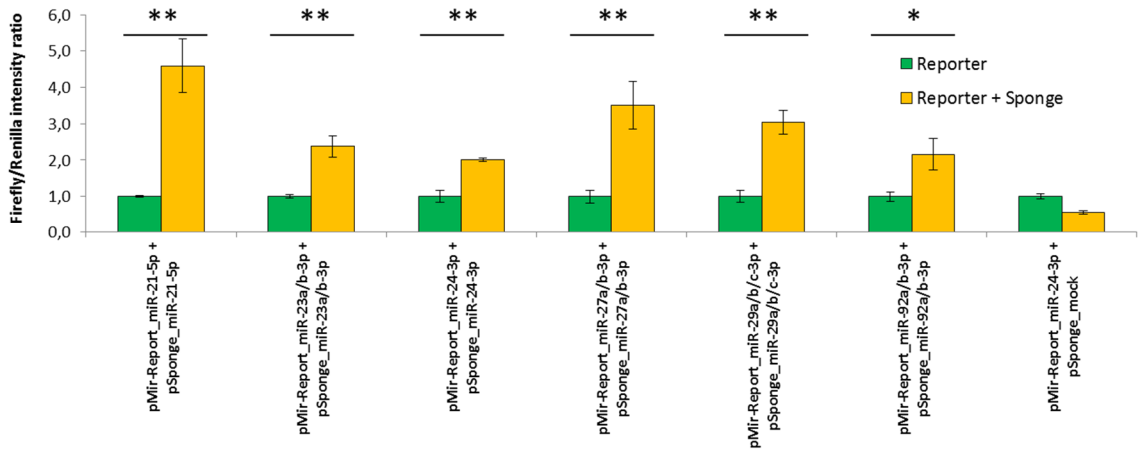

Fig. 4.31: Sponge functionality analysis by luciferase assay using hPCLs; pMir-Report-TK/RenillaLuc constructs and empty sponge constructs or matching sponges were cotransfected into hPCLs; luciferase intensity ratio was measured and set to 1 in cells not transfected with sponge constructs; *: $p < 0.05$; **: $p < 0.01$

Taken together, it could be shown by dual luciferase assay that sponges directed against miRNA families miR-23a/b-3p, miR-27a/b-3p, miR-29a/b/c-p and miR-92a/b-3p as well as against the mature miRNA miR-24-3p are able to bind their targets, thus downregulating miRNA levels in cells.

4.8 *In vivo* knockdown of miRNAs using *Vivo-Morpholinos*

For transient miRNA knockdown by the so-called *Vivo-Morpholinos* (GeneTools), male C57bl/6 mice which were eight weeks of age were split into groups of two and injected with two different *Vivo-Morpholinos* or control solutions. Two groups of mice received antisense oligonucleotides against miR-30a-5p and miR-322-3p, respectively. Since the first two animals receiving anti-miR-322-3p oligonucleotides died shortly after injection from general, not kidney related problems, the experiment was repeated with half the dose of anti-miR-322-3p *Vivo-Morpholinos*. The two control groups were injected with a negative control *Vivo-Morpholino* directed against a human β-globin intron mutation provided by the manufacturer or plain 1x PBS, respectively. The urine of these mice was collected before the experiment as spot urine and after the third injection 16 h overnight by metabolic cages.

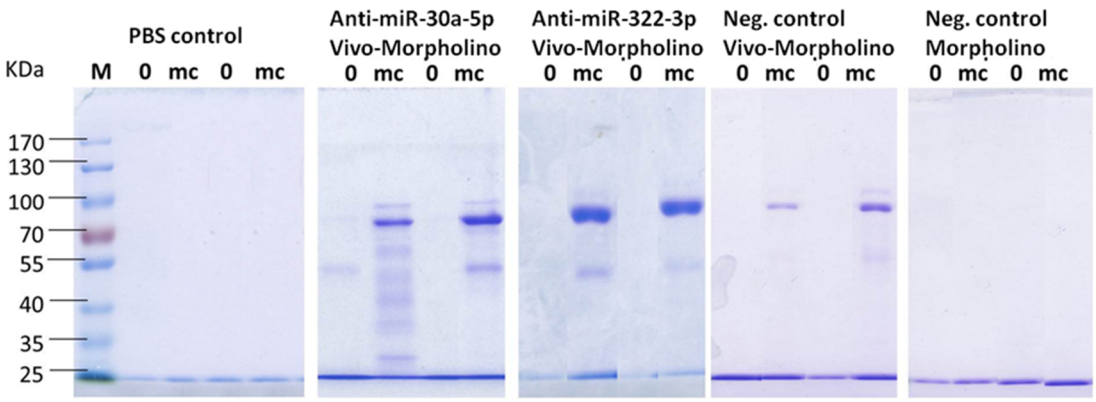

Fig. 4.32: Urine gel of vivo-Morpholino treated mice; Coomassie-stained SDS-gel of urines collected before experiment (0) and after the third injection from metabolic cages (mc); 0.5 µl urine per lane; size of albumin: ca. 66 kDa

Both *Vivo-Morpholinos* directed against two miRNAs highly enriched in podocytes, anti-miR-30a-5p and anti-miR-322-3p, lead to proteinuria in the treated animals. Since the mice which received the control *Vivo-Morpholino* also developed a proteinuria after treatment, an additional control group was injected with control *Morpholinos*. *Morpholinos* possess the same nucleotide sequence, but lack the octaguanidinium residue at the 3'-end. Opposed to the injection of the control *Vivo-Morpholino*, the control *Morpholino* did not lead to a proteinuria in the animals, hinting that the octaguanidinium residue is nephrotoxic and has a big influence itself, independent of the sequence of the attached oligonucleotide. Since the *Morpholinos* lack this residue, the control oligonucleotide seems to not affect the kidney, but the expected permeation of the cells is much worse. If the uptake into the cells is slower, it might lead to a severe problem in targeting the *Morpholinos* specifically to the kidney, as the time a kidney can be clamped is limited. The effect of anti-miRNA *Morpholinos* in the kidney could be tested in a similar experiment.

4.9 TALE-Nucleases for miR-30a knockout in HEK293T cell line

To characterize the role of miR-30a-5p, HEK293T knockout cell clones were generated with the help of a TALEN pair directed against the miR-30a locus (bachelor thesis C. Blessing, 2014).

The efficiency of the TALEN-mediated knockout was assessed by Northern Blotting analyses of the amount of mature miR-30a-5p in the 30 µg total RNA isolated from different putative knockout cell clones. Three knockout clones showed a reduced expression of mature miR-30a-5p compared to the wildtype control (Fig. 4.33 A). They were analyzed for their Notch1 expression levels by qPCR, since Notch1 is a validated target of miR-30a-5p in glomeruli (Wu et al. 2014).

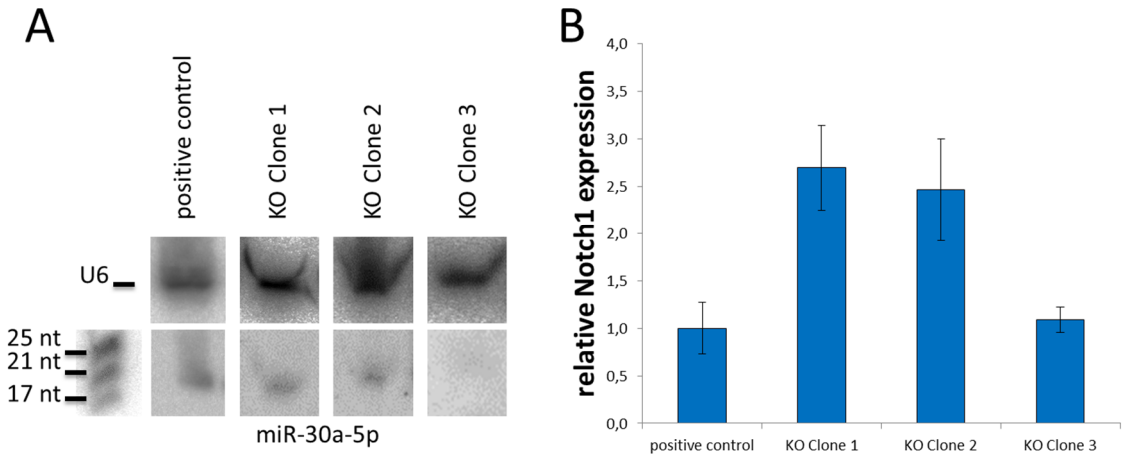

Fig. 4.33: Identification of miR-30a-5p knockout clones; (A) Northern Blotting for mature miR-30a-5p from 30 µg total RNA; internal control: snRNA U6; (B) qPCR of cDNA transcribed from long RNA fraction for Notch1 expression, a validated miR-30a-5p target in glomeruli

In the knockout clones 1 and 2, Notch1 was upregulated, while no changes in the expression levels are observed for knockout clone 3 (Fig. 4.33 B). To investigate the knockout on a genomic level, the genomic locus of mir-30a was amplified by PCR and the resulting PCR product was sequenced and aligned to the wildtype sequence for mutation analyses (Fig. 4.34).

```
Control: TGCTGTTGACAGTGAGCGACTGTAAACATCCTCGACTGGAAGCTGTGAAGCCACAGATGGGCTTTCAGTCGGATGTTTGCAGCTGCCTACTGCCTCGGACTTCAAGGGGCTACTTTAGGAGCAATTATCTTGTTTACTA

Clone 1: TGCTGTTGACAGTGAGCGA-------CATCCTCGACTGGAAGCTGTGAAGCCACAGATGGGCTTTCAGTCGGATGTTTGCAGCTGCCTACTGCCTCGGACTTCAAGGGGCTACTTTAGGAGCAATTATCTTGTTTACTA

Clone 2: TGCTGTTGAC----------------------------------------------------------------------------------------------------------TTGTTTACTA

Clone 3: TGCTGTTGACAGTGAGCGACTGTAAACATCCTCGACTGGAAGCTGTGAAGCCACAGATGGGCTTTCAGTCGGATGTTTGCAGCTGCCTACTGCCTCGGACTTCAAGGGGCTACTTTAGGAGCAATTATCTTGTTTACTA
         TGCTGTTGACAGTGAGCGACTGTAAAACATCCTCGACTGGAAGCTGTGAAGCCACAGATGGGCTTTCAGTCGGATGTTTGCAGCTGCCTACTGCCTCGGACTTCAAGGGGCTACTTTAGGAGCAATTATCTTGTTTACTA

pre-mir-30a    miR-30a-5p    miR-30a-3p
```

Fig. 4.34: Genomic organization of miR-30a-5p knockout clones; the genomic locus of mir-30a (chromosome:GRCh37:6:72113201:72113339:-1) was amplified by PCR and sequenced; underlined: sequence of pre-mir-30a; light blue: sequence of mature miR-30a-5p; dark blue: seed region of miR-30a-5p; light green: sequence of mature miR-30a-3p; dark green: seed region of miR-30a-3p; dash: gap in sequenced products; red: insertions in sequenced product

The three knockout clones show different reorganization patterns: in clone 1, the seed region of the miR-30a-5p is nearly completely deleted, in clone 2 the whole mir-30a precursor sequence is missing. Knockout clone 3 is heterozygous for the knockout: while one allele is not affected by the knockout at all, the other allele shows an insertion of one base. The presence of one wildtype allele in knockout clone 3 might explain why the Notch1 expression is not dysregulated in this clone.

Taken together, the TALEN mediated knockout can lead to different genomic reorganization patterns, resulting in downregulation of the mature miR-30a-5p expression and a dysregulation of a validated target gene, Notch1, in HEK293T cells.

4.10 Renal miRNA expression patterns in NPS disease models

The nail-patella syndrome is a human disease which is caused by mutations in the *LMX1B* gene. This gene codes for the transcription factor LMX1B which is known to be important for podocyte maintenance (Miner et al. 2002). Since the expression of miRNAs can be controlled by transcription factors, a reduced or absent function of LMX1B might also have an influence on miRNA expression in podocytes.

4.10.1 Profiles of glomerular and tubular miRNAs in *Lmx1b* knockout mice

To investigate if *Lmx1b* knockout has a direct or indirect influence on the miRNA levels in affected glomeruli, transgenic mice with a doxycycline inducible podocyte specific *Lmx1b* knockout were used (Fig. 4.35).

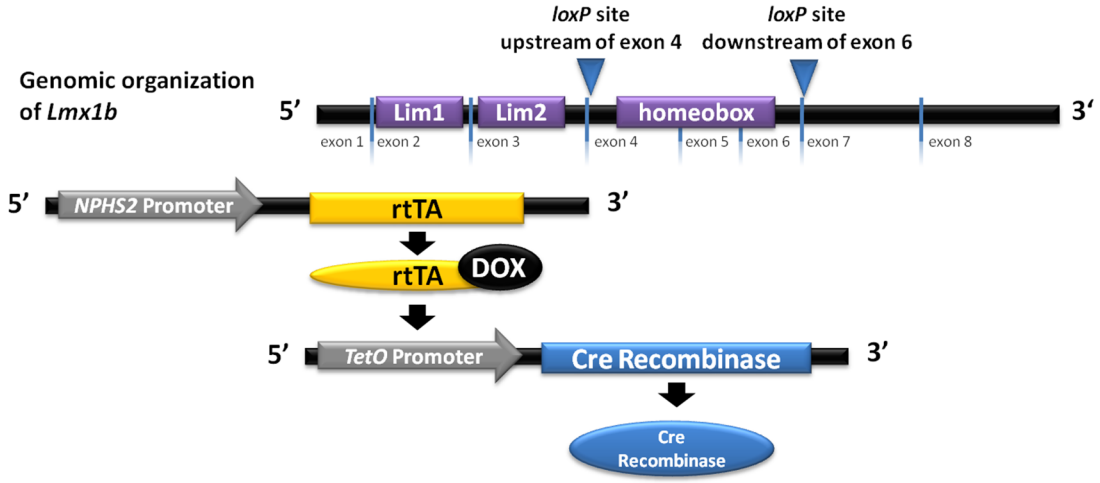

Fig. 4.35: Genomic organization of the triple transgenic *Lmx1b* knockout mice; exposure to doxycycline leads to podocyte specific reorganization of the genomic locus of *Lmx1b*; Abbreviations: Dox: doxycycline; Lim1, 2: Lim domain 1, 2; TetO: Tet-On promoter; rtTA: reverse tetracycline transactivator

Lmx1b knockout in mice was induced by adding doxycycline to their drinking water for 7 days. Spot urine of the *Lmx1b* knockout animals used for glomeruli isolation was checked for proteinuria by SDS-PAGE. All four mice used for glomeruli isolation showed a distinct proteinuria, which was not detected in the control urine (Fig. 4.36).

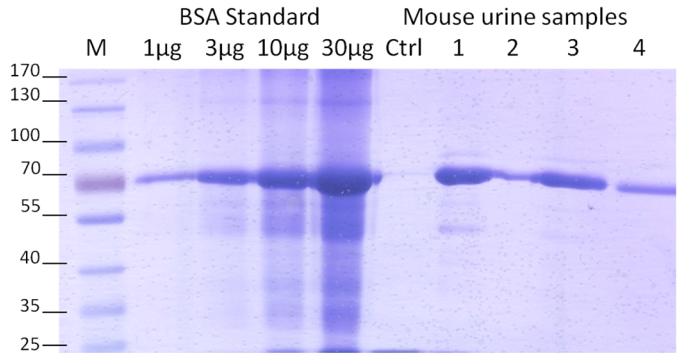

Fig. 4.36: Coomassie stained urine gel of triple transgenic *Lmx1b* knockout mice; urines of Cre^+ knockout animals (1 - 4) showing a distinct proteinuria after doxycycline induction and a control; 0.5 µl urine per lane; size of albumin: ca. 66 kDa

The glomeruli of four Cre^+ *Lmx1b* knockout mice and six Cre^- control mice, all female and aged between 12 and 14 weeks, were isolated by magnetic beads perfusion. RNA extraction and library preparation was performed by A. Dueck (Department of Biochemistry I, University of Regensburg). One *deep sequencing* profile was generated from the total RNA preparation, while the second profile was generated from the small RNA fraction enriched by gel electrophoresis. The RNA samples were sequenced on a HiSeq1000 sequencer (Illumina). The annotation of the sequenced libraries to the known miRNA sequences was performed by N. Eichner (Department of Biochemistry I, University of Regensburg).

The profiles from enriched small RNAs yielded 26.5 millions of miRNA reads of good quality from the control animals and 28.7 millions of miRNA reads from the *Lmx1b* knockout animals. The profile generated from total RNA consisted of 16.6 millions of miRNA reads in the control animals and 14.4 millions of miRNA reads from the *Lmx1b* knockout animals. For the profiles generated from small and total RNA, enrichments between the knockout animals and the control animals were calculated (Tab. 10.5).

In total, 247 mature miRNAs reached more than 430 total reads in all four libraries, which corresponds to more than five reads per million. There was no mature miRNA that was upregulated more than 2-fold in the knockout glomeruli in both profiles, but seven mature miRNAs that were downregulated more than 2-fold after the *Lmx1b* knockout, miR-28-5p, miR-200a-3p, miR-200b-3p, miR-200c-3p, miR-203-3p, miR-429-3p and miR-1839-5p.

The mature miRNAs miR-200a-3p, miR-200b-3p, miR-200c-3p, and miR-429-3p all belong to a miRNA family consisting of 5 members that is organized in two clusters. The fifth family member, miR-141-3p, was equally expressed with and without *Lmx1b* knockout according to both profiles.

4.10.2 Validation of miRNA expression by qPCR

To validate the *deep-sequencing* profiles generated from *Lmx1b* knockout mice and control mice, the expression of a subset of miRNAs was analyzed by qPCR. Two male 34 week old *Lmx1b* knockout mice and one male 34 week old control mouse received doxycycline containing drinking water for seven days. Their urine was checked for proteinuria after induction (Fig. 4.37 A). The glomeruli were isolated by magnetic beads perfusion (chapter 3.3.5). The long and small RNA fractions were isolated and reverse transcribed to cDNA (chapter 3.4.2 & 3.4.4). The cDNA generated from the long RNA sample was checked for Lmx1b expression. In the knockout mice, Lmx1b mRNA reduction to 59.8% was measured (Fig. 4.38 B).

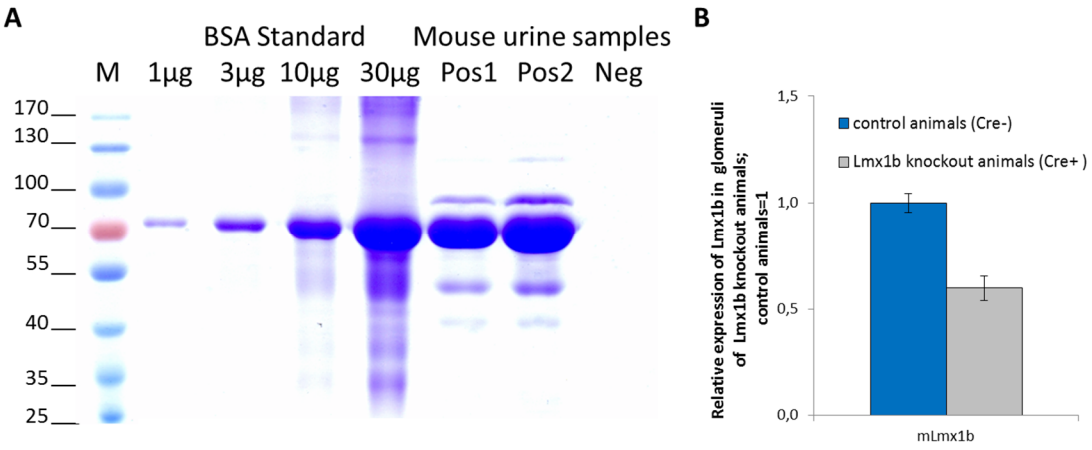

Fig. 4.37: Characterization of *Lmx1b* knockout validation animals; (A) Coomassie stained urine gel of triple transgenic *Lmx1b* knockout mice; both Cre^+ knockout animals (Pos1, Pos2) show a distinct proteinuria after doxycycline induction, while the urine sample from the Cre^- control animal (Neg) does not contain protein; 0.5 µl urine per lane; size of albumin: ca. 66 kDa (B) qPCR of Lmx1b transcript in Cre^+ *Lmx1b* knockout mice compared to Lmx1b transcript level in Cre^- control mice; internal control: snRNA U6

The enrichment of mature miRNAs between the control mouse sample and the sample generated from the knockout mice was calculated and compared to the result from the deep sequencing profiles.

All mature miRNAs from the subset to be validated seemed to be downregulated in the knockout animals compared to the control animals (Fig. 4.38). To check if the general reduction is due to a change in the miRNA processing pathway, the expression levels of Drosha, Dicer, and the Argonaute proteins were analyzed by qPCR, but no changes were found (bachelor thesis M. Billmeier, 2012, data not shown).

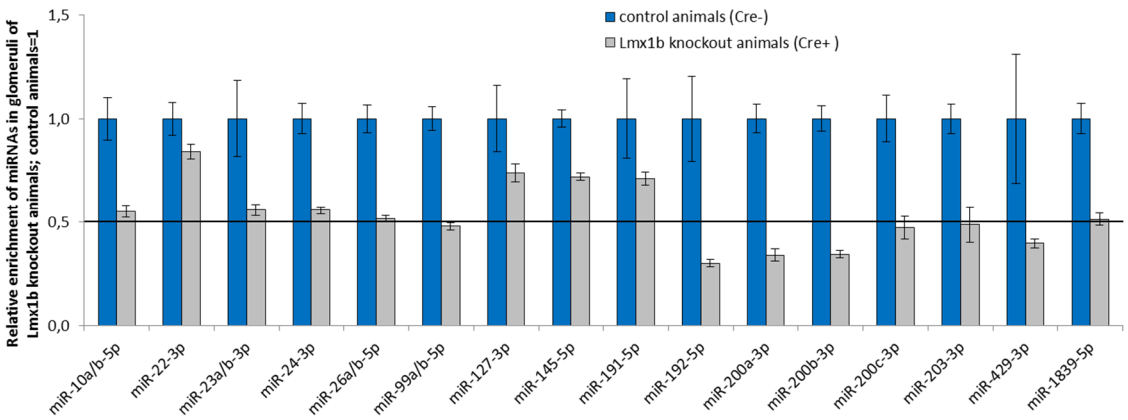

Fig. 4.38: Relative expression levels of mature miRNAs in *Lmx1b* knockout animals and control animals; internal standard: snRNA U6

It is known that miR-145-5p is a miRNA not expressed in the podocytes, but in the mesangial cells of the glomerulus (our data; Harvey et al. 2008), meaning that the *Lmx1b* knockout cannot have a direct effect on its expression levels. Therefore, for further analyses of the miRNA expression, the ratio of miR-145-5p between the knockout animals and the control animals was set to 1 (Fig. 4.39).

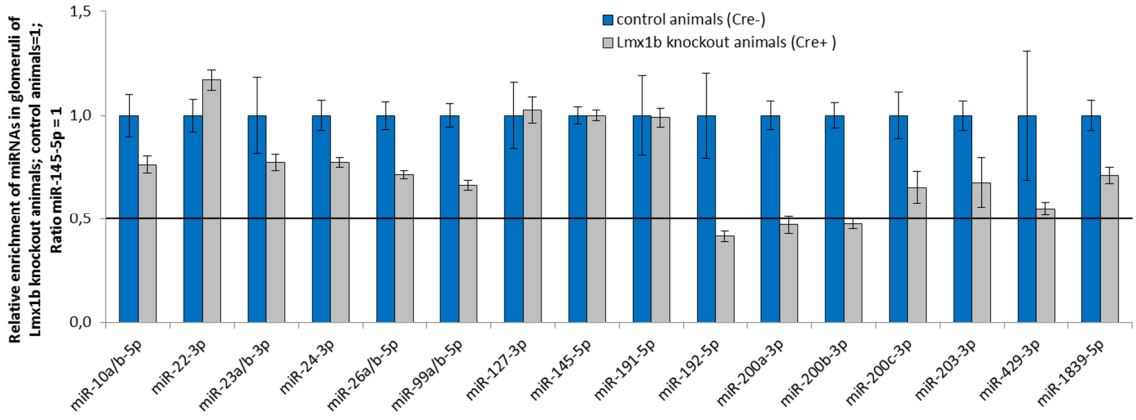

Fig. 4.39: Relative expression levels of mature miRNAs in *Lmx1b* knockout animals and control animals; miR-145-5p ratio set to 1; internal standard: snRNA U6

When the expression ratios are normalized to the expression of miR-145-5p, miR-200a-3p and miR-200b-3p are still reduced more than 2-fold in the knockout animals compared to the control. The miRNAs miR-200c-3p, miR-203-3p, miR-429-3p and miR-1839-5p are still reduced, but do not reach the threshold. Interestingly, an additional mature miRNA, miR-192-5p, also seemed to be reduced in the *Lmx1b* knockout animals. This miRNA was reduced to 51% expression in the profile generated from enriched small RNAs, but only reduced to 68% in the profile generated from total RNA.

4.10.3 Profiles of podocyte and endothelial/mesangial miRNAs in *Lmx1b* knockout mice

To assess if the miRNA levels changed in *Lmx1b* knockout glomeruli were caused by altered miRNA expression in the podocytes, the triple transgenic inducible podocyte specific *Lmx1b* knockout mice were crossed with the mT/mG reporter mice (Fig. 4.40). In these quadruple transgenic mice, doxycycline induction not only leads to *Lmx1b* knockout, but also to a switch from expression of the red fluorescent mTomato marker to expression of GFP, yielding mice with sortable green fluorescent *Lmx1b* knockout podocytes. As knockout samples, animals homozygous for the floxed *Lmx1b* locus harboring the transgenes for podocyte specific rtTA expression, the TetOn controlled Cre recombinase expression and the mT/mG reporter cassette, were used. As a control group, mice possessing two *Lmx1b* wildtype alleles were used.

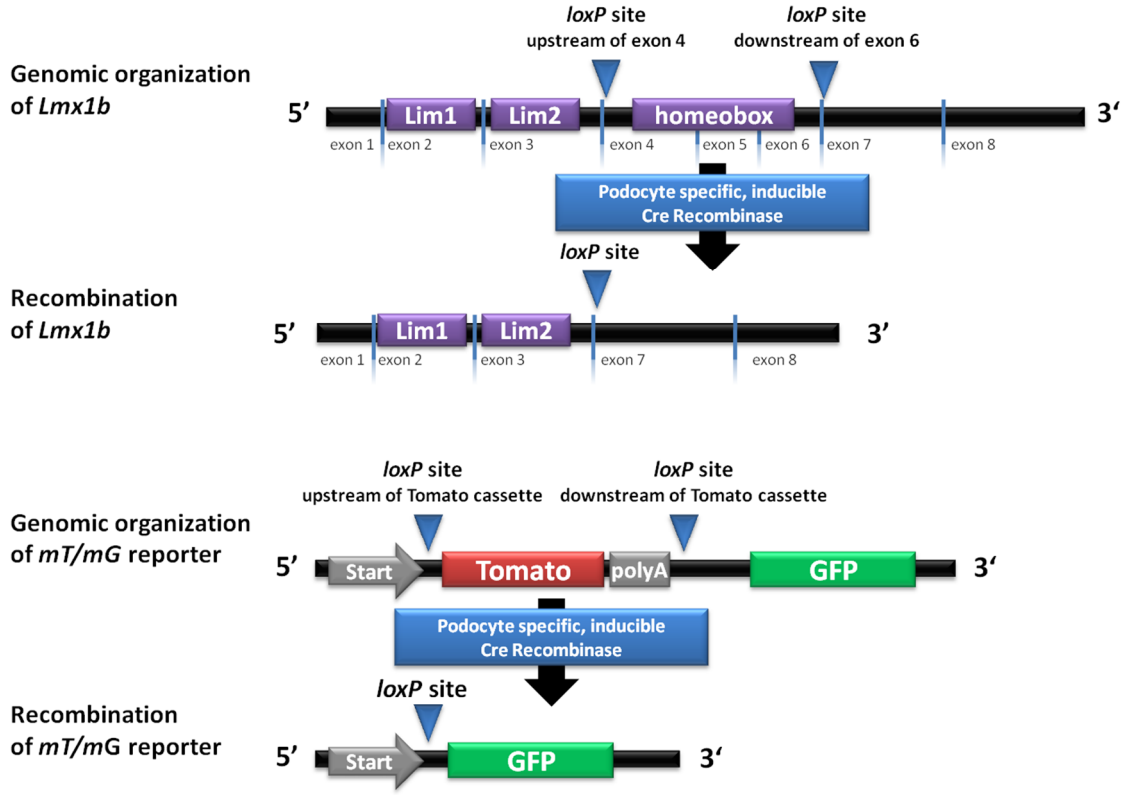

Fig. 4.40: Genomic organization of the quadruple transgenic *Lmx1b* knockout reporter mice; exposure to doxycycline leads to podocyte specific reorganization of the genomic loci of Lmx1b and of the mT/mG reporter cassette; Abbreviations: Lim1, 2: Lim domain 1, 2; GFP: green fluorescent protein; mT/mG: mTomato-GFP reporter cassette

The *Lmx1b* knockout mice and the control group received drinking water with doxycycline for eight days. On the seventh day of doxycycline induction, spot urine of the animals was checked for proteinuria by SDS-PAGE. Only knockout animals showing a clear proteinuria and control animals that did not show proteinuria were chosen for the experiment. Podocytes were isolated from the animals on the eighth day after induction.

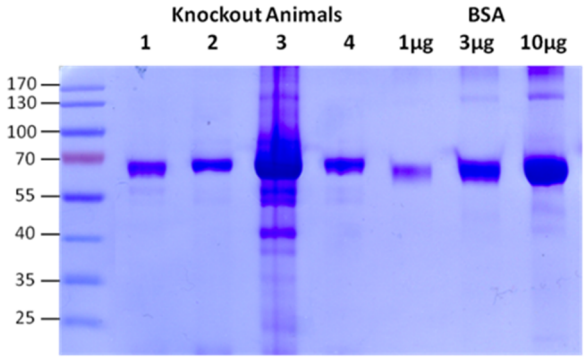

Fig. 4.41: Coomassie stained urine gel of quadruple transgenic *Lmx1b* knockout mice; all knockout animals (1-4) show a distinct proteinuria after doxycycline induction; 1µl urine per lane; size of albumin: ca. 66 kDa

All *Lmx1b* knockout animals showed a distinct proteinuria after doxycycline induction for eight days (Fig. 4.41), while the control animals did not show proteinuria after doxycycline induction for eight days (Fig. 4.42).

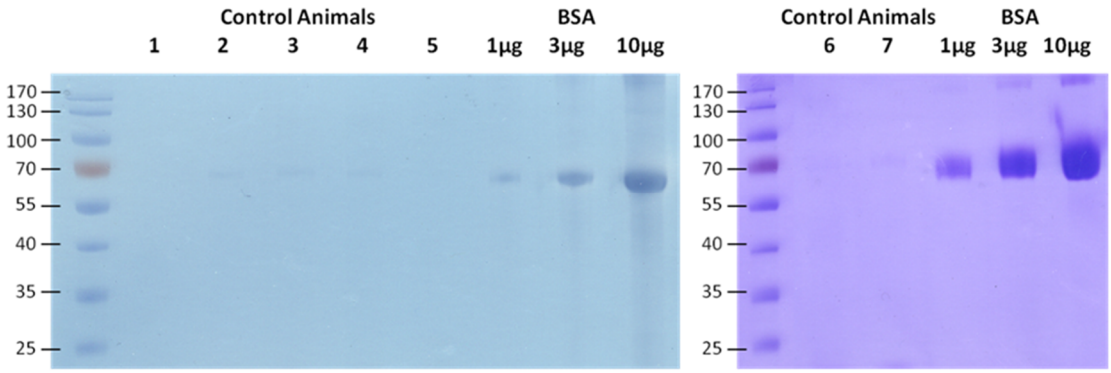

Fig. 4.42: Coomassie stained urine gel of quadruple transgenic control mice; all animals harboring a wildtype *Lmx1b* gene do not show proteinuria after doxycycline induction; 1µl urine per lane; size of albumin: ca. 66 kDa

In total, 98,000 green podocytes and 200,000 cells of the red cell population were isolated from four female *Lmx1b* knockout mice, while 91,000 green podocytes and 188,000 cells of the red cell population were isolated from seven female control mice. All animals used were aged between 12 and 14 weeks.

RNA extraction and library preparation from small RNAs was performed by A. Dueck (Department of Biochemistry I, University of Regensburg). The RNA samples were sequenced on a HiSeq1000 sequencer (Illumina). The annotation of the sequenced libraries to the known miRNA sequences was performed by N. Eichner (Department of Biochemistry I, University of Regensburg). The annotation of the sequenced libraries to the known miRNA sequences was performed by N. Eichner (Department of Biochemistry I, University of Regensburg).

From *Lmx1b* knockout podocytes and control podocytes, libraries with 2.97 million and 2.96 million sequence reads were generated. From the red cell population, libraries with 2.82 million reads from *Lmx1b* knockout animals and 2.96 million reads from control animals were generated (Tab. 10.6). In total, 262 mature miRNAs were identified to expressed over the threshold of more than five reads per million in at least one of the generated libraries. A total of 210 mature miRNAs were expressed in one of the podocyte samples. To identify miRNAs that might be regulated directly by Lmx1b, the profiles were searched for miRNAs with altered expression in the podocytes with and without *Lmx1b* knockout, while the expression in the red fluorescent cell population stays the same. In total, 48 mature miRNAs were upregulated after the *Lmx1b* knockout, while 40 mature miRNAs were downregulated. The miR-200 family was mainly expressed in the red fluorescent cell population, while miR-192-5p was expressed in control podocytes on a very low level and even more downregulated after the *Lmx1b* knockout.

Of the 38 podocyte miRNAs, all except one (mmu-miR-24-1-5p) could be identified in the miRNA profiles generated from the *Lmx1b* knockout mice as well as the control mice, underlining again the relyability of the generated data sets. For 21 mature miRNAs, expression levels in the podocytes and in the red fluorescent cell populations remained stable before and after the knockout. Five miRNAs, let-7e-3p, miR-30b-5p, miR-30c-5p, miR-125b-2-3p and miR-340-5p, were upregulated in the podocytes after the knockout and equally expressed in the red fluorescent cell population, while four miRNAs, miR-196b-5p, miR-330-3p, miR-450b-5p and miR-542-3p were downregulated in the podocytes after the knockout and equally expressed in the red fluorescent cell population. These nine miRNAs might be the most interesting targets for further analyses. Two miRNAs, miR-149-5p and miR-210-3p were upregulated in podocytes and downregulated in the red fluorescent cell population. Four miRNAs were downregulated in both cell populations, miR-30b-3p, miR-330-5p, miR-450a-5p and miR-615-3p. One single miRNA, miR-873a-5p, was downregulated in podocytes but upregulated in the red fluorescent cell population. Of the candidate miRNAs, miR-330-5p was the only one to totally vanish after the knockout, but only in the red fluorescent cell population, while residual expression persisted in the podocytes after knockout. As some miRNA are expressed at low levels, the calculated ratios might be more error-prone compared with miRNAs expressed at high levels. This underlines the need for a validation of the measured miRNA expression changes.

5 DISCUSSION

5.1 Models for investigation of podocytes

To investigate the role of miRNAs in glomeruli and podocytes, three main model systems can be used: immortalized cell lines in cell culture, podocytes isolated freshly from mice and manipulations inside the murine organism. In mammalian organisms, podocytes are placed in a very specific environment. *In vivo*, they cover the capillary of the glomerulus. The renal filtration barrier is composed of three layers: the fenestrated endothelium including the glycocalyx, the glomerular basement membrane between the endothelium and the podocytes and the slit diaphragm between the interdigitating podocyte foot processes. All three parts are crucial for successful blood filtration. The elaborate glycocalyx covering the endothelial cell and its fenestrae already restricts particulate blood components and larger molecules like immunoglobulins and albumin (Schlöndorff 2014). The glomerular basement membrane and the slit diaphragm come into play as second and third level of filtration, all together providing the highly effective permselectivity of the filter and preventing it from clogging up (Schlöndorff 2014). A very elaborate and tightly regulated cross-talk between the glomerular cells is necessary for a fully functional renal filtration barrier.

5.1.1 Differences between animal model and cell culture

In metanephric organ culture, it has been shown that podocytes develop before the other cell types, hinting that an intrinsic development program is used for podocyte differentiation during development (Schlöndorff 2014). However, it is not known how a podocyte recognizes its neighboring podocyte to build up the interdigitating foot processes and the slit diaphragms in-between the processes. It has been shown that the fenestrae formation in the endothelium is caused by VEGF (Vascular endothelial growth factor) signaling, a signal protein produced by podocytes (Chen et al. 2002). The fenestration of the endothelium and its characteristic glycocalyx is dependent on podocyte VEGFA (Vascular endothelial growth factor A) and the presence of the fitting receptor, VEGFR-2 (Vascular endothelial growth factor receptor 2), in the endothelium (Schlöndorff 2014). While studies have elucidated the molecular basis of signaling from podocyte to endothelial cell and from endothelial cell to mesangial cell, potential mediators have yet to be identified for cross-talk between podocytes and mesangial cells as well as unidirectional signaling from endothelial cells to podocytes and from mesangial to endothelial cells (Schlöndorff 2014). A first hint for signaling from endothelial cells to the podocytes was

given when medium conditioned from glomerular endothelial cells grown under permanent laminar shear stress decreased podocyte monolayer resistance and increased phosphorylation of vasodilator-stimulated phosphoprotein, showing a possible endothelium-to-podocyte crosstalk in cell culture (Slater et al. 2012).

The composition of the glomerular basement membrane has recently been studied by mass-spectrometry based proteomics (Byron et al. 2014). It was reported that cell type specific differences in the extra cellular matrix composition could be identified. Additionally, the extra cellular matrix deposition in co-cultured cells was different from the matrix in monocultures, hinting at cross-talk between the cell types. It has been tried to mimic the physiological state using hydrogel scaffolds (Bruggeman et al. 2012) or a bioartificial membranes containing collagen I (Slater et al. 2011) for culturing endothelial cells and podocytes on the two sides of a central substrate. But still, the very specialized three-dimensional podocyte architecture with the interdigitating foot processes of two neighboring podocytes embracing the capillaries has not been copied in cell culture yet.

Taken together, podocytes are placed in a very complex environment under physiological conditions, including a lot of signaling in-between the different cell types of the glomerulus. Additionally, the three-dimensional architecture of podocytes is not conserved in cells being cultured in two-dimensional cell culture. Thus, it is plausible that immortalized podocyte cell lines do not exhibit all characteristics of a podocyte *in vivo*.

5.1.2 Immortalized human cell line as model for podocytes

To investigate podocytes in cell culture, immortalized cell lines derived from isolated human and murine podocytes, that can be switched from a proliferating to a differentiated state, have been established (Saleem et al. 2002, Schiwek et al. 2004). For the human immortalized podocytes, the creators showed by immunofluorescence microscopy that the expression of nephrin as well as synaptopodin are low and diffuse in proliferating cells, but changes to a punctual pattern for nephrin and an actin associated pattern for synaptopodin in differentiated cells.

In the present work, the differentiation of immortalized human podocytes could also be nicely demonstrated by the changing localization of the podocyte marker nephrin, and the two actin associated adapter proteins synaptopodin and α-actinin-4 between the proliferating and the differentiated state of hPCLs. Similar to the to the results published before (Saleem et al. 2002), it could be shown that nephrin relocalizes from a weak nuclear staining to a spot-like or linear localization at the cellular membrane in differentiated human podocytes. Synaptopodin localizes

from nuclear staining with weak cytoplasmic staining to fibers spanning the whole differentiated cell, arguing for an actin colocalization of synaptopodin in differentiated hPCLs. Additionally, α-actinin-4, an actin crosslinking protein known to be mutated in some patients with familial focal segmental glomerulosclerosis (Henderson et al. 2008), could be shown to relocate from fibers spanning the whole cytoplasm to "spike"-like protrusions at the cortex of the cells. All three proteins known to be important for podocyte structure show a distinct relocation pattern between the proliferating and the differentiated state, indicating a reorganization of the actin cytoskeleton and enhanced expression of nephrin and synaptopodin after differentiation.

Additionally, the experiments showed that ten mature miRNAs that were found to be expressed in freshly isolated murine podocytes, miR-10b-5p, miR-92a-3p, miR-130a-3p, miR-30a-5p, miR-146b-5p, miR-29a-3p, miR-23b-3p, miR-22-3p, miR-107 and miR-27b-3p, are also expressed in immortalized human podocytes. These miRNAs show differential expression between proliferating and differentiated hPCLs, also arguing for an altered metabolic and structural state of the differentiated cells. In contrast, the expression of another set of five mature miRNAs expressed in freshly isolated murine podocytes, miR-148a-3p, miR-196b-5p, miR-424-5p, miR-542-3p and miR-503-5p, could neither be detected in the proliferating nor in the differentiated immortalized human podocytes. This shows either species specific expression of mature miRNAs or a gap between the situation of differentiated podocyte cell line and the physiological *in vivo* state. Since the immortalized murine podocytes can also be switched to the differentiated state by culturing them at 38°C for 14 days, expression of the miRNAs detected in freshly isolated murine podocytes might be checked in proliferating and differentiated mPCLs. Thus, it could be investigated if the differences are due to the different species or due to the difference between immortalized cell lines and *in vivo* podocytes.

The immortalized human podocytes show distinct differences between the proliferating and the differentiated state, in the expression and distribution of important structural proteins as well as their miRNA expression. Thus, they are a suitable model for regulatory mechanisms in human podocytes. There is, however, still a big difference between differentiated podocytes in the two-dimensional cell culture flask and the *in vivo* environment of podocytes. As freshly isolated human podocytes cannot be obtained, the immortalized human podocyte cell line is the best human model for experiments on the function of podocytes. For studies focusing on the delicate structure of podocytes in the mammalian organism, freshly isolated murine podocytes represent the most accurate model for podocyte structure and function under physiological conditions, since they are fully differentiated cells isolated from their natural environment.

5.1.3 Freshly isolated murine podocytes

The major limitation in working with podocytes freshly isolated from reporter mice is the yield. By modifications of the original podocyte isolation protocol (Boerries et al. 2013), adding an additional rinsing step prior to perfusion of the kidney and prolonging the podocyte digestion step by five minutes, it was possible to increase the cell yield to an average of around 200,000 green fluorescent podocytes per animal in this work. This makes the isolation of five to six million cells a possible, but laborious task demanding many laboratory animals. Immortalized podocyte cell lines like the hPCLs and mPCLs can be expanded to millions of cells quite easily in a relatively short amount of time, while breading of a sufficient amount of laboratory animals takes several months and is considerably costlier.

The number of cells per glomerulus was estimated to be 211 ± 29 by the dissector/fractionator method (Basgen et al. 2006), while the number of podocytes per glomerulus was estimated to be around 89 ± 10 with the fractionator/dissector method (Nicholas et al. 2011). The number of nephrons in a healthy murine kidney has been investigated by several studies. By physical dissector/fractionator combination, the number of nephrons per kidney in 129Sv/C57bl/6 hybrid mice after the sixth backcross to C57bl/6 background was estimated to be 13440 ± 1275 (Cullen-McEwen et al. 2003). In a study focusing on the nephron number during kidney development, the number of nephrons in the adult kidney of four week old C57bl/6J mice varied between 9266 and 13453 with an mean value of 11359 when analyzed with the fractionator/dissector method (Zhong et al. 2012). Differences of nephron numbers between male and female mice have been reported, when 19341 ± 859 nephrons in male C57bl/6 mice, but 22830 ± 1117 nephrons in female C57bl/6 mice were counted in individuals of eight weeks of age (Murawski et al. 2010).

By magnetic beads perfusion, 20,131 ± 4699 glomeruli could be isolated from mice with different backgrounds (C57bl/6, 129/SV or hybrids of the two strains, Takemoto 2002). Finally, it was reported that up to 500,000 podocytes can be isolated from one double fluorescent Cre reporter mouse (Boerries et al. 2013).

These numbers show that the number of nephrons, and thus, the number of podocytes per mouse varies with the age, sex, and genetic background of the laboratory animal, making an average of 200,000 podocytes per mouse a realistic yield.

5.2 miRNA expression in murine glomeruli and podocytes

To investigate the role of miRNAs for maintenance of structure and function of glomeruli and podocytes, the first step is the identification of miRNAs that are expressed in podocytes under physiological conditions. The starting point for the present study were miRNA *deep sequencing* profiles generated from glomeruli and tubules isolated from C57bl/6 wildtype mice.

5.2.1 Identification of glomerular and podocyte enriched miRNAs

In the *deep sequencing* profiles generated from glomeruli and tubules as well as from podocytes and the red cell population, enrichment factors were calculated for every miRNA between the two populations. A factor of ≥ 2 in either direction was considered enrichment, while a lower factor was considered as equal expression between two cell populations.

Identification glomerular enriched miRNAs

In total, 260 mature miRNA sequences have been identified to be expressed in murine glomeruli and tubules by two *deep sequencing* profiles. According to both profiles, 69 miRNAs were glomerular enriched, while 27 mature miRNAs were detected to be glomerular enriched in one of the profiles and equally expressed in the other profile. A total of 84 miRNAs were equally expressed in glomeruli and tubules, while 62 miRNAs were tubular enriched and 18 miRNAs were tubular enriched in one of the profiles and equally expressed in the other profile. Since glomeruli consist of at least three different cell types, the podocytes, endothelial and mesangial cells, a mature miRNA found to be enriched in glomeruli is not necessarily expressed in podocytes. Thus, double fluorescent Cre reporter mice were bred for further investigation of the expression of miRNAs in podocytes.

Identification of podocyte enriched miRNAs

Using the two *deep sequencing* profiles of podocytes and the red fluorescent cell population isolated from mice, 143 mature miRNAs that were detected in both profiles were identified. A total of 38 miRNAs were enriched more than 2-fold in the podocytes compared to the red fluorescent cell population in both profiles, while 69 miRNAs were equally expressed in both cell populations according to the profiles and 93 miRNAs were enriched in the red fluorescent cell population both times. One miRNA was enriched in podocytes in one profile but enriched in the red fluorescent cell population in the other profile. A total of 42 miRNAs were found to be enriched in one of the profiles while being equally expressed in the other profile.

The results of these two *deep sequencing* profiles were compared to the miRNAs detected to be enriched in glomeruli in the earlier profiles (Fig. 5.1, Tab. 5.1).

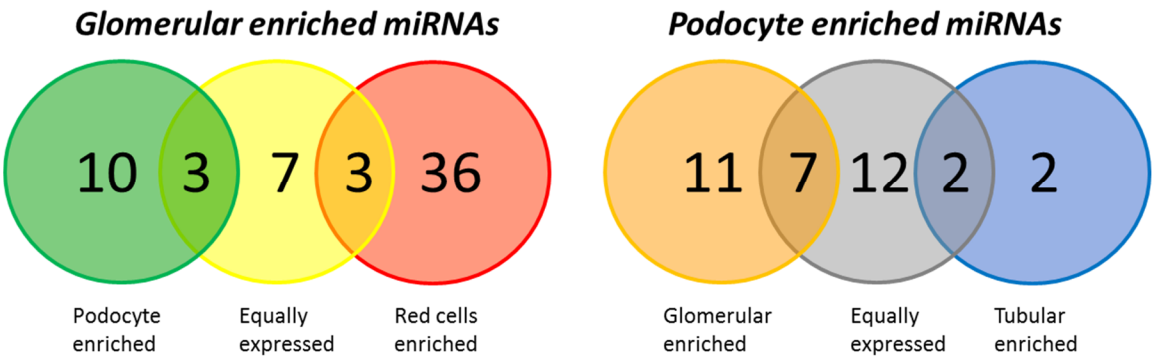

Fig. 5.1: Relative enrichment of miRNAs identified in murine glomeruli and podocytes; enrichment of glomerular enriched miRNAs in podocytes and the red fluorescent cell population (left) and enrichment of podocyte enriched miRNAs in the glomerular and tubular profiles (right)

A total number of 59 mature miRNAs identified to be glomerular enriched in both *deep sequencing* analyses performed with RNA isolated from murine glomeruli and tubules were identified in both *deep sequencing* profiles obtained from podocytes and the red fluorescent cell population. The majority of 36 miRNAs was found to be enriched in the red fluorescent cell population with some of them not being expressed in podocytes at all. Additionally, three miRNAs were enriched in the red fluorescent cells in one profile and equally expressed in the other profile, and seven miRNAs were equally expressed in both profiles. Strikingly, only ten of the glomerular enriched miRNAs were found to be podocyte enriched, with additionally three miRNAs being enriched in one of the profiles and equally expressed in the other profile. This underlined the importance of the double fluorescent reporter mouse model, meaning that studies concentrating on the glomerular miRNA expression might be dealing with non-podocyte miRNAs their effects.

Vice versa, 31 mature miRNAs enriched in podocytes had been identified previously in both the *deep sequencing* profiles of glomeruli and tubules. Eleven podocyte miRNAs had already been found to be glomerular enriched, while seven mature miRNAs were glomerular enriched in one of the profiles and equally expressed in the other profile. A total of twelve mature miRNAs was equally expressed in the profile derived from glomeruli and tubules, while two miRNAs were tubular enriched in one profile and two miRNAs were tubular enriched in both profiles.

Tab. 5.1: Glomerular and tubular expression of podocyte enriched miRNAs

miRNAs	accession number mature miRNA (murine)	podocytes vs. red fluorescent cells						glomeruli vs. tubules					
		1st profile			2nd profile			1st profile (total RNA)			2nd profile (small RNA)		
		Red Cells ‰	Podocytes ‰	Ratio (Pc/red)	Red Cells ‰	Podocytes ‰	Ratio (Pc/Red)	Tubular expression ‰	Glomerular Expression ‰	Ratio (Glom/Tub)	Tubular expression ‰	Glomerular Expression ‰	Ratio (Glom/Tub)
mmu-let-7e-3p	MIMAT0017016	0,02	0,04	2,7	0,01	0,04	2,8	0,002	0,005	2,6	0,003	0,009	3,3
mmu-miR-23b-3p	MIMAT0000125	1,68	3,84	2,3	1,46	4,25	2,9	0,306	2,345	7,7	0,187	0,325	1,7
mmu-miR-24-1-5p	MIMAT0000218	0,01	0,01	2,2	0,01	0,02	4,3	0,000	0,002	6,3	0,001	0,002	2,6
mmu-miR-27b-5p	MIMAT0004522	0,06	0,16	2,5	0,05	0,15	2,8	0,003	0,016	5,4	0,007	0,064	9,4
mmu-miR-30a-3p	MIMAT0000129	3,24	11,48	3,5	4,45	17,83	4,0	0,474	0,787	1,7	0,525	0,765	1,5
mmu-miR-30a-5p	MIMAT0000128	41,63	203,78	4,9	20,60	141,87	6,9	13,55	27,69	2,0	11,09	12,03	1,1
mmu-miR-30b-3p	MIMAT0004524	0,04	0,12	3,2	0,04	0,18	4,1	0,003	0,007	2,2	0,007	0,010	1,5
mmu-miR-30b-5p	MIMAT0000130	0,50	1,68	3,4	0,59	1,94	3,3	0,118	0,230	2,0	0,098	0,153	1,6
mmu-miR-30c-2-3p	MIMAT0005438	0,93	3,76	4,0	1,01	4,69	4,6	0,161	0,303	1,9	0,291	0,576	2,0
mmu-miR-30c-5p	MIMAT0000514	2,09	6,84	3,3	2,79	11,33	4,1	0,812	0,801	1,0	0,867	0,619	0,7
mmu-miR-30d-3p	MIMAT0017011	0,02	0,07	3,1	0,01	0,05	4,2	0,009	0,011	1,3	0,007	0,005	0,6
mmu-miR-30d-5p	MIMAT0000515	5,25	27,53	5,2	4,54	24,54	5,4	3,431	5,417	1,6	3,914	3,407	0,9
mmu-miR-99a-3p	MIMAT0016981	0,01	0,09	7,8	0,01	0,03	5,3	0,004	0,003	0,7	0,005	0,001	0,1
mmu-miR-99a-5p	MIMAT0000131	0,03	0,15	6,0	0,03	0,09	2,8	0,104	0,070	0,7	0,149	0,133	0,9
mmu-miR-107-3p	MIMAT0000647	0,10	0,47	4,8	0,15	0,61	4,2	0,092	0,033	0,4	0,070	0,015	0,2
mmu-miR-125b-2-3p	MIMAT0004529	0,01	0,08	6,3	0,01	0,05	4,3	0,012	0,011	0,9	0,012	0,002	0,2
mmu-miR-125b-5p	MIMAT0000136	0,06	0,18	2,9	0,12	0,24	2,0	0,083	0,074	0,9	0,137	0,131	1,0
mmu-miR-130a-3p	MIMAT0000141	0,19	0,88	4,7	0,19	0,59	3,2	0,064	0,161	2,5	0,078	0,111	1,4
mmu-miR-146b-5p	MIMAT0003475	0,10	2,51	24,6	0,08	1,49	17,6	0,263	0,997	3,8	0,339	1,186	3,5
mmu-miR-148a-3p	MIMAT0000516	0,26	1,19	4,6	0,43	0,98	2,3	0,573	0,831	1,5	0,362	0,308	0,9
mmu-miR-149-5p	MIMAT0000159	0,00	0,06	13,0	0,01	0,09	7,6	0,013	0,013	1,0	0,007	0,006	0,8
mmu-miR-196b-5p	MIMAT0001081	0,17	0,92	5,4	0,26	1,83	7,1	0,412	0,222	0,5	0,155	0,174	1,1
mmu-miR-210-3p	MIMAT0000658	0,04	0,30	8,0	0,03	0,16	5,3	0,005	0,006	1,2	0,007	0,007	1,0
mmu-miR-322-3p	MIMAT0000549	0,34	2,82	8,3	0,58	2,59	4,5	0,026	0,302	11,7	0,026	0,195	7,6
mmu-miR-330-3p	MIMAT0000569	0,00	0,04	8,9	0,00	0,02	5,4	0,001	0,001	2,8	---	0,001	---
mmu-miR-330-5p	MIMAT0004642	0,01	0,06	8,3	0,00	0,02	5,5	0,002	0,001	0,9	0,004	0,005	1,1
mmu-miR-340-5p	MIMAT0004651	0,24	0,67	2,8	0,17	0,63	3,6	0,200	0,092	0,5	0,142	0,029	0,2
mmu-miR-351-3p	MIMAT0017042	0,00	0,01	18,1	0,00	0,01	3,2	---	0,001	---	0,000	0,003	9,0
mmu-miR-351-5p	MIMAT0000609	0,25	1,59	6,4	0,26	1,00	3,8	0,036	0,489	13,5	0,058	0,730	12,7
mmu-miR-450a-5p	MIMAT0001546	0,05	0,18	3,5	0,07	0,19	2,7	0,002	0,025	11,8	0,003	0,027	8,0
mmu-miR-450b-5p	MIMAT0003511	0,01	0,06	5,2	0,01	0,06	4,8	0,001	0,010	18,6	0,001	0,002	1,9
mmu-miR-503-3p	MIMAT0004790	0,01	0,03	4,0	0,01	0,04	4,1	----	0,001	---	0,000	0,003	15,4
mmu-miR-503-5p	MIMAT0003188	0,11	0,50	4,5	0,13	0,35	2,7	0,003	0,017	5,3	0,004	0,036	8,9
mmu-miR-542-3p	MIMAT0003172	0,10	0,34	3,3	0,12	0,64	5,5	0,003	0,032	9,2	0,001	0,011	7,9
mmu-miR-574-3p	MIMAT0004894	0,07	0,28	4,0	0,13	0,39	2,9	0,007	0,046	6,2	0,002	0,007	4,2
mmu-miR-615-3p	MIMAT0003783	0,00	0,03	8,0	0,01	0,03	3,1	0,017	0,013	0,8	0,028	0,030	1,0
mmu-miR-652-3p	MIMAT0003711	0,06	0,17	2,8	0,05	0,16	3,1	0,032	0,125	3,9	0,045	0,159	3,5
mmu-miR-873a-5p	MIMAT0004936		0,03		0,00	0,02	82,6	---	0,000	---	0,000	0,000	2,6

Several miRNAs had already been identified to be expressed in glomeruli and to be important for glomerular function *in vivo*. It could be verified with the *deep sequencing* profiles generated from podocytes and red fluorescent cells, that miR-30a-5p is a miRNA highly expressed in podocytes, while miR-126-3p and miR-145-5p are expressed in the endothelial and mesangial cells, as it was reported before (Harvey et al. 2008). miR-30a-5p was identified to be the most abundant mature miRNA in podocytes. Also other miRNAs that were reported earlier to important for glomerular and podocyte function, like miR-21a-5p, miR-26a-5p, the miR-29 family, the whole miR-30 family and miR-92a/b-3p were detected as expressed in podocytes as well as in the red fluorescent cell population. Not all of them were podocyte enriched though. Interestingly, these miRNAs were among the most abundant miRNAs in glomeruli and podocytes. The miRNAs with lower expression levels might not have been in the focus until now, but they are interesting candidates for important regulatory functions in podocytes, as a miRNA expressed at low levels might still be the regulator of an important target gene. The mature miR-193a-5p was not detected in both *deep sequencing* profiles from podocytes. It was shown that miR-193a-5p expression in podocytes can induce focal segmental glomerulosclerosis (Gebeshuber et al. 2013) and that parietal epithelial cells loosing miR-193a-5p expression differentiate towards a podocyte like phenotype (Kietzmann et al. 2014). Both results fit the finding that miR-193a-5p is not expressed in podocytes under physiological conditions.

Little is known about the role of the miRNAs showing the highest enrichment in podoytes for podocyte function. However, some had already been identified to be expressed and functional in mammalian kidneys (Tab. 5.5). For miR-873a-5p, no function in kidney has been reported so far. It was identified to act as a tumor suppressor in in glioblastoma tumorigenesis and metastasis by downregulating the expression of IGF2BP1 (Insulin-like growth factor 2 mRNA-binding protein 1) (Wang et al. 2015B). miR-146a-5p and miR-146b-5p have been found to be induced by carbamylated albumin and to be enriched in renal cell carcinoma tumors (Ha et al. 2010). When delivered into the kidneys of a fibrosis mouse model using polyethylenimine nanoparticles, miR-146a-5p is able to attenuate renal fibrosis (Morishita et al. 2015). Additionally, miR-146a-5p levels are increased in mice suffering from chronic renal inflammation (Ichii et al. 2012). In the 3'-UTR of the renalase, a signaling molecule in cardiovascular and metabolic disease, a SNP (Single nucleotide polymorphism) that is common in humans creates a functional binding site for miR-146a-5p (Kalyani et al. 2015). The mature miRNA miR-330-3p was reported to be expressed in the juxtaglomerular cells, balancing its smooth muscle phenotype together with miR-125b-5p (Medrano et al. 2011). Additionally, miR-330-3p might regulate VEGF (Ye et al. 2008). In renal clear cell carcinoma, miR-107-3p was identified as a putative tumor

suppressor gene (Song et al. 2015) and a mutation in mir-149 has been linked to renal clear cell carcinoma (Wang et al. 2014). No role in the kidney has been assigned to miR-130a-3p, miR-148a-3p, and miR-196b-5p so far. The miR-130/301 family are signaling molecules in the crosstalk between endothelial cells and smooth muscle cells controlling vasoconstriction in pulmonary hypertension (Bertero et al. 2014), while the miR-148/152 family can modulate the innate response and antigen presenting capacity of dendritic cells (Liu et al. 2010B).

Expression levels and enrichment of miRNAs

To identify miRNAs that might be important for podocyte structure and function, the enrichment of the glomerular and podocyte miRNAs compared to a control cell population, tubules or the red fluorescent cell population of glomerular cells, was calculated. Only one miRNA, miR-873a-5p, might be exclusively expressed in podocytes, while all other miRNAs expressed in podocytes were also detected in the other glomerular cells or in the tubules. The enrichment is one possible way to sort for miRNAs that might be important for a podocyte specific function rather than a general regulatory mechanism. Nonetheless, miRNAs can have different functions in different cell populations, meaning that a miRNA not exclusively expressed in podocytes might still be a regulator of a podocyte specific transcript. In June 2015, the online database TarBase v7.0 (Vlachos et al. 2014) listed over 65,000 miRNA-gene interactions derived from specific and high-throughput experiments, proving that a mature miRNA regulates more than one specific target in different species, cell types and developmental stages. The expression level of a miRNA might also give hints to its physiological importance. The miR-92a-3p has a lower relative expression level in podocytes compared to the red fluorescent cells. However, in absolute numbers, it is the 19th highest expressed miRNA in podocytes, meaning it might also regulate a transcript important for podocyte function. It is reasonable to assume that a miRNA expressed in high levels plays a role in maintenance of cell function. Additionally, it is important to keep in mind that a rather rare miRNA can be extremely important for a cell.

Patterns of miRNAs expressed in podocytes

The miRNAs that were found to be podocyte enriched were analyzed for patterns to get hints concerning their role in podocyte function. In some cases, e.g. four members of the mir-30 family, mir-330 and mir-503, both mature miRNAs that are processed from the same precursor are enriched in podocytes (Tab. 5.1). The miRNA expressed at lower levels might just be the passenger strand, which is degraded after the other miRNA forms the functional RISC together with the Argonaute protein, but both miRNAs from the same precursor might also be functional miRNAs in the cell.

Tab. 5.2: Genomic organization of murine podocyte miRNAs

miRNAs	Genomic coordinates of the precursor mirna in mouse	Genomic organization in mouse (ensembl, UCSC, miRbase)	clustered miRNAs (<10 kb) in mouse
mmu-let-7e-3p	chr17: 17,830,352-17,830,444 [+]	antisense to gene Gm25927	mmu-let-7e, mmu-mir-99b, mmu-mir-125a
mmu-miR-23b-3p	chr13: 63,300,484-63,300,557 [+]	intron of protein coding gene 2010111I01Rik (together with mir-27b, mir-24-1, mir-3074 (antisense))	mmu-mir-23b mmu-mir-27b mmu-mir-24-1; antisense: mmu-mir-3074-1
mmu-miR-24-1-5p	chr13: 63,301,208-63,301,275 [+]	intron of protein coding gene 2010111I01Rik (together with mir-27b, mir-24-1, mir-3074 (antisense))	mmu-mir-23b mmu-mir-27b mmu-mir-24-1; antisense: mmu-mir-3074-1
mmu-miR-27b-5p	chr13: 63,300,712-63,300,784 [+]	intron of protein coding gene 2010111I01Rik (together with mir-27b, mir-24-1, mir-3074 (antisense))	mmu-mir-23b mmu-mir-27b mmu-mir-24-1; antisense: mmu-mir-3074-1
mmu-miR-30a-3p	chr1: 23,272,269-23,272,339 [+]	intergenic	
mmu-miR-30a-5p	chr1: 23,272,269-23,272,339 [+]	intergenic	
mmu-miR-30b-3p	chr15: 68,337,415-68,337,510 [-]	directly upstream of Gm26621	mmu-mir-30d, mmu-mir-30b
mmu-miR-30b-5p	chr15: 68,337,415-68,337,510 [-]	directly upstream of Gm26621	mmu-mir-30d, mmu-mir-30b
mmu-miR-30c-2-3p	chr1: 23,291,701-23,291,784 [+]	part of lincRNA Gm27028	
mmu-miR-30c-5p	locus 1: chr4: 120,769,534-120,769,622 [-] locus 2: chr1: 23,291,701-23,291,784 [+]	Locus 1: intron of NFYC (nuclear transcription factor Y gamma) Locus 2: part of lincRNA Gm27028	locus 1: mmu-mir-30f, mmu-mir-30e, mmu-mir-30c-1
mmu-miR-30d-3p	chr15: 68,341,208-68,341,289 [-]	part of lincRNA Gm20732	mmu-mir-30d, mmu-mir-30b
mmu-miR-30d-5p	chr15: 68,341,208-68,341,289 [-]	part of lincRNA Gm20732	mmu-mir-30d, mmu-mir-30b
mmu-miR-99a-3p	chr16: 77,598,936-77,599,000 [+]	intron of lincRNA MIR99AHG (mir-99a host gene)	mmu-mir-99a, mmu-let-7c-1
mmu-miR-99a-5p	chr16: 77,598,936-77,599,000 [+]	intron of lincRNA MIR99AHG (mir-99a host gene)	mmu-mir-99a, mmu-let-7c-1
mmu-miR-107-3p	chr19: 34,820,687-34,820,773 [-]	intron of Pank1 (pantothenate kinase 1)	
mmu-miR-125b-2-3p	chr16: 77,646,273-77,646,343 [+]	intron of lincRNA MIR99AHG (mir-99a host gene)	
mmu-miR-125b-5p	locus 1: chr9: 41,581,926-41,582,002 [+] locus2: chr16: 77,646,273-77,646,343 [+]	Locus 1: intron of lncRNA 2610203C20Rik Locus 2: intron of lincRNA MIR99AHG (mir-99a host gene)	
mmu-miR-130a-3p	chr2: 84,741,115-84,741,178 [-]	intergenic	
mmu-miR-146b-5p	chr19: 46,342,762-46,342,870 [+]	intron of Tmem180 (Transmembrane protein 180)	
mmu-miR-148a-3p	chr6: 51,269,812-51,269,910 [-]	intergenic	
mmu-miR-149-5p	chr1: 92,850,378-92,850,443 [+]	intron of Gpc1 (Glypican 1)	

miRNAs	Genomic coordinates of the precursor mirna in mouse	Genomic organization in mouse (ensembl, UCSC, miRbase)	clustered miRNAs (<10 kb) in mouse
mmu-miR-196b-5p	chr6: 52,230,081-52,230,165 [-]	intron of Hoxa9 (Homeobox A9) processed transcript exon of Hoxa9 retained intron exon of pseudogene 9930038K12	
mmu-miR-210-3p	chr7: 141,221,384-141,221,493 [-]	intergenic	
mmu-miR-322-3p	chrX: 53,054,255-53,054,349 [-]	ensembl: intergenic, downstream of lncRNA C430049B03 UCSC: part of lncRNA C430049B03	mmu-mir-322, mmu-mir-503, mmu-mir-351, mmu-mir-542, mmu-mir-450a-1, mmu-mir-450a-2, mmu-mir-450b
mmu-miR-330-3p	chr7: 19,181,465-19,181,562 [+]	intron of Eml2 (echinoderm microtubule associated protein like 2)	
mmu-miR-330-5p	chr7: 19,181,465-19,181,562 [+]	intron of Eml2 (echinoderm microtubule associated protein like 2)	
mmu-miR-340-5p	chr11: 50,069,702-50,069,799 [+]	intron of RNF130 (ring finger protein 130)	
mmu-miR-351-3p	chrX: 53,053,255-53,053,353 [-]	ensembl: intergenic, upstream of lincRNA Gm28730 UCSC: exon of lncRNA C430049B03	
mmu-miR-351-5p	chrX: 53,053,255-53,053,353 [-]	ensembl: intergenic, upstream of lincRNA Gm28730 UCSC: exon of lncRNA C430049B03	
mmu-miR-450a-5p	locus 1: chrX: 53,048,154-53,048,244 [-] locus 2: chrX: 53,048,299-53,048,367 [-]	intergenic	mmu-mir-322, mmu-mir-503, mmu-mir-351, mmu-mir-542, mmu-mir-450a-1, mmu-mir-450a-2, mmu-mir-450b
mmu-miR-450b-5p	chrX: 53,047,997-53,048,078 [-]	intergenic	
mmu-miR-503-3p	chrX: 53,053,984-53,054,054 [-]	ensembl: intergenic UCSC: exon of lncRNA C430049B03	
mmu-miR-503-5p	chrX: 53,053,984-53,054,054 [-]	ensembl: intergenic UCSC: exon of lncRNA C430049B03	
mmu-miR-542-3p	chrX: 53,049,403-53,049,487 [-]	intergenic	
mmu-miR-574-3p	chr5: 64,970,318-64,970,395 [+]	intron of Fam114a1 (family with sequence similarity 114, member A1)	
mmu-miR-615-3p	chr15: 103,014,910-103,015,001 [+]	intron of Hoxc5 (homeobox C5)	
mmu-miR-652-3p	chrX: 142,739,000-142,739,097 [+]	intron of Tmem164 (transmembrane protein 164)	
mmu-miR-873a-5p	chr4: 36,668,510-36,668,586 [-]	intron of Lingo2 (leucine rich repeat and Ig domain containing 2)	mmu-mir-873b, mmu-mir-873a

Another possibility to identify miRNAs that might have a cooperative function in podocytes is the analysis of the genomic organization. miRNAs which are processed from clusters, i.e. transcripts that contain several miRNA precursors, have been shown to perform cooperative tasks in cells, like the miR-17~92 cluster that enhances cell proliferation (Hayashita et al. 2005) and is crucial for developing nephrons during kidney development (Marrone et al. 2014) or the mir-23~27~24

clusters, which play an important role in angiogenesis, endothelial apoptosis in cardiac ischemia and retinal vascular development (reviewed by Bang et al. 2011).

The miRNAs were analyzed for genomic location and putative common precursor transcripts. Since the three precursors mmu-mir-23b, mmu-mir-27b and mmu-mir-24-1 are located in the same intron of the protein coding gene 2010111I01Rik, they are probably transcribed together. The precursors mir-30b and mir-30d are located in proximity in the genome, but since mir-30d is part of the lincRNA (long intergenic non-coding RNA) Gm20732 and mir-30b is located directly upstream of lincRNA Gm27028, they might be transcribed independently from each other. On the other hand, the distance between the mir-125b-2 and mir-99a position in the genome is > 50 kb, but they are located in the same lncRNA host gene, which supports a possible common transcription.

Interestingly, eight miRNAs that were found to be podocyte enriched in both *deep sequencing* profiles are encoded in a genomic area of ca. 5,800 bp on reverse strand of the X-chromosome (Fig. 5.2). The arrangement is conserved between human and mouse, with the mmu-mir-322 being exchanged for hsa-mir-424 and the mir-351 missing in human. In rat, the putative cluster is not only conserved, but two similar arrangements are present in the genome on the X chromosome. The genomic organization of the mirna precursors was analyzed using the UCSC genome browser and the ensembl database. For the comparison, the human genome (UCSC: GRCh38/hg38; ensembl: GRCh38.p3) and the murine genome (UCSC: GRCm38; ensembl: GRCm38.p4) were used.

According to the UCSC genome browser, mmu-mir-322, mmu-mir-503 and mmu-mir-351 are part of the lncRNA C430049B03, arguing for a common transcription. The transcriptional start site of this transcript is located ca. 2,800 bp upstream of the mir-322 precursor. In the database ensembl, however, the lncRNA is annotated to be shorter and its transcription ends upstream of the seven precursors (chromosome X: 53,055,046 - 53,057,190 according to ensembl). According to ensembl, lincRNA Gm28730 is located between mmu-mir-351 and mmu-mir-542 on the same strand, but does not stretch to the miRNA precursors downstream of it. The four precursors mmu-mir-542, mmu-mir-450a-2, mmu-mir-450a-1 and mmu-mir-450b are all annotated to be intergenic in the UCSC as well as in ensembl. However, it might be that a common primary transcript has not been identified yet, since the processing of the initial transcript, e.g. a lncRNA, might be very fast. Especially the very narrow gaps in-between the members of the mir-450 family might be a hint for common or alternate transcription.

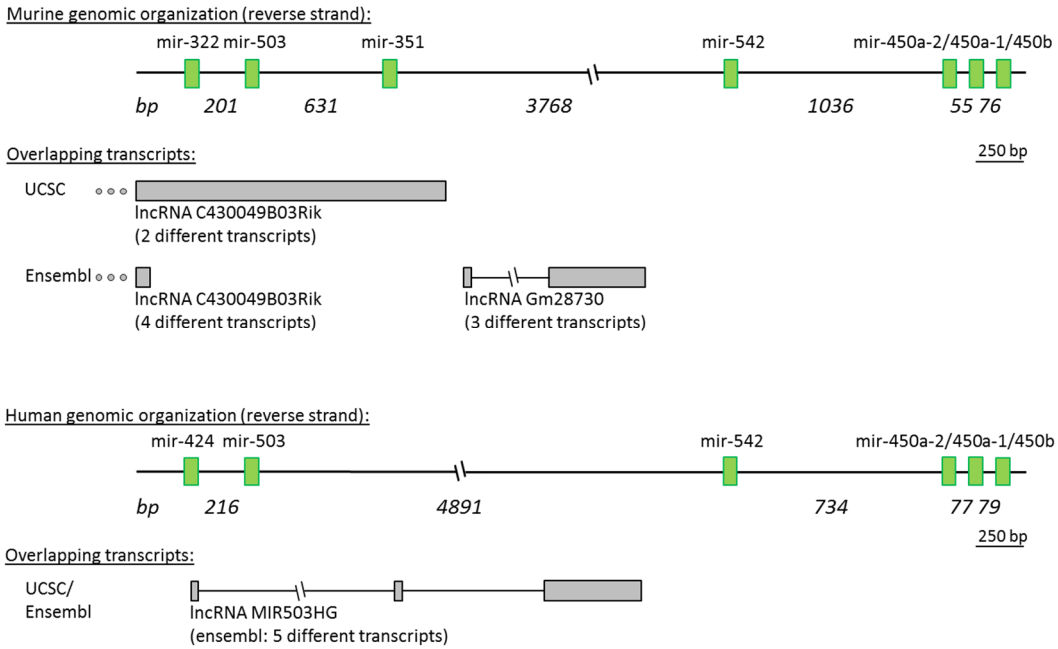

Fig. 5.2: Putative podocyte miRNA cluster; genomic arrangement of seven miRNA precursors (green boxes) coding for mature miRNAs enriched in murine podocytes and overlapping transcripts (grey boxes) in mouse (top) and human (bottom) on the reverse strand of the X-chromosome; numbers indicate the distances in basepairs between precursors; start of lncRNAs indicated by dotted lines

In human, hsa-mir-503 is located in an intron of lncRNA MIR503HG, the hsa-mir-503 host gene, while the location of hsa-mir-424 overlaps with the annotated first exon of this lncRNA. The four remaining precursors, hsa-mir-542, hsa-mir-450a-2, hsa-mir-450a-1 and hsa-mir-450b are all annotated to be intergenic according to the UCSC as well as ensembl in human like in mouse (Tab. 5.3; for all human podocyte miRNAs, Tab. 10.7).

Tab. 5.3: genomic organization of podocyte miRNAs in human

miRNAs	human accession number mature miRNA	Genomic coordinates of the precursor mirna in human	Genomic organization in human (UCSC, ensembl)
hsa-miR-424-3p	MIMAT0004749	chrX: 134,546,614-134,546,711 [-]	overlapping to lncRNA MIR503HG
hsa-miR-450a-5p	MIMAT0001545	Locus 1: chrX: 134,540,341-134,540,431 [-] Locus 2: chrX: 134,540,508-134,540,607 [-]	intergenic
hsa-miR-450b-5p	MIMAT0004909	chrX: 134,540,185-134,540,262 [-]	intergenic
hsa-miR-503-3p	MIMAT0022925	chrX: 134,546,328-134,546,398 [-]	Intron of lncRNA MIR503HG (mir-503 host gene)
hsa-miR-503-5p	MIMAT0002874	chrX: 134,546,328-134,546,398 [-]	Intron of lncRNA MIR503HG (mir-503 host gene)
hsa-miR-542-3p	MIMAT0003389	chrX: 134,541,341-134,541,437 [-]	intergenic

As the mature miRNAs derived from these precursors were enriched in both *deep sequencing* profiles from freshly isolated murine podocytes, they are an interesting target for knockout and

overexpression studies, representing putative regulators of genes important for podocyte structure and function. For some miRNAs encoded in the putative cluster, a regulatory role has been identified. However, a common function has not been described yet.

For some of these miRNAs, involvement in different regulatory processes has been proposed. For example, neural stem cell morphogenesis is mediated by miR-351-5p (Li et al. 2012). miR-322-3p mediates osteoblast differentiation (Gamez et al. 2013) and inhibits Smurf2 (SMAD specific E3 ubiquitin protein ligase 2) translation, thus modulating TGF-β/Smad2 signaling (Cao et al. 2014). Inhibiting G1/S translation by downregulation of cyclin D3 and E2F3 (E2F transcription factor 3) in hepatocellular carcinoma (Xiao et al. 2013) and inhibiting EMT in gastric cancer (Peng et al. 2014) are only two examples of different roles miR-503-5p has been shown to play in progression of different cancers. Also for miR-542-3p, different roles in the progression of cancers like suppressing cell growth of gastric cancer cells (Shen et al. 2015) or suppressing tumor growth by downregulating survivin in neuroblastomas (Althoff et al. 2015) have been reported. Little is known about the regulatory role of the mir-450 family in kidney so far. In rat kidney, rno-miR-450a-5p was identified to be enriched in the cortex compared to the medulla (Tian et al. 2008), which is consistent with a higher expression in the podocytes, since glomeruli are located in the cortex of mammalian kidneys. In the same study, Hnrpk (Heterogeneous nuclear ribonuclear protein K) was identified as a putative target of miR-450a-5p.

For three mature miRNAs, miR-424-3p, miR-503-5p and miR-542-3p, expression was investigated in proliferating and differentiated immortalized human podocytes (chapter 4.1.2). Neither in proliferating nor in differentiated cells, could expression be detected. This could be due to the expression levels of the mature miRNAs, which were also mid-level in the *deep sequencing* profiles. It might also show the differences between the differentiated immortalized podocytes and the freshly isolated podocytes. Additionally, a species dependent expression is possible, which can be tested by Northern Blotting of these miRNAs from proliferating and differentiated cells from the immortalized murine podocyte cell line.

5.2.2 miRNA expression validation

Using the modern sequencing techniques like *deep sequencing*, it is now possible to generate miRNA profiles from tissues or cell types that consist of millions of single reads, identifying hundreds of expressed miRNAs. However, many reaction steps are needed to gain the final results, like extraction, ligation of adaptors, reverse transcription and up-scaling PCRs, which can all be biased or distorted by statistical effects. Therefore, a profile can be used as a starting point, but has to be validated by different methods. For miRNA expression analyses, there are

two main methods, Northern Blotting and qPCR, which both harbor different advantages and disadvantages. Experiments have been performed to find a "housekeeping" miRNA to use as an internal standard for relative quantification, e.g. by comparing miRNA expression profiles of different colorectal cancer samples and normal tissue control samples (Chang et al. 2010). However, since all miRNAs might be functional regulatory miRNAs themselves and play different roles in different cell types, they might also still be differentially expressed between two distinct cell types. The small nuclear RNA U6, a part of the spliceosome, is often used as an internal standard in both qPCR and Northern Blotting, since it is expected to be rather equally expressed in all different cell types.

A general challenge for miRNA detection is their shortness. Northern Blotting probes as well as PCR primers need a minimum length of around 18 - 20 bp to hybridize with their target sequence, which is about the length of a miRNA. This prevents the selection of a sequence region suitable for hybridization, meaning that there might be miRNA sequences that are more suited for hybridization than others. In Northern Blotting, miRNAs are detected by hybridization of a fitting antisense strand. Dependent on the hybridization temperature that is used to hybridize a precise miRNA probe to the target miRNA, single mismatches can be detected, thus enabling the identification of miRNAs belonging to the same family (Fig. 4.28). Furthermore, due to the separation of the samples by gel electrophoresis, the miRNA precursor can be clearly distinguished from the mature miRNA (Fig. 5.3 A). Northern Blotting requires a lot of isolated RNA, making it the method of choice for experiments using cell culture material, but unfavorable for samples isolated from laboratory animals. In this study, 9 – 30 µg total RNA isolated from cell culture or laboratory animals was used for Northern Blotting, which translates to ca. three to four mice needed for one validated miRNA.

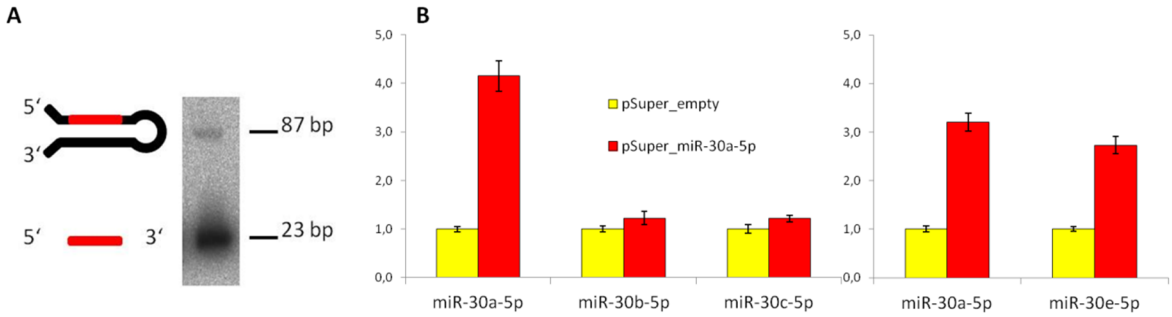

Fig. 5.3: Comparison of miRNA profile validation techniques; (A) Northern Blot of miR-19b expression in HeLa cells: hybridization signal of precursor (top) and mature miRNA (bottom); (B) qPCR of HeLa cells transfected with empty pSuper construct or pSuper construct overexpressing miR-30a-5p analyzed by qPCR with primers directed against miR-30 family members

By qPCR, the presence of miRNAs can be detected already at very low levels, making it a very suitable method if the amount of sample is limited. With less material than needed for one Northern Blotting lane, tens to more than one hundred miRNAs, dependent on their expression levels, can be detected. This enables qPCR based screening for a subset of miRNAs. Especially if the samples used are collected from laboratory animals, saving material is a huge advantage of this method. Additionally, miRNAs expressed at low levels might rather be detected by qPCR than by Northern Blotting.

When using normal DNA primer in the qPCR reaction, single mismatches between miRNAs belonging to the same family cannot be detected. When miR-30a-5p is overexpressed in cells, qPCR with the normal DNA primers against miR-30a-5p and miR-30e-5p both detect a similar level of upregulation (Fig. 5.3 B), showing that one mismatch between the mature miRNA sequences is not sufficient to distinguish between the two miRNAs. Both the primers directed against miR-30b-5p and miR-30c-5p, two miRNAs with 7 and 5 mismatches when compared to miR-30a-5p (Tab. 5.4), did not detect an upregulation of their target. This proves that qPCR is suitable for detection of miRNAs with several mismatches between their mature sequences.

Tab. 5.4: Sequences of mature miR-30 family members; mismatching nucleotides: marked in red

mature miRNA	Sequence seed region	number of mismatches
miR-30a-5p	UGUAAACAUCCUCGACUGGAAG	
miR-30b-5p	UGUAAACAUCCUACACUCAGCU	7 mismatches
miR-30c-5p	UGUAAACAUCCUACACUCUCAGC	5 mismatches
miR-30d-5p	UGUAAACAUCCCCGACUGGAAG	1 mismatch
miR-30e-5p	UGUAAACAUCCUUGACUGGAAG	1 mismatch

Furthermore, the miRNA precursors, which normally is present in cells at much lower levels than the mature miRNA, might also be amplified and give a signal. To check for amplification of molecules other than the desired mature miRNA, melting curves of the PCR products are recorded and checked for additional peaks indicating the presence of additional products. Especially for miRNAs derived from the 5'-end of the precursors, a longer product should be detected if the precursor is amplified. For all miRNAs, only one peak was observed. To bypass these disadvantages, especially designed primer molecules like LNA™ (locked nucleic acid; Exiqon) primers for detection of miRNAs without including the rest of the family, as well as Taqman® assays (lifetechnologies) for the detection of pri-miRNAs can be used.

Northern Blotting was used for the detection of ten miRNAs in proliferating and differentiated immortalized human podocytes and miR-30a-5p detection in HEK293T knockout cell clones. It

was also used for the expression validation of a subset of four miRNAs expressed in murine glomeruli and tubules isolated from C57bl/6 wildtype mice. For validation of miRNA expression of eleven miRNAs in murine glomeruli and tubules isolated from C57bl/6 wildtype mice, as well as for validation of relative expression of 18 miRNAs between podocytes and the red fluorescent cell population obtained from transgenic reporter animals, qPCR was used.

5.3 Identification of miRNA-mRNA pairs

The vast number of mRNAs and miRNAs expressed in podocytes contributes to the complexity of the physiological equilibrium in living cells, complicating the identification of single miRNA-mRNA interaction pairs. Different strategies were used to narrow down the candidates to find possible interaction partners. A combined approach using *in silico* predictions, Ago-IPs from immortalized human and murine podocytes and freshly isolated podocytes and luciferase assays was used to identify regulatory miRNA-mRNA pairs in podocytes. Four putative targets, CD2AP, FYN, NCK2 and NEPH1, all known to directly interact with the main component of the slit diaphragm, nephrin, were analyzed in detail (Tab. 5.5).

5.3.1 *In silico* prediction of miRNA-mRNA pairs

To generate a starting point for our experiments, *in silico* predictions were performed for transcripts coding for proteins known to be important for podocyte structure and function and miRNAs we identified to be enriched or highly expressed in podocytes. In the last years, several miRNA-mRNA interaction prediction programs have been published. Many of them can be run online one the respective websites. However, the amount of possible interaction partners obtained by these programs is rather overwhelming. Starting predictions with miRNAs, thousands of mRNAs that could potentially be regulated by these miRNAs are predicted. Vice versa, starting with a single mRNA, hundreds of miRNAs are predicted as possible regulators.

Prediction of interaction between podocyte miRNAs and genes important for podocyte maintenance

The *in silico* predictions were performed for putative miRNA-mRNA pairs. Binding sites for miRNAs that were enriched or highly expressed in podocytes were searched in the 3'-UTRs of transcripts coding for proteins that are known to be important for podocyte structure and function. This approach excludes possible interactions in the promoter regions of the genes as well as in the 5'-UTRs and coding regions of the transcripts, which are still a small minority in the

whole number of verified interactions. It also limits the predicted dataset to proteins that are already known to play an important role for podocyte structure and function. The first predictions were performed for 29 transcripts coding for proteins known to be important for podocyte structure and function using the miRWalk prediction platform. From this initial candidate set, four putative targets, CD2AP, FYN, NCK2 and NEPH1, all known to play an important role in the maintenance of the podocyte slit diaphragms, were selected as first candidates and analyzed in more detail using miRWalk2.

Boundaries of in silico *predictions*

To be able to concentrate on the most promising predictions in the further experiments, the prediction program miRWalk (Dweep et al. 2011) was used. miRWalk does not only predict interactions itself, but also obtains the predictions of up to eight different algorithms. Recently, the miRWalk2 program was released (Dweep et al. 2011), now also enabling prediction of binding sites in 3'-UTRs with twelve programs, in coding regions with seven programs and 5'-UTRs with six programs. Additionally, prediction of binding sites in the promoter regions is now possible with four programs. To shrink the enormous dataset obtained from the prediction programs, a score consisting of the number of programs that predict a certain interaction was introduced. An interaction was counted to be predicted when it was predicted by at least half of the used programs.

All *in silico* prediction programs use a kind of score or threshold to determine if a certain miRNA-mRNA pair is predicted for interaction. A second possible way to shrink the dataset, next to using different programs, could be a stricter adjustment of these thresholds in the prediction algorithms. These strategy harbors two possible disadvantages: Firstly, it is nearly impossible to determine which algorithm is the best in predicting miRNA-mRNA interaction pairs. They can be tested with miRNA-mRNA pairs that were proven to be functional, but that does not imply that they will be the best in predicting still unknown interaction pairs. Secondly, all programs work with models that are used to calculate the probability of binding, like the thermodynamic stability of the double stranded RNA to be built. Since these models may deviate from the situation in cells, physiological interactions might get rejected with a threshold that is set to strictly.

For the miRNAs enriched in podocytes, and some miRNAs that are not enriched, but highly expressed in podocytes, *in silico* target predictions were performed using the algorithms miRWalk and miRWalk2 (Dweep et al. 2011). For 20 candidate miRNAs, binding sites in the 3'-UTRs of human transcripts coding for podocyte proteins were predicted (Tab. 5.5).

Tab. 5.5: Podocyte miRNAs and targets – prediction and known functions

miRNAs identified in murine podocytes	predicted human targets by miRWalk & miRWalk2	Expression in mammalian kidney	Function in kidney
mmu-let-7e-3p		Expressed in murine glomeruli (smirnadb database)	
mmu-miR-23b-3p	ACTR2, EZR, PARD6B, TRPC6, VEGFA, WASL, WT1	Expressed in murine glomeruli (smirnadb database)	
mmu-miR-24-1-5p			
mmu-miR-27b-5p			
mmu-miR-30a-3p			
mmu-miR-30a-5p	CD2AP, IQGAP1, NCK2, TRPC6, WASL	Highly expressed in podocytes (Harvey et al. 2008) Expressed in murine glomeruli (smirnadb database) Expressed in podocytes (Boerries et al. 2013)	Affected in podocyte Dicer knockout (Harvey et al. 2008, Shi et al. 2008) Important for *Xenopus* kidney development (Agrawal et al. 2009) mir-30 family is involved in TGF-β signaling during glomerulosclerosis (Shi et al. 2013) Downregulation of mir-30 family facilitates podocyte injury, miR-30s target Notch1 (Wu et al. 2014) Upregulated in injured podocytes, prevents PAN induced podocyte apoptosis (Xie et a. 2015)
mmu-miR-30b-3p			
mmu-miR-30b-5p		Expressed in murine glomeruli (smirnadb database) Expressed in podocytes (Boerries et al. 2013)	
mmu-miR-30c-2-3p			
mmu-miR-30c-5p		Expressed in murine glomeruli (smirnadb database) Expressed in podocytes (Boerries et al. 2013)	
mmu-miR-30d-3p			
mmu-miR-30d-5p		Expressed in murine glomeruli (smirnadb database)	
mmu-miR-99a-3p			
mmu-miR-99a-5p		Expressed in rat kidney cortex and medulla (Tian et al. 2008)	
mmu-miR-107-3p	ACTR2, CD2AP, CDC42, EZR, GRB2, NEPH1, NPHS1, PODXL, VEGFA, WASL		Putative tumor suppressor in renal clear cell carcinoma (Song et al. 2015)
mmu-miR-125b-2-3p			
mmu-miR-125b-5p		Expressed in rat kidney cortex and medulla (Tian et al. 2008) Marks juxtaglomerular cells (Medrano et al. 2012)	Balances juxtaglomerular cells' smooth muscle phenotype (Medrano et al. 2012)
mmu-miR-130a-3p	CD2AP, EZR, WASL, FYN	Expressed in murine glomeruli (smirnadb database)	
mmu-miR-146b-5p	GRB2, FYN, IQGAP, PARD6B, RAC1, RHOA	Increased in renal cell carcinoma (Ha et al. 2010) Expressed in podocytes (Boerries et al. 2013)	Attenuates renal fibrosis (Morishita et al. 2015) Targets mutated renalase (Kalyani et al. 2015)
mmu-miR-148a-3p	EZR, PODXL, RAC1, WASL		
mmu-miR-149-5p	GRB2, LMX1B, NEPH1, NEPH3, PODXL	Expressed in murine glomeruli (smirnadb database)	When mutated, involved in renal clear cell carcinoma (Wang et al. 2014)
mmu-miR-196b-5p	NOSTRIN,PARD6B, TLN1, WASL	Expressed in murine glomeruli (smirnadb database)	
mmu-miR-210-3p	LMX1B		
mmu-miR-322-3p		Expressed in murine glomeruli (smirnadb database) Expressed in podocytes (Boerries et al. 2013)	

miRNAs identified in murine podocytes	predicted human targets by miRWalk & miRWalk2	Expression in mammalian kidney	Function in kidney
mmu-miR-330-3p		Marks juxtaglomerular cells (Medrano et al. 2012)	Balances juxtaglomerular cells' smooth muscle phenotype (Medrano et al. 2012) Regulates VEGF (Ye et al. 2008)
mmu-miR-330-5p			
mmu-miR-340-5p	ACTR2, CD2AP, CLIC5, IQGAP1, NCK1, NCK2, PARD6B, PODXL, RAC1, TRPC6, WASL, WT1		
mmu-miR-351-3p			
mmu-miR-351-5p			
mmu-miR-450a-5p		Expressed in murine glomeruli (smirnadb database) Enriched in rat kidney cortex (Tian et al. 2008) Expressed in podocytes (Boerries et al. 2013)	Regulates Hnrpk (Tian et al. 2008)
mmu-miR-450b-5p	ACTR2, CD2AP, EZR, GRB2, NCK2, NPHS2, RAC1		
mmu-miR-503-3p			
mmu-miR-503-5p	ACTR2, CD2AP, PARD6B, TLN1, VEGFA, WASL, WT1	Expressed in murine glomeruli (smirnadb database)	
mmu-miR-542-3p	IQGAP1, NCK1, NPHS2, PARD6B, RAC1		
mmu-miR-574-3p	RAC1	Expressed in murine glomeruli (smirnadb database) Expressed in podocytes (Boerries et al. 2013)	
mmu-miR-615-3p			
mmu-miR-652-3p			
mmu-miR-873a-5p			
mmu-miR-22-3p	ACTR2, EZR, GRB2, PODXL	Expressed in murine glomeruli (smirnadb database)	
mmu-miR-24-3p	IQGAP1, VEGFA	Expressed in rat kidney cortex and medulla (Tian et al. 2008)	
mmu-miR-26a-5p	CD2AP, CLIC5, FAT1, TRPC6	Expressed in murine glomeruli (smirnadb database) Lowered levels in post stenotic kidneys (Zhu et al. 2015) Lowered levels in patients with lupus nephritis or IgA nephropathy (Ichii et al. 2014)	Targets CTGF, involved in nephropathy (Koga et al. 2015)
mmu-miR-27a/b-3p	ACTR2, CD2AP, CDC42, EZR, FYN, GRB2, PARD6B, WASL	Expressed in murine glomeruli (smirnadb database) Expressed in rat kidney cortex and medulla (Tian et al. 2008)	
mmu-miR-29a-c-3p	CDC42, NEPH1, TRPC6, VEGFA	Expressed in murine glomeruli (smirnadb database) Signature miRNA under high glucose conditions (Long et al. 2011)	Regulates several collagens (Liu et al. 2010A) Targets Spry1 (Long et al. 2011) Blocks progressive renal fibrosis (Qin et al. 2011) Represses expression of collagens (Wang et al. 2012) Modulates nephrin acetylation (HDAC4) (Lin et al. 2014)
mmu-miR-92a-3p	CD2AP, CDC42, NCK2, PARD6B, WASL	Expressed in murine glomeruli (smirnadb database) Expressed in rat kidney cortex and medulla (Tian et al. 2008)	miR-17~92 cluster retards cyst growth (Patel et al. 2013) miR-17~92 cluster is crucial for kidney development (Marrone et al. 2014)

5.3.2 Regulated mRNAs identified by Ago-IP and microarray

To validate putative targets generated by *in silico* predictions, Ago-IP with a subsequent qPCR detection of four predicted targets was performed using proliferating immortalized human and murine podocytes. Enrichment could be detected for CD2AP, FYN, NCK2 and NEPH1 in the Ago-IP samples from the human as well as in the murine cells, proving them to be regulated by miRNAs in proliferating cells. Thus, with the combination of *in silico* prediction of putative miRNA regulation of genes important for podocyte structure and function and their detection by qPCR in the Ago-IP samples, four miRNA regulated genes could be identified.

Nonetheless, this approach only allows the detection of targets that are already known to be important in podocytes. For an unbiased identification of transcripts bound by miRNAs, Ago-IP was performed from freshly isolated murine podocytes. The transcripts isolated were analyzed on a microarray. Of the four targets that were *in silico* predicted and investigated more closely by Ago-IP from human and murine podocyte cell lines, two targets, Cd2ap and Fyn, were also enriched in the Ago-IP samples from freshly isolated murine podocytes. Additionally, seven more proteins known or expected to be important for podocyte structure and function, Itgb1, Vegfa, Actg1, Nphs2, Actbl2, Itgb5 and Wipf3 were detected to be enriched in the Ago2 bound sample when compared to the background control or the Ago-IP from the red fluorescent cells, being the next candidates for prediction of putative binding sites of podocyte miRNAs.

Limitations of first microarray

Since the Ago2 bound transcripts are only a part of the whole transcriptome, a certain number of cells is needed to generate enough RNA for subsequent microarray analysis. As samples from many animals are needed to perform the analyses, it has been done only once until now. To generate reliable results, the whole procedure will be repeated to test if the transcripts enrichment detected in the first microarray can be validated for the new candidate transcripts. The transcripts identified to be enriched in the Ago-IP samples will be the next interesting candidates for *in silico* predictions and miRNA-mRNA pair identification via luciferase assay.

The errors in detection of transcript expression occur according to the Gaussian distribution, meaning most enrichment factors are detected rather correctly, while some enrichment factors are highly over- or underestimated. With an independent second and ideally third microarray, regression to the mean should occur, strengthen the results and allowing the identification of truly enriched transcripts. For these statistical reasons, more repetitions would be desirable, but are hardly possible due to the amount of animals needed per experiment.

5.3.3 miRNA-mRNA pair validation by luciferase assays

Four or two targets important for the structure of the slit diaphragms of podocytes, respectively, could be identified as miRNA targets by *in silico* predictions followed by the isolation of transcripts by Ago-IP from immortalized human and murine podocytes or freshly isolated murine podocytes. To identify the miRNAs responsible for the regulation of these targets *in vivo*, luciferase assays were performed.

Confirmed miRNA-mRNA interaction

For the first set of four candidate target transcripts, CD2AP, FYN, NCK2 and NEPH1, the human 3'-UTRs were cloned into luciferase reporter assay constructs. To check for regulation by different miRNAs, the reporter constructs were cotransfected into HEK293T cells together with miRNA overexpressing pSuper constructs. For CD2AP, a putative regulation by miR-30a-5p and miR-92a-3p could be detected. For the tyrosine kinase FYN, miR-146b-5p might be a functional regulator, as indicated by the repression after cotransfection. The luciferase repression seems to vanish when the predicted miR-146b-5p binding sites are mutated (bachelor thesis K. Heizler). In the initial screening experiment, NCK2 seemed to be regulated by coexpression miR-30a-5p. With further experiment using a 3'-UTR construct containing a mutated binding site, binding might be confirmed.

Cd2ap and Fyn could be identified to be regulated *in vivo* by Ago-IP from freshly isolated murine podocytes (Tab. 5.6). The miR-92a/b-3p binding site is not only conserved between the human and the murine CD2AP transcript, but is also the binding site predicted with the highest score for each of them. The miR-30a-5p binding site is only present in and predicted for the human transcript. Thus, the miR-92-3p binding site might be active in murine podocytes *in vivo* as well as in humans. The miR-146b-5p binding site in the human FYN 3'-UTR is predicted with very good scores and appears to be functional in luciferase assays, but it is not conserved to the murine 3'-UTR. Thus, other miRNAs might be responsible for the regulation of the murine transcript *in vivo.* For miR-130a-3p, two binding sites are conserved between the human and murine 3'-UTR. However, regulation could not be confirmed by luciferase assay.

NCK2 appeared to be targeted in luciferase assays by miR-30a-5p but could not be isolated by Ago-IP from freshly isolated podocytes. One possible explanation might be different regulatory mechanism in human and mouse. A second explanation might be the fact that the luciferase assay is performed under artificial conditions, with the miRNAs being overexpressed to guarantee sufficient miRNA levels for the luciferase transcripts whose transcription is driven by

the TK promoter. An excess level of a certain miRNA might bind to a putative binding site that is not active under physiological conditions. In spite of the miRNA overexpression during the luciferase assay, several predicted binding pairs did not show regulation, which proves that overexpression of a possibly fitting miRNA is not enough to artificially activate a binding site.

Tab. 5.6: Analyzed miRNA targets in podocytes; X: interaction tested negative; ✓: interaction confirmed; ?: interaction not proven yet

Target	Physiological function	Detected by Ago-IP using hPCLs/ mPCLs/ freshly isolated podocytes	miRNAs predicted to target human/ murine 3'-UTR		conserved binding sites	Luciferase Assay using human 3'-UTR
CD2AP	adaptor protein linking nephrin to the cytoskeleton	yes/yes/yes		miR-23a/b-3p	no	
			miR-27a/b-3p	miR-27a/b-3p	yes	X
			miR-29a-c-3p	miR-29a-c-3p	no	X
			miR-30a-e-5p		no	✓
			miR-92a/b-3p	miR-92a/b-3p	yes	?
			miR-107(-3p)	miR-107-3p	yes	
			miR-130a-3p		no	
			miR-340-5p	miR-340-5p	no	
			miR-450a/b-5p		no	
			miR-503-5p	miR-503-5p	yes	
				miR-542-3p	no	
Fyn	phosphorylates slit diaphragm components nephrin (prerequisite to Nck recruitment and Ca^{2+} dependent signaling) and Neph1	yes/yes/yes	miR-23a/b-3p		yes/yes/no	X
			miR-24-3p		no	
			miR-27a/b-3p	miR-27a/b-3p	no	X
			miR-29a-c-3p	miR-29a-c-3p	yes	
			miR-30a-e-5p	miR-30a-e-5p	yes	
			miR-130a-3p		yes/yes	X
			miR-146b-5p		no/no	✓
			miR-149-5p		yes/no	
				miR-322-3p (miRNA not conserved)	yes	
			miR-340-5p		yes	
			miR-450b-5p		no	
Nck2	Adapter protein recruited after nephrin phosphorylation, regulates assembly of actin filaments	yes/yes/no		miR-23a/b-3p	yes	X
			miR-30a-e-5p	miR-30a-e-5p	yes	?
			miR-92a/b-3p		yes	X
				miR-196b-5p	no	
			miR-340-5p	miR-340-5p	yes/yes	
			miR-450b-5p	miR-450b-5p	yes	

Target	Physiological function	Detected by Ago-IP using hPCLs/ mPCLs/ freshly isolated podocytes	miRNAs predicted to target human/ murine 3'-UTR		conserved binding sites	Luciferase Assay using human 3'-UTR
Neph1	localized to the slit diaphragms, binds to nephrin	yes/yes/no		miR-23a/b-3p	no	
			miR-24-3p		no	
			miR-27a/b-3p	miR-27a/b-3p	?	
			miR-29a-c-3p	miR-29a-c-3p	yes	X
			miR-30b/c-3p	miR-30b/c-3p	yes	
				miR-30a-e-5p	no	
			miR-107(-3p)	miR-107-3p	?	
			miR-148a-3p		no	
			miR-149-5p		no	
				miR-196b-5p	no	
				miR-322-3p	no	
				miR-351-5p (miRNA not conserved)	no	
				miR-340-5p	no	
				miR-542-3p	no	

To verify the *in silico* predictions, putative regulatory pairs that seem to be active have to be further analyzed by mutation of the predicted binding site. In the experiments using the CD2AP 3'-UTR harboring the mutated miR-92a/b-3p binding site, the reduction of the luciferase assay activity by miR-92a/b-3p could not be validated, as the reduction could only be measured in some of the experiments. Luciferase assays are performed in cell culture, which leads to a high biological variance between the single experiments, since little deviations during the culturing might have a big influence on the state of the cells. This might explain the differing results in the different experiments. For miR-30a-5p, the predicted binding site in the 3'-UTR could be confirmed.

The 3'-UTR of FYN contains two putative binding sites for miR-146b-5p. Constructs containing the CD2AP 3'-UTR with single or double mutations will be used to identify the active binding site.

Consequences of miRNA level dysregulation in podocytes

The architecture of podocyte foot processes is regulated by a delicate interplay of several proteins that build up the slit diaphragm and link it to the cytoskeleton. It was shown by different studies that a podocyte specific deletion of the miRNA processing enzyme Dicer (Harvey et al. 2008, Ho et al. 2008, Shi et al. 2008) as well as an inducible podocyte specific deletion of the miRNA processing enzyme Drosha (Zhadanova et al. 2011) leads to a severe

phenotype alteration, including the loss of slit diaphragms and effacement of podocyte foot processes. This proves that miRNA levels are important for the development maintenance of podocyte structure and function, including the slit diaphragms.

CD2AP is an adapter protein important for the structure of the podocyte foot processes. It is localized to the slit diaphragm in murine glomeruli (Shih et al. 2001) and interacts directly with the actin cytoskeleton (Lehtonen et al. 2002), thus linking the slit diaphragm to the actin cytoskeleton. The CD2AP knockout mouse exhibits defects in epithelial foot processes and extra cellular matrix deposition (Shih et al. 1999). *In vivo*, CD2AP and nephrin interact with the p85 regulatory subunit of PI3K, which leads to recruitment of PI3K to the plasma membrane and stimulates PI3K-dependent AKT signaling in podocytes together with podocin (Huber et al. 2003A). If the available amount of CD2AP is the bottleneck of this initial signaling step, an upregulation of CD2AP would enhance AKT signaling in the podocyte. The serine/threonine kinase AKT, also known as PKB (Protein kinase B), is a central signaling node and controls many cellular processes like cell proliferation, survival and metabolism (Hers et al. 2011). Since AKT influences many pathways that favor tumorigenesis, like blocking the apoptosis pathway at several points, it is the most frequently hyper activated protein kinase in human cancer and a potential therapeutic target (Hers et al. 2011). Thus, a non-physiological upregulation of the AKT pathway might be one explanation for changes in podocytes after miRNA knockout.

CD2AP also interacts with podocin at the slit diaphragm (Schwarz et al. 2001). Since podocin, who was also identified to be miRNA regulated in the Ago-IP using freshly isolated murine podocytes, organizes a complex containing the ion channel TRPC6, a sensor of mechanically and osmotically induced membrane stretch (Huber et al. 2007), a dysregulated level of CD2AP might reduce the podocyte's ability to cope with changing pressure, easing podocyte injury.

The phosphorylation of the slit diaphragm main component nephrin by the tyrosine kinase FYN (Verma et al. 2003) is a prerequisite for the recruitment of the NCK adapter proteins, leading to the assembly of actin filaments (Verma et al. 2006). The NCK adapter proteins control actin polymerization through their activation of N-WASP and WASP, which are important for the regulation of the actin cytoskeleton via the ARP2/3 complex (Tomasevic et al. 2007). The upregulation of FYN levels by miRNA knockout might lead to increased phosphorylation of nephrin and, via the NCK mediated pathway, to an increase of actin polymerization.

Non-physiological levels of actin polymerization have been shown to disturb maintenance of podocyte structure and function. A higher binding activity of mutant α-actinin-4 to actin fibers,

thus stiffening the actin network, has been proposed as a possible mechanism in the development of familial FSGS caused by mutations in the *ACTN4* gene (Kaplan et al. 2000, Weins et al. 2005, Ward et al. 2008). A stiffer actin cytoskeleton has also been proposed to be a reason for podocyte injury in the nail-patella syndrome, a disease caused by mutations in the transcription factor LMX1B (Burghardt et al. 2013). The activity of cofilin A, an actin binding protein able to sever and depolymerize actin fibers to enable actin rearrangement, is necessary for maintenance of podocyte architecture (Garg et al. 2010), also proving that an inflexible actin cytoskeleton eases podocyte injury. Thus, a stiffer actin cytoskeleton due to a non-physiological stimulation of FYN activity might be one mechanism leading to podocyte injury.

FYN also phosphorylates the slit diaphragm component NEPH1, which results in the recruitment of the adaptor protein GRB2, an event important for NEPH1-induced actin polymerization (Garg et al. 2007). A dysregulation of the miRNAs regulating FYN presumably leads to an upregulating of FYN levels *in vivo*, which might lead to an increased phosphorylation of its targets. FYN phosphorylates NEPH1 at two tyrosine residues at the positions 637 and 638, a prerequisite for NEPH1-GRB2 binding, and an increased phosphorylation at the tyrosine residue 637 was observed in *in vivo* models of podocyte injury (Harita et al. 2008). As the phosphorylation dependent NEPH1-GRB2 binding also modulates ERK (Extracellular-signal regulated kinase) signaling, a process important for cell survival, differentiation, proliferation, metabolism and motility (reviewed by Mendoza et al. 2011, De Luca et al. 2012), it might be an explanation for miRNA-loss dependent podocyte injury, leading to foot process effacement and loss of podocyte cytoarchitecture.

Boundaries of luciferase assay

The luciferase reporter assay is a suitable system for the identification of miRNA-mRNA target pairs, including determination of the distinct binding site of a mature miRNA. However, the method also harbors some disadvantages. The assay is performed in immortalized cell lines, which might not fully reflect the *in vivo* situation, as binding partners or cofactors might be missing. Because of the overexpression of the targeted luciferase as well as the candidate miRNA, the relative expression level of 3'-UTR and putative regulator might be totally different from the *in vivo* situation. The assay was performed with an altered reporter plasmid already coding for the targeted luciferase as well as the untargeted control, enabling relative quantification of the signals. Still, double transfection of the reporter plasmid and the miRNA overexpression plasmid is needed for a functional assay. As the transfection efficiency is important, the assay was performed in HEK293T cells which are easy to transfect, instead of

hPCLs which might be closer to the *in vivo* situation, but show poor transfection efficiencies. The transfection efficiency of the assay was monitored by transfection of a plasmid coding for GFP in every experiment. To avoid the insecurities of a double transfection, cell lines with a stable miRNA overexpression using pSuperior constructs harboring a puromycin resistance might be used for a stable background for the reporter assay.

Alternative methods for miRNA-mRNA pair identification

As an alternative for luciferase assays, a dual fluorescence strategy has been proposed for miRNA-mRNA pair validation (Goldoni et al. 2012). Instead of using luminescence generating enzymes as reporters, fluorescent proteins can be used. The 3'-UTR to be investigated for miRNA binding sites is cloned downstream of a mCherry red fluorescent protein, while miRNAs were overexpressed with a vector also coding for eGFP. By calculating the red/green fluorescence intensity ratio by automated image analysis, the putative miRNA-mRNA pairs can be checked for binding. As the cells do not have to be lysed for analysis, time course experiments are possible and every cell can be treated as one data point, enabling more statistical analyses. With this method, miR-125a-5p was identified to target WT1 (Tatsumi et al. 2015).

In a protein-RNA complex immunoprecipitation, the complexes can be crosslinked with UV light to increase the yield. By CLIP (Cross-linking and immunoprecipitation) experiments, e.g. RNAs bound to the protein NOVA1 (Neuro-oncological ventral antigen 1) in the human brain were identified (Ule et al. 2003). The isolated RNAs can be analyzed by subsequent high-throughput sequencing, the HITS-CLIP (High-throughput sequencing of RNA isolated by crosslinking immunoprecipitation) (Licatalosi et al. 2008). It was shown that Ago-IPs can be combined with the CLIP method (Jaskiewicz et al. 2012), which could increase the RNA yield in the Ago-IPs from freshly isolated murine podocytes, increasing the amount of isolated RNA. The UV exposure might be performed directly after the first isolation of murine glomeruli or later, at the single cell suspension state. Additionally, a deep-sequencing analysis is an alternative to transcript identification by microarray. The PAR-CLIP (Photoactivatable-ribonucleoside-enhanced crosslinking and immunoprecipitation) method was developed to identify the binding sites of RNPs (Ribonucleoprotein complexes), including the RISCs, to RNA transcripts (Hafner et al. 2010). Cells are fed with a uridine analogon, which, after exposure to UV light and reverse transcription, leads to a T to C point mutation in the transcript sequence at the miRNA binding site. By mapping the sequenced products to the known transcripts, binding sites can be identified through their single base mutation and the regulating miRNA can be distinguished. The problem in applying this technique in laboratory animals is the delivery of the uridine

analogon. High amounts would have to be injected into the organism, which might be toxic or at least causing stress or other reactions, like inflammations, influencing the physiological state of the cells.

5.4 miRNA level manipulation methods

To influence the miRNA levels in living cells, different techniques have successfully applied in the present work. However, each technique possesses distinct advantages and disadvantages.

5.4.1 miRNA knockdown in cell culture by sponge expression

Sponges are transcripts possessing binding sites for miRNAs in their 3'-UTR, mimicking the natural situation between a target transcript and a fitting miRNA. Since perfect complementary of the miRNA sequence and the target sequence is not necessary for binding, members of miRNA families can bind to the same binding sites. Thus, expression of a sponge transcript leads to the knockdown of a whole family. The binding to the sponge only affects the mature miRNAs, meaning that the levels of the miRNA derived from the other strand of the same precursor are not affected.

For the knockdown of a whole family of mature miRNAs *in vivo*, competitive inhibitor transcripts, "sponges", harboring binding sites for miRNA families highly expressed in podocytes were designed. The expression of the target miRNAs was controlled by Northern Blotting of RNA isolated from proliferating hPCLs. The functionality of the sponges was monitored by luciferase assays. In hPCLs cotransfected with a targeted luciferase containing binding sites for a miRNA in its 3'-UTR and a matching sponge, the luciferase activity was rescued compared to the samples cotransfected with a sponge not harboring any binding sites. As first sponge candidates, miRNA families highly expressed in glomeruli and podocytes were selected. The sponge functionality could be confirmed for sponges targeting miR-23a/b-3p, miR-24-3p, miR-27a/b-3p, miR-29a-c-3p and miR-92a/b-3p. Since the precursors of the miR-23 and the mir-27 family as well as the two genomic loci of mir-24 are organized in two clusters, it was planned to design mixed sponges using the sequences tested successfully. Thus the generation of podocyte specific cluster knockdown mice as well as mice with a knockdown for the miR-29 and the miR-92 family, two families known to be important for glomerular functionality (Liu et al. 2010A, Long et al. 2011, Qin et al. 2011, Wang et al. 2012, Lin et al. 2014, Marrone et al. 2014), would have been possible. Since the genomic knockout system available at that time, the zinc finger nucleases,

showed varying knockout efficiencies as well as off-target effects, the knockdown of miRNA levels on the cytoplasmic level was a very promising way for miRNA level manipulation in cultured cells and laboratory animals.

A big disadvantage of this method is the need to freshly transfect cultured cells with the sponge coding plasmid. When working with immortalized podocyte cell lines, the cells can be differentiated by culturing at 37°C or 38°C, respectively, for two weeks. Since the differentiated cells are very hard to transfect, the transfection would have to be done with proliferating cells. Using plasmids coding for resistance genes, the generation of a stably transfected cell line would be possible. However, the presence of antibiotics would be necessary to maintain the selective pressure on the cells, which might influence the differentiation efficiency of the cells. Thus, a permanent depletion of miRNAs by an irreversable genomic knockout enables the differentiation of manipulated immortalized podocytes.

5.4.2 TALEN mediated genomic miRNA knockout

In 2013, TALE nucleases were introduced as a novel genome editing tool. A TALEN pair, each composed of a sequence specific TALE array and a part of an unspecific nuclease, binds to the DNA and generates double-strand breaks in the genome. This technique is more reliable than its predecessor, the zinc-finger nucleases.

For the genomic knockout of a miRNA highly expressed in podocytes, miR-30a-5p, HEK293T cells were cotransfected with plasmids coding for two TALENs directed against the human genomic locus of miR-30a-5p obtained from www.talenlibrary.net and a plasmid coding for antibiotics resistance into cells. After selection with antibiotics, clones were picked and investigated for miR-30a-5p expression. After a first screening by Northern Blotting, clones with a reduced expression of mature miR-30a-5p were selected and checked for Notch1 expression, a validated miR-30a-5p target in podocytes (Wu et al. 2014), by qPCR. Additionally, the genomic locus of mir-30a was amplified by PCR and sequenced. The three knockout clones show different reorganization patterns: While the seed region of the miR-30a-5p is nearly completely deleted in clone 1, the whole mir-30a precursor sequence is missing in clone 2. Knockout clone 3 is heterozygous for the knockout: While one allele is not affected by the knockout at all, the other allele shows an insertion of one base. The presence of one wildtype allele in knockout clone 3 might explain why the Notch1 expression is not dysregulated in this clone.

The sequencing of the PCR products of the genomic locus of mir-30a show different reorganization patterns. After the double strand break, the cell repairs the DNA double strand by

non homologous end-joining or homology directed repair. During both processes, parts of the genome can be deleted, like the seed region of miR-30a-5p in knockout clone 1 or the whole precursor in knockout clone 2. Additionally, insertions and homozygous mutations like both observed in knockout clone 3 are possible.

The different repairs of double strand breaks in cells might lead to different phenotypes. When the whole miRNA precursor is deleted, the expression of both mature miRNAs derived from the same precursor is disturbed. If the deleted region is very small or a small amount of bases is inserted, a changed hairpin precursor might be able to form, now coding for an altered miRNA, which might have completely different function in a cell. Thus, a detailed analysis of the genomic rearrangement after the double-strand break is important. One possibility to circumvent this problem is the addition of a donor in the cotransfection that can be integrated at the site of the double strand break by the cell by homology directed repair. With the insertion of a longer DNA fragment, not only a putatively altered precursor is disturbed, but also the insertion of a marker, like GFP expression, can be achieved.

Following the promising results obtained using HEK293T cells, immortalized human podocyte cell lines harboring a knockout of miR-30a-5p have been generated (L. Hübner, 2015). Knockout cell lines for miR-146b-5p and miR-92a-3p have also been generated and will be characterized accordingly. As miR-92a-3p is encoded in the genome at two different loci, the knockouts will be performed stepwise and a final clone harboring two genomic knockouts will be selected.

A relatively new system for genomic engineering is the CRISPR-Cas9 system, derived from a bacterial adaptive immune system that is also able to generate double strand breaks (Gupta & Musunuru 2014). By heterologous expression of the Cas9 protein from *Streptococcus pyogenes* together with a chimeric guide RNA, double strand breaks at the target sites of the guide RNAs can be generated (Gupta & Musunuru 2014). Since the so called protospacer sequence of the guide RNA of ca. 20 nt is responsible for the recognition of the target, the system can easily be adapted for different targets including the so-called “multiplexing”, i.e. using different guide RNAs together with one Cas9 protein for simultaneous knockout of different targets in one cell (Gupta & Musunuru, 2014). However, compared to the TALEN technology, the CRISPR-Cas9 system still harbors some disadvantages. Firstly, downstream of the desired location of the double strand break, a NGG nucleotide sequence, the so called PAM (Protospacer adjacent motif) is needed (Gupta & Musunuru 2014). While finding such a sequence might not be a problem in a long, protein coding gene, this sequence might not occur in the relatively short miRNA sequence of 20 nt. Secondly, the protospacer region of the guide RNA consists of 20 nt,

but allows single, sometimes even multiple mismatches, increasing the risk of off-target effects (Gupta & Musunuru, 2014). With the TALEN system, a perfect match of two times around 9 to 18 nt is needed, minimizing the risk of off-target effects. If the targeting of the CRISPR-Cas9 system can be improved to lower the risk of off-target effects, it might be a good and faster alternative to the TALEN system.

5.4.3 Podocyte specific knockdown/knockout techniques in mice

To investigate the role of a certain miRNA *in vivo*, a cell type specific, and preferably a inducible manipulation of a miRNA level is desirable. The application of the different knockdown and knockout methods harbors diverse advantages and disadvantages.

One possibility to influence miRNA levels *in vivo* is the application of antisense oligonucleotides, e.g. *Vivo-Morpholinos*. The molecules harboring an antisense sequence against the miRNA to be downregulated can be injected into the laboratory animals. Unfortunately, the targeting is rather unspecific. By direct injection into the renal aorta with parallel clamping of the renal vein, the retention time in the kidney and the uptake of the antisense oligonucleotides can be improved. Nonetheless, a specific targeting of a single cell population like the podocytes cannot be reached with this technique. A siRNA delivery system with a sheep anti-mouse podocyte antibody coupled to a siRNA was developed to exploit the endocytotic activity of podocytes for targeted siRNA delivery (Hauser et al. 2010). However, the injection of antisense oligonucleotides can only be used as a short term treatment.

The classical Cre/*loxP* system can be used for a genomic knockout, e.g. of the locus of the precursor of a single miRNA of a cluster, like the putative podocyte cluster. A broad variety of inducible, cell type specific Cre expressions and also fluorescent reporter strains can be used for the knockout and its visual control. As a disadvantage, a knock-in mouse harboring the mutation of a genomic locus containing the *loxP* sites has to be generated by embryonic stem cell injection followed by homologous recombination to yield a mouse with the desired genotype.

Another possibility for a genomic knockout is the TALEN mediated genomic knockout. Knockout of a miRNA locus in mice was performed by injection of the RNA coding for a TALEN pair directed against the mir-10a locus into the one cell stage of embryos (Takada et al. 2013). While the generation of TALEN knockout animals might be faster and straighter forward than the generation of a classical knock-in mouse, this model generated a constitutive knockout model, with no possibility to induce a cell-type specific alteration of a miRNA level at a later time point of development.

An interesting alternative for the genomic knockout of miRNAs by the Cre/*loxP* system or TALENs is the generation of a transgenic sponge mouse. The knockout of a genomic miRNA locus results in the disruption of the two miRNAs encoded in the same precursor. Sponge expression is only directed against one of the sequences encoded by a precursor, but is able to bind all mature miRNAs of the same family. It might be a helpful tool for a miRNA knockdown if the miRNA is encoded at different loci in the genome. Another application might be the knockdown of a whole miRNA family that is suspected to be interchangeable in their regulatory role. Transgenic mice expressing sponge transcripts have been constructed by microinjection (Ma et al. 2011) into fertilized eggs (Zhu et al. 2011). Combined with a cell type specific promoter like the P2.5 podocyte specific promoter, sponges are an interesting tool for family specific miRNA knockdown.

5.5 miRNA expression in podocytes of NPS mouse model

The NPS (Nail-patella syndrome) is a disease caused by mutations in the transcription factor LMX1B. A possible role for miRNAs in the progression of this disease was investigated using a mouse model.

miRNA expression regulation by transcription factors

It was shown for many miRNAs that their expression can be regulated by transcription factors. p73 and p63 have been identified as activators for miR-200 family upregulation (Knouf et al. 2011), while a regulatory circuit for Lmx1b and miR-135a-2 in brain development was described (Anderegg et al. 2013). Since Lmx1b is important for maintenance of murine podocyte structure and function, the effects of *Lmx1b* knockout on miRNA levels in glomeruli and podocytes were investigated. The knockout of *Lmx1b* in mice leads to the upregulation of its target genes Abra and Arl4c (Burghardt et al. 2013). Thus, Lmx1b seems to act as a transcriptional suppressor in podocytes for these genes. It might also act as an upregulating transcription factor as dendrin and semaphorin-3g are downregulated in glomeruli after the *Lmx1b* knockout (Burghardt et al. 2013). A possible way for indirect upregulation of a target gene might be inhibiting the transcription of miRNAs, indirectly influencing the target transcripts of these miRNAs (Fig. 5.4).

If LMX1B regulates the expression of miRNAs, it would increase the number of LMX1B regulated targets in podocytes and enable it to work in two directions for different target genes, as a direct suppressor and indirect enhancer.

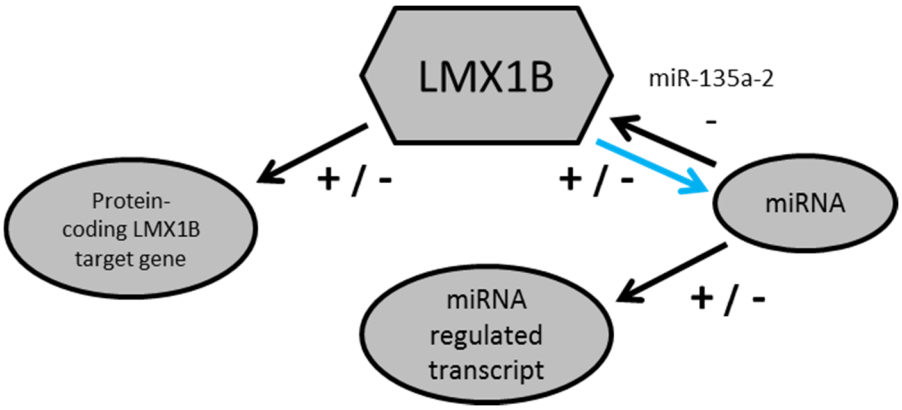

Fig. 5.4: Putative regulatory pathways of transcription factor LMX1B

miRNA expression in podocytes of Lmx1b *knockout animals*

In the inducible, podocyte specific *Lmx1b* knockout mice, the glomerular expression levels of seven miRNAs were reduced after the knockout, including four members of the miR-200 family, a family consisting of five members in human and mice that is genomically organized in two clusters.

The miR-200 has been described to be involved in kidney fibrosis and diabetic nephropathy, regulating the EMT (Epithelial mesenchymal transition) and the EndMT (Endothelial mesenchymal transition), two processes playing a role in the development of kidney fibrosis (Srivastava et al. 2013). The miR-200 family regulates renal tubular epithelial to mesenchymal transition induced by TGF-β through the Smad pathway by targeting ZEB1 and ZEB2 (Xiong et al. 2011). In the progression of breast cancer, it was shown that the miR-200 family and the miR-221 family play opposing effects for EMT progression (Howe et al. 2012). A feedback loop between the ZEB transcription factors and the miR-200 family, each controlling the expression of each other, was identified to be an important player in the progression of cancer, inducing stem-cell properties and preventing apoptosis and senescence (Brabletz & Brabletz 2010). This feedback loop was also termed a “cross road of signaling” in cancer, as it is linked to other signaling pathways like TGF-β, Notch, p53 and others (Hill et al. 2012).

Another mature miRNA downregulated in the *Lmx1b* knockout glomeruli is miR-192-5p. It has been described as a signature miRNA of renal ischemia reperfusion injury (Godwin et al. 2010), to mediate TGF-β/Smad3-driven renal fibrosis (Chung et al. 2010) and to regulate E-cadherin expression (Wang et al. 2010). Loss of miR-192-5p was reported to promote fibrosis in diabetic nephropathy (Krupa et al. 2010), while inhibiting miR-192-5p ameliorated diabetic nephropathy in a different study (Putta et al. 2012). These studies propose that a tightly regulated miR-192-5p level is important for prevention of renal fibrosis. Additionally, crosstalk between miR-192-5p

and the transcription factor p53 induced by TGF-β was observed in the pathogenesis of diabetic nephropathy (Deshpande et al. 2013). miR-192-5p represses the transcription factors ZEB1 and ZEB2, leading to pro- as well as anti-fibrotic effects (reviewed by Jenkins et al. 2012) and linking miR-192-5p dependent regulation to regulation by the miR-200 family.

To identify miRNAs directly affected by the *Lmx1b* knockout, inducible podocyte specific *Lmx1b* knockout mice were crossed with the Cre reporter mice to generate sortable, green fluorescent *Lmx1b* knockout podocytes. In the podocyte profiles generated from knockout and control mice, the miR-200 family was strongly enriched in the red fluorescent cell population with nearly no expression in podocytes, while miR-192-5p was expressed in podocytes as well as in the red fluorescent cell population.

The low transcription levels of the miR-200 family in podocytes together with their involvement in EMT hints that the altered expression level might be a secondary effect in the non-podocyte cells of the glomerulus. miR-192-5p is expressed in podocytes as well as in non-podocyte cells and plays a major role in the progression of kidney fibrosis. The altered level of miR-192-5p might be a direct or a secondary effect of the *Lmx1b* knockout.

The *deep sequencing* profiles of green fluorescent *Lmx1b* knockout podocytes revealed 48 mature miRNAs to be upregulated and 40 mature miRNAs to be downregulated in podocytes after the *Lmx1b* knockout. For this analysis, only miRNAs with expression levels unchanged in the red fluorescent cell population were counted in order to identify direct *Lmx1b* knockout effects. miR-192-5p was also downregulated in podocytes after *Lmx1b* knockout, making it, together with the other altered miRNAs, a very interesting target for further studies.

Using the profile generated from podocytes and red fluorescent glomerular cells from animals not harboring a mutated *Lmx1b* gene and thus, not suffering from the *Lmx1b* knockout, a third wildtype profile of miRNAs expressed in podocytes and mesangial and endothelial cells can be generated. However, several differences between the samples have to be considered. The original podocyte profiles were generated using male animals aged 12 to 14 weeks, while the third profile was generated from female mice aged 12 to 14 weeks. Secondly, both mouse strains possess a different background. The double fluorescent Cre reporter mice as well as the quadruple transgenic *Lmx1b* knockout strain possess a 50 : 50 mixed background of C57bl/6 and the Cre reporter mouse harboring the *mT/mG* cassette (Muzumdar et al. 2007), but both strands are bred independently from one another. The third big difference is the treatment of the animals before the isolation of glomerular cells. The control mice of the *Lmx1b* knockout

experiment received drinking water containing doxycycline for 9 days to induce the switch from expression of a red fluorescent protein to a green fluorescent protein, enabling also correction for doxycycline induced effect when being compared to the *Lmx1b* knockout animals. These doxycycline dependent effects are also an explanation for differences between the profiles. Nonetheless, 15 podocyte miRNAs, miR-125b-5p, miR-146b-5p, miR-148a-3p, miR-196b-5p, miR-27b-5p, miR-30a-3p, miR-30b-3p, miR-30d-5p, miR-322-3p, miR-330-5p, miR-340-5p, miR-351-5p, miR-503-3p, miR-503-5p and miR-615-3p were also identified to be enriched in the third podocyte library.

6 SUMMARY

In the last decade, thousands of small, highly conserved regulative RNAs, e.g. the miRNAs, could be identified to be expressed in various tissues and organs of many different species using the improved sequencing techniques. Meanwhile it is known that they play important roles in the post-transcriptional regulation of various cellular processes, e.g. different signaling pathways, in mammalian organisms.

Podocytes are unique, specialized cells with a very elaborate three-dimensional cytoarchitecture. Being located in the glomeruli of the kidney, they cover the glomerular capillaries with their interdigitating foot processes. In-between these processes, they build up slit diaphragms, complex protein structures responsible for the filtration of the blood, forming the primary urine. From different studies working with mice harboring a podocyte specific knockout for miRNA processing enzymes Dicer and Drosha (Harvey et al. 2008, Ho et al. 2008, Shi et al. 2008, Zhdanova et al. 2011), it is known that miRNAs are not only important for the development, but also responsible for maintenance of podocyte structure and function. Since this complex cytoarchitecture of the podocyte foot processes is lost in the described knockout mice, the proteins building up and stabilizing the slit diaphragms in-between the foot processes represent putative targets of miRNA dependent regulation.

In the present work, *deep sequencing* miRNA profiles were generated using glomeruli and tubules isolated from C57bl/6 wildtype mice and validated by Northern Blotting as well as qPCR analysis. However, to identify miRNAs enriched in podocytes, cells where freshly isolated from a double fluorescent Cre reporter mouse (Möller et al. 2003, Muzumdar et al. 2007). Analyzing *deep sequencing* profiles of miRNAs expressed in murine podocytes and the other glomerular cells, endothelial and mesangial cells, a subset of 38 mature miRNAs was identified to be enriched in podocytes compared to the other glomerular cell types. The enrichment of a subset of miRNAs in the glomerular cell populations, including podocyte candidate miRNAs, was validated by qPCR. By analyses of the human and murine 3'-UTR of transcripts coding for proteins important for podocyte structure and function and subsequent *in silico* predictions, putative regulatory miRNA-mRNA pairs in podocytes were predicted. A subset of four putative structural target genes: CD2AP, FYN, NCK2 and NEPH1 were analyzed in more detail. All of them are known to interact directly with the main protein building up the slit diaphragm, nephrin. To investigate these putative targets, luciferase assays were performed. HEK293T cells were transfected using a plasmid coding for a targeted luciferase together with a plasmid

overexpressing a mature miRNA or a control sequence. A possible regulation of CD2AP by miR-30a-5p could be identified via luciferase assay. A regulation by miR-92a-3p is likely, but could not be proven yet. Additionally, regulation of FYN by miR-146b-5p was detected. The effect of these miRNAs on the transcript and protein level of their targets will be analyzed in immortalized human podocytes, e.g. in miRNA knockout cell lines, in future studies.

To identify miRNA-target genes in podocytes *in vivo*, Ago-IP (Argonaute immunoprecipitation) combined with subsequent microarray analysis of the miRNA regulated targets was performed using freshly isolated murine podocytes. A new subset of candidate genes could be generated searching the Ago-bound transcripts for mRNAs coding for proteins important for podocyte structure and function. Additionally, Cd2ap and Fyn could both be identified to be enriched in the Ago-bound sample derived from podocytes, confirming the results from the luciferase assays. By repeating the analysis with an independent second sample, the enrichment of these candidates in the Ago-bound sample will be validated.

Two methods for miRNA level manipulation, "miRNA-sponges" for a knockdown of miRNA families and the genomic knockout of miRNAs using TALE nucleases were applied successfully in different cultured cell types. Sponges directed against several miRNA families highly expressed in podocytes were proven to be functional by luciferase assays in immortalized human podocytes. The genomic locus of mir-30a could be knocked out using TALE nucleases in HEK293T cells, yielding knockout cell lines. The downregulation of the mature miR-30a-5p as well as the upregulation of a known miR-30a-5p target in podocytes, Notch1 (Wu et al. 2014), could be shown in these knockout cell clones. With a TALE nuclease mediated knockout of miR-30a-5p, miR-92a-3p and miR-146b-5p in immortalized human podocytes, the role of these miRNAs will be investigated further, including the role they play in the regulation of CD2AP and FYN levels in the cells. As the genomic miRNA knockout is stable, the effect on the cellular structure can be analyzed in differentiated cells.

The transcription factor LMX1B plays an important role for the maintenance of podocyte structure and function. To investigate its possible effect on miRNA levels *in vivo*, glomeruli and podocytes were isolated from inducible *Lmx1b* knockout mice and compared to control mice. In the *Lmx1b* knockout podocytes, 48 mature miRNAs were found to be upregulated and 40 miRNAs were found to be downregulated compared to the control animals. This indicates a role of this transcription factor in controlling miRNA expression in podocytes. A miRNA family that was earlier found to be downregulated in glomeruli after *Lmx1b* knockout, the miR-200 family, was identified to be expressed in the non-podocyte glomerular cells, indicating a secondary

effect of the transcription factor inactivation. The miRNAs showing altered expression levels after *Lmx1b* knockout are putative starting points for further analyses of the genesis of the nail-patella syndrome, a human genomic disease caused by mutations in the *LMX1B* gene.

The overall goal of the present work was the investigation of the processes leading to podocyte injury and foot process effacement after dysregulation of miRNA levels. Firstly, it was required to identify podocyte miRNAs from the generated glomerular profiles, which was achieved using freshly isolated murine podocytes from the double fluorescent Cre reporter mice. By a combination of *in silico* predictions, Ago-IPs and luciferase assays, two transcripts coding for proteins important for podocyte structure and function, CD2AP and FYN, could be identified to be regulated by miRNAs. Specific interaction could be shown between FYN and miR-146b-5p. Furthermore, CD2AP might be regulated by miR-30a-5p as well as miR-92a-3p. In an Ago-IP from freshly isolated murine podocytes followed by microarray analysis, these targets could also be validated. Additionally, a new subset of target genes to be further analyzed has been generated. Techniques for miRNA level manipulation were successfully applied and will be used to characterize the identified specific regulatory miRNA-mRNA pairs.

The present work sheds light on the miRNA-mediated regulatory network in podocytes, which aids in the maintenance of their complex cytoarchitecture and function in renal filtration.

7 ZUSAMMENFASSUNG

Mit Hilfe verbesserter Sequenzierungstechniken konnte in den letzten zehn Jahren die Expression tausender kleiner, hoch konservierter RNAs, der miRNAs, in einer Vielzahl von Geweben und Organen in ganz unterschiedlichen Organismen identifiziert werden. Inzwischen ist bekannt, dass sie in Säugetieren eine wichtige Rolle in der post-transkriptionellen Regulation vieler zellulärer Prozesse, beispielsweise in verschiedenen Signalwegen, spielen.

Podozyten sind hochspezialisierte Zellen, die eine komplexe, dreidimensionale Zytoarchitektur besitzen. Sie befinden sich in den Nierenkörperchen, wo sie die Kapillaren mit ihren ineinandergreifenden Fußfortsätzen bedecken. Zwischen diesen bilden sie eine komplexe Proteinstruktur, das Schlitzdiaphragma, aus, das für die Filtration des Blutes zum Primärharn verantwortlich ist. Durch mehrere Studien an Mäusen, die unter einem podozyten-spezifischen Knockout der miRNA prozessierenden Enzyme Drosha und Dicer leiden (Harvey et al. 2008, Ho et al. 2008, Shi et al. 2008, Zhdanova et al. 2011), wurde gezeigt, dass miRNAs nicht nur für die Entwicklung, sondern auch für die Erhaltung der Podozytenstruktur und -funktion essentiell sind. Da die komplexe Zytoarchitektur der Podozytenfußfortsätze in diesen Knockout-Mäusen verloren geht, stellen die Proteine, die für den Aufbau und die Stabilisierung der Schlitzdiaphragmen zwischen den Fußfortsätzen verantwortlich sind, potentielle Ziele für die miRNA vermittelte Regulation dar.

Im Rahmen der vorliegenden Arbeit konnten aus Glomeruli und Tubuli, die aus C57/bl6-wildtyp Mäusen isoliert wurden, miRNA-Expressionsprofile mittels *deep sequencing* generiert und durch Northern Blotting und qPCR-Analyse validiert werden. Zur Identifizierung von miRNAs, die in Podozyten angereichert sind, wurden diese frisch aus einer doppelt-fluoreszierenden Cre-Reporter-Maus isoliert (Möller et al. 2003, Muzumdar et al. 2007). Die generierten miRNA-*deep sequencing*-Profile der murinen Podozyten und der glomerulären Endothel- und den Mesangialzellen wurden analysiert. Auf diese Weise wurden 38 miRNAs identifiziert, die in Podozyten gegenüber den Endothel- und Mesangialzellen angereichert sind. Die Anreicherung spezifischer miRNAs in den glomerulären Zellpopulationen, einschließlich der podozytären miRNA-Kandidaten, wurde stichprobenartig per qPCR-Analyse validiert. Durch die Analyse der 3'-UTRs humaner und muriner Transkripte, die für Proteine kodieren, welche für die Podozytenstruktur und –funktion wichtig sind, und anschließende *in silico*-Vorhersagen wurden mögliche regulatorische miRNA-mRNA Paare vorhergesagt. Eine Gruppe von vier möglichen Zielgenen: CD2AP, FYN, NCK2 und NEPH1, wurde genauer untersucht. Von diesen Proteinen ist eine direkte Interaktion mit dem wichtigsten Protein des Schlitzdiaphragmas, Nephrin, bekannt.

Zur Untersuchung dieser möglichen Zielgene wurden Luciferase Assays durchgeführt. Dazu wurden HEK293T Zellen mit einem Plasmid, das eine Luciferase mit der jeweiligen 3'-UTR kodiert und einem Plasmid, das entsprechend eine spezifische reife miRNA oder eine Kontrollsequenz überexprimiert, transfiziert. Im Luciferase Assay konnte eine mögliche Regulation von CD2AP durch miR-30a-5p identifiziert werden. Eine Regulation durch miR-92a-3p erscheint wahrscheinlich, konnte jedoch noch nicht bewiesen werden. Zusätzlich wurde eine Regulation von FYN durch miR-146b-5p detektiert. Die Effekte dieser miRNAs auf die Transkript- und Proteinspiegel der Zielgene werden in immortalisierten humanen Podozyten, beispielsweise in miRNA Knockout-Zelllinien, weiter analysiert werden.

Darüber hinaus wurde zur Identifikation von miRNA Zielgenen *in vivo* eine Ago-IP (Argonaute Immunprezipitation) aus frisch isolierten murinen Podozyten durchgeführt und mit einer anschließenden Microarray-Analyse der miRNA regulierten Transkripte kombiniert. Durch die Suche nach Transkripten möglicher Zielgene, die in der podozytären Ago-gebundenen Probe angereichert und für die Podozytenstruktur und –funktion wichtig sind, konnte eine neue Gruppe von möglichen Zielgenen generiert werden. Zusätzlich konnten Cd2ap und Fyn in der podozytären Ago-angereicherten Probe identifiziert werden, was die Ergebnisse der Luciferase Assays bestätigt. Die Anreicherung dieser Kandidaten in der Ago-gebundenen Probe soll durch die Wiederholung des Experiments mit einer zweiten, unabhängigen Probe validiert werden.

Zwei Methoden zur Manipulation der miRNA-Spiegel, „miRNA-sponges" für den Knockdown von miRNA-Familien und der genomische Knockout von miRNAs mit Hilfe von TALE Nukleasen, wurden erfolgreich in verschiedenen immortalisierten Zelllinien angewendet. Die Funktionalität von „miR-sponges" gegen mehrere miRNA-Familien, die in Podozyten stark exprimiert sind, konnte mit Hilfe von Luciferase Assays in humanen immortalisierten Podozyten nachgewiesen werden. Mit Hilfe von TALE-Nukleasen konnten mir-30a Knockout-Zelllinien aus HEK293T Zellen hergestellt werden. Sowohl die verminderte Expression der reifen miR-30a-5p als auch die vermehrte Expression eines bekannten miR-30a-5p Zielgens in Podozyten, Notch1 (Wu et al. 2014), konnte in diesen Klonen gezeigt werden. Durch einen TALE-Nuklease vermittelten Knockout von miR-30a-5p, miR-92a-3p und miR-146b-5p in immortalisierten, humanen Podozyten, wird die Rolle dieser miRNAs, einschließlich ihrer Rolle bei der Regulation der CD2AP- und FYN-Spiegel in den Zellen untersucht werden. Die Folgen des stabilen miRNA knock-outs für die Zellstruktur können so in differenzierten Zellen analysiert werden.

Der Transkriptionsfaktor LMX1B spielt für die Erhaltung der Podozytenstruktur und –funktion eine wichtige Rolle. Um seinen möglichen Einfluss auf die miRNA-Spiegel *in vivo* zu analysieren,

wurden Glomeruli und Podozyten von *Lmx1b* Knockout-Mäusen isoliert und mit Kontrollmäusen verglichen. In *Lmx1b* Knockout-Podozyten wurden 48 reife hochregulierte und 40 herunterregulierte miRNAs gefunden. Dies weist auf eine Rolle dieses Transkriptionsfaktors in der Expressionskontrolle von miRNAs in Podozyten hin. In *Lmx1b* Knockout-Glomeruli wurde eine Reduktion der miR-200 Familie festgestellt. Diese miRNA-Familie wurde später als in den nicht-podozytären, glomerulären Zellen exprimiert identifiziert, was auf einen sekundären Effekt des *Lmx1b* Knockouts hinweist. Die miRNAs mit veränderten Expressionsspiegeln nach dem *Lmx1b* Knockout sind mögliche Ausgangspunkte für die Aufklärung der Entstehung des Nagel-Patella-Syndroms, einer humanen genetischen Erkrankung, die durch Mutationen im *LMX1B* Gen verursacht wird, sein.

In der vorliegenden Arbeit wurden die Vorgänge, die zur Störung der Podozytenarchitektur nach einer Dysregulation der podozytären miRNA-Spiegel führen, untersucht. Zunächst konnten die in Podozyten endogen exprimierten miRNAs konnten mit Hilfe der frisch isolierten Zellen aus den gekreuzten doppelt-fluoreszenten Cre-Reportermäusen identifiziert werden. Durch eine Kombination von *in silico*-Vorhersagen, Ago-IPs und Luciferase Assays konnte die Regulation zweier Transkripte, CD2AP und FYN, identifiziert werden. Eine spezifische Interaktion zwischen FYN und miR-146b-5p konnte gezeigt werden. Zusätzlich könnte CD2AP sowohl durch miR-30a-5p als auch durch miR-92a-3p reguliert werden. Durch eine Ago-IP mit frisch isolierten murinen Podozyten, die mit einem Microarray kombiniert wurde, konnten diese Zielgene bestätigt und darüber hinaus neue potentielle Zielgene identifiziert werden. Methoden zur Manipulation der miRNA-Spiegel wurden in Zellkulturen erfolgreich angewendet und stehen zur weiteren Charakterisierung der spezifischen regulativen miRNA-mRNA Paare zur Verfügung.

Die vorliegende Arbeit trägt zur Aufklärung über das miRNA-gesteuerte regulative Netzwerk in Podozyten, das die Erhaltung der komplexen Zytoarchitektur und die Funktion in der renalen Filtration unterstützt, bei.

8 LIST OF ABBREVIATIONS

Human proteins are written in all capital letters, murine proteins written starting with a capital letter; the corresponding genes are written in italics.

27G	Needle size; outer diameter: 0.4128 mm; inner diameter: 0.210 mm
3'-end	Strand terminating at the hydroxyl group of the third carbon in the sugar-ring
5'-end	Strand terminating at the hydroxyl group of the fifth carbon in the sugar-ring
3p	Mature miRNA derived from the 3'-end of the precursor
5p	Mature miRNA derived from the 5'-end of the precursor
β	Mass concentration
λ	Wave length
µg	Microgram(s)
µl	Microliter(s)
µm	Micrometer(s)
A	Adenine
Abra	Actin-Binding Rho Activating Protein
Actbl2	Actin, beta-like 2
Actg1	Actin, gamma, cytoplasmic 1
ACTN4	α-Actinin-4 gene
ACTR2	Actin related protein 2
Ago1-4	Argonaute protein 1-4
Ago-IP	Argonaute immunoprecipitation
AGTII	Angiotensin 2
AKT	Protein kinase B
Apa	*Acetobacter pasteurianus* sub. *pasteurianus*
aPKC	Atypical protein kinase C
APS	Ammoniumpersulfate
Arl4c	ADP-Ribosylation Factor-Like 4C
Arp2/3	Arp2/3 complex
Asn	Asparagine
Asp	Aspartic acid
AT1 receptor	Angiotensin II receptor type 1
ATP	Adenosine triphosphate
BCL2	B-cell lymphoma 2
Bgl	*Bacillus globigii*
BLAST	Basic Local Alignment Search Tool
bp	Base pairs
BSA	Bovine serum albumin
c	Molar concentration
C	Cytosine
C. elegans	*Caenorhabditis elegans*
c-terminus	Carboxyl-terminus
C57bl/6	C57black6 mouse strain
Ca^{2+}	Bivalent calcium ion
$CaCl_2$	Calcium chloride
CaMKII	Ca^{2+}/calmodulin-dependent protein kinase
CAMTA1	Calmodulin binding transcription activator 1
CapZ	Capping protein (actin filament) muscle Z-line
Cas9	CRISPR associated protein 9
CCR4	Chemokine (C-C Motif) Receptor 4
CD2AP	CD2 associated protein
CD31	Cluster of differentiation 31
CDC42	Cell division control protein 42 homolog
cDNA	Complementary DNA
chr	Chromosome
ciRS-7	Circular RNA sponge for miR-7
CLIP	Cross-linking and immunoprecipitation
CLIC5	Chloride intracellular channel protein 5
CMV	Cytomegalovirus
CO_2	Carbon dioxide
ColE1 origin	Origin of replication of ColE1 plasmid (carrying gene for colicin E1)
c_p	Crossing point
Cre	Cre Recombinase
CRISPR	Clustered regularly interspaced short palindromic repeats
CTGF	Connective tissues growth factor
cxcr4	C-X-C chemokine receptor type 4
D	Differentiated
d2eGFP	Destabilized GFP
DAG	Diacylglycerol
DABCO	1, 4-Diazabicyclo[2.2.2]octane
DAPI	4', 6-Diamidin-2-phenylindol
db/db mice	Mice with deficient leptin receptor activity

DEPC	Diethylpyrocarbonate
DG	Dystroglycan
DGCR8	DiGeorge syndrome critical region gene 8
DMEM	Dulbecco's modified Eagle's medium
DMSO	Dimethyl sulfoxide
DNA	Deoxyribonucleic acid
DNase	Deoxyribonuclease
dNTPs	Deoxynucleotide triphosphates
Dox	Doxycycline
DTT	1, 4-Dithio-DL-threitol
e.g.	examples given
E11/E12/E13	Embryonic days: day 11, day 12, day 13
E2F1	Transcription factor E2F1
E2F3	Transcription factor E2F3
EcoR	*Escherichia coli RY13*
EDC	1-Ethyl-3-(3-dimethylamino-propyl)carbodiimid
EDTA	Ethylenediaminetetraacetic acid
EF	Fenestrated endothelium
eGFP	Enhanced green fluorescent protein
Eml2	Echinoderm microtubule associated protein like 2
EMT	Epithelial mesenchymal transition
ENCODE	Encyclopedia of DNA Elements
EndMT	Endothelial mesenchymal transition
EPAP	*E.coli* poly-A polymerase
ER	Endoplasmic reticulum
ERK	Extracellular-signal-regulated kinase
EZR	Ezrin
F	Forward
FACS	Fluorescent activated cell sorting
FAK	Focal adhesion kinase
Fam114a1	Family with sequence similarity 114, member A1
FAT1	Protocadherin Fat 1
FCS	Fetal calf serum
Fig	Figure
FLAT	Far linked AT rich elements
FP	Foot process
FSGS	Focal segmental glomerulosclerosis
FYN	Proto-oncogene tyrosin kinase Fyn
G	Guanine
g	Gram(s)
g	Multiple of acceleration of gravity
G1 phase	Growth 1/Gap 1 phase
G418	Geneticin
GBM	Glomerular basement membrane
genloc	Genomic locus
GFP	Green fluorescent protein
Glom	Glomeruli
Gly	Glycine
Gpc1	Glypican 1
GRB2	Growth factor receptor-bound protein 2
GRCh	Genome Reference Consortium Human genome
GTPase	Guanine triphosphate hydrolyzing enzyme
GW	Glycin-tryptophan repeat containing
h	Hour(s)
H-2K^b	Mouse major histocompatibility complex promoter
H_2O	Water
HBSS	Hank's buffered saline solution
HCl	Hydrochloric acid
HDAC4	Histone deacetylase 4
HDR	Homology directed repair
HEK293T	Human Embryonic Kidney 293 cells containing SV40 Large T-antigen
HeLa	HeLa cell line, human cervical cancer cell line
HEPES	4-(2-Hydroxyethyl)-1-piperazineethanesulfonic acid
HF	High Fidelity
Hind	*Haemophilus influenzae*
His	Histidine
Hnrpk	Heterogeneous nuclear ribonuclear protein K
Hoxa9	Homeobox A9
Hoxc5	Homeobox C5
hPCL	Human podocyte cell line
HRP	Horse radish peroxidase
hsa	Homo sapiens
Hsp90	Heat shock protein 90
i.e.	it est
IgA	Immunoglobulin A
IgG	Immunoglobulin G
Ile	Isoleucine
ILK	Integrin-linked kinase
IP	Immunoprecipitation

IP3	Inositol triphosphate
IQGAP-1	IQ motif containing GTPase activating protein
Itga3	Integrin alpha 3
Itgb1	Integrin beta 1
JAM4	Junctional cell adhesion molecule 4
kb	Kilobase(s)
KCl	Potassium chloride
kDa	Kilodalton
KFB	Kompetenzzentrum fluoreszente Bioanalytik
KH_2PO_4	Potassiumdihydrogen phosphate
Kirrel1	Kin of IRRE like protein 1
KO	knockout
l	Liter(s)
LB	Lysogeny broth
LC1	Tet-On inducible Cre recombinase
Lim domain	Domain discovered in Lin11, Isl-1, Mec-3
lincRNA	Long intergenic non-coding RNA
Lingo2	Leucine rich repeat and Ig domain containing 2
Lmx1b	LIM Homeobox Transcription Factor 1, Beta
LNA	Locked nucleic acid
loxP sites	Locus of X-over P1, Cre recombinase recognition site
LPS	Lipopolysaccharide
M	Molar
MAGI-1/2	Membrane-associated guanylate kinase, WW and PDZ domain-containing protein 1/2
MET	Mesenchymal–epithelial transition
mG	Monomeric green fluorescent protein
$MgCl_2$	Magnesiumchloride
$MgSO_4$	Magnesiumsulfate
min	Minute(s)
miR	Mature miRNA
mir	Precursor miRNA
ml	Milliliter(s)
mM	Millimolar
mmHg	Millimeters of mercury
mmu	Mus musculus
MO	Missouri
mPCL	Murine podocyte cell line
mT	Targeted tandem dimer Tomato
mT/mG	Tomato mouse reporter cassette
mut	Mutant
n-terminus	Aminoterminus of a protein
N-Wasp	Neural Wiskott-Aldrich syndrome protein
n.s.	Not significant
NaCl	Sodiumchloride
NaF	Sodiumfluoride
Na_2HPO_4	Sodiumhydrogenphosphate
NaN_3	Sodiumazide
Nck1/2	Non-catalytic region of tyrosine kinase adaptor protein 1/2
neg	Negative
Neph1	Kin of IRRE-like protein 1
Neph2	Kin of IRRE-like protein 3
Neph3	Kin of IRRE-like protein 2
NFYC	Nuclear transcription factor Y gamma
ng	Nanogram(s)
NHEJ	Non homologous end-joining
NHERF1/2	Sodium-hydrogen antiporter 3 regulator 1/2
nm	Nanometer(s)
nonRT	Not reversely transcribed sample
NOSTRIN	Nitric oxide synthase trafficking
NOT9	RCD1 required for cell differentiation1 homolog
Notch1	Notch homolog 1, translocation-associated
NPC	Nuclear pore complex
NPHS1	Nephrin
NPHS2	Podocin
NPS	Nail patella syndrome
nt	Nucleotide
O	Oxygen
P	Proliferating
p27	Cyclin-Dependent Kinase Inhibitor 1B
p53	Tumor protein P53
p63	Tumor protein p63
p73	Tumor protein p73
PAGE	Polyacrylamide gel electrophoresis
PAKs	p21 activated kinases
PAM	Protospacer adjacent motif
PAN	Puromycin amino-glycoside
PAN2	Poly(A) Specific Ribonuclease Subunit 2
PAN3	Poly(A) Specific Ribonuclease Subunit 3
Pank1	Pantothenate kinase 1

Par3	Partitioning defective 3 homolog
Par6	Partitioning defective 6 homolog
PARN	Poly(A) specific ribonuclease
PBS	Phosphate buffered saline
PCNA	Proliferating cell nuclear antigen
PCR	*Polymerase chain reaction*
PDZ domain	Protein domain found in PSD95, Dlg1 and ZO-1
PECs	Pariethal endothelial cells
PEI	Polyethylenimine
PFA	Paraformaldehyde
Pfu	*Pyrococcus furiosus*
PI3K	Phosphatidylinositol-4,5-bisphosphate 3-kinase
PINCH-1	Particularly interesting new cysteine-histidine-rich protein
PIP2	Phosphatidylinositol 4,5-bisphosphate
PLCε1	Phospholipase C, epsilon 1
PLCG1	Phospholipase C, gamma 1
PNK	Polynucleotide Kinase
PODXL	Podocalyxin
pos	Positive
ppm	Parts per million
pre-miRNA	miRNA precursor
pri-miRNA	Primary transcript of a miRNA
Protein G	Immunoglobulin-binding protein
PVDF	Polyvinylidene fluoride
PVP	Polyvinylpyrrolidone
qPCR	Quantitative polymerase chain reaction
R	Reverse
RAC1	Ras-related C3 botulinum toxin substrate 1
RHOA	Ras homolog gene family, member A
RISC	RNA induced silencing complex
RMC	Complement system protein
RNA	Ribonucleic acic
RNAse	Ribonuclease, RNA degrading enzyme
RNF130	Ring finger protein 130
rno	*Rattus norvegicus*
RNP	Ribonucleoprotein complex
RPMI	Roswell Park Memorial Institute
RQCD1	RCD1 required for cell differentiation1 homolog
RT	Room temperature
RT-PCR	Reverse transcription polymerase chain reaction
rtTA	Reverse tetracyclin transactivator
s	Second(s)
S phase	Synthesis phase
Sac	*Streptomyces achromogenes*
SDS	Sodium dodecylsulfate
SH2/3 domain	Src homology 2/3 domain
shRNA	short hairpin RNA
siRNAs	small interference RNA
Smad2/3	Smad family member 2/3
Smurf1	E3 ubiquitin-protein ligase
Smurf2	SMAD specific E3 ubiquitin protein ligase 2
SNP	Single nucleotide polymorphism
snRNA	small nuclear RNA
SOCS1	Suppressor of cytokine signaling 1
Spe	*Sphaerotilus natans*
Spry1	Sprouty homolog 1
SS-13^{BN} rats	Control strain for Dahl sensitive rats
SSC	Sodium citrate/sodium chloride buffer
Src	SRC proto-oncogene, non-receptor tyrosine kinase
Sry	Sex-determining region Y
SV40	Simian vacuolating virus 40
Synpo	Synaptopodin
T	Thymine
Tab	Table
TAE buffer	Tris-acetate-EDTA buffer
TALE	Transcription activator-like effector
TALEN	Transcription activator-like effector nuclease
Taq	*Thermus aquaticus*
TBE buffer	Tris-borate-EDTA buffer
TEMED	Tetramethylethylenediamine
Tet-On	Tetracycline-Controlled Transcriptional Activation
TGF-β1	Transforming growth factor beta 1
TK	Thymidin kinase promoter
TLN1	Talin-1
Tmem164	Transmembrane protein 164
Tmem180	Transmembrane protein 180
TNRC6A-C	Trinucleotide repeat containing 6 A-C
TRIS	Tris(hydroxymethyl)-aminomethan

TRPC1	Transient receptor potential cation channel, subfamily C, member 1
TRPC6	Transient receptor potential cation channel, subfamily C, member 6
Tub	Tubules
U	Enzyme unit (1 µm/min)
U6	U6 snRNA, spliceosomal RNA
URT primer	Universal reverse transcription primer
UTR	Untranslated region
UV	Ultraviolet
V	Volt(s)
VEGF(A)	Vascular endothelial growth factor (A)
VEGFR-2	Vascular endothelial growth factor receptor 2
WASL	Neural Wiskott-Aldrich syndrome protein
WASP	Wiskott-Aldrich syndrome protein
Wipf3	WAS/WASL interacting protein family, member 3
Wnt1	Proto-oncogene protein Wnt-1/Wnt
wt	Wildtype
WT1	Wilms Tumor protein 1
Xho	*Xanthomonas holcicola*
Xlim1/Lhx1	Lim homeobox 1
XPO-5	Exportin-5
YDxV domain	Domain consisting of Tyrosine – Aspartic Acid – any amino acid - Valine
ZEB1	Zinc Finger E-Box Binding Homeobox 1
ZEB2	Zinc Finger E-Box Binding Homeobox 2
ZO-1	Zonula occludens 1

9 REFERENCE LIST

Agrawal, Raman; Tran, Uyen; Wessely, Oliver (2009): The miR-30 miRNA family regulates Xenopus pronephros development and targets the transcription factor Xlim1/Lhx1. In: *Development (Cambridge, England)* 136 (23), S. 3927–3936. DOI: 10.1242/dev.037432.

Aguilar, Ana Laura Gutierrez; Piskol, Robert; Beitzinger, Michaela; Zhu, Jia Yun; Kruspe, Dagmar; Aszodi, Attila et al. (2010): The small RNA expression profile of the developing murine urinary and reproductive systems. In: *FEBS letters* 584 (21), S. 4426–4434. DOI: 10.1016/j.febslet.2010.09.050.

Aitsebaomo, Julius; Portbury, Andrea L.; Schisler, Jonathan C.; Patterson, Cam (2008): Brothers and sisters: molecular insights into arterial-venous heterogeneity. In: *Circulation research* 103 (9), S. 929–939. DOI: 10.1161/CIRCRESAHA.108.184937.

Althoff, Kristina; Lindner, Sven; Odersky, Andrea; Mestdagh, Pieter; Beckers, Anneleen; Karczewski, Sarah et al. (2015): miR-542-3p exerts tumor suppressive functions in neuroblastoma by downregulating Survivin. In: *International journal of cancer. Journal international du cancer* 136 (6), S. 1308–1320. DOI: 10.1002/ijc.29091.

Anderegg, Angela; Lin, Hsin-Pin; Chen, Jun-An; Caronia-Brown, Giuliana; Cherepanova, Natalya; Yun, Beth et al. (2013): An Lmx1b-miR135a2 regulatory circuit modulates Wnt1/Wnt signaling and determines the size of the midbrain dopaminergic progenitor pool. In: *PLoS genetics* 9 (12), S. e1003973. DOI: 10.1371/journal.pgen.1003973.

Appel, Daniel; Kershaw, David B.; Smeets, Bart; Yuan, Gang; Fuss, Astrid; Frye, Björn et al. (2009): Recruitment of podocytes from glomerular parietal epithelial cells. In: *Journal of the American Society of Nephrology : JASN* 20 (2), S. 333–343. DOI: 10.1681/ASN.2008070795.

Asanuma, Katsuhiko; Kim, Kwanghee; Oh, Jun; Giardino, Laura; Chabanis, Sophie; Faul, Christian et al. (2005): Synaptopodin regulates the actin-bundling activity of α-actinin in an isoform-specific manner. In: *J. Clin. Invest.* 115 (5), S. 1188–1198. DOI: 10.1172/JCI200523371.

Asanuma, Katsuhiko; Yanagida-Asanuma, Etsuko; Faul, Christian; Tomino, Yasuhiko; Kim, Kwanghee; Mundel, Peter (2006): Synaptopodin orchestrates actin organization and cell motility via regulation of RhoA signalling. In: *Nature cell biology* 8 (5), S. 485–491. DOI: 10.1038/ncb1400.

Bang, Claudia; Fiedler, Jan; Thum, Thomas (2012): Cardiovascular importance of the microRNA-23/27/24 family. In: *Microcirculation (New York, N.Y. : 1994)* 19 (3), S. 208–214. DOI: 10.1111/j.1549-8719.2011.00153.x.

Barletta, Gina-Marie; Kovari, Iulia A.; Verma, Rakesh K.; Kerjaschki, Dontscho; Holzman, Lawrence B. (2003): Nephrin and Neph1 co-localize at the podocyte foot process intercellular junction and form cis hetero-oligomers. In: *The Journal of biological chemistry* 278 (21), S. 19266–19271. DOI: 10.1074/jbc.M301279200.

Basgen JM, Nicholas SB, Mauer M, Rozen S, Nyengaard JR (2006): Comparison of Methods for Counting Cells in the Mouse Glomerulus. In: *Nephron Exp Nephrol* 103 (4), S. e139–e148.

Beitzinger, Michaela; Peters, Lasse; Zhu, Jia Yun; Kremmer, Elisabeth; Meister, Gunter (2007): Identification of Human microRNA Targets From Isolated Argonaute Protein Complexes. In: *RNA Biology* 4 (2), S. 76–84. DOI: 10.4161/rna.4.2.4640.

Berger, Katja; Schulte, Kevin; Boor, Peter; Kuppe, Christoph; van Kuppevelt, Toin H; Floege, Jürgen et al. (2014): The regenerative potential of parietal epithelial cells in adult mice. In: *Journal of the American Society of Nephrology : JASN* 25 (4), S. 693–705. DOI: 10.1681/ASN.2013050481.

Bertero, Thomas; Cottrill, Katherine; Krauszman, Adrienn; Lu, Yu; Annis, Sofia; Hale, Andrew et al. (2015): The microRNA-130/301 family controls vasoconstriction in pulmonary hypertension. In: *The Journal of biological chemistry* 290 (4), S. 2069–2085. DOI: 10.1074/jbc.M114.617845.

Billmeier, Martina (2012): Funktionelle Analyse von microRNAs in der Niere: Bedeutung für die glomeruläre Filtration und die Entwicklung von Nierenerkrankungen; Bachelor thesis, University of Regensburg

Bladt, F.; Aippersbach, E.; Gelkop, S.; Strasser, G. A.; Nash, P.; Tafuri, A. et al. (2003): The Murine Nck SH2/SH3 Adaptors Are Important for the Development of Mesoderm-Derived Embryonic Structures and for Regulating the Cellular Actin Network. In: *Molecular and cellular biology* 23 (13), S. 4586–4597. DOI: 10.1128/MCB.23.13.4586-4597.2003.

Blessing, Charlotte (2014): Herstellung und Anwendung von TALE-Nukleasen zur Etablierung einer miR-30a Knock-out-Zelllinie; Bachelor thesis, University of Regensburg

Boerries, Melanie; Grahammer, Florian; Eiselein, Sven; Buck, Moritz; Meyer, Charlotte; Goedel, Markus et al. (2013): Molecular fingerprinting of the podocyte reveals novel gene and protein regulatory networks. In: *Kidney international* 83 (6), S. 1052–1064. DOI: 10.1038/ki.2012.487.

Boute, N.; Gribouval, O.; Roselli, S.; Benessy, F.; Lee, H.; Fuchshuber, A. et al. (2000): NPHS2, encoding the glomerular protein podocin, is mutated in autosomal recessive steroid-resistant nephrotic syndrome. In: *Nature genetics* 24 (4), S. 349–354. DOI: 10.1038/74166.

Brabletz, Simone; Brabletz, Thomas (2010): The ZEB/miR-200 feedback loop--a motor of cellular plasticity in development and cancer? In: *EMBO reports* 11 (9), S. 670–677. DOI: 10.1038/embor.2010.117.

Brandt, Dominique T.; Grosse, Robert (2007): Get to grips: steering local actin dynamics with IQGAPs. In: *EMBO reports* 8 (11), S. 1019–1023. DOI: 10.1038/sj.embor.7401089.

Bruggeman, Leslie A.; Doan, Ryan P.; Loftis, Jacqueline; Darr, Aniq; Calabro, Anthony (2012): A cell culture system for the structure and hydrogel properties of basement membranes; Application to capillary walls. In: *Cellular and molecular bioengineering* 5 (2), S. 194–204. DOI: 10.1007/s12195-012-0221-3.

Brummelkamp, Thijn R.; Bernards, René; Agami, Reuven (2002): A system for stable expression of short interfering RNAs in mammalian cells. In: *Science (New York, N.Y.)* 296 (5567), S. 550–553. DOI: 10.1126/science.1068999.

Brümmer, Anneke; Hausser, Jean (2014): MicroRNA binding sites in the coding region of mRNAs: extending the repertoire of post-transcriptional gene regulation. In: *BioEssays : news and reviews in molecular, cellular and developmental biology* 36 (6), S. 617–626. DOI: 10.1002/bies.201300104.

Burghardt, Tillmann; Kastner, Jürgen; Suleiman, Hani; Rivera-Milla, Eric; Stepanova, Natalya; Lottaz, Claudio et al. (2013): LMX1B is essential for the maintenance of differentiated podocytes in adult kidneys. In: *Journal of the American Society of Nephrology : JASN* 24 (11), S. 1830–1848. DOI: 10.1681/ASN.2012080788.

Burroughs, Alexander Maxwell; Ando, Yoshinari; de Hoon, Michiel Laurens; Tomaru, Yasuhiro; Suzuki, Harukazu; Hayashizaki, Yoshihide; Daub, Carsten Olivier (2011): Deep-sequencing of human Argonaute-associated small RNAs provides insight into miRNA sorting and reveals Argonaute association with RNA fragments of diverse origin. In: *RNA Biology* 8 (1), S. 158–177. DOI: 10.4161/rna.8.1.14300.

Byron, Adam; Randles, Michael J.; Humphries, Jonathan D.; Mironov, Aleksandr; Hamidi, Hellyeh; Harris, Shelley et al. (2014): Glomerular cell cross-talk influences composition and assembly of extracellular matrix. In: *Journal of the American Society of Nephrology : JASN* 25 (5), S. 953–966. DOI: 10.1681/ASN.2013070795.

Cao, Shan; Xiao, Lan; Rao, Jaladanki N.; Zou, Tongtong; Liu, Lan; Zhang, Dee et al. (2014): Inhibition of Smurf2 translation by miR-322/503 modulates TGF-β/Smad2 signaling and intestinal epithelial homeostasis. In: *Molecular biology of the cell* 25 (8), S. 1234–1243. DOI: 10.1091/mbc.E13-09-0560.

Carthew, Richard W.; Sontheimer, Erik J. (2009): Origins and Mechanisms of miRNAs and siRNAs. In: *Cell* 136 (4), S. 642–655. DOI: 10.1016/j.cell.2009.01.035.

Cazalla, Demián; Yario, Therese; Steitz, Joan A.; Steitz, Joan (2010): Down-regulation of a host microRNA by a Herpesvirus saimiri noncoding RNA. In: *Science (New York, N.Y.)* 328 (5985), S. 1563–1566. DOI: 10.1126/science.1187197.

Chandrasekaran, Karthikeyan; Karolina, Dwi S.; Sepramaniam, Sugunavathi; Armugam, Arunmozhiarasi; Wintour, E. Marelyn; Bertram, John F.; Jeyaseelan, Kandiah (2012): Role of microRNAs in kidney homeostasis and disease. In: *Kidney international* 81 (7), S. 617–627. DOI: 10.1038/ki.2011.448.

Chang, Kah Hoong; Mestdagh, Pieter; Vandesompele, Jo; Kerin, Michael J.; Miller, Nicola (2010): MicroRNA expression profiling to identify and validate reference genes for relative quantification in colorectal cancer. In: *BMC cancer* 10, S. 173. DOI: 10.1186/1471-2407-10-173.

Chau, B. Nelson; Xin, Cuiyan; Hartner, Jochen; Ren, Shuyu; Castano, Ana P.; Linn, Geoffrey et al. (2012): MicroRNA-21 promotes fibrosis of the kidney by silencing metabolic pathways. In: *Science translational medicine* 4 (121), S. 121ra18. DOI: 10.1126/scitranslmed.3003205.

Cheloufi, Sihem; Dos Santos, Camila O; Chong, Mark M W; Hannon, Gregory J. (2010): A dicer-independent miRNA biogenesis pathway that requires Ago catalysis. In: *Nature* 465 (7298), S. 584–589. DOI: 10.1038/nature09092.

Chen, Jun; Braet, Filip; Brodsky, Sergey; Weinstein, Talia; Romanov, Victor; Noiri, Eisei; Goligorsky, Michael S. (2002): VEGF-induced mobilization of caveolae and increase in permeability of endothelial cells. In: *American journal of physiology. Cell physiology* 282 (5), S. C1053-63. DOI: 10.1152/ajpcell.00292.2001.

Chen, Yu-Qiang; Wang, Xiao-Xia; Yao, Xing-Mei; Zhang, Dong-Liang; Yang, Xu-Feng; Tian, Shou-Fu; Wang, Nian-Song (2011): MicroRNA-195 promotes apoptosis in mouse podocytes via enhanced caspase activity driven by BCL2 insufficiency. In: *American journal of nephrology* 34 (6), S. 549–559. DOI: 10.1159/000333809.

Chong, Mark M W; Rasmussen, Jeffrey P.; Rudensky, Alexander Y.; Rundensky, Alexander Y.; Littman, Dan R. (2008): The RNAseIII enzyme Drosha is critical in T cells for preventing lethal inflammatory disease. In: *The Journal of experimental medicine* 205 (9), S. 2005–2017. DOI: 10.1084/jem.20081219.

Chung, Arthur C K; Huang, Xiao R.; Meng, Xiaoming; Lan, Hui Y. (2010): miR-192 mediates TGF-beta/Smad3-driven renal fibrosis. In: *Journal of the American Society of Nephrology : JASN* 21 (8), S. 1317–1325. DOI: 10.1681/ASN.2010020134.

Cifuentes, Daniel; Xue, Huiling; Taylor, David W.; Patnode, Heather; Mishima, Yuichiro; Cheloufi, Sihem et al. (2010): A novel miRNA processing pathway independent of Dicer requires Argonaute2 catalytic activity. In: *Science (New York, N.Y.)* 328 (5986), S. 1694–1698. DOI: 10.1126/science.1190809.

Cockett, M. I.; Ochalski, R.; Benwell, K.; Franco, R.; Wardwell-Swanson, J. (1997): Simultaneous expression of multi-subunit proteins in mammalian cells using a convenient set of mammalian cell expression vectors. In: *Biotechniques* 23 (3), S. 402-4, 406-7.

Codocedo, Juan F.; Ríos, Juvenal A.; Godoy, Juan A.; Inestrosa, Nibaldo C. (2015): Are microRNAs the Molecular Link Between Metabolic Syndrome and Alzheimer's Disease? In: *Molecular neurobiology. DOI:* 10.1007/s12035-015-9201-7.

Cullen-McEwen, L. A.; Kett, M. M.; Dowling, J.; Anderson, W. P.; Bertram, J. F. (2003): Nephron Number, Renal Function, and Arterial Pressure in Aged GDNF Heterozygous Mice. In: *Hypertension* 41 (2), S. 335–340. DOI: 10.1161/01.HYP.0000050961.70182.56.

Cunningham, Fiona; Amode, M. Ridwan; Barrell, Daniel; Beal, Kathryn; Billis, Konstantinos; Brent, Simon et al. (2015): Ensembl 2015. In: *Nucleic acids research* 43 (Database issue), S. D662-9. DOI: 10.1093/nar/gku1010.

Dandapani, Savita V.; Sugimoto, Hikaru; Matthews, Benjamin D.; Kolb, Robert J.; Sinha, Sumita; Gerszten, Robert E. et al. (2007): Alpha-actinin-4 is required for normal podocyte adhesion. In: *The Journal of biological chemistry* 282 (1), S. 467–477. DOI: 10.1074/jbc.M605024200.

Deller, Thomas; Korte, Martin; Chabanis, Sophie; Drakew, Alexander; Schwegler, Herbert; Stefani, Giulia Good et al. (2003): Synaptopodin-deficient mice lack a spine apparatus and show deficits in synaptic plasticity. In: *Proceedings of the National Academy of Sciences of the United States of America* 100 (18), S. 10494–10499. DOI: 10.1073/pnas.1832384100.

Denli, Ahmet M.; Tops, Bastiaan B J; Plasterk, Ronald H A; Ketting, René F.; Hannon, Gregory J. (2004): Processing of primary microRNAs by the Microprocessor complex. In: *Nature* 432 (7014), S. 231–235. DOI: 10.1038/nature03049.

Deshpande, Supriya D.; Putta, Sumanth; Wang, Mei; Lai, Jennifer Y.; Bitzer, Markus; Nelson, Robert G. et al. (2013): Transforming growth factor-β-induced cross talk between p53 and a microRNA in the pathogenesis of diabetic nephropathy. In: *Diabetes* 62 (9), S. 3151–3162. DOI: 10.2337/db13-0305.

Dieci, Giorgio; Fiorino, Gloria; Castelnuovo, Manuele; Teichmann, Martin; Pagano, Aldo (2007): The expanding RNA polymerase III transcriptome. In: *Trends in genetics : TIG* 23 (12), S. 614–622. DOI: 10.1016/j.tig.2007.09.001.

Donoviel, D. B.; Freed, D. D.; Vogel, H.; Potter, D. G.; Hawkins, E.; Barrish, J. P. et al. (2001): Proteinuria and perinatal lethality in mice lacking NEPH1, a novel protein with homology to NEPHRIN. In: *Molecular and cellular biology* 21 (14), S. 4829–4836. DOI: 10.1128/MCB.21.14.4829-4836.2001.

Doyon, Yannick; Vo, Thuy D.; Mendel, Matthew C.; Greenberg, Shon G.; Wang, Jianbin; Xia, Danny F. et al. (2011): Enhancing zinc-finger-nuclease activity with improved obligate heterodimeric architectures. In: *Nature methods* 8 (1), S. 74–79. DOI: 10.1038/nmeth.1539.

Dreyer, S. D.; Zhou, G.; Baldini, A.; Winterpacht, A.; Zabel, B.; Cole, W. et al. (1998): Mutations in LMX1B cause abnormal skeletal patterning and renal dysplasia in nail patella syndrome. In: *Nature genetics* 19 (1), S. 47–50. DOI: 10.1038/ng0598-47.

Dueck, Anne; Ziegler, Christian; Eichner, Alexander; Berezikov, Eugene; Meister, Gunter (2012): microRNAs associated with the different human Argonaute proteins. In: *Nucleic acids research* 40 (19), S. 9850–9862. DOI: 10.1093/nar/gks705.

Dustin, Michael L.; Olszowy, Michael W.; Holdorf, Amy D.; Li, Jun; Bromley, Shannon; Desai, Naishadh et al. (1998): A Novel Adaptor Protein Orchestrates Receptor Patterning and Cytoskeletal Polarity in T-Cell Contacts. In: *Cell* 94 (5), S. 667–677. DOI: 10.1016/S0092-8674(00)81608-6.

Dweep, Harsh; Sticht, Carsten; Pandey, Priyanka; Gretz, Norbert (2011): miRWalk--database: prediction of possible miRNA binding sites by \"walking\" the genes of three genomes. In: *Journal of biomedical informatics* 44 (5), S. 839–847. DOI: 10.1016/j.jbi.2011.05.002.

Ebert, Margaret S.; Neilson, Joel R.; Sharp, Phillip A. (2007): MicroRNA sponges: competitive inhibitors of small RNAs in mammalian cells. In: *Nature methods* 4 (9), S. 721–726. DOI: 10.1038/nmeth1079.

Ebert, Margaret S.; Sharp, Phillip A. (2010): Emerging roles for natural microRNA sponges. In: *Current biology : CB* 20 (19), S. R858-61. DOI: 10.1016/j.cub.2010.08.052.

Ebert, Margaret S.; Sharp, Phillip A. (2010): MicroRNA sponges: progress and possibilities. In: *RNA (New York, N.Y.)* 16 (11), S. 2043–2050. DOI: 10.1261/rna.2414110.

Eng, Diana G.; Sunseri, Maria W.; Kaverina, Natalya V.; Roeder, Sebastian S.; Pippin, Jeffrey W.; Shankland, Stuart J. (2015): Glomerular parietal epithelial cells contribute to adult podocyte regeneration in experimental focal segmental glomerulosclerosis. In: *Kidney international. DOI:* 10.1038/ki.2015.152.

Faul, Christian; Asanuma, Katsuhiko; Yanagida-Asanuma, Etsuko; Kim, Kwanghee; Mundel, Peter (2007): Actin up: regulation of podocyte structure and function by components of the actin cytoskeleton. In: *Trends in cell biology* 17 (9), S. 428–437. DOI: 10.1016/j.tcb.2007.06.006.

Femminella, Grazia D.; Ferrara, Nicola; Rengo, Giuseppe (2015): The emerging role of microRNAs in Alzheimer's disease. In: *Frontiers in physiology* 6, S. 40. DOI: 10.3389/fphys.2015.00040.

Friedman, Robin C.; Farh, Kyle Kai-How; Burge, Christopher B.; Bartel, David P. (2009): Most mammalian mRNAs are conserved targets of microRNAs. In: *Genome research* 19 (1), S. 92–105. DOI: 10.1101/gr.082701.108.

Gámez, Beatriz; Rodríguez-Carballo, Edgardo; Bartrons, Ramon; Rosa, José Luis; Ventura, Francesc (2013): MicroRNA-322 (miR-322) and its target protein Tob2 modulate Osterix (Osx) mRNA stability. In: *The Journal of biological chemistry* 288 (20), S. 14264–14275. DOI: 10.1074/jbc.M112.432104.

Garg, Puneet; Verma, Rakesh; Nihalani, Deepak; Johnstone, Duncan B.; Holzman, Lawrence B. (2007): Neph1 cooperates with nephrin to transduce a signal that induces actin polymerization. In: *Molecular and cellular biology* 27 (24), S. 8698–8712. DOI: 10.1128/MCB.00948-07.

Garg, Puneet; Verma, Rakesh; Cook, Leslie; Soofi, Abdul; Venkatareddy, Madhusudan; George, Britta et al. (2010): Actin-depolymerizing factor cofilin-1 is necessary in maintaining mature podocyte architecture. In: *The Journal of biological chemistry* 285 (29), S. 22676–22688. DOI: 10.1074/jbc.M110.122929.

Gebeshuber, Christoph A.; Kornauth, Christoph; Dong, Lihua; Sierig, Ralph; Seibler, Jost; Reiss, Martina et al. (2013): Focal segmental glomerulosclerosis is induced by microRNA-193a and its downregulation of WT1. In: *Nature medicine* 19 (4), S. 481–487. DOI: 10.1038/nm.3142.

Gerke, Peter; Sellin, Lorenz; Kretz, Oliver; Petraschka, Daniel; Zentgraf, Hanswalter; Benzing, Thomas; Walz, Gerd (2005): NEPH2 is located at the glomerular slit diaphragm, interacts with nephrin and is cleaved from podocytes by metalloproteinases. In: *Journal of the American Society of Nephrology : JASN* 16 (6), S. 1693–1702. DOI: 10.1681/ASN.2004060439.

Gerke P, Huber TB, Sellin L, Benzing T and Walz G (2003): Homodimerization and Heterodimerization of the Glomerular Podocyte Proteins Nephrin and NEPH1. In: *JASN* vol. 14 (no. 4), S. 918–926.

Godwin, Jonathan G.; Ge, Xupeng; Stephan, Kristin; Jurisch, Anke; Tullius, Stefan G.; Iacomini, John (2010): Identification of a microRNA signature of renal ischemia reperfusion injury. In: *Proceedings of the National Academy of Sciences of the United States of America* 107 (32), S. 14339–14344. DOI: 10.1073/pnas.0912701107.

Goldoni, Dana; Yarham, Janet M.; McGahon, Mary K.; O'Connor, Anna; Guduric-Fuchs, Jasenka; Edgar, Kevin et al. (2012): A novel dual-fluorescence strategy for functionally validating microRNA targets in 3' untranslated regions: regulation of the inward rectifier potassium channel K(ir)2.1 by miR-212. In: *The Biochemical journal* 448 (1), S. 103–113. DOI: 10.1042/BJ20120578.

Gomez, Ivan G.; MacKenna, Deidre A.; Johnson, Bryce G.; Kaimal, Vivek; Roach, Allie M.; Ren, Shuyu et al. (2015): Anti-microRNA-21 oligonucleotides prevent Alport nephropathy progression by stimulating metabolic pathways. In: *The Journal of clinical investigation* 125 (1), S. 141–156. DOI: 10.1172/JCI75852.

Grahammer, Florian; Wanner, Nicola; Huber, Tobias B. (2013): Podocyte regeneration: who can become a podocyte? In: *The American Journal of Pathology* 183 (2), S. 333–335. DOI: 10.1016/j.ajpath.2013.04.009.

Griffiths-Jones, Sam (2004): The microRNA Registry. In: *Nucleic acids research* 32 (Database issue), S. D109-11. DOI: 10.1093/nar/gkh023.

Griffiths-Jones, Sam; Grocock, Russell J.; van Dongen, Stijn; Bateman, Alex; Enright, Anton J. (2006): miRBase: microRNA sequences, targets and gene nomenclature. In: *Nucleic acids research* 34 (Database issue), S. D140-4. DOI: 10.1093/nar/gkj112.

Griffiths-Jones, Sam; Saini, Harpreet Kaur; van Dongen, Stijn; Enright, Anton J. (2008): miRBase: tools for microRNA genomics. In: *Nucleic acids research* 36 (Database issue), S. D154-8. DOI: 10.1093/nar/gkm952.

Guay, Claudiane; Roggli, Elodie; Nesca, Valeria; Jacovetti, Cécile; Regazzi, Romano (2011): Diabetes mellitus, a microRNA-related disease? In: *Translational research : the journal of laboratory and clinical medicine* 157 (4), S. 253–264. DOI: 10.1016/j.trsl.2011.01.009.

Gupta, Rajat M.; Musunuru, Kiran (2014): Expanding the genetic editing tool kit: ZFNs, TALENs, and CRISPR-Cas9. In: *The Journal of clinical investigation* 124 (10), S. 4154–4161. DOI: 10.1172/JCI72992.

Ha, Eunyoung; Bang, Ji-Hye; Son, Jung N.; Cho, Ho-Chan; Mun, Kyo-Chul (2010): Carbamylated albumin stimulates microRNA-146, which is increased in human renal cell carcinoma. In: *Molecular medicine reports* 3 (2), S. 275–279. DOI: 10.3892/mmr_00000251.

Ha, Minju; Kim, V. Narry (2014): Regulation of microRNA biogenesis. In: *Nature reviews. Molecular cell biology* 15 (8), S. 509–524. DOI: 10.1038/nrm3838.

Hafner, Markus; Landgraf, Pablo; Ludwig, Janos; Rice, Amanda; Ojo, Tolulope; Lin, Carolina et al. (2008): Identification of microRNAs and other small regulatory RNAs using cDNA library sequencing. In: *Methods (San Diego, Calif.)* 44 (1), S. 3–12. DOI: 10.1016/j.ymeth.2007.09.009.

Hafner M, Landthaler M, Burger L, Khorshid M, Hausser J, Berninger P, Rothballer A, Ascano M Jr, Jungkamp AC, Munschauer M, Ulrich A, Wardle GS, Dewell S, Zavolan M, Tuschl T (2010): Transcriptome-wide identification of RNA-binding protein and microRNA target sites by PAR-CLIP. In: *Cell* 141 (1), S. 129–141.

Hansen, Thomas B.; Jensen, Trine I.; Clausen, Bettina H.; Bramsen, Jesper B.; Finsen, Bente; Damgaard, Christian K.; Kjems, Jørgen (2013): Natural RNA circles function as efficient microRNA sponges. In: *Nature* 495 (7441), S. 384–388. DOI: 10.1038/nature11993.

Harfe, Brian D.; McManus, Michael T.; Mansfield, Jennifer H.; Hornstein, Eran; Tabin, Clifford J. (2005): The RNaseIII enzyme Dicer is required for morphogenesis but not patterning of the vertebrate limb. In: *Proceedings of the National Academy of Sciences of the United States of America* 102 (31), S. 10898–10903. DOI: 10.1073/pnas.0504834102.

Harita, Yutaka; Kurihara, Hidetake; Kosako, Hidetaka; Tezuka, Tohru; Sekine, Takashi; Igarashi, Takashi; Hattori, Seisuke (2008): Neph1, a component of the kidney slit diaphragm, is tyrosine-phosphorylated by the Src family tyrosine kinase and modulates intracellular signaling by binding to Grb2. In: *The Journal of biological chemistry* 283 (14), S. 9177–9186. DOI: 10.1074/jbc.M707247200.

Harita, Yutaka; Kurihara, Hidetake; Kosako, Hidetaka; Tezuka, Tohru; Sekine, Takashi; Igarashi, Takashi et al. (2009): Phosphorylation of Nephrin Triggers Ca2+ Signaling by Recruitment and Activation of Phospholipase C-{gamma}1. In: *The Journal of biological chemistry* 284 (13), S. 8951–8962. DOI: 10.1074/jbc.M806851200.

Hartleben, Björn; Schweizer, Heiko; Lübben, Pauline; Bartram, Malte P.; Möller, Clemens C.; Herr, Ronja et al. (2008): Neph-Nephrin proteins bind the Par3-Par6-atypical protein kinase C (aPKC) complex to regulate podocyte cell polarity. In: *The Journal of biological chemistry* 283 (34), S. 23033–23038. DOI: 10.1074/jbc.M803143200.

Harvey, Scott J.; Jarad, George; Cunningham, Jeanette; Goldberg, Seth; Schermer, Bernhard; Harfe, Brian D. et al. (2008): Podocyte-specific deletion of dicer alters cytoskeletal dynamics and causes glomerular disease. In: *Journal of the American Society of Nephrology : JASN* 19 (11), S. 2150–2158. DOI: 10.1681/ASN.2008020233.

Hata, Akiko; Lieberman, Judy (2015): Dysregulation of microRNA biogenesis and gene silecing in cancer. In: *ScienceSignaling* 8 (368). DOI: 10.1126/scisignal.2005825.

Hauser, Peter V.; Pippin, Jeffrey W.; Kaiser, Cora; Krofft, Ronald D.; Brinkkoetter, Paul T.; Hudkins, Kelly L. et al. (2010): Novel siRNA delivery system to target podocytes in vivo. In: *PloS one* 5 (3), S. e9463. DOI: 10.1371/journal.pone.0009463.

Hausser, Jean; Berninger, Philipp; Rodak, Christoph; Jantscher, Yvonne; Wirth, Stefan; Zavolan, Mihaela (2009): MirZ: an integrated microRNA expression atlas and target prediction resource. In: *Nucleic acids research* 37 (Web Server issue), S. W266-72. DOI: 10.1093/nar/gkp412.

Hayashita, Yoji; Osada, Hirotaka; Tatematsu, Yoshio; Yamada, Hideki; Yanagisawa, Kiyoshi; Tomida, Shuta et al. (2005): A polycistronic microRNA cluster, miR-17-92, is overexpressed in human lung cancers and enhances cell proliferation. In: *Cancer research* 65 (21), S. 9628–9632. DOI: 10.1158/0008-5472.CAN-05-2352.

He, Bing; Ebarasi, Lwaki; Zhao, Zhe; Guo, Jing; Ojala, Juha R M; Hultenby, Kjell et al. (2014): Lmx1b and FoxC combinatorially regulate podocin expression in podocytes. In: *Journal of the American Society of Nephrology : JASN* 25 (12), S. 2764–2777. DOI: 10.1681/ASN.2012080823.

He, Feng; Peng, Fenfen; Xia, Xi; Zhao, Chen; Luo, Qimei; Guan, Weiming et al. (2014): MiR-135a promotes renal fibrosis in diabetic nephropathy by regulating TRPC1. In: *Diabetologia* 57 (8), S. 1726–1736. DOI: 10.1007/s00125-014-3282-0.

He, Lin; Thomson, J. Michael; Hemann, Michael T.; Hernando-Monge, Eva; Mu, David; Goodson, Summer et al. (2005): A microRNA polycistron as a potential human oncogene. In: *Nature* 435 (7043), S. 828–833. DOI: 10.1038/nature03552.

Heikkilä, Eija; Ristola, Mervi; Havana, Marika; Jones, Nina; Holthöfer, Harry; Lehtonen, Sanna (2011): Trans-interaction of nephrin and Neph1/Neph3 induces cell adhesion that associates with decreased tyrosine phosphorylation of nephrin. In: *The Biochemical journal* 435 (3), S. 619–628. DOI: 10.1042/BJ20101599.

Heizler, Kevin (2015): Untersuchung spezifischer miRNA-mRNA Interaktionen und ihre Bedeutung in den Podozyten der Niere; Bachelor thesis, University of Regensburg

Henderson, J. M.; Al-Waheeb, S.; Weins, A.; Dandapani, S. V.; Pollak, M. R. (2008): Mice with altered alpha-actinin-4 expression have distinct morphologic patterns of glomerular disease. In: *Kidney international* 73 (6), S. 741–750. DOI: 10.1038/sj.ki.5002751.

Hers, Ingeborg; Vincent, Emma E.; Tavaré, Jeremy M. (2011): Akt signalling in health and disease. In: *Cellular signalling* 23 (10), S. 1515–1527. DOI: 10.1016/j.cellsig.2011.05.004.

Hill, Louise; Browne, Gareth; Tulchinsky, Eugene (2013): ZEB/miR-200 feedback loop: at the crossroads of signal transduction in cancer. In: *International journal of cancer. Journal international du cancer* 132 (4), S. 745–754. DOI: 10.1002/ijc.27708.

Ho, Jacqueline; Ng, Kar Hui; Rosen, Seymour; Dostal, Ales; Gregory, Richard I.; Kreidberg, Jordan A. (2008): Podocyte-specific loss of functional microRNAs leads to rapid glomerular and tubular injury. In: *Journal of the American Society of Nephrology : JASN* 19 (11), S. 2069–2075. DOI: 10.1681/ASN.2008020162.

Holoch, Daniel; Moazed, Danesh (2015): RNA-mediated epigenetic regulation of gene expression. In: *Nature reviews. Genetics* 16 (2), S. 71–84. DOI: 10.1038/nrg3863.

Howe, Erin N.; Cochrane, Dawn R.; Richer, Jennifer K. (2012): The miR-200 and miR-221/222 microRNA families: opposing effects on epithelial identity. In: *Journal of mammary gland biology and neoplasia* 17 (1), S. 65–77. DOI: 10.1007/s10911-012-9244-6.

Huber, T. B.; Hartleben, B.; Kim, J.; Schmidts, M.; Schermer, B.; Keil, A. et al. (2003): Nephrin and CD2AP Associate with Phosphoinositide 3-OH Kinase and Stimulate AKT-Dependent Signaling. In: *Molecular and cellular biology* 23 (14), S. 4917–4928. DOI: 10.1128/MCB.23.14.4917-4928.2003.

Huber, Tobias B.; Schermer, Bernhard; Benzing, Thomas (2007): Podocin organizes ion channel-lipid supercomplexes: implications for mechanosensation at the slit diaphragm. In: *Nephron. Experimental nephrology* 106 (2), S. e27-31. DOI: 10.1159/000101789.

Huber, Tobias B.; Schmidts, Miriam; Gerke, Peter; Schermer, Bernhard; Zahn, Anne; Hartleben, Björn et al. (2003): The carboxyl terminus of Neph family members binds to the PDZ domain protein zonula occludens-1. In: *The Journal of biological chemistry* 278 (15), S. 13417–13421. DOI: 10.1074/jbc.C200678200.

Huntzinger, Eric; Izaurralde, Elisa (2011): Gene silencing by microRNAs: contributions of translational repression and mRNA decay. In: *Nature reviews. Genetics* 12 (2), S. 99–110. DOI: 10.1038/nrg2936.

Hurteau, Gregory J.; Spivack, Simon D.; Brock, Graham J. (2006): Potential mRNA Degradation Targets of hsa-miR-200c. In: Cell Cycle 5 (17), S. 1951–1956. DOI: 10.4161/cc.5.17.3133.

Ichii, Osamu; Otsuka, Saori; Sasaki, Nobuya; Namiki, Yuka; Hashimoto, Yoshiharu; Kon, Yasuhiro (2011): Altered expression of microRNA miR-146a correlates with the development of chronic renal inflammation. In: *Kidney Int* 81 (3), S. 280–292. DOI: 10.1038/ki.2011.345.

Ichii, Osamu; Otsuka-Kanazawa, Saori; Horino, Taro; Kimura, Junpei; Nakamura, Teppei; Matsumoto, Manabu et al. (2014): Decreased miR-26a expression correlates with the progression of podocyte injury in autoimmune glomerulonephritis. In: *PloS one* 9 (10), S. e110383. DOI: 10.1371/journal.pone.0110383.

Jansson, Martin D.; Lund, Anders H. (2012): MicroRNA and cancer. In: *Molecular oncology* 6 (6), S. 590–610. DOI: 10.1016/j.molonc.2012.09.006.

Jaskiewicz, Lukasz; Bilen, Biter; Hausser, Jean; Zavolan, Mihaela (2012): Argonaute CLIP--a method to identify in vivo targets of miRNAs. In: *Methods (San Diego, Calif.)* 58 (2), S. 106–112. DOI: 10.1016/j.ymeth.2012.09.006.

Jenkins, Robert H.; Martin, John; Phillips, Aled O.; Bowen, Timothy; Fraser, Donald J. (2012): Pleiotropy of microRNA-192 in the kidney. In: *Biochemical Society transactions* 40 (4), S. 762–767. DOI: 10.1042/BST20120085.

Jiang, Qinghua; Wang, Yadong; Hao, Yangyang; Juan, Liran; Teng, Mingxiang; Zhang, Xinjun et al. (2009): miR2Disease: a manually curated database for microRNA deregulation in human disease. In: *Nucleic acids research* 37 (Database issue), S. D98-104. DOI: 10.1093/nar/gkn714.

Jinek, Martin; Chylinski, Krzysztof; Fonfara, Ines; Hauer, Michael; Doudna, Jennifer A.; Charpentier, Emmanuelle (2012): A programmable dual-RNA-guided DNA endonuclease in adaptive bacterial immunity. In: *Science (New York, N.Y.)* 337 (6096), S. 816–821. DOI: 10.1126/science.1225829.

Jonas, Stefanie; Izaurralde, Elisa (2015): Towards a molecular understanding of microRNA-mediated gene silencing. In: *Nature reviews. Genetics* 16 (7), S. 421–433. DOI: 10.1038/nrg3965.

Jones, Nina; Blasutig, Ivan M.; Eremina, Vera; Ruston, Julie M.; Bladt, Friedhelm; Li, Hongping et al. (2006): Nck adaptor proteins link nephrin to the actin cytoskeleton of kidney podocytes. In: *Nature* 440 (7085), S. 818–823. DOI: 10.1038/nature04662.

Jones, Nina; New, Laura A.; Fortino, Megan A.; Eremina, Vera; Ruston, Julie; Blasutig, Ivan M. et al. (2009): Nck proteins maintain the adult glomerular filtration barrier. In: *Journal of the American Society of Nephrology : JASN* 20 (7), S. 1533–1543. DOI: 10.1681/ASN.2009010056.

Joung, J. Keith; Sander, Jeffry D. (2013): TALENs: a widely applicable technology for targeted genome editing. In: *Nature reviews. Molecular cell biology* 14 (1), S. 49–55. DOI: 10.1038/nrm3486.

Kalyani, Ananthamohan; Sonawane, Parshuram J.; Khan, Abrar Ali; Subramanian, Lakshmi; Ehret, Georg B.; Mullasari, Ajit S.; Mahapatra, Nitish R. (2015): Post-Transcriptional Regulation of Renalase Gene by miR-29 and miR-146 MicroRNAs: Implications for Cardiometabolic Disorders. In: *Journal of molecular biology* 427 (16), S. 2629–2646. DOI: 10.1016/j.jmb.2015.07.003.

Kaplan JM, Kim SH, North KN, Rennke H, Correia LA, Tong HQ, Mathis BJ, Rodriguez-Perez JC, Allen PG, Beggs AH, Pollak MR (2000): Mutations in ACTN4, encoding α-actinin-4, cause familial focal segmental glomerulosclerosis. In: *Nat Genet* 24 (3), S. 251–256.

Kato, Mitsuo; Natarajan, Rama (2015): MicroRNAs in diabetic nephropathy: functions, biomarkers, and therapeutic targets. In: *Annals of the New York Academy of Sciences. DOI:* 10.1111/nyas.12758.

Kato, Mitsuo; Park, Jung Tak; Natarajan, Rama (2012): MicroRNAs and the glomerulus. In: *Experimental cell research* 318 (9), S. 993–1000. DOI: 10.1016/j.yexcr.2012.02.034.

Kent, W. J.; Sugnet, C. W.; Furey, T. S.; Roskin, K. M.; Pringle, T. H.; Zahler, A. M.; Haussler, a. D. (2002): The Human Genome Browser at UCSC. In: *Genome research* 12 (6), S. 996–1006. DOI: 10.1101/gr.229102.

Kestilä, Marjo; Lenkkeri, Ulla; Männikkö, Minna; Lamerdin, Jane; McCready, Paula; Putaala, Heli et al. (1998): Positionally Cloned Gene for a Novel Glomerular Protein—Nephrin—Is Mutated in Congenital Nephrotic Syndrome. In: *Molecular Cell* 1 (4), S. 575–582. DOI: 10.1016/S1097-2765(00)80057-X.

Kietzmann, Leonie; Guhr, Sebastian S O; Meyer, Tobias N.; Ni, Lan; Sachs, Marlies; Panzer, Ulf et al. (2014): MicroRNA-193a Regulates the Transdifferentiation of Human Parietal Epithelial Cells toward a Podocyte Phenotype. In: *Journal of the American Society of Nephrology : JASN. DOI:* 10.1681/ASN.2014020190.

Kim, V. Narry (2005): MicroRNA biogenesis: coordinated cropping and dicing. In: *Nature reviews. Molecular cell biology* 6 (5), S. 376–385. DOI: 10.1038/nrm1644.

Kim, Young-Kook; Wee, Gabbine; Park, Joha; Kim, Jongkyu; Baek, Daehyun; Kim, Jin-Soo; Kim, V. Narry (2013): TALEN-based knockout library for human microRNAs. In: *Nature structural & molecular biology* 20 (12), S. 1458–1464. DOI: 10.1038/nsmb.2701.

Knouf, Emily C.; Garg, Kavita; Arroyo, Jason D.; Correa, Yesenia; Sarkar, Deepayan; Parkin, Rachael K. et al. (2012): An integrative genomic approach identifies p73 and p63 as activators of miR-200 microRNA family transcription. In: *Nucleic acids research* 40 (2), S. 499–510. DOI: 10.1093/nar/gkr731.

Koga, Kenichi; Yokoi, Hideki; Mori, Kiyoshi; Kasahara, Masato; Kuwabara, Takashige; Imamaki, Hirotaka et al. (2015): MicroRNA-26a inhibits TGF-β-induced extracellular matrix protein expression in podocytes by targeting CTGF and is downregulated in diabetic nephropathy. In: *Diabetologia. DOI:* 10.1007/s00125-015-3642-4.

Koressaar, Triinu; Remm, Maido (2007): Enhancements and modifications of primer design program Primer3. In: *Bioinformatics (Oxford, England)* 23 (10), S. 1289–1291. DOI: 10.1093/bioinformatics/btm091.

Kozomara, Ana; Griffiths-Jones, Sam (2011): miRBase: integrating microRNA annotation and deep-sequencing data. In: *Nucleic acids research* 39 (Database issue), S. D152-7. DOI: 10.1093/nar/gkq1027.

Kozomara, Ana; Griffiths-Jones, Sam (2014): miRBase: annotating high confidence microRNAs using deep sequencing data. In: *Nucleic acids research* 42 (Database issue), S. D68-73. DOI: 10.1093/nar/gkt1181.

Krupa, Aleksandra; Jenkins, Robert; Luo, Dong Dong; Lewis, Aled; Phillips, Aled; Fraser, Donald (2010): Loss of MicroRNA-192 promotes fibrogenesis in diabetic nephropathy. In: *Journal of the American Society of Nephrology : JASN* 21 (3), S. 438–447. DOI: 10.1681/ASN.2009050530.

Krützfeldt, Jan; Rajewsky, Nikolaus; Braich, Ravi; Rajeev, Kallanthottathil G.; Tuschl, Thomas; Manoharan, Muthiah; Stoffel, Markus (2005): Silencing of microRNAs in vivo with 'antagomirs'. In: *Nature* 438 (7068), S. 685–689. DOI: 10.1038/nature04303.

Lagos-Quintana, Mariana; Rauhut, Reinhard; Yalcin, Abdullah; Meyer, Jutta; Lendeckel, Winfried; Tuschl, Thomas (2002): Identification of Tissue-Specific MicroRNAs from Mouse. In: *Current Biology* 12 (9), S. 735–739. DOI: 10.1016/S0960-9822(02)00809-6.

Lai, Jennifer Y.; Luo, Jinghui; O'Connor, Christopher; Jing, Xiaohong; Nair, Viji; Ju, Wenjun et al. (2015): MicroRNA-21 in glomerular injury. In: *Journal of the American Society of Nephrology : JASN* 26 (4), S. 805–816. DOI: 10.1681/ASN.2013121274.

Landgraf, Pablo; Rusu, Mirabela; Sheridan, Robert; Sewer, Alain; Iovino, Nicola; Aravin, Alexei et al. (2007): A Mammalian microRNA Expression Atlas Based on Small RNA Library Sequencing. In: *Cell* 129 (7), S. 1401–1414. DOI: 10.1016/j.cell.2007.04.040.

Lee, Rosalind C.; Feinbaum, Rhonda L.; Ambros, Victor (1993): The C. elegans heterochronic gene lin-4 encodes small RNAs with antisense complementarity to lin-14. In: *Cell* 75 (5), S. 843–854. DOI: 10.1016/0092-8674(93)90529-Y.

Lehtonen, Sanna; Zhao, Fang; Lehtonen, Eero (2002): CD2-associated protein directly interacts with the actin cytoskeleton. In: *American journal of physiology. Renal physiology* 283 (4), S. F734-43. DOI: 10.1152/ajprenal.00312.2001.

Lei, Yong; Guo, Xiaogang; Liu, Yun; Cao, Yang; Deng, Yi; Chen, Xiongfeng et al. (2012): Efficient targeted gene disruption in Xenopus embryos using engineered transcription activator-like effector nucleases (TALENs). In: *Proceedings of the National Academy of Sciences of the United States of America* 109 (43), S. 17484–17489. DOI: 10.1073/pnas.1215421109.

Li, Dong; Lu, Zhenyu; Jia, Junya; Zheng, Zhenfeng; Lin, Shan (2013): Changes in microRNAs associated with podocytic adhesion damage under mechanical stress. In: *Journal of the renin-angiotensin-aldosterone system : JRAAS* 14 (2), S. 97–102. DOI: 10.1177/1470320312460071.

Li, Dong; Lu, Zhenyu; Jia, Junya; Zheng, Zhenfeng; Lin, Shan (2013): Curcumin ameliorates Podocytic adhesive capacity damage under mechanical stress by inhibiting miR-124 expression. In: *Kidney & blood pressure research* 38 (1), S. 61–71. DOI: 10.1159/000355755.

Li, Xiao; Feng, Ruili; Huang, Chen; Wang, Haifeng; Wang, Jiao; Zhang, Zhifeng et al. (2012): MicroRNA-351 regulates TMEM 59 (DCF1) expression and mediates neural stem cell morphogenesis. In: *RNA Biology* 9 (3), S. 292–301. DOI: 10.4161/rna.19100.

Li, Ya-Feng; Jing, Ying; Hao, Jielu; Frankfort, Nathan C.; Zhou, Xiaoshuang; Shen, Bing et al. (2013): MicroRNA-21 in the pathogenesis of acute kidney injury. In: *Protein & cell* 4 (11), S. 813–819. DOI: 10.1007/s13238-013-3085-y.

Liang, Tingming; Yu, JiaFeng; Liu, Chang; Guo, Li (2014): An exploration of evolution, maturation, expression and function relationships in mir-23 ~ 27 ~ 24 cluster. In: *PloS one* 9 (8), S. e106223. DOI: 10.1371/journal.pone.0106223.

Licatalosi, Donny D.; Mele, Aldo; Fak, John J.; Ule, Jernej; Kayikci, Melis; Chi, Sung Wook et al. (2008): HITS-CLIP yields genome-wide insights into brain alternative RNA processing. In: *Nature* 456 (7221), S. 464–469. DOI: 10.1038/nature07488.

Lin, Chun-Liang; Lee, Pei-Hsien; Hsu, Yung-Chien; Lei, Chen-Chou; Ko, Jih-Yang; Chuang, Pei-Chin et al. (2014): MicroRNA-29a promotion of nephrin acetylation ameliorates hyperglycemia-induced podocyte dysfunction. In: *Journal of the American Society of Nephrology : JASN* 25 (8), S. 1698–1709. DOI: 10.1681/ASN.2013050527.

Lin, Xu; You, Yanwu; Wang, Jie; Qin, Youling; Huang, Peng; Yang, Fafen (2015): MicroRNA-155 deficiency promotes nephrin acetylation and attenuates renal damage in hyperglycemia-induced nephropathy. In: *Inflammation* 38 (2), S. 546–554. DOI: 10.1007/s10753-014-9961-7.

Liu, Gang; Kaw, Beenu; Kurfis, Jayson; Rahmanuddin, Syed; Kanwar, Yashpal S.; Chugh, Sumant S. (2003): Neph1 and nephrin interaction in the slit diaphragm is an important determinant of glomerular permeability. In: *J. Clin. Invest.* 112 (2), S. 209–221. DOI: 10.1172/JCI200318242.

Liu, Yong; Taylor, Norman E.; Lu, Limin; Usa, Kristie; Cowley, Allen W.; Ferreri, Nicholas R. et al. (2010): Renal medullary microRNAs in Dahl salt-sensitive rats: miR-29b regulates several collagens and related genes. In: *Hypertension* 55 (4), S. 974–982. DOI: 10.1161/HYPERTENSIONAHA.109.144428.

Liu, Xingguang; Zhan, Zhenzhen; Xu, Li; Ma, Feng; Li, Dong; Guo, Zhenhong et al. (2010): MicroRNA-148/152 impair innate response and antigen presentation of TLR-triggered dendritic cells by targeting CaMKIIα. In: *Journal of immunology (Baltimore, Md. : 1950)* 185 (12), S. 7244–7251. DOI: 10.4049/jimmunol.1001573.

Long, Justin M.; Lahiri, Debomoy K. (2012): Advances in microRNA experimental approaches to study physiological regulation of gene products implicated in CNS disorders. In: *Experimental neurology* 235 (2), S. 402–418. DOI: 10.1016/j.expneurol.2011.12.043.

Long, Jianyin; Wang, Yin; Wang, Wenjian; Chang, Benny H J; Danesh, Farhad R. (2010): Identification of microRNA-93 as a novel regulator of vascular endothelial growth factor in hyperglycemic conditions. In: *The Journal of biological chemistry* 285 (30), S. 23457–23465. DOI: 10.1074/jbc.M110.136168.

Long, Jianyin; Wang, Yin; Wang, Wenjian; Chang, Benny H J; Danesh, Farhad R. (2011): MicroRNA-29c is a signature microRNA under high glucose conditions that targets Sprouty homolog 1, and its in vivo knockdown prevents progression of diabetic nephropathy. In: *The Journal of biological chemistry* 286 (13), S. 11837–11848. DOI: 10.1074/jbc.M110.194969.

Luca, Antonella de; Maiello, Monica R.; D'Alessio, Amelia; Pergameno, Maria; Normanno, Nicola (2012): The RAS/RAF/MEK/ERK and the PI3K/AKT signalling pathways: role in cancer pathogenesis and implications for therapeutic approaches. In: *Expert opinion on therapeutic targets* 16 Suppl 2, S. S17-27. DOI: 10.1517/14728222.2011.639361.

Ma, Feng; Xu, Sheng; Liu, Xingguang; Zhang, Qian; Xu, Xiongfei; Liu, Mofang et al. (2011): The microRNA miR-29 controls innate and adaptive immune responses to intracellular bacterial infection by targeting interferon-γ. In: *Nature immunology* 12 (9), S. 861–869. DOI: 10.1038/ni.2073.

Machuca, Eduardo; Benoit, Geneviève; Antignac, Corinne (2009): Genetics of nephrotic syndrome: connecting molecular genetics to podocyte physiology. In: *Human molecular genetics* 18 (R2), S. R185-94. DOI: 10.1093/hmg/ddp328.

Marrone, April K.; Stolz, Donna B.; Bastacky, Sheldon I.; Kostka, Dennis; Bodnar, Andrew J.; Ho, Jacqueline (2014): MicroRNA-17~92 is required for nephrogenesis and renal function. In: *Journal of the American Society of Nephrology : JASN* 25 (7), S. 1440–1452. DOI: 10.1681/ASN.2013040390.

McIntosh, I.; Dreyer, S. D.; Clough, M. V.; Dunston, J. A.; Eyaid, W.; Roig, C. M. et al. (1998): Mutation analysis of LMX1B gene in nail-patella syndrome patients. In: *American journal of human genetics* 63 (6), S. 1651–1658. DOI: 10.1086/302165.

Medrano, Silvia; Monteagudo, Maria C.; Sequeira-Lopez, Maria Luisa S; Pentz, Ellen S.; Gomez, R. Ariel (2012): Two microRNAs, miR-330 and miR-125b-5p, mark the juxtaglomerular cell and balance its smooth muscle phenotype. In: *American journal of physiology. Renal physiology* 302 (1), S. F29-37. DOI: 10.1152/ajprenal.00460.2011.

Meister, Gunter (2013): Argonaute proteins: functional insights and emerging roles. In: *Nature reviews. Genetics* 14 (7), S. 447–459. DOI: 10.1038/nrg3462.

Meister, Gunter; Tuschl, Thomas (2004): Mechanisms of gene silencing by double-stranded RNA. In: *Nature* 431 (7006), S. 343–349. DOI: 10.1038/nature02873.

MEISTER, G.; Landthaler, M.; Dorsett, Y.; Tuschl, T. (2004): Sequence-specific inhibition of microRNA- and siRNA-induced RNA silencing. In: *RNA* 10 (3), S. 544–550. DOI: 10.1261/rna.5235104.

Melo, Sonia A.; Esteller, Manel (2011): Dysregulation of microRNAs in cancer: playing with fire. In: *FEBS letters* 585 (13), S. 2087–2099. DOI: 10.1016/j.febslet.2010.08.009.

Mendoza, Michelle C.; Er, E. Emrah; Blenis, John (2011): The Ras-ERK and PI3K-mTOR pathways: cross-talk and compensation. In: *Trends in biochemical sciences* 36 (6), S. 320–328. DOI: 10.1016/j.tibs.2011.03.006.

Miner, Jeffrey H.; Morello, Roy; Andrews, Kaya L.; Li, Cong; Antignac, Corinne; Shaw, Andrey S.; Lee, Brendan (2002): Transcriptional induction of slit diaphragm genes by Lmx1b is required in podocyte differentiation. In: *The Journal of clinical investigation* 109 (8), S. 1065–1072. DOI: 10.1172/JCI13954.

Moeller, Marcus J.; Sanden, Silja K.; Soofi, Abdulsalam; Wiggins, Roger C.; Holzman, Lawrence B. (2003): Podocyte-specific expression of cre recombinase in transgenic mice. In: *Genesis (New York, N.Y. : 2000)* 35 (1), S. 39–42. DOI: 10.1002/gene.10164.

Morcos, Paul A.; Li, Yongfu; Jiang Shan (2008): Vivo-Morpholinos: A non-peptide transporter delivers Morpholinos into a wide array of mouse tissues. In: *BioTechniques* 45 (6), S. 616–626.

Morishita, Yoshiyuki; Imai, Toshimi; Yoshizawa, Hiromichi; Watanabe, Minami; Ishibashi, Kenichi; Muto, Shigeaki; Nagata, Daisuke (2015): Delivery of microRNA-146a with polyethylenimine nanoparticles inhibits renal fibrosis in vivo. In: *International journal of nanomedicine* 10, S. 3475–3488. DOI: 10.2147/IJN.S82587.

Morris, Kevin V.; Mattick, John S. (2014): The rise of regulatory RNA. In: *Nature reviews. Genetics* 15 (6), S. 423–437. DOI: 10.1038/nrg3722.

Mount, David B. (2014): Thick ascending limb of the loop of Henle. In: *Clinical journal of the American Society of Nephrology : CJASN* 9 (11), S. 1974–1986. DOI: 10.2215/CJN.04480413.

Mundel P, Heid HW, Mundel TM, Krüger M, Reiser J, Kriz W (1997): Synaptopodin: An Actin-associated Protein in Telencephalic Dendrites and Renal Podocytes. In: *The Journal of Cell Biology* 139 (1), S. 193–204. DOI: 10.1083/jcb.139.1.193.

Murawski, Inga J.; Maina, Rita W.; Gupta, Indra R. (2014): The relationship between nephron number, kidney size and body weight in two inbred mouse strains. In: *Organogenesis* 6 (3), S. 189–194. DOI: 10.4161/org.6.3.12125.

Muzumdar, Mandar Deepak; Tasic, Bosiljka; Miyamichi, Kazunari; Li, Ling; Luo, Liqun (2007): A global double-fluorescent Cre reporter mouse. In: *Genesis (New York, N.Y. : 2000)* 45 (9), S. 593–605. DOI: 10.1002/dvg.20335.

Newman, P.; Berndt, M.; Gorski, J.; White, G.; Lyman, S.; Paddock, C.; Muller, W. (1990): PECAM-1 (CD31) cloning and relation to adhesion molecules of the immunoglobulin gene superfamily. In: *Science* 247 (4947), S. 1219–1222. DOI: 10.1126/science.1690453.

Nguyen, Tuan Anh; Jo, Myung Hyun; Choi, Yeon-Gil; Park, Joha; Kwon, S. Chul; Hohng, Sungchul et al. (2015): Functional Anatomy of the Human Microprocessor. In: *Cell* 161 (6), S. 1374–1387. DOI: 10.1016/j.cell.2015.05.010.

Nicholas, Susanne B.; Basgen, John M.; Sinha, Satyesh (2011): Using stereologic techniques for podocyte counting in the mouse: shifting the paradigm. In: *American journal of nephrology* 33 Suppl 1, S. 1–7. DOI: 10.1159/000327564.

Otey, Carol A.; Carpen, Olli (2004): Alpha-actinin revisited: a fresh look at an old player. In: *Cell motility and the cytoskeleton* 58 (2), S. 104–111. DOI: 10.1002/cm.20007.

Patel, Vishal; Noureddine, Lama (2012): MicroRNAs and fibrosis. In: *Current opinion in nephrology and hypertension* 21 (4), S. 410–416. DOI: 10.1097/MNH.0b013e328354e559.

Patel, Vishal; Williams, Darren; Hajarnis, Sachin; Hunter, Ryan; Pontoglio, Marco; Somlo, Stefan; Igarashi, Peter (2013): miR-17~92 miRNA cluster promotes kidney cyst growth in polycystic kidney disease. In: *Proceedings of the National Academy of Sciences of the United States of America* 110 (26), S. 10765–10770. DOI: 10.1073/pnas.1301693110.

Patrie, Kevin M.; Drescher, Andrew J.; Welihinda, Ajith; Mundel, Peter; Margolis, Ben (2002): Interaction of two actin-binding proteins, synaptopodin and alpha-actinin-4, with the tight junction protein MAGI-1. In: *The Journal of biological chemistry* 277 (33), S. 30183–30190. DOI: 10.1074/jbc.M203072200.

Peng, Yang; Liu, Yan-Min; Li, Lu-Chun; Wang, Lu-Lu; Wu, Xiao-Ling (2014): microRNA-503 inhibits gastric cancer cell growth and epithelial-to-mesenchymal transition. In: *Oncology letters* 7 (4), S. 1233–1238. DOI: 10.3892/ol.2014.1868.

Pennisi, Elizabeth (2012): ENCODE Project writes eulogy for junk DNA. In: *Science* 337 (6099), S. 1159–1161. DOI: 10.1126/science.337.6099.1159.

Pollak, Martin R.; Quaggin, Susan E.; Hoenig, Melanie P.; Dworkin, Lance D. (2014): The glomerulus: the sphere of influence. In: *Clinical journal of the American Society of Nephrology : CJASN* 9 (8), S. 1461–1469. DOI: 10.2215/CJN.09400913.

Pozzi, Ambra; Zent, Roy (2012): Hold tight or you'll fall off: CD151 helps podocytes stick in high-pressure situations. In: *The Journal of clinical investigation* 122 (1), S. 13–16. DOI: 10.1172/JCI61858.

Putta, Sumanth; Lanting, Linda; Sun, Guangdong; Lawson, Gregory; Kato, Mitsuo; Natarajan, Rama (2012): Inhibiting microRNA-192 ameliorates renal fibrosis in diabetic nephropathy. In: *Journal of the American Society of Nephrology : JASN* 23 (3), S. 458–469. DOI: 10.1681/ASN.2011050485.

Qin, Wei; Chung, Arthur C K; Huang, Xiao R.; Meng, Xiao-Ming; Hui, David S C; Yu, Cheuk-Man et al. (2011): TGF-β/Smad3 signaling promotes renal fibrosis by inhibiting miR-29. In: *Journal of the American Society of Nephrology : JASN* 22 (8), S. 1462–1474. DOI: 10.1681/ASN.2010121308.

Reinhart, B. J.; Slack, F. J.; Basson, M.; Pasquinelli, A. E.; Bettinger, J. C.; Rougvie, A. E. et al. (2000): The 21-nucleotide let-7 RNA regulates developmental timing in Caenorhabditis elegans. In: *Nature* 403 (6772), S. 901–906. DOI: 10.1038/35002607.

Rinkevich, Yuval; Montoro, Daniel T.; Contreras-Trujillo, Humberto; Harari-Steinberg, Orit; Newman, Aaron M.; Tsai, Jonathan M. et al. (2014): In vivo clonal analysis reveals lineage-restricted progenitor characteristics in mammalian kidney development, maintenance, and regeneration. In: *Cell reports* 7 (4), S. 1270–1283. DOI: 10.1016/j.celrep.2014.04.018.

Rüdel, Sabine; Flatley, Andrew; Weinmann, Lasse; Kremmer, Elisabeth; Meister, Gunter (2008): A multifunctional human Argonaute2-specific monoclonal antibody. In: *RNA (New York, N.Y.)* 14 (6), S. 1244–1253. DOI: 10.1261/rna.973808.

Rüdel, Sabine; Wang, Yanli; Lenobel, René; Körner, Roman; Hsiao, He-Hsuan; Urlaub, Henning et al. (2011): Phosphorylation of human Argonaute proteins affects small RNA binding. In: *Nucleic acids research* 39 (6), S. 2330–2343. DOI: 10.1093/nar/gkq1032.

Sachs, Norman; Sonnenberg, Arnoud (2013): Cell-matrix adhesion of podocytes in physiology and disease. In: *Nature reviews. Nephrology* 9 (4), S. 200–210. DOI: 10.1038/nrneph.2012.291.

Saleem M, O'Hare MJ, Reiser J,Coward RJ, Inward CD, Farren T., Xing CY, Ni L, Mathieson PW and Mundel P (2002): A Conditionally Immortalized Human Podocyte Cell Line Demonstrating Nephrin and Podocin Expression. In: *JASN* 13 (3), S. 630–638.

Schiwek, Daniel; Endlich, Nicole; Holzman, Lawrence; Holthöfer, Harry; Kriz, Wilhelm; Endlich, Karlhans (2004): Stable expression of nephrin and localization to cell-cell contacts in novel murine podocyte cell lines. In: *Kidney international* 66 (1), S. 91–101. DOI: 10.1111/j.1523-1755.2004.00711.x.

Schlöndorff, Detlef (2014): Putting the glomerulus back together: per aspera ad astra (\"a rough road leads to the stars\"). In: *Kidney international* 85 (5), S. 991–998. DOI: 10.1038/ki.2014.51.

Schraivogel, Daniel; Weinmann, Lasse; Beier, Dagmar; Tabatabai, Ghazaleh; Eichner, Alexander; Zhu, Jia Yun et al. (2011): CAMTA1 is a novel tumour suppressor regulated by miR-9/9* in glioblastoma stem cells. In: *The EMBO journal* 30 (20), S. 4309–4322. DOI: 10.1038/emboj.2011.301.

Schwarz, K.; Simons, M.; Reiser, J.; Saleem, M. A.; Faul, C.; Kriz, W. et al. (2001): Podocin, a raft-associated component of the glomerular slit diaphragm, interacts with CD2AP and nephrin. In: *The Journal of clinical investigation* 108 (11), S. 1621–1629. DOI: 10.1172/JCI12849.

Sellin, Lorenz; Huber, Tobias B.; Gerke, Peter; Quack, Ivo; Pavenstädt, Hermann; Walz, Gerd (2003): NEPH1 defines a novel family of podocin interacting proteins. In: *FASEB journal : official publication of the Federation of American Societies for Experimental Biology* 17 (1), S. 115–117. DOI: 10.1096/fj.02-0242fje.

Servín-González, Luis Steven; Granados-López, Angelica Judith; López, Jesús Adrián (2015): Families of microRNAs Expressed in Clusters Regulate Cell Signaling in Cervical Cancer. In: *International journal of molecular sciences* 16 (6), S. 12773–12790. DOI: 10.3390/ijms160612773.

Shen, Xinsheng; Si, Yaqing; Yang, Zhugong; Wang, Qun; Yuan, Jiaxiang; Zhang, Xiefu (2015): MicroRNA-542-3p suppresses cell growth of gastric cancer cells via targeting oncogene astrocyte-elevated gene-1. In: *Medical oncology (Northwood, London, England)* 32 (1), S. 361. DOI: 10.1007/s12032-014-0361-5.

Shenoy, Archana; Blelloch, Robert H. (2014): Regulation of microRNA function in somatic stem cell proliferation and differentiation. In: *Nature reviews. Molecular cell biology* 15 (9), S. 565–576. DOI: 10.1038/nrm3854.

Shi, Shaolin; Yu, Liping; Chiu, Celine; Sun, Yezhou; Chen, Jin; Khitrov, Greg et al. (2008): Podocyte-selective deletion of dicer induces proteinuria and glomerulosclerosis. In: *Journal of the American Society of Nephrology : JASN* 19 (11), S. 2159–2169. DOI: 10.1681/ASN.2008030312.

Shi, Shaolin; Yu, Liping; Zhang, Taoran; Qi, Haiying; Xavier, Sandhya; Ju, Wenjun; Bottinger, Erwin (2013): Smad2-dependent downregulation of miR-30 is required for TGF-β-induced apoptosis in podocytes. In: *PloS one* 8 (9), S. e75572. DOI: 10.1371/journal.pone.0075572.

Shih, Neng-Yao; Li, Jun; Cotran, Ramzi; Mundel, Peter; Miner, Jeffrey H.; Shaw, Andrey S. (2001): CD2AP Localizes to the Slit Diaphragm and Binds to Nephrin via a Novel C-Terminal Domain. In: *The American Journal of Pathology* 159 (6), S. 2303–2308. DOI: 10.1016/S0002-9440(10)63080-5.

Shih NY, Li J, Karpitskii V, Nguyen A, Dustin ML, Kanagawa O, Miner JH, Shaw AS (1999): Congenital Nephrotic Syndrome in Mice Lacking CD2-Associated Protein. In: *Science* 286 (5438), S. 312–315. DOI: 10.1126/science.286.5438.312.

Shono, Akemi; Tsukaguchi, Hiroyasu; Yaoita, Eishin; Nameta, Masaaki; Kurihara, Hidetake; Qin, Xiao-Song et al. (2007): Podocin participates in the assembly of tight junctions between foot processes in nephrotic podocytes. In: *Journal of the American Society of Nephrology : JASN* 18 (9), S. 2525–2533. DOI: 10.1681/ASN.2006101084.

Slater, Sadie C.; Beachley, Vince; Hayes, Thomas; Zhang, Daming; Welsh, Gavin I.; Saleem, Moin A. et al. (2011): An in vitro model of the glomerular capillary wall using electrospun collagen nanofibres in a bioartificial composite basement membrane. In: *PloS one* 6 (6), S. e20802. DOI: 10.1371/journal.pone.0020802.

Slater, Sadie C.; Ramnath, Raina D.; Uttridge, Kate; Saleem, Moin A.; Cahill, Paul A.; Mathieson, Peter W. et al. (2012): Chronic exposure to laminar shear stress induces Kruppel-like factor 2 in glomerular endothelial cells and modulates interactions with co-cultured podocytes. In: *The international journal of biochemistry & cell biology* 44 (9), S. 1482–1490. DOI: 10.1016/j.biocel.2012.05.020.

Song, Nan; Ma, Xin; Li, Hongzhao; Zhang, Yu; Wang, Xiaoxiong; Zhou, Pingkun; Zhang, Xu (2015): microRNA-107 functions as a candidate tumor suppressor gene in renal clear cell carcinoma involving multiple genes. In: *Urologic oncology* 33 (5), S. 205.e1-205.e11. DOI: 10.1016/j.urolonc.2015.02.003.

Srivastava, Swayam Prakash; Koya, Daisuke; Kanasaki, Keizo (2013): MicroRNAs in kidney fibrosis and diabetic nephropathy: roles on EMT and EndMT. In: *BioMed research international* 2013, S. 125469. DOI: 10.1155/2013/125469.

Su Zhenyi, Yang Zuozhang, Xu Yongqing, Chen Yongbin, Yu Qiang (2015): MicroRNAs in apoptosis, autophagy and necroptosis. In: *Oncotarget* 6 (11), S. 8474–8490.

Sun, Ning; Zhao, Huimin (2013): Transcription activator-like effector nucleases (TALENs): a highly efficient and versatile tool for genome editing. In: *Biotechnology and bioengineering* 110 (7), S. 1811–1821. DOI: 10.1002/bit.24890.

Sweeney, E. (2003): Nail patella syndrome: a review of the phenotype aided by developmental biology. In: *Journal of Medical Genetics* 40 (3), S. 153–162. DOI: 10.1136/jmg.40.3.153.

Takada, Shuji; Sato, Tempei; Ito, Yoshiaki; Yamashita, Satoshi; Kato, Tomoko; Kawasumi, Miyuri et al. (2013): Targeted gene deletion of miRNAs in mice by TALEN system. In: *PloS one* 8 (10), S. e76004. DOI: 10.1371/journal.pone.0076004.

Takemoto, Minoru; Asker, Noomi; Gerhardt, Holger; Lundkvist, Andrea; Johansson, Bengt R.; Saito, Yasushi; Betsholtz, Christer (2002): A New Method for Large Scale Isolation of Kidney Glomeruli from Mice. In: *The American Journal of Pathology* 161 (3), S. 799–805. DOI: 10.1016/S0002-9440(10)64239-3.

Tang, Rui; Li, Limin; Zhu, Dihan; Hou, Dongxia; Cao, Ting; Gu, Hongwei et al. (2012): Mouse miRNA-709 directly regulates miRNA-15a/16-1 biogenesis at the posttranscriptional level in the nucleus: evidence for a microRNA hierarchy system. In: *Cell research* 22 (3), S. 504–515. DOI: 10.1038/cr.2011.137.

Tatsumi N, Hojo N, Yamada O, Ogawa M, Katsura Y, Kawata S, Morii E, Sakamoto H, Inaba R, Tsuda A, Fukuda I, Moriguchi N, Hasuwa H, Okabe M, Fujiki F, Nishida S, Nakajima H, Tsuboi A, Oka Y, Hosen N, Sugiyama H, Oji Y: Deficiency in WT1-targeting microRNA-125a leads to myeloid malignancies and urogenital abnormalities. In: *Oncogene* advanced online publication 11 May 2015.

Tian, Zhongmin; Greene, Andrew S.; Pietrusz, Jennifer L.; Matus, Isaac R.; Liang, Mingyu (2008): MicroRNA-target pairs in the rat kidney identified by microRNA microarray, proteomic, and bioinformatic analysis. In: *Genome research* 18 (3), S. 404–411. DOI: 10.1101/gr.6587008.

Tomasevic, Nenad; Jia, Zhiheng; Russell, Alan; Fujii, Toby; Hartman, James J.; Clancy, Sheila et al. (2007): Differential regulation of WASP and N-WASP by Cdc42, Rac1, Nck, and PI(4,5)P2. In: *Biochemistry* 46 (11), S. 3494–3502. DOI: 10.1021/bi062152y.

Tryggvason, Karl; Patrakka, Jaakko; Wartiovaara, Jorma (2006): Hereditary proteinuria syndromes and mechanisms of proteinuria. In: *The New England journal of medicine* 354 (13), S. 1387–1401. DOI: 10.1056/NEJMra052131.

Uhde-Stone, Claudia; Sarkar, Nandita; Antes, Travis; Otoc, Nicole; Kim, Young; Jiang, Yan J.; Lu, Biao (2014): A TALEN-based strategy for efficient bi-allelic miRNA ablation in human cells. In: *RNA (New York, N.Y.)* 20 (6), S. 948–955. DOI: 10.1261/rna.042010.113.

Ule, Jernej; Jensen, Kirk B.; Ruggiu, Matteo; Mele, Aldo; Ule, Aljaz; Darnell, Robert B. (2003): CLIP identifies Nova-regulated RNA networks in the brain. In: *Science (New York, N.Y.)* 302 (5648), S. 1212–1215. DOI: 10.1126/science.1090095.

Untergasser, Andreas; Cutcutache, Ioana; Koressaar, Triinu; Ye, Jian; Faircloth, Brant C.; Remm, Maido; Rozen, Steven G. (2012): Primer3--new capabilities and interfaces. In: *Nucleic acids research* 40 (15), S. e115. DOI: 10.1093/nar/gks596.

Verma, Rakesh; Wharram, Bryan; Kovari, Iulia; Kunkel, Robin; Nihalani, Deepak; Wary, Kishore K. et al. (2003): Fyn binds to and phosphorylates the kidney slit diaphragm component Nephrin. In: *The Journal of biological chemistry* 278 (23), S. 20716–20723. DOI: 10.1074/jbc.M301689200.

Verma, Rakesh; Kovari, Iulia; Soofi, Abdul; Nihalani, Deepak; Patrie, Kevin; Holzman, Lawrence B. (2006): Nephrin ectodomain engagement results in Src kinase activation, nephrin phosphorylation, Nck recruitment, and actin polymerization. In: *The Journal of clinical investigation* 116 (5), S. 1346–1359. DOI: 10.1172/JCI27414.

Vlachos, Ioannis S.; Paraskevopoulou, Maria D.; Karagkouni, Dimitra; Georgakilas, Georgios; Vergoulis, Thanasis; Kanellos, Ilias et al. (2015): DIANA-TarBase v7.0: indexing more than half a million experimentally supported miRNA:mRNA interactions. In: *Nucleic acids research* 43 (Database issue), S. D153-9. DOI: 10.1093/nar/gku1215.

Volinia, Stefano; Galasso, Marco; Costinean, Stefan; Tagliavini, Luca; Gamberoni, Giacomo; Drusco, Alessandra et al. (2010): Reprogramming of miRNA networks in cancer and leukemia. In: *Genome research* 20 (5), S. 589–599. DOI: 10.1101/gr.098046.109.

Vollrath, D.; Jaramillo-Babb, V. L.; Clough, M. V.; McIntosh, I.; Scott, K. M.; Lichter, P. R.; Richards, J. E. (1998): Loss-of-Function Mutations in the LIM-Homeodomain Gene, LMX1B, in Nail-Patella Syndrome. In: *Human molecular genetics* 7 (7), S. 1091–1098. DOI: 10.1093/hmg/7.7.1091.

Wang, Bo; Herman-Edelstein, Michal; Koh, Philip; Burns, Wendy; Jandeleit-Dahm, Karin; Watson, Anna et al. (2010): E-cadherin expression is regulated by miR-192/215 by a mechanism that is independent of the profibrotic effects of transforming growth factor-beta. In: *Diabetes* 59 (7), S. 1794–1802. DOI: 10.2337/db09-1736.

Wang, Bo; Komers, Radko; Carew, Rosemarie; Winbanks, Catherine E.; Xu, Bei; Herman-Edelstein, Michal et al. (2012): Suppression of microRNA-29 expression by TGF-β1 promotes collagen expression and renal fibrosis. In: *Journal of the American Society of Nephrology : JASN* 23 (2), S. 252–265. DOI: 10.1681/ASN.2011010055.

Wang, Jin; Chen, Jinyun; Sen, Subrata (2015): microRNA as Biomarkers and Diagnostics. In: *Journal of cellular physiology. DOI:* 10.1002/jcp.25056.

Wang, Ren-jie; Li, Jian-wei; Bao, Bu-he; Wu, Huan-cheng; Du, Zhen-hua; Su, Jing-liang et al. (2015): MicroRNA-873 (miRNA-873) inhibits glioblastoma tumorigenesis and metastasis by suppressing the expression of IGF2BP1. In: *The Journal of biological chemistry* 290 (14), S. 8938–8948. DOI: 10.1074/jbc.M114.624700.

Wang, Zhigang; Wei, Meng; Ren, Yi; Liu, Hua; Wang, Meng; Shi, Kehui; Jiang, Hongli (2014): miR149 rs71428439 polymorphism and risk of clear cell renal cell carcinoma: a case-control study. In: *Tumour biology : the journal of the International Society for Oncodevelopmental Biology and Medicine* 35 (12), S. 12127–12130. DOI: 10.1007/s13277-014-2517-5.

Wanner, Nicola; Hartleben, Björn; Herbach, Nadja; Goedel, Markus; Stickel, Natalie; Zeiser, Robert et al. (2014): Unraveling the role of podocyte turnover in glomerular aging and injury. In: *Journal of the American Society of Nephrology : JASN* 25 (4), S. 707–716. DOI: 10.1681/ASN.2013050452.

Ward, Sabine M Volkmer; Weins, Astrid; Pollak, Martin R.; Weitz, David A. (2008): Dynamic viscoelasticity of actin cross-linked with wild-type and disease-causing mutant alpha-actinin-4. In: *Biophysical journal* 95 (10), S. 4915–4923. DOI: 10.1529/biophysj.108.131722.

Weins, Astrid; Kenlan, Peter; Herbert, Stephanie; Le, Tu C.; Villegas, Ivan; Kaplan, Bernard S. et al. (2005): Mutational and Biological Analysis of alpha-actinin-4 in focal segmental glomerulosclerosis. In: *Journal of the American Society of Nephrology : JASN* 16 (12), S. 3694–3701. DOI: 10.1681/ASN.2005070706.

Welsh, Gavin I.; Saleem, Moin A. (2012): The podocyte cytoskeleton--key to a functioning glomerulus in health and disease. In: *Nature reviews. Nephrology* 8 (1), S. 14–21. DOI: 10.1038/nrneph.2011.151.

Witzgall, Ralph (2008): How are podocytes affected in nail-patella syndrome? In: *Pediatric nephrology (Berlin, Germany)* 23 (7), S. 1017–1020. DOI: 10.1007/s00467-007-0714-9.

Wu, Junnan; Zheng, Chunxia; Fan, Yun; Zeng, Caihong; Chen, Zhaohong; Qin, Weisong et al. (2014): Downregulation of microRNA-30 facilitates podocyte injury and is prevented by glucocorticoids. In: *Journal of the American Society of Nephrology : JASN* 25 (1), S. 92–104. DOI: 10.1681/ASN.2012111101.

Xiao, Fenqiang; Zhang, Wu; Chen, Liming; Chen, Fei; Xie, Haiyang; Xing, Chunyang et al. (2013): MicroRNA-503 inhibits the G1/S transition by downregulating cyclin D3 and E2F3 in hepatocellular carcinoma. In: *Journal of translational medicine* 11, S. 195. DOI: 10.1186/1479-5876-11-195.

Xie, Hua; Lin, Hong-Li; Wang, Nan; Sun, Yan-Ling; Kan, Yu; Guo, Hui et al. (2015): Inhibition of microRNA-30a prevents puromycin aminonucleoside-induced podocytic apoptosis by upregulating the glucocorticoid receptor α. In: *Molecular medicine reports. DOI:* 10.3892/mmr.2015.4226.

Xiong M, Jiang L, Zhou Y, Qiu W, Fang L, Tan R, Wen P, Yang J (2012): The miR-200 family regulates TGF-β1-induced renal tubular epithelial to mesenchymal transition through Smad pathway by targeting ZEB1 and ZEB2 expression. In: *Am J Physiol Renal Physiol* 302 (3), S. 369–379.

Yanagida-Asanuma, Etsuko; Asanuma, Katsuhiko; Kim, Kwanghee; Donnelly, Mary; Young Choi, Hoon; Hyung Chang, Jae et al. (2007): Synaptopodin protects against proteinuria by disrupting Cdc42:IRSp53:Mena signaling complexes in kidney podocytes. In: *The American Journal of Pathology* 171 (2), S. 415–427. DOI: 10.2353/ajpath.2007.070075.

Ye, Wenbin; Lv, Qing; Wong, Chung-Kwun Amy; Hu, Sean; Fu, Chao; Hua, Zhong et al. (2008): The effect of central loops in miRNA:MRE duplexes on the efficiency of miRNA-mediated gene regulation. In: *PloS one* 3 (3), S. e1719. DOI: 10.1371/journal.pone.0001719.

Yoda, Mayuko; Cifuentes, Daniel; Izumi, Natsuko; Sakaguchi, Yuriko; Suzuki, Tsutomu; Giraldez, Antonio J.; Tomari, Yukihide (2013): Poly(A)-specific ribonuclease mediates 3'-end trimming of Argonaute2-cleaved precursor microRNAs. In: *Cell reports* 5 (3), S. 715–726. DOI: 10.1016/j.celrep.2013.09.029.

Zhdanova, Olga; Srivastava, Shekhar; Di, Lie; Li, Zhai; Tchelebi, Leila; Dworkin, Sara et al. (2011): The inducible deletion of Drosha and microRNAs in mature podocytes results in a collapsing glomerulopathy. In: *Kidney international* 80 (7), S. 719–730. DOI: 10.1038/ki.2011.122.

Zhong, Jianyong; Perrien, Daniel Scott; Yang, Hai-Chun; Kon, Valentina; Fogo, Agnes B.; Ichikawa, Iekuni; Ma, Ji (2012): Maturational regression of glomeruli determines the nephron population in normal mice. In: *Pediatric research* 72 (3), S. 241–248. DOI: 10.1038/pr.2012.81.

Zhou, Hua; Hasni, Sarfaraz A.; Perez, Paola; Tandon, Mayank; Jang, Shyh-Ing; Zheng, Changyu et al. (2013): miR-150 promotes renal fibrosis in lupus nephritis by downregulating SOCS1. In: *Journal of the American Society of Nephrology : JASN* 24 (7), S. 1073–1087. DOI: 10.1681/ASN.2012080849.

Zhu, Jianxin; Attias, Ortal; Aoudjit, Lamine; Jiang, Ruihua; Kawachi, Hiroshi; Takano, Tomoko (2010): p21-activated kinases regulate actin remodeling in glomerular podocytes. In: *American journal of physiology. Renal physiology* 298 (4), S. F951-61. DOI: 10.1152/ajprenal.00536.2009.

Zhu, Qubo; Sun, Wenyu; Okano, Kiichiro; Chen, Yu; Zhang, Ning; Maeda, Tadao; Palczewski, Krzysztof (2011): Sponge transgenic mouse model reveals important roles for the microRNA-183 (miR-183)/96/182 cluster in postmitotic photoreceptors of the retina. In: *The Journal of biological chemistry* 286 (36), S. 31749–31760. DOI: 10.1074/jbc.M111.259028.

Zhu, Xiang-Yang; Ebrahimi, Behzad; Eirin, Alfonso; Woollard, John R.; Tang, Hui; Jordan, Kyra L. et al. (2015): Renal Vein Levels of MicroRNA-26a Are Lower in the Poststenotic Kidney. In: *Journal of the American Society of Nephrology : JASN* 26 (6), S. 1378–1388. DOI: 10.1681/ASN.2014030248

10 APPENDIX

Tab. 10.1: miRNAs expressed in murine glomeruli and tubules

miRNA	Glomeruli total RNA		Tubules Total RNA			Glomeruli small RNA		Tubules small RNA		
	good reads	‰ of good reads	good reads	‰ of good reads	Ratio Glom/ Tub	good reads	‰ of good reads	good reads	‰ of good reads	Ratio Glom/ Tub
	5,381,269		3,775,151			4,436,757		5,710,310		
mmu-let-7a-1-3p, mmu-let-7c-2-3p	63	0.01	22	0.01	2.01	93	0.02	52	0.01	2.30
mmu-let-7a-5p	41,255	7.67	18,219	4.83	1.59	27,034	6.09	19,687	3.45	1.77
mmu-let-7a-5p, mmu-let-7c-5p	122	0.02	113	0.03	0.76	311	0.07	116	0.02	3.45
mmu-let-7b-3p	25	0.00	2	0.00	8.77	21	0.00	12	0.00	2.25
mmu-let-7b-5p	16,312	3.03	5,872	1.56	1.95	27,601	6.22	16,891	2.96	2.10
mmu-let-7c-5p	33,524	6.23	13,516	3.58	1.74	39,557	8.92	26,053	4.56	1.95
mmu-let-7d-3p	454	0.08	168	0.04	1.90	1,923	0.43	1,218	0.21	2.03
mmu-let-7d-5p	2,790	0.52	1,619	0.43	1.21	1,454	0.33	1,815	0.32	1.03
mmu-let-7e-3p	26	0.00	7	0.00	2.61	39	0.01	15	0.00	3.35
mmu-let-7e-5p	5,950	1.11	2,387	0.63	1.75	4,530	1.02	1,865	0.33	3.13
mmu-let-7f-2-3p	41	0.01	23	0.01	1.25	58	0.01	43	0.01	1.74
mmu-let-7f-5p	42,422	7.88	42,569	11.28	0.70	36,019	8.12	27,564	4.83	1.68
mmu-let-7g-5p	12,689	2.36	11,051	2.93	0.81	2,990	0.67	7,736	1.35	0.50
mmu-let-7i-5p	13,809	2.57	7,849	2.08	1.23	10,489	2.36	6,920	1.21	1.95
mmu-miR-100-5p	426	0.08	131	0.03	2.28	521	0.12	272	0.05	2.47
mmu-miR-101a-3p	296	0.06	122	0.03	1.70	254	0.06	210	0.04	1.56
mmu-miR-101a-3p, mmu-miR-101c	14,770	2.74	7,352	1.95	1.41	11,694	2.64	12,966	2.27	1.16
mmu-miR-101b-3p	1,038	0.19	643	0.17	1.13	655	0.15	806	0.14	1.05
mmu-miR-101c	9,487	1.76	7,214	1.91	0.92	8,019	1.81	11,534	2.02	0.89
mmu-miR-103-3p	3,275	0.61	2,440	0.65	0.94	1,233	0.28	2,543	0.45	0.62
mmu-miR-103-3p, mmu-miR-107-3p	339	0.06	426	0.11	0.56	319	0.07	809	0.14	0.51
mmu-miR-106b-3p	125	0.02	83	0.02	1.06	98	0.02	107	0.02	1.18
mmu-miR-106b-5p	43	0.01	28	0.01	1.08	28	0.01	28	0.00	1.29
mmu-miR-107-3p	175	0.03	348	0.09	0.35	67	0.02	398	0.07	0.22
mmu-miR-10a-3p	50	0.01	40	0.01	0.88	47	0.01	92	0.02	0.66
mmu-miR-10a-5p	1,299,061	241.40	860,036	227.81	1.06	1,158,586	261.13	1,292,589	226.36	1.15
mmu-miR-10b-5p	1,342,787	249.53	756,932	200.50	1.24	991,872	223.56	997,889	174.75	1.28
mmu-miR-1198-5p	70	0.01	60	0.02	0.82	153	0.03	256	0.04	0.77
mmu-miR-1247-5p						2	0.00	29	0.01	0.09
mmu-miR-125a-3p	8	0.00	3	0.00	1.87	25	0.01	19	0.00	1.69
mmu-miR-125a-5p	8,639	1.61	2,912	0.77	2.08	11,467	2.58	6,081	1.06	2.43
mmu-miR-125b-2-3p	59	0.01	44	0.01	0.94	11	0.00	69	0.01	0.21
mmu-miR-125b-5p	396	0.07	313	0.08	0.89	582	0.13	784	0.14	0.96
mmu-miR-126-3p	7,271	1.35	512	0.14	9.96	14,215	3.20	1,104	0.19	16.57
mmu-miR-126-5p	18,476	3.43	900	0.24	14.40	20,770	4.68	2,000	0.35	13.37

miRNA	Glomeruli total RNA		Tubules Total RNA			Glomeruli small RNA		Tubules small RNA		
	good reads	‰ of good reads	good reads	‰ of good reads	Ratio Glom/ Tub	good reads	‰ of good reads	good reads	‰ of good reads	Ratio Glom/ Tub
	5,381,269		3,775,151			4,436,757		5,710,310		
mmu-miR-127-3p	26,515	4.93	1,122	0.30	16.58	24,763	5.58	1,775	0.31	17.96
mmu-miR-128-3p	32	0.01	47	0.01	0.48	29	0.01	143	0.03	0.26
mmu-miR-130a-3p	867	0.16	242	0.06	2.51	492	0.11	447	0.08	1.42
mmu-miR-132-3p	314	0.06	30	0.01	7.34	108	0.02	32	0.01	4.34
mmu-miR-133a-3p	70	0.01	4	0.00	12.28	33	0.01	16	0.00	2.65
mmu-miR-134-5p	21	0.00	2	0.00	7.37	30	0.01	1	0.00	38.61
mmu-miR-139-3p	44	0.01	5	0.00	6.17	340	0.08	22	0.00	19.89
mmu-miR-139-5p	297	0.06	22	0.01	9.47	141	0.03	26	0.00	6.98
mmu-miR-140-3p	2,300	0.43	1,767	0.47	0.91	1,387	0.31	2,512	0.44	0.71
mmu-miR-143-3p	1,075,605	199.88	84,425	22.36	8.94	969,109	218.43	157,049	27.50	7.94
mmu-miR-143-5p	17	0.00	5	0.00	2.39	72	0.02	8	0.00	11.58
mmu-miR-145-5p	2,860	0.53	178	0.05	11.27	195	0.04	81	0.01	3.10
mmu-miR-146a-5p	437	0.08	85	0.02	3.61	3,999	0.90	574	0.10	8.97
mmu-miR-146b-5p	5,365	1.00	992	0.26	3.79	5,264	1.19	1,935	0.34	3.50
mmu-miR-148a-3p	4,470	0.83	2,162	0.57	1.45	1,368	0.31	2,069	0.36	0.85
mmu-miR-148b-3p	1,132	0.21	1,318	0.35	0.60	109	0.02	542	0.09	0.26
mmu-miR-149-5p	70	0.01	49	0.01	1.00	25	0.01	41	0.01	0.78
mmu-miR-150-5p	523	0.10	47	0.01	7.81	387	0.09	76	0.01	6.55
mmu-miR-151-3p	4,631	0.86	1,561	0.41	2.08	10,885	2.45	4,955	0.87	2.83
mmu-miR-151-5p	3,216	0.60	1,006	0.27	2.24	2,924	0.66	1,977	0.35	1.90
mmu-miR-152-3p	1,340	0.25	675	0.18	1.39	512	0.12	812	0.14	0.81
mmu-miR-152-5p	399	0.07	216	0.06	1.30	276	0.06	337	0.06	1.05
mmu-miR-15a-5p	314	0.06	109	0.03	2.02	156	0.04	202	0.04	0.99
mmu-miR-15b-5p	74	0.01	67	0.02	0.77	9	0.00	46	0.01	0.25
mmu-miR-16-5p	5,047	0.94	2,034	0.54	1.74	1,598	0.36	2,222	0.39	0.93
mmu-miR-17-5p	30	0.01	24	0.01	0.88	5	0.00	19	0.00	0.34
mmu-miR-181a-1-3p	183	0.03	145	0.04	0.89	103	0.02	191	0.03	0.69
mmu-miR-181a-5p	39,180	7.28	18,799	4.98	1.46	35,869	8.08	39,948	7.00	1.16
mmu-miR-181b-5p	2,348	0.44	2,202	0.58	0.75	1,359	0.31	3,946	0.69	0.44
mmu-miR-181c-3p	74	0.01	43	0.01	1.21	69	0.02	68	0.01	1.31
mmu-miR-181c-5p	2,737	0.51	769	0.20	2.50	1,562	0.35	1,237	0.22	1.63
mmu-miR-181d-5p	356	0.07	140	0.04	1.78	295	0.07	222	0.04	1.71
mmu-miR-182-5p	428	0.08	4,456	1.18	0.07	197	0.04	5,356	0.94	0.05
mmu-miR-183-5p	219	0.04	1,152	0.31	0.13	151	0.03	1,773	0.31	0.11
mmu-miR-1839-5p	386	0.07	776	0.21	0.35	117	0.03	529	0.09	0.28
mmu-miR-1843-3p	35	0.01	34	0.01	0.72	13	0.00	72	0.01	0.23
mmu-miR-1843-5p	197	0.04	156	0.04	0.89	204	0.05	275	0.05	0.95
mmu-miR-1843-5p, mmu-miR-1843b-5p	125	0.02	124	0.03	0.71	144	0.03	228	0.04	0.81
mmu-miR-1843b-5p	97	0.02	72	0.02	0.95	117	0.03	170	0.03	0.89
mmu-miR-184-3p	113	0.02	53	0.01	1.50	98	0.02	135	0.02	0.93

miRNA	Glomeruli total RNA		Tubules Total RNA			Glomeruli small RNA		Tubules small RNA		
	good reads	‰ of good reads	good reads	‰ of good reads	Ratio Glom/ Tub	good reads	‰ of good reads	good reads	‰ of good reads	Ratio Glom/ Tub
	5,381,269		3,775,151			4,436,757		5,710,310		
mmu-miR-185-3p	5	0.00	23	0.01	0.15	8	0.00	53	0.01	0.19
mmu-miR-185-5p	59	0.01	257	0.07	0.16	49	0.01	236	0.04	0.27
mmu-miR-186-5p	311	0.06	104	0.03	2.10	275	0.06	492	0.09	0.72
mmu-miR-190-5p	5	0.00	199	0.05	0.02	3	0.00	172	0.03	0.02
mmu-miR-191-5p	8,505	1.58	6,414	1.70	0.93	7,043	1.59	10,601	1.86	0.86
mmu-miR-192-5p	942	0.18	16,630	4.41	0.04	722	0.16	25,275	4.43	0.04
mmu-miR-194-5p	66	0.01	523	0.14	0.09	19	0.00	744	0.13	0.03
mmu-miR-195-3p	84	0.02	5	0.00	11.79	103	0.02	11	0.00	12.05
mmu-miR-195-5p	1,371	0.25	149	0.04	6.46	356	0.08	133	0.02	3.45
mmu-miR-196a-5p	1,773	0.33	2,208	0.58	0.56	555	0.13	1,268	0.22	0.56
mmu-miR-196b-5p	1,193	0.22	1,557	0.41	0.54	770	0.17	887	0.16	1.12
mmu-miR-1981-5p	19	0.00	54	0.01	0.25	22	0.00	210	0.04	0.13
mmu-miR-199a-3p, mmu-miR-199b-3p	2,736	0.51	243	0.06	7.90	973	0.22	259	0.05	4.84
mmu-miR-19a-3p	39	0.01	12	0.00	2.28	38	0.01	71	0.01	0.69
mmu-miR-19b-3p	495	0.09	123	0.03	2.82	270	0.06	534	0.09	0.65
mmu-miR-1a-3p	1,193	0.22	162	0.04	5.17	382	0.09	67	0.01	7.34
mmu-miR-200a-3p	304	0.06	5,126	1.36	0.04	142	0.03	6,676	1.17	0.03
mmu-miR-200a-5p	19	0.00	281	0.07	0.05	5	0.00	318	0.06	0.02
mmu-miR-200b-3p	170	0.03	3,374	0.89	0.04	261	0.06	8,239	1.44	0.04
mmu-miR-200c-3p	22	0.00	382	0.10	0.04	50	0.01	1,218	0.21	0.05
mmu-miR-203-3p	138	0.03	340	0.09	0.28	48	0.01	400	0.07	0.15
mmu-miR-204-5p	632	0.12	389	0.10	1.14	190	0.04	403	0.07	0.61
mmu-miR-205-5p	9	0.00	71	0.02	0.09	1	0.00	108	0.02	0.01
mmu-miR-20a-5p	98	0.02	93	0.02	0.74	35	0.01	71	0.01	0.63
mmu-miR-210-3p	32	0.01	18	0.00	1.25	29	0.01	39	0.01	0.96
mmu-miR-21-5p	4,046	0.75	10,579	2.80	0.27	890	0.20	8,037	1.41	0.14
mmu-miR-218-5p	5	0.00	95	0.03	0.04	4	0.00	113	0.02	0.05
mmu-miR-221-3p	161	0.03	241	0.06	0.47	94	0.02	592	0.10	0.20
mmu-miR-222-3p	664	0.12	1,431	0.38	0.33	735	0.17	4,582	0.80	0.21
mmu-miR-22-3p	14,742	2.74	17,655	4.68	0.59	33,150	7.47	66,147	11.58	0.65
mmu-miR-224-5p	30	0.01	9	0.00	2.34	24	0.01	30	0.01	1.03
mmu-miR-23a-3p	3,286	0.61	321	0.09	7.18	513	0.12	383	0.07	1.72
mmu-miR-23b-3p	12,617	2.34	1,155	0.31	7.66	1,442	0.33	1,069	0.19	1.74
mmu-miR-23b-3p, mmu-miR-23a-3p	29	0.01	7	0.00	2.91	15	0.00	6	0.00	3.22
mmu-miR-24-2-5p	81	0.02	7	0.00	8.12	62	0.01	19	0.00	4.20
mmu-miR-24-3p	10,906	2.03	1,228	0.33	6.23	4,810	1.08	2,236	0.39	2.77
mmu-miR-25-3p	2,709	0.50	1,237	0.33	1.54	725	0.16	1,395	0.24	0.67
mmu-miR-26a-5p	58,229	10.82	14,473	3.83	2.82	21,052	4.74	18,816	3.30	1.44
mmu-miR-26b-5p	6,252	1.16	2,936	0.78	1.49	896	0.20	1,991	0.35	0.58
mmu-miR-27a-3p	2,728	0.51	343	0.09	5.58	949	0.21	325	0.06	3.76

miRNA	Glomeruli total RNA good reads 5,381,269	Glomeruli total RNA ‰ of good reads	Tubules Total RNA good reads 3,775,151	Tubules Total RNA ‰ of good reads	Ratio Glom/ Tub	Glomeruli small RNA good reads 4,436,757	Glomeruli small RNA ‰ of good reads	Tubules small RNA good reads 5,710,310	Tubules small RNA ‰ of good reads	Ratio Glom/ Tub
mmu-miR-27a-5p	42	0.01	2	0.00	14.73	44	0.01	7	0.00	8.09
mmu-miR-27b-3p	61,434	11.42	9,252	2.45	4.66	53,473	12.05	14,268	2.50	4.82
mmu-miR-27b-3p, mmu-miR-27a-3p	79	0.01	12	0.00	4.62	67	0.02	21	0.00	4.11
mmu-miR-27b-5p	85	0.02	11	0.00	5.42	284	0.06	39	0.01	9.37
mmu-miR-28-3p	183	0.03	182	0.05	0.71	91	0.02	194	0.03	0.60
mmu-miR-28-5p	37	0.01	35	0.01	0.74	23	0.01	36	0.01	0.82
mmu-miR-28-5p, mmu-miR-28c	208	0.04	168	0.04	0.87	144	0.03	244	0.04	0.76
mmu-miR-299-3p, mmu-miR-299b-3p	46	0.01	4	0.00	8.07	45	0.01	1	0.00	57.92
mmu-miR-29a-3p	1,623	0.30	669	0.18	1.70	2,202	0.50	1,674	0.29	1.69
mmu-miR-29b-3p	73	0.01	40	0.01	1.28	41	0.01	109	0.02	0.48
mmu-miR-29c-3p	429	0.08	148	0.04	2.03	503	0.11	406	0.07	1.59
mmu-miR-300-3p	76	0.01	1	0.00	53.32	33	0.01			
mmu-miR-301a-3p	78	0.01	45	0.01	1.22	13	0.00	67	0.01	0.25
mmu-miR-3068-5p	71	0.01	84	0.02	0.59	19	0.00	93	0.02	0.26
mmu-miR-30a-3p	4,234	0.79	1,790	0.47	1.66	3,396	0.77	3,000	0.53	1.46
mmu-miR-30a-5p	149,029	27.69	51,143	13.55	2.04	53,363	12.03	63,316	11.09	1.08
mmu-miR-30b-3p	35	0.01	11	0.00	2.23	44	0.01	38	0.01	1.49
mmu-miR-30b-5p	1,236	0.23	444	0.12	1.95	677	0.15	558	0.10	1.56
mmu-miR-30c-1-3p	14	0.00	25	0.01	0.39	33	0.01	85	0.01	0.50
mmu-miR-30c-2-3p	1,632	0.30	606	0.16	1.89	2,557	0.58	1,662	0.29	1.98
mmu-miR-30c-5p	4,313	0.80	3,064	0.81	0.99	2,748	0.62	4,950	0.87	0.71
mmu-miR-30d-3p	61	0.01	33	0.01	1.30	20	0.00	40	0.01	0.64
mmu-miR-30d-5p	29,149	5.42	12,954	3.43	1.58	15,116	3.41	22,349	3.91	0.87
mmu-miR-30e-3p	420	0.08	1,233	0.33	0.24	279	0.06	1,279	0.22	0.28
mmu-miR-30e-5p	4,057	0.75	11,397	3.02	0.25	1,722	0.39	15,183	2.66	0.15
mmu-miR-31-5p	23	0.00	55	0.01	0.29	23	0.01	92	0.02	0.32
mmu-miR-320-3p	1,254	0.23	779	0.21	1.13	1,676	0.38	1,341	0.23	1.61
mmu-miR-322-3p	1,623	0.30	97	0.03	11.74	865	0.19	146	0.03	7.63
mmu-miR-322-5p	440	0.08	25	0.01	12.35	101	0.02	33	0.01	3.94
mmu-miR-326-3p	30	0.01	5	0.00	4.21	27	0.01	7	0.00	4.96
mmu-miR-328-3p	253	0.05	191	0.05	0.93	422	0.10	600	0.11	0.91
mmu-miR-335-3p	241	0.04	18	0.00	9.39	41	0.01	11	0.00	4.80
mmu-miR-335-5p	156	0.03	12	0.00	9.12	103	0.02	18	0.00	7.36
mmu-miR-338-3p	94	0.02	6	0.00	10.99	75	0.02	6	0.00	16.09
mmu-miR-339-5p	33	0.01	24	0.01	0.96	41	0.01	52	0.01	1.01
mmu-miR-340-5p	495	0.09	756	0.20	0.46	128	0.03	811	0.14	0.20
mmu-miR-342-3p	147	0.03	51	0.01	2.02	13	0.00	33	0.01	0.51
mmu-miR-34a-5p	30	0.01	97	0.03	0.22	17	0.00	54	0.01	0.41
mmu-miR-350-5p	24	0.00	4	0.00	4.21	26	0.01	5	0.00	6.69

miRNA	Glomeruli total RNA		Tubules Total RNA			Glomeruli small RNA		Tubules small RNA		
	good reads	‰ of good reads	good reads	‰ of good reads	Ratio Glom/ Tub	good reads	‰ of good reads	good reads	‰ of good reads	Ratio Glom/ Tub
	5,381,269		3,775,151			4,436,757		5,710,310		
mmu-miR-351-5p	2,633	0.49	137	0.04	13.48	3,239	0.73	329	0.06	12.67
mmu-miR-361-3p	27	0.01	11	0.00	1.72	26	0.01	24	0.00	1.39
mmu-miR-361-5p	108	0.02	57	0.02	1.33	120	0.03	159	0.03	0.97
mmu-miR-365-3p	258	0.05	386	0.10	0.47	224	0.05	550	0.10	0.52
mmu-miR-374-5p	28	0.01	30	0.01	0.65	32	0.01	25	0.00	1.65
mmu-miR-375-3p	38	0.01	619	0.16	0.04	65	0.01	2,061	0.36	0.04
mmu-miR-378-3p	9,418	1.75	32,214	8.53	0.21	9,549	2.15	56,099	9.82	0.22
mmu-miR-378b	28	0.01	59	0.02	0.33	12	0.00	69	0.01	0.22
mmu-miR-379-5p	715	0.13	46	0.01	10.90	446	0.10	13	0.00	44.16
mmu-miR-381-3p	128	0.02	4	0.00	22.45	38	0.01	5	0.00	9.78
mmu-miR-382-5p	64	0.01	6	0.00	7.48	27	0.01	6	0.00	5.79
mmu-miR-383-5p	29	0.01	83	0.02	0.25	28	0.01	228	0.04	0.16
mmu-miR-409-3p	69	0.01	1	0.00	48.41	116	0.03	8	0.00	18.66
mmu-miR-410-3p	53	0.01	3	0.00	12.39	12	0.00	3	0.00	5.15
mmu-miR-411-5p	211	0.04	9	0.00	16.45	196	0.04	7	0.00	36.04
mmu-miR-421-3p	14	0.00	32	0.01	0.31	7	0.00	74	0.01	0.12
mmu-miR-423-3p	378	0.07	379	0.10	0.70	453	0.10	1,128	0.20	0.52
mmu-miR-423-5p	425	0.08	386	0.10	0.77	878	0.20	630	0.11	1.79
mmu-miR-425-3p	41	0.01	43	0.01	0.67	43	0.01	60	0.01	0.92
mmu-miR-425-5p	50	0.01	83	0.02	0.42	38	0.01	162	0.03	0.30
mmu-miR-429-3p	72	0.01	1,325	0.35	0.04	75	0.02	2,584	0.45	0.04
mmu-miR-434-3p	199	0.04	7	0.00	19.94	73	0.02	18	0.00	5.22
mmu-miR-450a-5p	135	0.03	8	0.00	11.84	118	0.03	19	0.00	7.99
mmu-miR-450b-3p	34	0.01	4	0.00	5.96	6	0.00	1	0.00	7.72
mmu-miR-450b-5p	53	0.01	2	0.00	18.59	9	0.00	6	0.00	1.93
mmu-miR-455-5p	30	0.01	169	0.04	0.12	19	0.00	258	0.05	0.09
mmu-miR-484	914	0.17	738	0.20	0.87	432	0.10	642	0.11	0.87
mmu-miR-486-5p, mmu-miR-3107-5p	6,380	1.19	945	0.25	4.74	7,653	1.72	1,761	0.31	5.59
mmu-miR-497-5p	20	0.00	2	0.00	7.02	193	0.04	27	0.00	9.20
mmu-miR-503-5p	90	0.02	12	0.00	5.26	159	0.04	23	0.00	8.90
mmu-miR-5099	170	0.03	267	0.07	0.45	176	0.04	580	0.10	0.39
mmu-miR-532-5p	299	0.06	436	0.12	0.48	200	0.05	520	0.09	0.50
mmu-miR-541-5p	597	0.11	22	0.01	19.04	978	0.22	62	0.01	20.30
mmu-miR-542-3p	171	0.03	13	0.00	9.23	49	0.01	8	0.00	7.88
mmu-miR-574-3p	246	0.05	28	0.01	6.16	33	0.01	10	0.00	4.25
mmu-miR-574-5p	82	0.02	6	0.00	9.59	84	0.02	13	0.00	8.32
mmu-miR-598-3p	93	0.02	42	0.01	1.55	10	0.00	15	0.00	0.86
mmu-miR-615-3p	69	0.01	64	0.02	0.76	131	0.03	162	0.03	1.04
mmu-miR-652-3p	670	0.12	121	0.03	3.88	706	0.16	259	0.05	3.51
mmu-miR-664-5p	16	0.00	23	0.01	0.49	63	0.01	98	0.02	0.83

miRNA	Glomeruli total RNA		Tubules Total RNA			Glomeruli small RNA		Tubules small RNA		
	good reads	‰ of good reads	good reads	‰ of good reads	Ratio Glom/ Tub	good reads	‰ of good reads	good reads	‰ of good reads	Ratio Glom/ Tub
	5,381,269		3,775,151			4,436,757		5,710,310		
mmu-miR-669c-5p	64	0.01	58	0.02	0.77	33	0.01	36	0.01	1.18
mmu-miR-671-3p	149	0.03	82	0.02	1.27	124	0.03	176	0.03	0.91
mmu-miR-672-5p	46	0.01	80	0.02	0.40	53	0.01	123	0.02	0.55
mmu-miR-676-3p	89	0.02	61	0.02	1.02	146	0.03	199	0.03	0.94
mmu-miR-676-5p	23	0.00	26	0.01	0.62	11	0.00	33	0.01	0.43
mmu-miR-744-5p	404	0.08	93	0.02	3.05	457	0.10	300	0.05	1.96
mmu-miR-7a-5p	69	0.01	180	0.05	0.27	31	0.01	68	0.01	0.59
mmu-miR-872-3p	46	0.01	44	0.01	0.73	32	0.01	61	0.01	0.68
mmu-miR-872-5p	108	0.02	105	0.03	0.72	59	0.01	141	0.02	0.54
mmu-miR-92a-3p	31,280	5.81	10,066	2.67	2.18	14,169	3.19	16,593	2.91	1.10
mmu-miR-9-5p	14	0.00	271	0.07	0.04	5	0.00	331	0.06	0.02
mmu-miR-98-5p	265	0.05	777	0.21	0.24	180	0.04	471	0.08	0.49
mmu-miR-99a-5p	375	0.07	393	0.10	0.67	589	0.13	852	0.15	0.89
mmu-miR-99b-3p	106	0.02	51	0.01	1.46	82	0.02	75	0.01	1.41
mmu-miR-99b-5p	24,751	4.60	10,139	2.69	1.71	26,197	5.90	16,620	2.91	2.03

Tab. 10.2: miRNAs expressed in glomerular cells: podocytes and red fluorescent cell population

miRNA	podocytes vs. red fluorescent cells									
	1st profile					2nd profile				
	Podocytes reads	Podocytes ‰	red Cells reads	red Cells ‰	Ratio (Pod/red cells)	Podocytes reads	Podocytes ‰	red Cells reads	red Cells ‰	Ratio (Pod/red cells)
mmu-let-7a-1-3p, mmu-let-7c-2-3p	636	0.12	602	0.11	1.06	826	0.16	527	0.10	1.62
mmu-let-7a-5p	343,792	64.83	251,694	47.30	1.37	554,218	106.46	281,820	52.45	2.03
mmu-let-7a-5p, mmu-let-7c-5p	3,979	0.75	3,577	0.67	1.12	4,787	0.92	2,413	0.45	2.05
mmu-let-7b-3p	26	0.00	74	0.01	0.35	34	0.01	79	0.01	0.44
mmu-let-7b-5p	147,755	27.86	209,201	39.31	0.71	212,135	40.75	189,786	35.32	1.15
mmu-let-7c-5p	250,916	47.32	324,273	60.94	0.78	431,323	82.85	364,208	67.78	1.22
mmu-let-7d-3p	6,967	1.31	3,784	0.71	1.85	4,144	0.80	1,619	0.30	2.64
mmu-let-7d-5p	30,753	5.80	23,440	4.40	1.32	37,053	7.12	27,523	5.12	1.39
mmu-let-7e-3p	214	0.04	81	0.02	2.65	211	0.04	79	0.01	2.76
mmu-let-7e-5p	51,770	9.76	37,054	6.96	1.40	47,319	9.09	36,237	6.74	1.35
mmu-let-7f-2-3p	634	0.12	422	0.08	1.51	495	0.10	209	0.04	2.44
mmu-let-7f-5p	538,119	101.48	408,158	76.70	1.32	551,521	105.94	363,598	67.67	1.57
mmu-let-7g-5p	30,231	5.70	54,258	10.20	0.56	83,554	16.05	71,891	13.38	1.20
mmu-let-7i-3p	33	0.01	49	0.01	0.68					
mmu-let-7i-5p	31,929	6.02	81,456	15.31	0.39	30,657	5.89	46,055	8.57	0.69
mmu-let-7k	111	0.02	164	0.03	0.68	158	0.03	145	0.03	1.12
mmu-miR-100-5p	10	0.00	206	0.04	0.05	2	0.00	365	0.07	0.01
mmu-miR-101a-3p	812	0.15	1,746	0.33	0.47	371	0.07	806	0.15	0.48
mmu-miR-101a-3p, mmu-miR-101c	51,740	9.76	76,830	14.44	0.68	50,791	9.76	44,912	8.36	1.17
mmu-miR-101b-3p	7,099	1.34	6,011	1.13	1.19	9,394	1.80	3,927	0.73	2.47
mmu-miR-101c	6,880	1.30	13,294	2.50	0.52	6,197	1.19	7,477	1.39	0.86
mmu-miR-103-3p	9,529	1.80	21,329	4.01	0.45	13,119	2.52	16,960	3.16	0.80
mmu-miR-103-3p, mmu-miR-107-3p	2,828	0.53	5,054	0.95	0.56	2,102	0.40	3,515	0.65	0.62
mmu-miR-106b-3p	311	0.06	601	0.11	0.52	370	0.07	517	0.10	0.74
mmu-miR-106b-5p	169	0.03	230	0.04	0.74	297	0.06	182	0.03	1.68
mmu-miR-107-3p	2.513	0.47	530	0.10	4.76	3.170	0.61	788	0.15	4.15
mmu-miR-10a-3p	40	0.01	704	0.13	0.06	40	0.01	491	0.09	0.08
mmu-miR-10a-5p	38,001	7.17	583,123	109.58	0.07	55,607	10.68	652,874	121.50	0.09
mmu-miR-10b-5p	428,640	80.83	173,877	32.67	2.47	529,253	101.66	348,000	64.76	1.57
mmu-miR-1198-5p	250	0.05	460	0.09	0.55	279	0.05	535	0.10	0.54
mmu-miR-122-5p						10	0.00	45	0.01	0.23
mmu-miR-125a-3p	170	0.03	141	0.03	1.21	102	0.02	98	0.02	1.07
mmu-miR-125a-5p	6,102	1.15	3,523	0.66	1.74	12,728	2.44	4,506	0.84	2.92
mmu-miR-125b-2-3p	436	0.08	70	0.01	6.25	248	0.05	59	0.01	4.34

miRNA	podocytes vs. red fluorescent cells									
	1st profile					2nd profile				
	Podocytes reads	Podocytes ‰	red Cells reads	red Cells ‰	Ratio (Pod/red cells)	Podocytes reads	Podocytes ‰	red Cells reads	red Cells ‰	Ratio (Pod/red cells)
mmu-miR-125b-5p	952	0.18	333	0.06	2.87	1,273	0.24	642	0.12	2.05
mmu-miR-1249-3p						20	0.00	77	0.01	0.27
mmu-miR-126-3p	37	0.01	62,042	11.66	0.00	17	0.00	56,544	10.52	0.00
mmu-miR-126-5p	96	0.02	137,998	25.93	0.00	38	0.01	93,880	17.47	0.00
mmu-miR-127-3p	9	0.00	21,542	4.05	0.00	4	0.00	3,792	0.71	0.00
mmu-miR-127-5p			519	0.10				104	0.02	
mmu-miR-128-3p	53	0.01	91	0.02	0.58	72	0.01	84	0.02	0.88
mmu-miR-129-5p	21	0.00	481	0.09	0.04	26	0.00	328	0.06	0.08
mmu-miR-130a-3p	4.660	0.88	994	0.19	4.70	3,059	0.59	998	0.19	3.16
mmu-miR-132-3p	408	0.08	1,478	0.28	0.28	285	0.05	1,627	0.30	0.18
mmu-miR-133a-3p	2	0.00	1,268	0.24	0.00	2	0.00	613	0.11	0.00
mmu-miR-134-5p			337	0.06				130	0.02	
mmu-miR-136-3p			92	0.02						
mmu-miR-139-3p	3	0.00	1,600	0.30	0.00			972	0.18	
mmu-miR-139-5p	5	0.00	1,635	0.31	0.00			1,457	0.27	
mmu-miR-140-3p	3,348	0.63	7,536	1.42	0.45	2,741	0.53	6,700	1.25	0.42
mmu-miR-140-5p	256	0.05	397	0.07	0.65	178	0.03	433	0.08	0.42
mmu-miR-1249-3p								126	0.02	
mmu-miR-143-3p	26,606	5.02	457,545	85.98	0.06	16,557	3.18	415,094	77.25	0.04
mmu-miR-143-5p	13	0.00	103	0.02	0.13	5	0.00	162	0.03	0.03
mmu-miR-145a-3p						9	0.00	93	0.02	0.10
mmu-miR-145a-5p	16	0.00	317	0.06	0.05	61	0.01	745	0.14	0.08
mmu-miR-146a-5p	25	0.00	3,807	0.72	0.01	20	0.00	2,278	0.42	0.01
mmu-miR-146b-5p	13,295	2.51	542	0.10	24.62	7,755	1.49	455	0.08	17.59
mmu-miR-148a-3p	6,333	1.19	1,376	0.26	4.62	5,082	0.98	2,292	0.43	2.29
mmu-miR-148b-3p	1,066	0.20	1,462	0.27	0.73	955	0.18	1,058	0.20	0.93
mmu-miR-149-5p	310	0.06	24	0.00	12.96	448	0.09	61	0.01	7.58
mmu-miR-150-5p	1	0.00	397	0.07	0.00	1	0.00	550	0.10	0.00
mmu-miR-151-3p	2,171	0.41	14,094	2.65	0.15	2,072	0.40	10,653	1.98	0.20
mmu-miR-151-5p	1,705	0.32	13,157	2.47	0.13	1,681	0.32	10,544	1.96	0.16
mmu-miR-152-3p	6,545	1.23	7,340	1.38	0.89	6,460	1.24	6,011	1.12	1.11
mmu-miR-152-5p	73	0.01	58	0.01	1.26	77	0.01	60	0.01	1.32
mmu-miR-154-5p			69	0.01						
mmu-miR-15a-5p	158	0.03	691	0.13	0.23	108	0.02	457	0.09	0.24
mmu-miR-15b-5p	63	0.01	132	0.02	0.48	86	0.02	82	0.02	1.08
mmu-miR-16-1-3p	15	0.00	50	0.01	0.30	20	0.00	42	0.01	0.49
mmu-miR-16-2-3p						33	0.01	54	0.01	0.63
mmu-miR-16-5p	2,012	0.38	5,927	1.11	0.34	2,307	0.44	6,465	1.20	0.37
mmu-miR-17-3p	40	0.01	62	0.01	0.65	18	0.00	40	0.01	0.46

miRNA	podocytes vs. red fluorescent cells									
	1st profile					2nd profile				
	Podocytes reads	Podocytes ‰	red Cells reads	red Cells ‰	Ratio (Pod/red cells)	Podocytes reads	Podocytes ‰	red Cells reads	red Cells ‰	Ratio (Pod/red cells)
mmu-miR-17-5p	148	0.03	135	0.03	1.10	526	0.10	202	0.04	2.69
mmu-miR-181a-1-3p	320	0.06	775	0.15	0.41	423	0.08	697	0.13	0.63
mmu-miR-181a-5p	44,145	8.33	48,910	9.19	0.91	34,773	6.68	28,659	5.33	1.25
mmu-miR-181b-5p	4,911	0.93	9,007	1.69	0.55	4,415	0.85	5,996	1.12	0.76
mmu-miR-181c-3p	2	0.00	198	0.04	0.01			123	0.02	
mmu-miR-181c-5p	94	0.02	4,027	0.76	0.02	53	0.01	2,470	0.46	0.02
mmu-miR-181d-5p	6	0.00	936	0.18	0.01	16	0.00	712	0.13	0.02
mmu-miR-182-5p	18	0.00	1,286	0.24	0.01	11	0.00	2,250	0.42	0.01
mmu-miR-183-5p	3	0.00	132	0.02	0.02			192	0.04	
mmu-miR-1839-5p	1,122	0.21	1,014	0.19	1.11	2,419	0.46	1,131	0.21	2.21
mmu-miR-1843a-3p	515	0.10	311	0.06	1.66	534	0.10	377	0.07	1.46
mmu-miR-1843a-5p	427	0.08	354	0.07	1.21	453	0.09	287	0.05	1.63
mmu-miR-1843a-5p, mmu-miR-1843b-5p	459	0.09	308	0.06	1.50	538	0.10	190	0.04	2.92
mmu-miR-1843b-3p	150	0.03	123	0.02	1.22	102	0.02	96	0.02	1.10
mmu-miR-1843b-5p	418	0.08	330	0.06	1.27	341	0.07	230	0.04	1.53
mmu-miR-184-3p	46	0.01	117	0.02	0.39	54	0.01	117	0.02	0.48
mmu-miR-185-3p	38	0.01	66	0.01	0.58	39	0.01	37	0.01	1.09
mmu-miR-185-5p	151	0.03	220	0.04	0.69	165	0.03	226	0.04	0.75
mmu-miR-186-5p	588	0.11	610	0.11	0.97	445	0.09	379	0.07	1.21
mmu-miR-187-3p						20	0.00	42	0.01	0.49
mmu-miR-190a-5p						44	0.01	46	0.01	0.99
mmu-miR-190b-5p	16	0.00	69	0.01	0.23	37	0.01	54	0.01	0.71
mmu-miR-191-5p	4,267	0.80	3,615	0.68	1.18	3,590	0.69	3,622	0.67	1.02
mmu-miR-192-5p	315	0.06	208	0.04	1.52	271	0.05	146	0.03	1.92
mmu-miR-193a-5p	9	0.00	104	0.02	0.09	15	0.00	128	0.02	0.12
mmu-miR-1943-5p	8	0.00	63	0.01	0.13					
mmu-miR-194-5p	92	0.02	54	0.01	1.71	175	0.03	87	0.02	2.08
mmu-miR-194-2-3p						75	0.01	48	0.01	1.61
mmu-miR-195a-3p			464	0.09				215	0.04	
mmu-miR-195a-5p	4	0.00	1,358	0.26	0.00	2	0.00	1,476	0.27	0.00
mmu-miR-196a-5p	2,062	0.39	1,333	0.25	1.55	3,282	0.63	4,048	0.75	0.84
mmu-miR-196b-5p	4,904	0.92	908	0.17	5.42	9,553	1.83	1,396	0.26	7.06
mmu-miR-1966-3p						38	0.01	16	0.00	2.45
mmu-miR-1981-5p	206	0.04	196	0.04	1.05	170	0.03	231	0.04	0.76
mmu-miR-199a-3p, mmu-miR-199b-3p	366	0.07	3,475	0.65	0.11	639	0.12	4,950	0.92	0.13
mmu-miR-199a-5p			56	0.01						
mmu-miR-19a-3p	196	0.04	892	0.17	0.22	346	0.07	416	0.08	0.86

miRNA	podocytes vs. red fluorescent cells									
	1st profile					2nd profile				
	Podocytes reads	Podocytes ‰	red Cells reads	red Cells ‰	Ratio (Pod/red cells)	Podocytes reads	Podocytes ‰	red Cells reads	red Cells ‰	Ratio (Pod/red cells)
mmu-miR-19b-3p	1,750	0.33	4,894	0.92	0.36	3,428	0.66	3,096	0.58	1.14
mmu-miR-1a-3p	45	0.01	11,056	2.08	0.00	52	0.01	6,815	1.27	0.01
mmu-miR-200a-3p	54	0.01	2,315	0.44	0.02	46	0.01	5,660	1.05	0.01
mmu-miR-200a-5p	2	0.00	59	0.01	0.03			139	0.03	
mmu-miR-200b-3p	34	0.01	1,093	0.21	0.03	21	0.00	6,198	1.15	0.00
mmu-miR-200b-5p						2	0.00	62	0.01	0.03
mmu-miR-200c-3p	2	0.00	636	0.12	0.00	11	0.00	2,479	0.46	0.00
mmu-miR-203-3p	236	0.04	1,296	0.24	0.18	534	0.10	1,581	0.29	0.35
mmu-miR-204-3p	5	0.00	96	0.02	0.05	2	0.00	94	0.02	0.02
mmu-miR-204-5p	200	0.04	4,648	0.87	0.04	272	0.05	7,460	1.39	0.04
mmu-miR-205-5p	13	0.00	223	0.04	0.06	1	0.00	192	0.04	0.01
mmu-miR-20a-5p	376	0.07	354	0.07	1.07	1,469	0.28	548	0.10	2.77
mmu-miR-210-3p	1,595	0.30	199	0.04	8.04	856	0.16	166	0.03	5.32
mmu-miR-218-5p			66	0.01				224	0.04	
mmu-miR-219-1-3p	42	0.01	40	0.01	1.05					
mmu-miR-21a-5p	7,418	1.40	16,657	3.13	0.45	7,822	1.50	15,671	2.92	0.52
mmu-miR-221-3p	44	0.01	1,908	0.36	0.02	99	0.02	2,829	0.53	0.04
mmu-miR-222-3p	25	0.00	1,943	0.37	0.01	24	0.00	1,857	0.35	0.01
mmu-miR-22-3p	86,470	16.31	31,672	5.95	2.74	52,295	10.05	28,347	5.28	1.90
mmu-miR-224-5p			86	0.02				54	0.01	
mmu-miR-22-5p	65	0.01	35	0.01	1.86	36	0.01	34	0.01	1.09
mmu-miR-23a-3p	1,746	0.33	9,443	1.77	0.19	2,180	0.42	7,369	1.37	0.31
mmu-miR-23a-5p	35	0.01	32	0.01	1.10	40	0.01	31	0.01	1.33
mmu-miR-23b-3p	20,360	3.84	8,916	1.68	2.29	22,111	4.25	7,866	1.46	2.90
mmu-miR-23b-3p, mmu-miR-23a-3p	335	0.06	678	0.13	0.50	246	0.05	361	0.07	0.70
mmu-miR-24-1-5p	60	0.01	27	0.01	2.23	113	0.02	27	0.01	4.32
mmu-miR-24-2-5p	159	0.03	471	0.09	0.34	136	0.03	191	0.04	0.73
mmu-miR-24-3p	43,356	8.18	33,083	6.22	1.32	42,487	8.16	29,820	5.55	1.47
mmu-miR-25-3p	5,532	1.04	14,795	2.78	0.38	6,267	1.20	13,808	2.57	0.47
mmu-miR-26a-2-3p						58	0.01	17	0.00	3.52
mmu-miR-26a-5p	211,150	39.82	141,726	26.63	1.50	214,852	41.27	103,799	19.32	2.14
mmu-miR-26b-3p						54	0.01	16	0.00	3.48
mmu-miR-26b-5p	32,816	6.19	43,370	8.15	0.76	46,077	8.85	35,647	6.63	1.33
mmu-miR-27a-3p	1,278	0.24	6,425	1.21	0.20	821	0.16	3,022	0.56	0.28
mmu-miR-27a-5p	486	0.09	364	0.07	1.34	2.065	0.40	922	0.17	2.31
mmu-miR-27b-3p	125,181	23.61	84,018	15.79	1.50	78,425	15.06	46,432	8.64	1.74
mmu-miR-27b-3p, mmu-miR-27a-3p	4,008	0.76	4,003	0.75	1.00	2,943	0.57	2,780	0.52	1.09

miRNA	podocytes vs. red fluorescent cells									
	1st profile					2nd profile				
	Podocytes reads	Podocytes ‰	red Cells reads	red Cells ‰	Ratio (Pod/red cells)	Podocytes reads	Podocytes ‰	red Cells reads	red Cells ‰	Ratio (Pod/red cells)
mmu-miR-27b-5p	847	0.16	339	0.06	2.51	760	0.15	279	0.05	2.81
mmu-miR-28a-3p	228	0.04	1,189	0.22	0.19	392	0.08	1,595	0.30	0.25
mmu-miR-28a-5p	36	0.01	112	0.02	0.32	32	0.01	187	0.03	0.18
mmu-miR-28a-5p, mmu-miR-28c	193	0.04	820	0.15	0.24	130	0.02	744	0.14	0.18
mmu-miR-28c	31	0.01	125	0.02	0.25	28	0.01	107	0.02	0.27
mmu-miR-296-3p	23	0.00	32	0.01	0.72					
mmu-miR-298-5p	5	0.00	58	0.01	0.09					
mmu-miR-299a-3p, mmu-miR-299b-3p	1	0.00	558	0.10	0.00	2	0.00	166	0.03	0.01
mmu-miR-299b-3p			166	0.03				79	0.01	
mmu-miR-29a-3p	10,846	2.05	7,963	1.50	1.37	8,226	1.58	4,288	0.80	1.98
mmu-miR-29b-3p	234	0.04	187	0.04	1.26	75	0.01	71	0.01	1.09
mmu-miR-29c-3p	1,411	0.27	1,698	0.32	0.83	686	0.13	887	0.17	0.80
mmu-miR-300-3p			427	0.08				103	0.02	
mmu-miR-301a-3p	112	0.02	87	0.02	1.29	57	0.01	42	0.01	1.40
mmu-miR-3068-5p	31	0.01	26	0.00	1.20	52	0.01	17	0.00	3.16
mmu-miR-3096a-5p, mmu-miR-3096b-5p	69	0.01	96	0.02	0.72					
mmu-miR-3096b-5p	83	0.02	83	0.02	1.00					
mmu-miR-30a-3p	60,898	11.48	17,250	3.24	3.54	92,817	17.83	23,919	4.45	4.01
mmu-miR-30a-5p	1,080,588	203.78	221,539	41.63	4.90	738,560	141.87	110,666	20.60	6.89
mmu-miR-30b-3p	623	0.12	195	0.04	3.21	946	0.18	237	0.04	4.12
mmu-miR-30b-5p	8,906	1.68	2,663	0.50	3.36	10,086	1.94	3,197	0.59	3.26
mmu-miR-30b-5p, mmu-miR-30c-5p	94	0.02	58	0.01	1.63	60	0.01	21	0.00	2.95
mmu-miR-30c-1-3p	63	0.01	69	0.01	0.92	90	0.02	139	0.03	0.67
mmu-miR-30c-2-3p	19,948	3.76	4,969	0.93	4.03	24,398	4.69	5,423	1.01	4.64
mmu-miR-30c-5p	36,253	6.84	11,104	2.09	3.28	58,989	11.33	14,980	2.79	4.06
mmu-miR-30d-3p	355	0.07	114	0.02	3.13	282	0.05	70	0.01	4.16
mmu-miR-30d-5p	146,004	27.53	27,942	5.25	5.24	127,730	24.54	24,399	4.54	5.40
mmu-miR-30e-3p	1,558	0.29	1,370	0.26	1.14	2,779	0.53	3,130	0.58	0.92
mmu-miR-30e-5p	12,171	2.30	8,685	1.63	1.41	7,907	1.52	6,984	1.30	1.17
mmu-miR-31-5p			59	0.01		2	0.00	169	0.03	0.01
mmu-miR-320-3p	1,439	0.27	3,967	0.75	0.36	2,810	0.54	3,795	0.71	0.76
mmu-miR-322-3p	14,940	2.82	1,810	0.34	8.28	13,469	2.59	3,093	0.58	4.49
mmu-miR-322-5p	1,374	0.26	1,194	0.22	1.15	528	0.10	910	0.17	0.60
mmu-miR-324-5p	28	0.01	26	0.00	1.08					
mmu-miR-326-3p	184	0.03	129	0.02	1.43	103	0.02	60	0.01	1.77

miRNA	podocytes vs. red fluorescent cells									
	1st profile					2nd profile				
	Podocytes reads	Podocytes ‰	red Cells reads	red Cells ‰	Ratio (Pod/red cells)	Podocytes reads	Podocytes ‰	red Cells reads	red Cells ‰	Ratio (Pod/red cells)
mmu-miR-328-3p	4,426	0.83	2,862	0.54	1.55	3,806	0.73	2,782	0.52	1.41
mmu-miR-329-5p	2	0.00	283	0.05	0.01			117	0.02	
mmu-miR-330-3p	222	0.04	25	0.00	8.91	120	0.02	23	0.00	5.39
mmu-miR-330-5p	306	0.06	37	0.01	8.30	112	0.02	21	0.00	5.50
mmu-miR-335-3p	1	0.00	1,579	0.30	0.00			1,508	0.28	
mmu-miR-335-5p	4	0.00	1,800	0.34	0.00			1,680	0.31	
mmu-miR-338-3p	1	0.00	263	0.05	0.00			116	0.02	
mmu-miR-339-5p	397	0.07	1,077	0.20	0.37	212	0.04	592	0.11	0.37
mmu-miR-340-5p	3,535	0.67	1,281	0.24	2.77	3,263	0.63	925	0.17	3.64
mmu-miR-341-3p			93	0.02						
mmu-miR-342-3p	1	0.00	54	0.01	0.02	3	0.00	85	0.02	0.04
mmu-miR-3473b	5	0.00	62	0.01	0.08					
mmu-miR-34a-5p	276	0.05	357	0.07	0.78	396	0.08	242	0.05	1.69
mmu-miR-34c-5p	11	0.00	80	0.02	0.14					
mmu-miR-350-5p	59	0.01	178	0.03	0.33	55	0.01	126	0.02	0.45
mmu-miR-351-3p	54	0.01	3	0.00	18.06	46	0.01	15	0.00	3.17
mmu-miR-351-5p	8,439	1.59	1,332	0.25	6.36	5,192	1.00	1,400	0.26	3.83
mmu-miR-3535						240	0.05	233	0.04	1.06
mmu-miR-361-3p	254	0.05	391	0.07	0.65	228	0.04	335	0.06	0.70
mmu-miR-361-5p	173	0.03	318	0.06	0.55	125	0.02	282	0.05	0.46
mmu-miR-362-3p	123	0.02	142	0.03	0.87	50	0.01	66	0.01	0.78
mmu-miR-365-3p	13	0.00	121	0.02	0.11	5	0.00	155	0.03	0.03
mmu-miR-369-3p			78	0,01						
mmu-miR-374b-5p	84	0.02	35	0,01	2.41	73	0.01	45	0.01	1.67
mmu-miR-374b-5p, mmu-miR-374c-5p	100	0.02	69	0,01	1.45	85	0.02	45	0.01	1.95
mmu-miR-375-3p	2	0.00	207	0,04	0.01	5	0.00	1,164	0.22	0.00
mmu-miR-376b-3p			78	0,01						
mmu-miR-376c-3p			75	0,01						
mmu-miR-378a-3p	26,410	4.98	14,695	2,76	1.80	22,955	4.41	21,464	3.99	1.10
mmu-miR-378a-3p, mmu-miR-378c	3,205	0.60	1,686	0,32	1.91	1,916	0.37	2,055	0.38	0.96
mmu-miR-378a-3p, mmu-miR-378b, mmu-miR-378c						33	0.01	29	0.01	1.17
mmu-miR-378a-5p	115	0.02	75	0,01	1.54	78	0.01	50	0.01	1.61
mmu-miR-378b	212	0.04	161	0,03	1.32	274	0.05	152	0.03	1.86
mmu-miR-379-5p	7	0.00	5,558	1,04	0.00			2,489	0.46	
mmu-miR-381-3p			568	0,11		1	0.00	177	0.03	0.01

miRNA	podocytes vs. red fluorescent cells									
	1st profile					2nd profile				
	Podocytes reads	Podocytes ‰	red Cells reads	red Cells ‰	Ratio (Pod/red cells)	Podocytes reads	Podocytes ‰	red Cells reads	red Cells ‰	Ratio (Pod/red cells)
mmu-miR-382-5p			758	0,14		2	0.00	539	0.10	0.00
mmu-miR-383-5p			78	0,01				68	0.01	
mmu-miR-409-3p			551	0,10				265	0.05	
mmu-miR-410-3p			226	0,04				104	0.02	
mmu-miR-411-3p			84	0,02						
mmu-miR-411-5p			1,486	0,28				627	0.12	
mmu-miR-421-3p	59	0.01	70	0,01	0.85	43	0.01	28	0.01	1.59
mmu-miR-423-3p	726	0.14	1,956	0,37	0.37	464	0.09	1,040	0.19	0.46
mmu-miR-423-5p	653	0.12	1,853	0,35	0.35	389	0.07	1,459	0.27	0.28
mmu-miR-425-3p	127	0.02	102	0,02	1.25	69	0.01	57	0.01	1.25
mmu-miR-425-5p	143	0.03	205	0,04	0.70	113	0.02	194	0.04	0.60
mmu-miR-429-3p	6	0.00	753	0,14	0.01	10	0.00	3,355	0.62	0.00
mmu-miR-433-3p			197	0,04				69	0.01	
mmu-miR-434-3p			1,396	0,26				897	0.17	
mmu-miR-434-5p			274	0,05				128	0.02	
mmu-miR-450a-5p	962	0.18	272	0,05	3.55	1,000	0.19	378	0.07	2.73
mmu-miR-450a-1-3p						35	0.01	30	0.01	1.20
mmu-miR-450b-3p	283	0.05	120	0,02	2.37	364	0.07	266	0.05	1.41
mmu-miR-450b-5p	334	0.06	64	0,01	5.24	296	0.06	64	0.01	4.77
mmu-miR-455-5p	3	0.00	143	0,03	0.02			113	0.02	
mmu-miR-455-5p								163	0.03	
mmu-miR-484	70	0.01	202	0,04	0.35	95	0.02	183	0.03	0.54
mmu-miR-485-5p			61	0,01						
mmu-miR-486-5p, mmu-miR-3107-5p	211	0.04	218	0,04	0.97	140	0.03	317	0.06	0.46
mmu-miR-488-3p			67	0,01						
mmu-miR-497-5p	4	0.00	688	0,13	0.01			391	0.07	
mmu-miR-503-3p	152	0.03	38	0,01	4.01	197	0.04	50	0.01	4.07
mmu-miR-503-5p	2,677	0.50	591	0,11	4.55	1,832	0.35	713	0.13	2.65
mmu-miR-5099	754	0.14	5,438	1,02	0.14	507	0.10	1,285	0.24	0.41
mmu-miR-5109	81	0.02	98	0,02	0.83					
mmu-miR-5117-3p	109	0.02	76	0,01	1.44					
mmu-miR-532-5p	1,704	0.32	2,527	0,47	0.68	1,532	0.29	2,099	0.39	0.75
mmu-miR-540-3p			116	0,02						
mmu-miR-541-5p	2	0.00	3,050	0,57	0.00			1,550	0.29	
mmu-miR-542-3p	1,829	0.34	550	0,10	3.34	3,334	0.64	626	0.12	5.50
mmu-miR-542-5p	100	0.02	41	0,01	2.45	42	0.01	43	0.01	1.01
mmu-miR-543-3p			333	0,06				70	0.01	
mmu-miR-574-3p	1,473	0.28	369	0,07	4.01	2,017	0.39	725	0.13	2.87

miRNA	podocytes vs. red fluorescent cells									
	1st profile					2nd profile				
	Podocytes reads	Podocytes ‰	red Cells reads	red Cells ‰	Ratio (Pod/red cells)	Podocytes reads	Podocytes ‰	red Cells reads	red Cells ‰	Ratio (Pod/red cells)
mmu-miR-574-5p	498	0.09	330	0,06	1.51	307	0.06	366	0.07	0.87
mmu-miR-598-3p	173	0.03	584	0,11	0.30	161	0.03	515	0.10	0.32
mmu-miR-615-3p	167	0.03	21	0,00	7.98	134	0.03	45	0.01	3.07
mmu-miR-615-5p	49	0.01	12	0,00	4.10					
mmu-miR-6240	25	0.00	39	0,01	0.64	2	0.00	62	0.01	0.03
mmu-miR-6243	174	0.03	251	0,05	0.70					
mmu-miR-652-3p	878	0.17	315	0,06	2.80	847	0.16	278	0.05	3.14
mmu-miR-664-3p						67	0.01	42	0.01	1.65
mmu-miR-664-5p	166	0.03	110	0,02	1.51	98	0.02	85	0.02	1.19
mmu-miR-669c-5p	153	0.03	110	0,02	1.40	405	0.08	359	0.07	1.16
mmu-miR-671-3p	492	0.09	257	0,05	1.92	448	0.09	255	0.05	1.81
mmu-miR-672-5p	99	0.02	511	0,10	0.19	74	0.01	638	0.12	0.12
mmu-miR-673-5p			126	0,02						
mmu-miR-674-3p	29	0.01	66	0,01	0.44	39	0.01	90	0.02	0.45
mmu-miR-676-3p	895	0.17	380	0,07	2.36	858	0.16	692	0.13	1.28
mmu-miR-676-5p	57	0.01	20	0,00	2.86	43	0.01	39	0.01	1.14
mmu-miR-709						8	0.00	64	0.01	0.13
mmu-miR-744-5p	3,493	0.66	3,769	0,71	0.93	1,411	0.27	1,449	0.27	1.01
mmu-miR-7a-5p	181	0.03	522	0,10	0.35	481	0.09	475	0.09	1.05
mmu-miR-8103						19	0.00	59	0.01	0.33
mmu-miR-872-3p	33	0.01	63	0,01	0.53	44	0.01	42	0.01	1.08
mmu-miR-872-5p	424	0.08	578	0,11	0.74	343	0.07	430	0.08	0.82
mmu-miR-873a-5p	170	0.03				80	0.02	1	0.00	82.57
mmu-miR-874-3p						15	0.00	59	0.01	0.26
mmu-miR-92a-1-5p	25	0.00	74	0,01	0.34	25	0.00	74	0.01	0.35
mmu-miR-92a-3p	32,326	6.10	80,733	15,17	0.40	38,591	7.41	93,747	17.45	0.42
mmu-miR-92b-3p	493	0.09	190	0,04	2.60	111	0.02	259	0.05	0.44
mmu-miR-92b-5p	463	0.09	76	0,01	6.11	81	0.02	63	0.01	1.33
mmu-miR-93-5p	1,924	0.36	1,857	0,35	1.04	4,921	0.95	1,798	0.33	2.82
mmu-miR-9-5p	13	0.00	993	0,19	0.01	7	0.00	1,446	0.27	0.00
mmu-miR-98-3p						29	0.01	27	0.01	1.11
mmu-miR-98-5p	2,581	0.49	3,625	0.68	0.71	2,699	0.52	2,793	0.52	1.00
mmu-miR-99a-3p	495	0.09	64	0.01	7.76	169	0.03	33	0.01	5.29
mmu-miR-99a-5p	795	0.15	134	0.03	5.95	485	0.09	182	0.03	2.75
mmu-miR-99b-3p	1,273	0.24	797	0.15	1.60	970	0.19	460	0.09	2.18
mmu-miR-99b-5p	7,750	1.46	8,455	1.59	0.92	9,927	1.91	10,472	1.95	0.98

Tab. 10.3: Alignment of RT-PCR products with mRNA sequences of potential human target genes; cDNA from RNA derived from proliferating hPCLs; top rows: sequenced products; bottom rows: sequence of mRNA transcripts;

<table>
<tr><th>Potential Target</th><th>Sequence used for BLAST</th><th>Alignment</th></tr>
<tr><td>E2F1</td><td>NM_005225</td><td>GCCTGGGTGATTTATTTATTGGGAAAGTGAGGGAGG
||||||||||||||||||||||||||||||||||||
GCCTGGGTGATTTATTTATTGGGAAAGTGAGGGAGG</td></tr>
<tr><td>CD2AP</td><td>NM_012120</td><td>AGGCTGGTGGAGTGGAACCCTGAATAACAAGTTGGGACTGTTTCCCTCAAA
|||||||||||||||||||||||||||||||||||||||||||||||||||
AGGCTGGTGGAGTGGAACCCTGAATAACAAGTTGGGACTGTTTCCCTCAAA</td></tr>
<tr><td>FYN</td><td>NM_002037</td><td>CCGCGACAGAGCCCCAGTACCAACCTGGTGAAAACCTGTAAGGCC
|||||||||||||||||||||||||||||||||||||||||||||
CCGCGACAGAGCCCCAGTACCAACCTGGTGAAAACCTGTAAGGCC</td></tr>
<tr><td>NCK2</td><td>NM_003581</td><td>GGCCGAGCGGGAGGATGAGTTGTCCCTGGTGA
||||||||||||||||||||||||||||||||
GGCCGAGCGGGAGGATGAGTTGTCCCTGGTGA</td></tr>
<tr><td>NEPH1</td><td>NM_018240</td><td>GGGATAGCCTGGCCAGTCCCTCTGTT
||||||||||||||||||||||||||
GGGATAGCCTGGCCAGTCCCTCTGTT</td></tr>
</table>

Tab. 10.4: Alignment of RT-PCR products with mRNA sequences of potential murine target genes; cDNA from RNA derived from proliferating hPCLs; top rows: sequenced products; bottom rows: sequence of mRNAs;

<table>
<tr><th>Potential target gene</th><th>Sequence used for alignment</th><th>Alignment</th></tr>
<tr><td>E2f1</td><td>NM_007891</td><td>GGGGTTTGGTTGCTGCCACATTGAGCAGACCAAAATGGGAAGGATGTTG
|||||||||||||||||||||||||||||||||||||||||||||||||
GGGGTTTGGTTGCTGCCACATTGAGCAGACCAAAATGGGAAGGATGTTG</td></tr>
<tr><td>Cd2ap</td><td>NM_009847</td><td>ACCGTTGCCATCTCCGGGGAATGGGAGTGAACCTGCTCCCGGATCAGTTGCACA
||||||||||||||||||||||||||||||||||||||||||||||||||||||
ACCGTTGCCATCTCCGGGGAATGGGAGTGAACCTGCTCCCGGATCAGTTGCACA</td></tr>
<tr><td>Fyn</td><td>NM_008054</td><td>AGATTGCTGACTTTGGATTGGCTCGGTTGATTGAAGA
|||||||||||||||||||||||||||||||||||||
AGATTGCTGACTTTGGATTGGCTCGGTTGATTGAAGA</td></tr>
<tr><td>Nck2</td><td>NM_010879</td><td>AATTTTTCCAGTCACCTCTTGTAACTGCGTGCCAAA
||||||||||||||||||||||||||||||||||||
AATTTTTCCAGTCACCTCTTGTAACTGCGTGCCAAA</td></tr>
<tr><td>Neph1</td><td>NM_130867</td><td>AGTAGGTCCCTCCTATGGAAATAAGAGCAGCACTAAGGAGAACTCTGAGAGTCAAGCGCA
||||||||||||||||||||||||||||||||||||||||||||||||||||||||||||
AGTAGGTCCCTCCTATGGAAATAAGAGCAGCACTAAGGAGAACTCTGAGAGTCAAGCGCA

CAGCCATGCGAGGGACAGGAAACAG
|||||||||||||||||||||||||
CAGCCATGCGAGGGACAGGAAACAG</td></tr>
</table>

Tab. 10.5: miRNA expression in Cre⁻ control mice and Cre⁺ Lmx1b knockout mice

	Cre⁻ Control mice			Cre⁺ Lmx1b-KO mice						
miRNA	**total RNA valid reads: 16,483,415**	**‰ reads**	**small RNAs valid reads: 26,499,566**	**‰ reads**	**total RNA valid reads: 14,350,712**	**‰ reads**	**small RNAs valid reads: 28,671,121**	**‰ reads**	total RNA Libs: KO/Ctrl	small RNA Libs: KO/Ctrl
mmu-let-7a	329,353	19.98	433,901	16.37	441,238	30.75	389,478	13.58	1.54	0.83
mmu-let-7a, mmu-let-7b, mmu-let-7c	258	0.02	1,184	0.04	132	0.01	1,017	0.04	0.59	0.79
mmu-let-7a, mmu-let-7c	5,017	0.30	17,355	0.65	7,060	0.49	15,450	0.54	1.62	0.82
mmu-let-7a-1*, mmu-let-7c-2*	188	0.01	2,919	0.11	151	0.01	3,450	0.12	0.92	1.09
mmu-let-7b	119,980	7.28	244,374	9.22	186,472	12.99	282,348	9.85	1.79	1.07
mmu-let-7b*	186	0.01	756	0.03	183	0.01	1,687	0.06	1.13	2.06
mmu-let-7c	208,655	12.66	455,783	17.20	269,706	18.79	459,478	16.03	1.48	0.93
mmu-let-7c-1*			68	0.00			58	0.00		0.79
mmu-let-7d	14,510	0.88	38,195	1.44	18,300	1.28	34,004	1.19	1.45	0.82
mmu-let-7d*	6,464	0.39	46,553	1.76	8,808	0.61	76,591	2.67	1.57	1.52
mmu-let-7e	26,693	1.62	47,002	1.77	31,713	2.21	61,650	2.15	1.36	1.21
mmu-let-7e*	56	0.00	668	0.03	140	0.01	909	0.03	2.87	1.26
mmu-let-7f	215,092	13.05	648,555	24.47	184,519	12.86	506,785	17.68	0.99	0.72
mmu-let-7f-1*	19	0.00	251	0.01	47	0.00	338	0.01	2.84	1.24
mmu-let-7f-2*	3	0.00	366	0.01			441	0.02		1.11
mmu-let-7g	71,068	4.31	55,398	2.09	58,877	4.10	43,651	1.52	0.95	0.73
mmu-let-7g*			7	0.00			28	0.00		3.70
mmu-let-7g, mmu-let-7i	25	0.00	73	0.00	1	0.00	94	0.00	0.05	1.19
mmu-let-7g, mmu-miR-3962			4	0.00			5	0.00		1.16
mmu-let-7i	19,561	1.19	37,221	1.40	11,737	0.82	31,591	1.10	0.69	0.78
mmu-let-7i*	1	0.00	168	0.01	55	0.00	196	0.01	63.17	1.08
mmu-miR-100	3,533	0.21	5,317	0.20	2,400	0.17	6,783	0.24	0.78	1.18
mmu-miR-101a	243	0.01	1,600	0.06	120	0.01	1,162	0.04	0.57	0.67
mmu-miR-101a*	16	0.00	52	0.00	1	0.00	25	0.00	0.07	0.44
mmu-miR-101a, mmu-miR-101b			16	0.00			21	0.00		1.21
mmu-miR-101a, mmu-miR-101c	8,017	0.49	25,259	0.95	5,140	0.36	22,057	0.77	0.74	0.81
mmu-miR-101b	732	0.04	2,170	0.08	443	0.03	1,660	0.06	0.70	0.71
mmu-miR-101c	8,937	0.54	30,826	1.16	6,986	0.49	28,324	0.99	0.90	0.85
mmu-miR-103	2,572	0.16	5,316	0.20	1,471	0.10	4,637	0.16	0.66	0.81
mmu-miR-103, mmu-miR-107	188	0.01	733	0.03	388	0.03	424	0.01	2.37	0.53
mmu-miR-106b	200	0.01	299	0.01	219	0.02	574	0.02	1.26	1.77
mmu-miR-106b*	125	0.01	777	0.03	63	0.00	536	0.02	0.58	0.64
mmu-miR-107	167	0.01	264	0.01			62	0.00		0.22
mmu-miR-107*							16	0.00		
mmu-miR-10a	1,298,399	78.77	4,658,335	175.79	1,130,198	78.76	4,824,356	168.27	1.00	0.96

miRNA	Cre⁻ Control mice				Cre⁺ Lmx1b-KO mice					
	total RNA valid reads: 16,483,415	‰ reads	small RNAs valid reads: 26,499,566	‰ reads	total RNA valid reads: 14,350,712	‰ reads	small RNAs valid reads: 28,671,121	‰ reads	total RNA Libs: KO/Ctrl	small RNA Libs: KO/Ctrl
mmu-miR-10a*	121	0.01	1,001	0.04	210	0.01	705	0.02	1.99	0.65
mmu-miR-10b	798,042	48.41	4,025,869	151.92	835,609	58.23	5,176,028	180.53	1.20	1.19
mmu-miR-10b*			202	0.01	71	0.00	251	0.01		1.15
mmu-miR-1186b			15	0.00						
mmu-miR-1187	24	0.00	18	0.00						
mmu-miR-1191	10	0.00								
mmu-miR-1193-3p			80	0.00			86	0.00		0.99
mmu-miR-1194	21	0.00					1	0.00		
mmu-miR-1195	51	0.00	340	0.01	17	0.00	246	0.01	0.38	0.67
mmu-miR-1196	12	0.00	70	0.00	1	0.00	55	0.00	0.10	0.73
mmu-miR-1198-5p	369	0.02	1,487	0.06	290	0.02	1,176	0.04	0.90	0.73
mmu-miR-1199			9	0.00						
mmu-miR-122					22	0.00				
mmu-miR-1247			16	0.00			29	0.00		1.68
mmu-miR-1249	183	0.01	50	0.00	99	0.01	121	0.00	0.62	2.24
mmu-miR-125a-3p	66	0.00	203	0.01	19	0.00	158	0.01	0.33	0.72
mmu-miR-125a-5p	35,991	2.18	132,335	4.99	52,410	3.65	230,763	8.05	1.67	1.61
mmu-miR-125b-1-3p			61	0.00						
mmu-miR-125b-2-3p	49	0.00	134	0.01			202	0.01		1.39
mmu-miR-125b-5p	4,339	0.26	16,172	0.61	4,784	0.33	20,684	0.72	1.27	1.18
mmu-miR-126-3p	20,417	1.24	249,701	9.42	28,995	2.02	214,712	7.49	1.63	0.79
mmu-miR-126-5p	33,115	2.01	509,117	19.21	47,552	3.31	467,650	16.31	1.65	0.85
mmu-miR-127	682,210	41.39	734,753	27.73	505,247	35.21	687,951	23.99	0.85	0.87
mmu-miR-127*			6	0.00	34	0.00	37	0.00		5.70
mmu-miR-128	93	0.01	391	0.01	149	0.01	320	0.01	1.84	0.76
mmu-miR-128-1*	19	0.00					24	0.00		
mmu-miR-129-1-3p			58	0.00			59	0.00		0.94
mmu-miR-129-2-3p			6	0.00						
mmu-miR-129-5p	40	0.00	162	0.01	63	0.00	108	0.00	1.81	0.62
mmu-miR-1306-3p			13	0.00			36	0.00		2.56
mmu-miR-1306-5p	7	0.00	29	0.00			17	0.00		0.54
mmu-miR-130a	1,090	0.07	16,617	0.63	1,136	0.08	14,878	0.52	1.20	0.83
mmu-miR-130a*			36	0.00			61	0.00		1.57
mmu-miR-130b	19	0.00	106	0.00			122	0.00		1.06
mmu-miR-130b*	18	0.00	253	0.01	48	0.00	144	0.01	3.06	0.53
mmu-miR-132	239	0.01	1,767	0.07	601	0.04	1,157	0.04	2.89	0.61
mmu-miR-132*	25	0.00	44	0.00			251	0.01		5.27
mmu-miR-133a	71	0.00	173	0.01	62	0.00	289	0.01	1.00	1.54
mmu-miR-133a, mmu-miR-133b			74	0.00			80	0.00		1.00
mmu-miR-134	158	0.01	212	0.01	132	0.01	311	0.01	0.96	1.36

miRNA	Cre⁻ Control mice				Cre⁺ Lmx1b-KO mice					
	total RNA valid reads: 16,483,415	‰ reads	small RNAs valid reads: 26,499,566	‰ reads	total RNA valid reads: 14,350,712	‰ reads	small RNAs valid reads: 28,671,121	‰ reads	total RNA Libs: KO/Ctrl	small RNA Libs: KO/Ctrl
mmu-miR-134*			37	0.00			8	0.00		0.20
mmu-miR-135a			4	0.00			30	0.00		6.93
mmu-miR-136	19	0.00	128	0.00			129	0.00		0.93
mmu-miR-136*	44	0.00	999	0.04			854	0.03		0.79
mmu-miR-138			11	0.00						
mmu-miR-139-3p	284	0.02	2,115	0.08	201	0.01	3,445	0.12	0.81	1.51
mmu-miR-139-5p	1,133	0.07	4,861	0.18	1,119	0.08	5,476	0.19	1.13	1.04
mmu-miR-140	41	0.00	294	0.01			120	0.00		0.38
mmu-miR-140*	1,590	0.10	4,727	0.18	1,586	0.11	5,200	0.18	1.15	1.02
mmu-miR-141	48	0.00	427	0.02	60	0.00	244	0.01	1.44	0.53
mmu-miR-142-3p	25	0.00	210	0.01	40	0.00	58	0.00	1.84	0.26
mmu-miR-142-5p	218	0.01	2,560	0.10	120	0.01	2,201	0.08	0.63	0.79
mmu-miR-143	1,118,613	67.86	3,587,001	135.36	790,543	55.09	3,526,839	123.01	0.81	0.91
mmu-miR-143*	33	0.00	209	0.01			402	0.01		1.78
mmu-miR-144	38	0.00	113	0.00	64	0.00	94	0.00	1.93	0.77
mmu-miR-144*			14	0.00						
mmu-miR-145	33,375	2.02	54,323	2.05	40,392	2.81	72,925	2.54	1.39	1.24
mmu-miR-145*	2,395	0.15	19,001	0.72	3,985	0.28	19,144	0.67	1.91	0.93
mmu-miR-146a	943	0.06	64,991	2.45	2,730	0.19	60,210	2.10	3.33	0.86
mmu-miR-146a, mmu-miR-146b	10	0.00	969	0.04	61	0.00	992	0.03	7.01	0.95
mmu-miR-146b	2,470	0.15	14,684	0.55	3,706	0.26	24,201	0.84	1.72	1.52
mmu-miR-148a	2,195	0.13	7,367	0.28	2,169	0.15	8,889	0.31	1.14	1.12
mmu-miR-148a*	40	0.00	45	0.00			116	0.00		2.38
mmu-miR-148b	1,885	0.11	2,436	0.09	1,276	0.09	1,903	0.07	0.78	0.72
mmu-miR-148b*			30	0.00						
mmu-miR-149	544	0.03	803	0.03	533	0.04	843	0.03	1.13	0.97
mmu-miR-150	4,816	0.29	12,200	0.46	5,961	0.42	15,033	0.52	1.42	1.14
mmu-miR-150*			9	0.00						
mmu-miR-151-3p	6,062	0.37	74,465	2.81	9,818	0.68	84,051	2.93	1.86	1.04
mmu-miR-151-5p	7,367	0.45	50,645	1.91	12,516	0.87	47,985	1.67	1.95	0.88
mmu-miR-152	3,475	0.21	14,563	0.55	4,361	0.30	10,714	0.37	1.44	0.68
mmu-miR-152*	259	0.02	920	0.03	279	0.02	1,809	0.06	1.24	1.82
mmu-miR-154	13	0.00	3	0.00						
mmu-miR-154*			15	0.00						
mmu-miR-155	9	0.00	27	0.00			39	0.00		1.34
mmu-miR-15a	559	0.03	2,827	0.11	927	0.06	2,666	0.09	1.90	0.87
mmu-miR-15b	705	0.04	1,663	0.06	542	0.04	900	0.03	0.88	0.50
mmu-miR-15b*	15	0.00	142	0.01	116	0.01			8.88	
mmu-miR-16	10,542	0.64	44,092	1.66	9,699	0.68	34,326	1.20	1.06	0.72
mmu-miR-16-1*			21	0.00			12	0.00		0.53

miRNA	Cre⁻ Control mice				Cre⁺ Lmx1b-KO mice					
	total RNA valid reads: 16,483,415	‰ reads	small RNAs valid reads: 26,499,566	‰ reads	total RNA valid reads: 14,350,712	‰ reads	small RNAs valid reads: 28,671,121	‰ reads	total RNA Libs: KO/Ctrl	small RNA Libs: KO/Ctrl
mmu-miR-16-2*			58	0.00						
mmu-miR-17	101	0.01	95	0.00	69	0.00	138	0.00	0.78	1.34
mmu-miR-17*	19	0.00	95	0.00			66	0.00		0.64
mmu-miR-181a	19,149	1.16	87,386	3.30	21,917	1.53	74,755	2.61	1.31	0.79
mmu-miR-181a-1*	165	0.01	453	0.02	188	0.01	371	0.01	1.31	0.76
mmu-miR-181a-2*			51	0.00			88	0.00		1.59
mmu-miR-181b	1,394	0.08	4,468	0.17	1,206	0.08	4,341	0.15	0.99	0.90
mmu-miR-181b-1*			9	0.00	67	0.00	31	0.00		3.18
mmu-miR-181c	695	0.04	4,213	0.16	664	0.05	4,316	0.15	1.10	0.95
mmu-miR-181c*	32	0.00	83	0.00	97	0.01	162	0.01	3.48	1.80
mmu-miR-181d	264	0.02	614	0.02	122	0.01	687	0.02	0.53	1.03
mmu-miR-182	380	0.02	1,913	0.07	504	0.04	1,724	0.06	1.52	0.83
mmu-miR-183	865	0.05	901	0.03	352	0.02	703	0.02	0.47	0.72
mmu-miR-1839-3p	31	0.00	7	0.00			31	0.00		4.09
mmu-miR-1839-5p	733	0.04	1,423	0.05	246	0.02	708	0.02	0.39	0.46
mmu-miR-184			123	0.00	98	0.01	400	0.01		3.01
mmu-miR-1843-3p	91	0.01	497	0.02	62	0.00	516	0.02	0.78	0.96
mmu-miR-1843-5p	80	0.00	392	0.01	56	0.00	269	0.01	0.80	0.63
mmu-miR-1843-5p, mmu-miR-1843b-5p	116	0.01	347	0.01			254	0.01		0.68
mmu-miR-1843b-3p	31	0.00	228	0.01	144	0.01	216	0.01	5.34	0.88
mmu-miR-1843b-5p	43	0.00	153	0.01			14	0.00		0.08
mmu-miR-185	356	0.02	659	0.02	362	0.03	806	0.03	1.17	1.13
mmu-miR-185*	13	0.00	36	0.00			71	0.00		1.82
mmu-miR-186	177	0.01	3,054	0.12	384	0.03	3,037	0.11	2.49	0.92
mmu-miR-187	63	0.00	411	0.02			368	0.01		0.83
mmu-miR-187*	36	0.00	90	0.00	50	0.00	57	0.00	1.60	0.59
mmu-miR-188-3p			10	0.00						
mmu-miR-188-5p			24	0.00			13	0.00		0.50
mmu-miR-1892							17	0.00		
mmu-miR-18a			9	0.00	52	0.00				
mmu-miR-190			65	0.00						
mmu-miR-190*			27	0.00						
mmu-miR-190b			11	0.00						
mmu-miR-191	22,076	1.34	107,527	4.06	23,465	1.64	99,680	3.48	1.22	0.86
mmu-miR-191*	39	0.00	180	0.01			233	0.01		1.20
mmu-miR-192	6,431	0.39	22,915	0.86	3,820	0.27	12,763	0.45	0.68	0.51
mmu-miR-193	7	0.00	47	0.00			101	0.00		1.99
mmu-miR-193*	30	0.00	85	0.00	46	0.00	57	0.00	1.76	0.62
mmu-miR-1930			9	0.00						
mmu-miR-1931			15	0.00						
mmu-miR-1933-3p			9	0.00						

miRNA	Cre⁻ Control mice				Cre⁺ Lmx1b-KO mice					
	total RNA valid reads: 16,483,415	‰ reads	small RNAs valid reads: 26,499,566	‰ reads	total RNA valid reads: 14,350,712	‰ reads	small RNAs valid reads: 28,671,121	‰ reads	total RNA Libs: KO/Ctrl	small RNA Libs: KO/Ctrl
mmu-miR-1934*							18	0.00		
mmu-miR-1936	1	0.00								
mmu-miR-193b	62	0.00	123	0.00	151	0.01	77	0.00	2.80	0.58
mmu-miR-193b*			6	0.00			30	0.00		4.62
mmu-miR-194	574	0.03	734	0.03	523	0.04	285	0.01	1.05	0.36
mmu-miR-1940	970	0.06	66	0.00	2,850	0.20	78	0.00	3.37	1.09
mmu-miR-1941-3p							107	0.00		
mmu-miR-1941-5p			31	0.00			73	0.00		2.18
mmu-miR-194-2*			2	0.00			25	0.00		11.55
mmu-miR-1943	398	0.02	1,412	0.05	452	0.03	2,135	0.07	1.30	1.40
mmu-miR-1943*					45	0.00				
mmu-miR-1946a			9	0.00						
mmu-miR-1946a, mmu-miR-1946b	17	0.00								
mmu-miR-1947	18	0.00	16	0.00						
mmu-miR-195*	29	0.00	521	0.02	87	0.01	739	0.03	3.45	1.31
mmu-miR-1951			10	0.00						
mmu-miR-1954			5	0.00						
mmu-miR-1955-5p			33	0.00			34	0.00		0.95
mmu-miR-1964-3p			155	0.01			122	0.00		0.73
mmu-miR-1965			4	0.00						
mmu-miR-1966							32	0.00		
mmu-miR-1968			12	0.00			61	0.00		4.70
mmu-miR-196a	3,394	0.21	7,285	0.27	2,485	0.17	6,778	0.24	0.84	0.86
mmu-miR-196a-1*			9	0.00						
mmu-miR-196a-2*			26	0.00			72	0.00		2.56
mmu-miR-196b	1,014	0.06	2,023	0.08	705	0.05	1,924	0.07	0.80	0.88
mmu-miR-1981	84	0.01	160	0.01			386	0.01		2.23
mmu-miR-1981*	7	0.00	43	0.00	1	0.00	100	0.00	0.16	2.15
mmu-miR-1982.1, mmu-miR-1982.2							29	0.00		
mmu-miR-1983			9	0.00						
mmu-miR-199a-3p, mmu-miR-199b	3,013	0.18	33,618	1.27	4,272	0.30	32,710	1.14	1.63	0.90
mmu-miR-199a-5p	1,540	0.09	3,587	0.14	1,588	0.11	4,693	0.16	1.18	1.21
mmu-miR-199b*			2	0.00	2	0.00	35	0.00		16.17
mmu-miR-19a	56	0.00	128	0.00			359	0.01		2.59
mmu-miR-19b	1,030	0.06	1,261	0.05	232	0.02	3,265	0.11	0.26	2.39
mmu-miR-19b-1*	10	0.00								
mmu-miR-1a	5,606	0.34	5,641	0.21	2,423	0.17	4,173	0.15	0.50	0.68
mmu-miR-1b-3p	13	0.00								
mmu-miR-200a	598	0.04	4,188	0.16	93	0.01	1,449	0.05	0.18	0.32
mmu-miR-200a*	140	0.01	167	0.01	46	0.00	111	0.00	0.38	0.61

miRNA	Cre⁻ Control mice				Cre⁺ Lmx1b-KO mice					
	total RNA valid reads: 16,483,415	‰ reads	small RNAs valid reads: 26,499,566	‰ reads	total RNA valid reads: 14,350,712	‰ reads	small RNAs valid reads: 28,671,121	‰ reads	total RNA Libs: KO/Ctrl	small RNA Libs: KO/Ctrl
mmu-miR-200b	770	0.05	6,601	0.25	176	0.01	2,683	0.09	0.26	0.38
mmu-miR-200b*	22	0.00	200	0.01			1	0.00		0.00
mmu-miR-200c	246	0.01	707	0.03			256	0.01		0.33
mmu-miR-203	774	0.05	658	0.02	161	0.01	350	0.01	0.24	0.49
mmu-miR-203*					54	0.00				
mmu-miR-204	3,485	0.21	10,290	0.39	2,999	0.21	10,315	0.36	0.99	0.93
mmu-miR-204*			26	0.00						
mmu-miR-205	15	0.00	31	0.00						
mmu-miR-20a	85	0.01	205	0.01	88	0.01	185	0.01	1.19	0.83
mmu-miR-20a*			18	0.00	41	0.00	17	0.00		0.87
mmu-miR-20b			1	0.00						
mmu-miR-21	4,576	0.28	12,458	0.47	2,806	0.20	10,455	0.36	0.70	0.78
mmu-miR-21*			26	0.00						
mmu-miR-210	50	0.00	116	0.00	73	0.01	169	0.01	1.68	1.35
mmu-miR-210*	20	0.00	23	0.00						
mmu-miR-211			8	0.00			2	0.00		0.23
mmu-miR-212-3p	81	0.00	87	0.00			45	0.00		0.48
mmu-miR-212-5p	128	0.01	980	0.04	231	0.02	791	0.03	2.07	0.75
mmu-miR-2137	14	0.00					1	0.00		
mmu-miR-214	522	0.03	1,502	0.06	641	0.04	1,140	0.04	1.41	0.70
mmu-miR-214*	47	0.00	78	0.00			74	0.00		0.88
mmu-miR-215			18	0.00			31	0.00		1.59
mmu-miR-216b			14	0.00						
mmu-miR-218			143	0.01						
mmu-miR-218-1*			12	0.00						
mmu-miR-219-3p*	20	0.00	142	0.01	34	0.00	188	0.01	1.95	1.22
mmu-miR-22	10,888	0.66	100,511	3.79	14,540	1.01	118,201	4.12	1.53	1.09
mmu-miR-22*	36	0.00	4	0.00	76	0.01	30	0.00	2.42	6.93
mmu-miR-221	144	0.01	884	0.03	260	0.02	843	0.03	2.07	0.88
mmu-miR-221*	28	0.00	131	0.00			284	0.01		2.00
mmu-miR-222	216	0.01	1,811	0.07	190	0.01	2,579	0.09	1.01	1.32
mmu-miR-222*	14	0.00	44	0.00	63	0.00	34	0.00	5.17	0.71
mmu-miR-223	104	0.01	744	0.03	150	0.01	730	0.03	1.66	0.91
mmu-miR-223*	7	0.00					41	0.00		
mmu-miR-224	50	0.00	604	0.02	141	0.01	621	0.02	3.24	0.95
mmu-miR-224*			14	0.00						
mmu-miR-23a	8,656	0.53	45,003	1.70	15,906	1.11	41,650	1.45	2.11	0.86
mmu-miR-23a*			10	0.00			57	0.00		5.27
mmu-miR-23b	23,909	1.45	98,629	3.72	53,022	3.69	97,985	3.42	2.55	0.92
mmu-miR-23b*	33	0.00	172	0.01			188	0.01		1.01
mmu-miR-23b, mmu-miR-23a	127	0.01	1,336	0.05	295	0.02	1,185	0.04	2.67	0.82

miRNA	Cre⁻ Control mice				Cre⁺ Lmx1b-KO mice				total RNA Libs: KO/Ctrl	small RNA Libs: KO/Ctrl
	total RNA valid reads: 16,483,415	‰ reads	small RNAs valid reads: 26,499,566	‰ reads	total RNA valid reads: 14,350,712	‰ reads	small RNAs valid reads: 28,671,121	‰ reads		
mmu-miR-24	20,211	1.23	107,157	4.04	25,634	1.79	128,607	4.49	1.46	1.11
mmu-miR-24-1*	69	0.00	134	0.01	50	0.00	253	0.01	0.83	1.75
mmu-miR-24-2*	477	0.03	2,360	0.09	734	0.05	2,739	0.10	1.77	1.07
mmu-miR-25	2,583	0.16	6,169	0.23	2,396	0.17	4,723	0.16	1.07	0.71
mmu-miR-25*	16	0.00	104	0.00			190	0.01		1.69
mmu-miR-26a	82,760	5.02	455,141	17.18	87,123	6.07	411,157	14.34	1.21	0.83
mmu-miR-26a-1*			81	0.00	49	0.00	29	0.00		0.33
mmu-miR-26a-2*	30	0.00	42	0.00	64	0.00	54	0.00	2.45	1.19
mmu-miR-26b	12,616	0.77	21,918	0.83	7,496	0.52	14,103	0.49	0.68	0.59
mmu-miR-26b*	386	0.02	1,648	0.06	537	0.04	1,132	0.04	1.60	0.63
mmu-miR-27a	9,463	0.57	43,317	1.63	19,336	1.35	50,733	1.77	2.35	1.08
mmu-miR-27a*	42	0.00	168	0.01	44	0.00	227	0.01	1.20	1.25
mmu-miR-27b	102,065	6.19	358,974	13.55	136,149	9.49	340,264	11.87	1.53	0.88
mmu-miR-27b*	144	0.01	696	0.03	318	0.02	874	0.03	2.54	1.16
mmu-miR-27b, mmu-miR-27a	605	0.04	7,214	0.27	748	0.05	8,897	0.31	1.42	1.14
mmu-miR-28	99	0.01	367	0.01	1	0.00	199	0.01	0.01	0.50
mmu-miR-28*	729	0.04	979	0.04	784	0.05	1,301	0.05	1.24	1.23
mmu-miR-28, mmu-miR-28c	363	0.02	2,036	0.08	583	0.04	1,823	0.06	1.84	0.83
mmu-miR-28c	35	0.00	120	0.00	2	0.00	132	0.00	0.07	1.02
mmu-miR-296-3p	24	0.00	49	0.00			35	0.00		0.66
mmu-miR-296-5p			18	0.00						
mmu-miR-297b-5p			14	0.00						
mmu-miR-298			30	0.00			152	0.01		4.68
mmu-miR-299	60	0.00	47	0.00	135	0.01	132	0.00	2.58	2.60
mmu-miR-299*	22	0.00	44	0.00			163	0.01		3.42
mmu-miR-29a	4,261	0.26	76,287	2.88	7,795	0.54	78,483	2.74	2.10	0.95
mmu-miR-29a*			32	0.00			35	0.00		1.01
mmu-miR-29b	678	0.04	5,900	0.22	1,341	0.09	5,437	0.19	2.27	0.85
mmu-miR-29b, mmu-miR-29c	35	0.00	20	0.00			49	0.00		2.26
mmu-miR-29b-1*	16	0.00	7	0.00						
mmu-miR-29b-2*			11	0.00			29	0.00		2.44
mmu-miR-29c	653	0.04	15,839	0.60	875	0.06	18,730	0.65	1.54	1.09
mmu-miR-29c*	14	0.00			17	0.00	22	0.00	1.39	
mmu-miR-300	38	0.00	140	0.01	59	0.00	275	0.01	1.78	1.82
mmu-miR-301a	59	0.00	374	0.01	49	0.00	398	0.01	0.95	0.98
mmu-miR-301a*			27	0.00			31	0.00		1.06
mmu-miR-3057-5p	61	0.00	120	0.00	72	0.01	35	0.00	1.36	0.27
mmu-miR-3058	22	0.00	4	0.00						
mmu-miR-3062	5	0.00								
mmu-miR-3064-3p	4	0.00	2	0.00						

miRNA	Cre⁻ Control mice				Cre⁺ Lmx1b-KO mice					
	total RNA valid reads: 16,483,415	‰ reads	small RNAs valid reads: 26,499,566	‰ reads	total RNA valid reads: 14,350,712	‰ reads	small RNAs valid reads: 28,671,121	‰ reads	total RNA Libs: KO/Ctrl	small RNA Libs: KO/Ctrl
mmu-miR-3064-5p	10	0.00	12	0.00			68	0.00		5.24
mmu-miR-3068	62	0.00	325	0.01	213	0.01	451	0.02	3.95	1.28
mmu-miR-3068*			9	0.00			1	0.00		0.10
mmu-miR-3076-3p							46	0.00		
mmu-miR-3081			27	0.00			62	0.00		2.12
mmu-miR-3082-3p	13	0.00	25	0.00						
mmu-miR-3083*			4	0.00						
mmu-miR-3086-5p			73	0.00			122	0.00		1.54
mmu-miR-3087			12	0.00						
mmu-miR-3087*			21	0.00						
mmu-miR-3096-5p	75	0.00	16	0.00	82	0.01	38	0.00	1.26	2.20
mmu-miR-3096-5p, mmu-miR-3096b-5p	17,864	1.08	31	0.00	11,032	0.77	147	0.01	0.71	4.38
mmu-miR-3096b-5p	24,957	1.51	12	0.00	17,012	1.19	162	0.01	0.78	12.48
mmu-miR-30a	363,847	22.07	531,009	20.04	394,925	27.52	562,411	19.62	1.25	0.98
mmu-miR-30a*	4,854	0.29	25,426	0.96	5,633	0.39	18,234	0.64	1.33	0.66
mmu-miR-30a*, mmu-miR-30e*	1	0.00	44	0.00	1	0.00	2	0.00	1.15	0.04
mmu-miR-30b	2,976	0.18	25,477	0.96	3,689	0.26	15,255	0.53	1.42	0.55
mmu-miR-30b*	86	0.01	346	0.01	61	0.00	538	0.02	0.81	1.44
mmu-miR-30b, mmu-miR-30c	65	0.00	101	0.00			60	0.00		0.55
mmu-miR-30c	10,702	0.65	98,037	3.70	14,256	0.99	94,186	3.29	1.53	0.89
mmu-miR-30c-1*	26	0.00	117	0.00	58	0.00	161	0.01	2.56	1.27
mmu-miR-30c-2*	1,148	0.07	10,142	0.38	1,039	0.07	12,185	0.42	1.04	1.11
mmu-miR-30d	170,860	10.37	345,010	13.02	206,643	14.40	318,133	11.10	1.39	0.85
mmu-miR-30d*			443	0.02			260	0.01		0.54
mmu-miR-30e	17,728	1.08	37,934	1.43	14,258	0.99	34,504	1.20	0.92	0.84
mmu-miR-30e*	622	0.04	3,779	0.14	554	0.04	1,596	0.06	1.02	0.39
mmu-miR-31	22	0.00	58	0.00						
mmu-miR-3102	1,074	0.07	735	0.03	1,450	0.10	817	0.03	1.55	1.03
mmu-miR-3102-3p.2	14	0.00	78	0.00	95	0.01	204	0.01	7.79	2.42
mmu-miR-3102-5p.2			30	0.00			112	0.00		3.45
mmu-miR-3103			7	0.00						
mmu-miR-3105-3p	72	0.00	38	0.00						
mmu-miR-3109			15	0.00						
mmu-miR-3110							30	0.00		
mmu-miR-3112			17	0.00						
mmu-miR-3112*			18	0.00						
mmu-miR-32	48	0.00	237	0.01			95	0.00		0.37
mmu-miR-320	1,830	0.11	2,338	0.09	1,864	0.13	2,436	0.08	1.17	0.96
mmu-miR-322	770	0.05	3,753	0.14	1,011	0.07	3,444	0.12	1.51	0.85
mmu-miR-322*	10,212	0.62	41,696	1.57	13,678	0.95	38,682	1.35	1.54	0.86

miRNA	Cre⁻ Control mice				Cre⁺ Lmx1b-KO mice					
	total RNA valid reads: 16,483,415	‰ reads	small RNAs valid reads: 26,499,566	‰ reads	total RNA valid reads: 14,350,712	‰ reads	small RNAs valid reads: 28,671,121	‰ reads	total RNA Libs: KO/Ctrl	small RNA Libs: KO/Ctrl
mmu-miR-323-3p	11	0.00	26	0.00			28	0.00		1.00
mmu-miR-324-3p			84	0.00						
mmu-miR-324-5p	21	0.00	37	0.00			299	0.01		7.47
mmu-miR-326	79	0.00	485	0.02	280	0.02	592	0.02	4.07	1.13
mmu-miR-328	1,364	0.08	8,577	0.32	1,870	0.13	10,431	0.36	1.57	1.12
mmu-miR-328*			3	0.00						
mmu-miR-329			62	0.00	47	0.00	149	0.01		2.22
mmu-miR-329*			13	0.00	50	0.00	37	0.00		2.63
mmu-miR-33			26	0.00			93	0.00		3.31
mmu-miR-330			139	0.01			116	0.00		0.77
mmu-miR-330*	15	0.00	96	0.00			42	0.00		0.40
mmu-miR-331-3p	101	0.01	156	0.01	357	0.02	139	0.00	4.06	0.82
mmu-miR-331-5p			13	0.00						
mmu-miR-335-3p	774	0.05	1,953	0.07	798	0.06	1,583	0.06	1.18	0.75
mmu-miR-335-5p	488	0.03	2,581	0.10	689	0.05	1,365	0.05	1.62	0.49
mmu-miR-337-3p			11	0.00						
mmu-miR-338-3p	51	0.00	722	0.03	57	0.00	957	0.03	1.28	1.23
mmu-miR-338-5p	40	0.00	285	0.01	132	0.01	206	0.01	3.79	0.67
mmu-miR-339-3p			109	0.00			78	0.00		0.66
mmu-miR-339-5p	42	0.00	246	0.01	73	0.01	139	0.00	2.00	0.52
mmu-miR-340-3p			115	0.00	55	0.00	80	0.00		0.64
mmu-miR-340-5p	468	0.03	679	0.03	58	0.00	534	0.02	0.14	0.73
mmu-miR-341			12	0.00			33	0.00		2.54
mmu-miR-342-3p	3,570	0.22	2,786	0.11	1,785	0.12	2,153	0.08	0.57	0.71
mmu-miR-342-5p	21	0.00	43	0.00			63	0.00		1.35
mmu-miR-345-3p							28	0.00		
mmu-miR-345-5p	13	0.00	61	0.00	78	0.01	57	0.00	6.89	0.86
mmu-miR-3470a	156	0.01	95	0.00	5	0.00	125	0.00	0.04	1.22
mmu-miR-3470a, mmu-miR-3470b	6	0.00					29	0.00		
mmu-miR-3470b	514	0.03	402	0.02	124	0.01	410	0.01	0.28	0.94
mmu-miR-3471			40	0.00						
mmu-miR-3473	1	0.00	13	0.00	57	0.00	15	0.00	65.47	1.07
mmu-miR-3473, mmu-miR-3473b	30	0.00								
mmu-miR-3473b	389	0.02	3,364	0.13	773	0.05	5,481	0.19	2.28	1.51
mmu-miR-3474			32	0.00	42	0.00				
mmu-miR-3475			11	0.00						
mmu-miR-34a	103	0.01	169	0.01	91	0.01	179	0.01	1.01	0.98
mmu-miR-34a*	10	0.00	2	0.00			8	0.00		3.70
mmu-miR-34b-3p	104	0.01	125	0.00			189	0.01		1.40
mmu-miR-34b-5p			54	0.00			36	0.00		0.62

miRNA	Cre⁻ Control mice				Cre⁺ Lmx1b-KO mice					
	total RNA valid reads: 16,483,415	‰ reads	small RNAs valid reads: 26,499,566	‰ reads	total RNA valid reads: 14,350,712	‰ reads	small RNAs valid reads: 28,671,121	‰ reads	total RNA Libs: KO/Ctrl	small RNA Libs: KO/Ctrl
mmu-miR-34c	136	0.01	951	0.04	350	0.02	976	0.03	2.96	0.95
mmu-miR-34c*	23	0.00	14	0.00			74	0.00		4.89
mmu-miR-350	89	0.01	48	0.00	28	0.00	33	0.00	0.36	0.64
mmu-miR-350*	14	0.00					100	0.00		
mmu-miR-351	21,676	1.32	38,131	1.44	16,224	1.13	39,112	1.36	0.86	0.95
mmu-miR-351*	103	0.01	865	0.03	102	0.01	1,423	0.05	1.14	1.52
mmu-miR-3572							10	0.00		
mmu-miR-361	101	0.01	1,566	0.06	172	0.01	1,181	0.04	1.96	0.70
mmu-miR-361*	39	0.00	209	0.01	21	0.00	234	0.01	0.62	1.03
mmu-miR-362-3p			24	0.00						
mmu-miR-362-5p	6	0.00	25	0.00			115	0.00		4.25
mmu-miR-363-3p	19	0.00	15	0.00			30	0.00		1.85
mmu-miR-363-5p			6	0.00						
mmu-miR-365	1,294	0.08	4,168	0.16	1,500	0.10	4,795	0.17	1.33	1.06
mmu-miR-365-2*	22	0.00	43	0.00			64	0.00		1.38
mmu-miR-369-3p			15	0.00	60	0.00				
mmu-miR-369-5p			33	0.00			21	0.00		0.59
mmu-miR-370	1	0.00	46	0.00	55	0.00	33	0.00	63.17	0.66
mmu-miR-374	129	0.01	780	0.03	172	0.01	876	0.03	1.53	1.04
mmu-miR-374, mmu-miR-374c	96	0.01	403	0.02	115	0.01	563	0.02	1.38	1.29
mmu-miR-374c			14	0.00	1	0.00	2	0.00		0.13
mmu-miR-375	105	0.01	1,603	0.06	166	0.01	1,017	0.04	1.82	0.59
mmu-miR-376a			20	0.00	51	0.00	92	0.00		4.25
mmu-miR-376b	15	0.00	62	0.00	67	0.00	85	0.00	5.13	1.27
mmu-miR-376b*			45	0.00			92	0.00		1.89
mmu-miR-376c			15	0.00			68	0.00		4.19
mmu-miR-377	16	0.00	33	0.00	41	0.00	54	0.00	2.94	1.51
mmu-miR-377*	17	0.00								
mmu-miR-378	24,783	1.50	54,879	2.07	10,549	0.74	54,551	1.90	0.49	0.92
mmu-miR-378*	29	0.00	63	0.00	52	0.00	67	0.00	2.06	0.98
mmu-miR-378, mmu-miR-378b	159	0.01	342	0.01	136	0.01	257	0.01	0.98	0.69
mmu-miR-378b	66	0.00	210	0.01	46	0.00	75	0.00	0.80	0.33
mmu-miR-379	2,088	0.13	3,568	0.13	1,471	0.10	3,001	0.10	0.81	0.78
mmu-miR-379*			15	0.00						
mmu-miR-380-3p	42	0.00	199	0.01	67	0.00	204	0.01	1.83	0.95
mmu-miR-380-5p	23	0.00								
mmu-miR-381	45	0.00	74	0.00	245	0.02	71	0.00	6.25	0.89
mmu-miR-382	206	0.01	158	0.01	238	0.02	181	0.01	1.33	1.06
mmu-miR-382*			12	0.00						
mmu-miR-383	14	0.00	50	0.00			111	0.00		2.05

miRNA	Cre⁻ Control mice				Cre⁺ Lmx1b-KO mice					
	total RNA valid reads: 16,483,415	‰ reads	small RNAs valid reads: 26,499,566	‰ reads	total RNA valid reads: 14,350,712	‰ reads	small RNAs valid reads: 28,671,121	‰ reads	total RNA Libs: KO/Ctrl	small RNA Libs: KO/Ctrl
mmu-miR-3960			8	0.00			1	0.00		0.12
mmu-miR-3962	7	0.00	2	0.00	4	0.00	1	0.00	0.66	0.46
mmu-miR-3963	2	0.00	3	0.00			1	0.00		0.31
mmu-miR-409-3p	623	0.04	2,513	0.09	550	0.04	2,330	0.08	1.01	0.86
mmu-miR-409-5p	17	0.00	65	0.00	30	0.00			2.03	
mmu-miR-410			25	0.00			126	0.00		4.66
mmu-miR-411	196	0.01	1,402	0.05	320	0.02	1,121	0.04	1.88	0.74
mmu-miR-411*	35	0.00	241	0.01			57	0.00		0.22
mmu-miR-421	41	0.00	838	0.03			792	0.03		0.87
mmu-miR-423-3p	381	0.02	12,483	0.47	1,140	0.08	17,243	0.60	3.44	1.28
mmu-miR-423-5p	546	0.03	5,282	0.20	1,051	0.07	10,093	0.35	2.21	1.77
mmu-miR-425	51	0.00	740	0.03	73	0.01	735	0.03	1.64	0.92
mmu-miR-425*	77	0.00	794	0.03	59	0.00	755	0.03	0.88	0.88
mmu-miR-429	484	0.03	1,983	0.07	43	0.00	788	0.03	0.10	0.37
mmu-miR-431			8	0.00			33	0.00		3.81
mmu-miR-431*							8	0.00		
mmu-miR-433			144	0.01			171	0.01		1.10
mmu-miR-434-3p	1,369	0.08	2,727	0.10	1,750	0.12	2,653	0.09	1.47	0.90
mmu-miR-434-5p	21	0.00	342	0.01			363	0.01		0.98
mmu-miR-449a			45	0.00	69	0.00	17	0.00		0.35
mmu-miR-450a	262	0.02	2,746	0.10	453	0.03	2,892	0.10	1.99	0.97
mmu-miR-450a-1*			81	0.00	41	0.00	74	0.00		0.84
mmu-miR-450b-3p	35	0.00	102	0.00			82	0.00		0.74
mmu-miR-450b-5p	69	0.00	251	0.01	36	0.00	333	0.01	0.60	1.23
mmu-miR-451	96	0.01	403	0.02			226	0.01		0.52
mmu-miR-455	103	0.01	1,382	0.05	219	0.02	965	0.03	2.44	0.65
mmu-miR-455*	20	0.00	265	0.01	55	0.00	154	0.01	3.16	0.54
mmu-miR-466a-3p, mmu-miR-466b-3p, mmu-miR-466c-3p, mmu-miR-466e-3p, mmu-miR-466p-3p			8	0.00						
mmu-miR-466c-5p			8	0.00						
mmu-miR-466d-3p			18	0.00			14	0.00		0.72
mmu-miR-466h-3p			12	0.00						
mmu-miR-466i-5p	516	0.03	371	0.01	516	0.04	246	0.01	1.15	0.61
mmu-miR-467a			13	0.00			34	0.00		2.42
mmu-miR-467a*, mmu-miR-467d*			13	0.00						
mmu-miR-467c							67	0.00		
mmu-miR-467d							29	0.00		
mmu-miR-470			82	0.00	64	0.00	24	0.00		0.27
mmu-miR-484	2,928	0.18	6,263	0.24	3,709	0.26	8,976	0.31	1.45	1.32

miRNA	Cre⁻ Control mice				Cre⁺ Lmx1b-KO mice					
	total RNA valid reads: 16,483,415	‰ reads	small RNAs valid reads: 26,499,566	‰ reads	total RNA valid reads: 14,350,712	‰ reads	small RNAs valid reads: 28,671,121	‰ reads	total RNA Libs: KO/Ctrl	small RNA Libs: KO/Ctrl
mmu-miR-485			38	0.00	43	0.00	60	0.00		1.46
mmu-miR-485*	14	0.00								
mmu-miR-486*, mmu-miR-3107*			24	0.00			31	0.00		1.19
mmu-miR-486, mmu-miR-3107	135,099	8.20	149,285	5.63	119,531	8.33	143,459	5.00	1.02	0.89
mmu-miR-487b			10	0.00						
mmu-miR-488	44	0.00	310	0.01			101	0.00		0.30
mmu-miR-490-3p			11	0.00						
mmu-miR-493*			4	0.00						
mmu-miR-494	17	0.00	45	0.00			57	0.00		1.17
mmu-miR-495	15	0.00	80	0.00	56	0.00			4.29	
mmu-miR-496			34	0.00			25	0.00		0.68
mmu-miR-497	34	0.00	1,333	0.05			1,662	0.06		1.15
mmu-miR-500			97	0.00			87	0.00		0.83
mmu-miR-501-3p	163	0.01	189	0.01	328	0.02	235	0.01	2.31	1.15
mmu-miR-503	292	0.02	1,305	0.05	84	0.01	1,073	0.04	0.33	0.76
mmu-miR-503*	73	0.00	248	0.01	51	0.00	499	0.02	0.80	1.86
mmu-miR-505-3p	7	0.00					13	0.00		
mmu-miR-505-5p							36	0.00		
mmu-miR-5097			1	0.00						
mmu-miR-5099	12,430	0.75	644	0.02	17,723	1.23	1,267	0.04	1.64	1.82
mmu-miR-5100	17	0.00								
mmu-miR-5101			5	0.00						
mmu-miR-5105	3	0.00	26	0.00	199	0.01	173	0.01	76.19	6.15
mmu-miR-5109	135	0.01	466	0.02	897	0.06	1,927	0.07	7.63	3.82
mmu-miR-5113			18	0.00						
mmu-miR-511-3p	15	0.00								
mmu-miR-5115	7	0.00	23	0.00	5	0.00	7	0.00	0.82	0.28
mmu-miR-511-5p			14	0.00			51	0.00		3.37
mmu-miR-5117	284	0.02			79	0.01			0.32	
mmu-miR-5121	20	0.00	105	0.00			118	0.00		1.04
mmu-miR-5122			10	0.00			7	0.00		0.65
mmu-miR-5126	14	0.00	43	0.00			64	0.00		1.38
mmu-miR-5128			8	0.00			2	0.00		0.23
mmu-miR-5130			4	0.00						
mmu-miR-532-3p	20	0.00	166	0.01	60	0.00	118	0.00	3.45	0.66
mmu-miR-532-5p	351	0.02	649	0.02	162	0.01	810	0.03	0.53	1.15
mmu-miR-539-5p			23	0.00						
mmu-miR-540-3p	13	0.00	153	0.01			26	0.00		0.16
mmu-miR-540-5p			28	0.00						
mmu-miR-541	759	0.05	2,660	0.10	448	0.03	2,564	0.09	0.68	0.89

miRNA	Cre⁻ Control mice				Cre⁺ Lmx1b-KO mice					
	total RNA valid reads: 16,483,415	‰ reads	small RNAs valid reads: 26,499,566	‰ reads	total RNA valid reads: 14,350,712	‰ reads	small RNAs valid reads: 28,671,121	‰ reads	total RNA Libs: KO/Ctrl	small RNA Libs: KO/Ctrl
mmu-miR-541*			8	0.00						
mmu-miR-542-3p	232	0.01	416	0.02	57	0.00	339	0.01	0.28	0.75
mmu-miR-542-5p	44	0.00	834	0.03	129	0.01	830	0.03	3.37	0.92
mmu-miR-543			131	0.00			132	0.00		0.93
mmu-miR-547							36	0.00		
mmu-miR-574-3p	1,359	0.08	4,047	0.15	1,803	0.13	5,523	0.19	1.52	1.26
mmu-miR-574-5p	1,382	0.08	914	0.03	1,344	0.09	685	0.02	1.12	0.69
mmu-miR-582-3p							13	0.00		
mmu-miR-582-5p	18	0.00	39	0.00						
mmu-miR-598	95	0.01	174	0.01	275	0.02	71	0.00	3.32	0.38
mmu-miR-598*			12	0.00						
mmu-miR-615-3p	235	0.01	952	0.04	483	0.03	2,164	0.08	2.36	2.10
mmu-miR-615-5p			63	0.00			66	0.00		0.97
mmu-miR-652	834	0.05	6,639	0.25	1,991	0.14	7,418	0.26	2.74	1.03
mmu-miR-664	76	0.00	190	0.01			118	0.00		0.57
mmu-miR-664*	79	0.00	273	0.01	32	0.00	420	0.01	0.47	1.42
mmu-miR-665							34	0.00		
mmu-miR-667	7	0.00	50	0.00			98	0.00		1.81
mmu-miR-668			49	0.00	57	0.00	68	0.00		1.28
mmu-miR-669a-3p, mmu-miR-669o-3p		23	0.00							
mmu-miR-669a-5p, mmu-miR-669p						30	0.00			
mmu-miR-669c	83	0.01	69	0.00	107	0.01	73	0.00	1.48	0.98
mmu-miR-671-3p	642	0.04	2,613	0.10	1,124	0.08	3,080	0.11	2.01	1.09
mmu-miR-671-5p	40	0.00	23	0.00						
mmu-miR-672	165	0.01	324	0.01	222	0.02	447	0.02	1.55	1.28
mmu-miR-673-3p			26	0.00			33	0.00		1.17
mmu-miR-673-5p	235	0.01	859	0.03	356	0.02	782	0.03	1.74	0.84
mmu-miR-674	51	0.00	278	0.01			159	0.01		0.53
mmu-miR-674*	62	0.00	616	0.02	298	0.02	1,314	0.05	5.52	1.97
mmu-miR-676	146	0.01	498	0.02	159	0.01	338	0.01	1.25	0.63
mmu-miR-676*			94	0.00	67	0.00				
mmu-miR-677			19	0.00						
mmu-miR-690	59	0.00	249	0.01	58	0.00	135	0.00	1.13	0.50
mmu-miR-696	25	0.00	24	0.00						
mmu-miR-700	31	0.00	448	0.02	124	0.01	425	0.01	4.59	0.88
mmu-miR-700*	78	0.00	39	0.00			77	0.00		1.82
mmu-miR-701	16	0.00								
mmu-miR-702			15	0.00			72	0.00		4.44
mmu-miR-703					7	0.00				
mmu-miR-706			12	0.00						

miRNA	Cre⁻ Control mice				Cre⁺ Lmx1b-KO mice					
	total RNA valid reads: 16,483,415	‰ reads	small RNAs valid reads: 26,499,566	‰ reads	total RNA valid reads: 14,350,712	‰ reads	small RNAs valid reads: 28,671,121	‰ reads	total RNA Libs: KO/Ctrl	small RNA Libs: KO/Ctrl
mmu-miR-708	15	0.00	69	0.00						
mmu-miR-708*	13	0.00								
mmu-miR-709	7,420	0.45	383	0.01	3,992	0.28	454	0.02	0.62	1.10
mmu-miR-712	56	0.00	83	0.00	165	0.01	60	0.00	3.38	0.67
mmu-miR-714	15	0.00								
mmu-miR-720	272	0.02	2,645	0.10	484	0.03	4,431	0.15	2.04	1.55
mmu-miR-744	1,310	0.08	5,265	0.20	1,935	0.13	7,242	0.25	1.70	1.27
mmu-miR-744*	77	0.00	249	0.01	264	0.02	149	0.01	3.94	0.55
mmu-miR-758			10	0.00						
mmu-miR-760-3p			6	0.00						
mmu-miR-770-3p	21	0.00								
mmu-miR-7a	367	0.02	296	0.01	280	0.02	505	0.02	0.88	1.58
mmu-miR-7a-1*			33	0.00			15	0.00		0.42
mmu-miR-802	10	0.00	38	0.00						
mmu-miR-802*			19	0.00						
mmu-miR-871-3p			34	0.00						
mmu-miR-872	134	0.01	622	0.02	201	0.01	485	0.02	1.72	0.72
mmu-miR-872*	308	0.02	889	0.03	592	0.04	758	0.03	2.21	0.79
mmu-miR-873	22	0.00	24	0.00			35	0.00		1.35
mmu-miR-873*	45	0.00	236	0.01			236	0.01		0.92
mmu-miR-874	1,148	0.07	2,045	0.08	1,094	0.08	1,348	0.05	1.09	0.61
mmu-miR-874*	81	0.00	95	0.00	97	0.01	42	0.00	1.38	0.41
mmu-miR-876-5p			28	0.00						
mmu-miR-877	34	0.00	106	0.00			146	0.01		1.27
mmu-miR-877*	14	0.00	77	0.00						
mmu-miR-9			167	0.01	42	0.00	11	0.00		0.06
mmu-miR-92a	13,364	0.81	34,805	1.31	13,138	0.92	40,839	1.42	1.13	1.08
mmu-miR-92a-1*			30	0.00			174	0.01		5.36
mmu-miR-92a-2*			14	0.00						
mmu-miR-92b	383	0.02	2,485	0.09	752	0.05	3,700	0.13	2.26	1.38
mmu-miR-93	866	0.05	1,030	0.04	652	0.05	673	0.02	0.86	0.60
mmu-miR-93*	5	0.00	288	0.01	52	0.00	289	0.01	11.95	0.93
mmu-miR-96	32	0.00	126	0.00						
mmu-miR-98	519	0.03	1,034	0.04	579	0.04	963	0.03	1.28	0.86
mmu-miR-98*	114	0.01	618	0.02			565	0.02		0.84
mmu-miR-99a	5,289	0.32	23,486	0.89	4,413	0.31	22,388	0.78	0.96	0.88
mmu-miR-99a*							41	0.00		
mmu-miR-99b	453,297	27.50	699,412	26.39	485,756	33.85	694,570	24.23	1.23	0.92
mmu-miR-99b*	25	0.00	224	0.01	12	0.00	500	0.02	0.55	2.06

Tab. 10.6: miRNA expression in Lmx1b knockout podocytes and red fluorescent cell population

miRNA	Total reads of miRNA sequences				fraction of miRNA reads in rpm				Ratio		
	podocytes (WT)	podocytes (Lmx1b KO)	red cells (WT)	red cells (Lmx1b KO)	podocytes (WT) rpm	podocytes (Lmx1b KO) rpm	red cells (WT) rpm	red cells (Lmx1b KO) rpm	Podocytes WT/KO	red cells WT/KO	PodocytesWT/ red cells WT
mmu-let-7a-1-3p. mmu-let-7c-2-3p	3	32	17	20	0.5	7.4	3.0	5.7	0.1	0.5	0.2
mmu-let-7a-5p	10927	7841	8143	2996	1874.2	1802.3	1435.1	848.2	1.0	1.7	1.3
mmu-let-7a-5p. mmu-let-7c-5p	678	844	429	646	116.3	194.0	75.6	182.9	0.6	0.4	1.5
mmu-let-7b-3p	33	6		11	5.7	1.4	0.0	3.1	4.1	0.0	-----
mmu-let-7b-5p	20531	31851	23246	19681	3521.4	7321.2	4096.8	5571.6	0.5	0.7	0.9
mmu-let-7c-5p	37946	37056	28447	20748	6508.4	8517.6	5013.4	5873.7	0.8	0.9	1.3
mmu-let-7d-3p	1297	330	404	119	222.5	75.9	71.2	33.7	2.9	2.1	3.1
mmu-let-7d-5p	465	883	1362	368	79.8	203.0	240.0	104.2	0.4	2.3	0.3
mmu-let-7e-3p	27	58	17	17	4.6	13.3	3.0	4.8	0.3	0.6	1.5
mmu-let-7e-5p	3063	1924	1629	885	525.4	442.2	287.1	250.5	1.2	1.1	1.8
mmu-let-7f-2-3p	19	30	12	5	3.3	6.9	2.1	1.4	0.5	1.5	1.5
mmu-let-7f-5p	4721	3212	4321	1387	809.7	738.3	761.5	392.7	1.1	1.9	1.1
mmu-let-7g-5p	502	1152	1623	882	86.1	264.8	286.0	249.7	0.3	1.1	0.3
mmu-let-7i-5p	29271	44335	62203	43345	5020.5	10190.8	10962.3	12270.8	0.5	0.9	0.5
mmu-miR-100-5p	32	6	113	83	5.5	1.4	19.9	23.5	4.0	0.8	0.3
mmu-miR-101a-3p	25	117	181	213	4.3	26.9	31.9	60.3	0.2	0.5	0.1
mmu-miR-101a-3p. mmu-miR-101c	14913	35279	28830	25002	2557.8	8109.2	5080.9	7077.9	0.3	0.7	0.5
mmu-miR-101b-3p	1443	3495	2509	1979	247.5	803.4	442.2	560.2	0.3	0.8	0.6
mmu-miR-101c	1630	4696	3712	3879	279.6	1079.4	654.2	1098.1	0.3	0.6	0.4
mmu-miR-103-3p	5943	6431	6456	6370	1019.3	1478.2	1137.8	1803.3	0.7	0.6	0.9
mmu-miR-103-3p. mmu-miR-107-3p	2779	2729	3319	2591	476.6	627.3	584.9	733.5	0.8	0.8	0.8
mmu-miR-106b-3p	1552	947	2212	862	266.2	217.7	389.8	244.0	1.2	1.6	0.7
mmu-miR-106b-5p	57	3	25	35	9.8	0.7	4.4	9.9	14.2	0.4	2.2
mmu-miR-107-3p	177	89	95	36	30.4	20.5	16.7	10.2	1.5	1.6	1.8
mmu-miR-10a-3p	20	8	38	25	3.4	1.8	6.7	7.1	1.9	0.9	0.5
mmu-miR-10a-5p	58809	64911	381110	495521	10086.7	14920.4	67164.9	140279.5	0.7	0.5	0.2
mmu-miR-10b-5p	658494	214717	91598	74553	112942.4	49354.6	16142.8	21105.6	2.3	0.8	7.0
mmu-miR-1191b-5p	15	29	1	20	2.6	6.7	0.2	5.7	0.4	0.0	14.6
mmu-miR-1198-5p	233	73	106	68	40.0	16.8	18.7	19.3	2.4	1.0	2.1
mmu-miR-122-5p	79	4	41	16	13.5	0.9	7.2	4.5	14.7	1.6	1.9
mmu-miR-1249-3p		6	29	10	0.0	1.4	5.1	2.8	0.0	1.8	0.0
mmu-miR-125a-3p	78	107	166	53	13.4	24.6	29.3	15.0	0.5	1.9	0.5
mmu-miR-125a-5p	2915	2449	1829	1130	500.0	562.9	322.3	319.9	0.9	1.0	1.6
mmu-miR-125b-2-3p	314	529	209	90	53.9	121.6	36.8	25.5	0.4	1.4	1.5
mmu-miR-125b-5p	513	437	245	131	88.0	100.4	43.2	37.1	0.9	1.2	2.0
mmu-miR-126a-3p	17	107	11062	12712	2.9	24.6	1949.5	3598.7	0.1	0.5	0.0

miRNA	Total reads of miRNA sequences				fraction of miRNA reads in rpm				Ratio		
	podocytes (WT)	podocytes (Lmx1b KO)	red cells (WT)	red cells (Lmx1b KO)	podocytes (WT) rpm	podocytes (Lmx1b KO) rpm	red cells (WT) rpm	red cells (Lmx1b KO) rpm	Podocytes WT/KO	red cells WT/KO	PodocytesWT/ red cells WT
mmu-miR-126a-5p		8	2951	1099	0.0	1.8	520.1	311.1	0.0	1.7	0.0
mmu-miR-127-3p	398	13	11811	89	68.3	3.0	2081.5	25.2	22.8	82.6	0.0
mmu-miR-127-5p			245	1	0.0	0.0	43.2	0.3	-----	152.5	0.0
mmu-miR-128-1-5p	37	19	6	8	6.3	4.4	1.1	2.3	1.5	0.5	6.0
mmu-miR-129-5p	125	2292	497	481	21.4	526.8	87.6	136.2	0.0	0.6	0.2
mmu-miR-130a-3p	366	272	371	104	62.8	62.5	65.4	29.4	1.0	2.2	1.0
mmu-miR-130b-3p		11	25	9	0.0	2.5	4.4	2.5	0.0	1.7	0.0
mmu-miR-132-3p		83	57	52	0.0	19.1	10.0	14.7	0.0	0.7	0.0
mmu-miR-133a-3p		10	189	184	0.0	2.3	33.3	52.1	0.0	0.6	0.0
mmu-miR-134-5p			289	1	0.0	0.0	50.9	0.3	-----	179.9	0.0
mmu-miR-139-3p		16	1657	1136	0.0	3.7	292.0	321.6	0.0	0.9	0.0
mmu-miR-139-5p		10	348	416	0.0	2.3	61.3	117.8	0.0	0.5	0.0
mmu-miR-140-3p	6312	5277	6484	4687	1082.6	1213.0	1142.7	1326.9	0.9	0.9	0.9
mmu-miR-140-5p	46	16	24	15	7.9	3.7	4.2	4.2	2.1	1.0	1.9
mmu-miR-143-3p	219276	784667	1E+06	2E+06	37609.4	180362.7	180205.2	428194.2	0.2	0.4	0.2
mmu-miR-143-5p	37	54	55	74	6.3	12.4	9.7	20.9	0.5	0.5	0.7
mmu-miR-145a-5p	112	697	872	2040	19.2	160.2	153.7	577.5	0.1	0.3	0.1
mmu-miR-146a-5p	37	542	2752	3013	6.3	124.6	485.0	853.0	0.1	0.6	0.0
mmu-miR-146b-5p	32276	24281	14618	2945	5535.9	5581.2	2576.2	833.7	1.0	3.1	2.1
mmu-miR-148a-3p	10541	5390	4314	1277	1808.0	1238.9	760.3	361.5	1.5	2.1	2.4
mmu-miR-148a-5p	35	86	29	8	6.0	19.8	5.1	2.3	0.3	2.3	1.2
mmu-miR-148b-3p	166	94	62	103	28.5	21.6	10.9	29.2	1.3	0.4	2.6
mmu-miR-149-5p	80	196	112	33	13.7	45.1	19.7	9.3	0.3	2.1	0.7
mmu-miR-150-5p		15	128	106	0.0	3.4	22.6	30.0	0.0	0.8	0.0
mmu-miR-151-3p	6896	2855	15848	8053	1182.8	656.2	2793.0	2279.8	1.8	1.2	0.4
mmu-miR-151-5p	148	35	379	290	25.4	8.0	66.8	82.1	3.2	0.8	0.4
mmu-miR-152-3p	3359	2461	1711	1315	576.1	565.7	301.5	372.3	1.0	0.8	1.9
mmu-miR-152-5p	109	80	40	44	18.7	18.4	7.0	12.5	1.0	0.6	2.7
mmu-miR-15a-5p	7	14	11	19	1.2	3.2	1.9	5.4	0.4	0.4	0.6
mmu-miR-15b-5p			56	3	0.0	0.0	9.9	0.8	-----	11.6	0.0
mmu-miR-16-1-3p	77	26	44	27	13.2	6.0	7.8	7.6	2.2	1.0	1.7
mmu-miR-16-5p	102	84	321	178	17.5	19.3	56.6	50.4	0.9	1.1	0.3
mmu-miR-17-3p	8	21	30	44	1.4	4.8	5.3	12.5	0.3	0.4	0.3
mmu-miR-17-5p		7	34	16	0.0	1.6	6.0	4.5	0.0	1.3	0.0
mmu-miR-181a-1-3p	970	655	677	492	166.4	150.6	119.3	139.3	1.1	0.9	1.4
mmu-miR-181a-5p	14452	9642	7860	6410	2478.8	2216.3	1385.2	1814.6	1.1	0.8	1.8
mmu-miR-181b-5p	2041	1048	1144	929	350.1	240.9	201.6	263.0	1.5	0.8	1.7
mmu-miR-181c-3p	25	9	174	152	4.3	2.1	30.7	43.0	2.1	0.7	0.1
mmu-miR-181c-5p	1	13	228	226	0.2	3.0	40.2	64.0	0.1	0.6	0.0

miRNA	Total reads of miRNA sequences				fraction of miRNA reads in rpm				Ratio		
	podocytes (WT)	podocytes (Lmx1b KO)	red cells (WT)	red cells (Lmx1b KO)	podocytes (WT) rpm	podocytes (Lmx1b KO) rpm	red cells (WT) rpm	red cells (Lmx1b KO) rpm	Podocytes WT/KO	red cells WT/KO	PodocytesWT/ red cells WT
mmu-miR-181d-5p	46	10	431	484	7.9	2.3	76.0	137.0	3.4	0.6	0.1
mmu-miR-182-5p	85	61	1119	406	14.6	14.0	197.2	114.9	1.0	1.7	0.1
mmu-miR-183-5p	1		52	23	0.2	0.0	9.2	6.5	-----	1.4	0.0
mmu-miR-1839-5p	340	411	231	263	58.3	94.5	40.7	74.5	0.6	0.5	1.4
mmu-miR-184-3p	41		6	5	7.0	0.0	1.1	1.4	-----	0.7	6.7
mmu-miR-1843a-5p	1205	579	539	336	206.7	133.1	95.0	95.1	1.6	1.0	2.2
mmu-miR-1843a-5p. mmu-miR-1843b-5p	652	700	443	184	111.8	160.9	78.1	52.1	0.7	1.5	1.4
mmu-miR-1843b-3p	34	1		4	5.8	0.2	0.0	1.1	25.4	0.0	----
mmu-miR-1843b-5p	533	564	575	265	91.4	129.6	101.3	75.0	0.7	1.4	0.9
mmu-miR-185-5p	191	570	401	230	32.8	131.0	70.7	65.1	0.3	1.1	0.5
mmu-miR-186-5p	219	282	203	154	37.6	64.8	35.8	43.6	0.6	0.8	1.0
mmu-miR-191-5p	2982	1924	2008	1249	511.5	442.2	353.9	353.6	1.2	1.0	1.4
mmu-miR-192-5p	106	33	55	26	18.2	7.6	9.7	7.4	2.4	1.3	1.9
mmu-miR-1934-3p	86	35	9	15	14.8	8.0	1.6	4.2	1.8	0.4	9.3
mmu-miR-193a-5p	67	57	31	40	11.5	13.1	5.5	11.3	0.9	0.5	2.1
mmu-miR-194-2-3p	78	7	26	27	13.4	1.6	4.6	7.6	8.3	0.6	2.9
mmu-miR-194-5p	138	32	36	17	23.7	7.4	6.3	4.8	3.2	1.3	3.7
mmu-miR-1940		15	3	24	0.0	3.4	0.5	6.8	0.0	0.1	0.0
mmu-miR-1943-5p	11	18	53	46	1.9	4.1	9.3	13.0	0.5	0.7	0.2
mmu-miR-1955-3p		25		2	0.0	5.7	0.0	0.6	0.0	0.0	----
mmu-miR-195a-3p	17	6	98	67	2.9	1.4	17.3	19.0	2.1	0.9	0.2
mmu-miR-195a-5p			109	144	0.0	0.0	19.2	40.8	----	0.5	0.0
mmu-miR-196a-2-3p	22	31	29	9	3.8	7.1	5.1	2.5	0.5	2.0	0.7
mmu-miR-196a-5p	193	125	57	56	33.1	28.7	10.0	15.9	1.2	0.6	3.3
mmu-miR-196b-5p	2831	4121	1327	974	485.6	947.2	233.9	275.7	0.5	0.8	2.1
mmu-miR-1981-5p	358	107	140	89	61.4	24.6	24.7	25.2	2.5	1.0	2.5
mmu-miR-199a-3p. mmu-miR-199b-3p	93	199	163	326	16.0	45.7	28.7	92.3	0.3	0.3	0.6
mmu-miR-199a-5p			30	29	0.0	0.0	5.3	8.2	----	0.6	0.0
mmu-miR-199b-5p		22			0.0	5.1	0.0	0.0	0.0	----	-----
mmu-miR-19a-3p	40	158	172	444	6.9	36.3	30.3	125.7	0.2	0.2	0.2
mmu-miR-19b-3p	687	2669	3123	5555	117.8	613.5	550.4	1572.6	0.2	0.3	0.2
mmu-miR-1a-3p			47	31	0.0	0.0	8.3	8.8	----	0.9	0.0
mmu-miR-200a-3p		23	254	139	0.0	5.3	44.8	39.4	0.0	1.1	0.0
mmu-miR-200a-5p			31	4	0.0	0.0	5.5	1.1	----	4.8	0.0
mmu-miR-200b-3p		2	40	39	0.0	0.5	7.0	11.0	0.0	0.6	0.0
mmu-miR-200c-3p		3	47	13	0.0	0.7	8.3	3.7	0.0	2.3	0.0
mmu-miR-203-3p	176	306	397	303	30.2	70.3	70.0	85.8	0.4	0.8	0.4

miRNA	Total reads of miRNA sequences				fraction of miRNA reads in rpm				Ratio		
	podocytes (WT)	podocytes (Lmx1b KO)	red cells (WT)	red cells (Lmx1b KO)	podocytes (WT) rpm	podocytes (Lmx1b KO) rpm	red cells (WT) rpm	red cells (Lmx1b KO) rpm	Podocytes WT/KO	red cells WT/KO	PodocytesWT/ red cells WT
mmu-miR-204-3p		15	68	29	0.0	3.4	12.0	8.2	0.0	1.5	0.0
mmu-miR-204-5p	45	8	158	156	7.7	1.8	27.8	44.2	4.2	0.6	0.3
mmu-miR-20a-5p	13	42	25	54	2.2	9.7	4.4	15.3	0.2	0.3	0.5
mmu-miR-210-3p	1732	4662	2670	616	297.1	1071.6	470.5	174.4	0.3	2.7	0.6
mmu-miR-214-3p	1	2	16	31	0.2	0.5	2.8	8.8	0.4	0.3	0.1
mmu-miR-21a-3p	1	117	14	15	0.2	26.9	2.5	4.2	0.0	0.6	0.1
mmu-miR-21a-5p	1173	7308	2026	3483	201.2	1679.8	357.1	986.0	0.1	0.4	0.6
mmu-miR-22-3p	118760	110370	45048	29023	20369.3	25369.5	7939.0	8216.3	0.8	1.0	2.6
mmu-miR-22-5p		29	25	9	0.0	6.7	4.4	2.5	0.0	1.7	0.0
mmu-miR-221-3p	30	36	185	122	5.1	8.3	32.6	34.5	0.6	0.9	0.2
mmu-miR-222-3p	103	119	487	393	17.7	27.4	85.8	111.3	0.6	0.8	0.2
mmu-miR-23a-3p	54	325	682	507	9.3	74.7	120.2	143.5	0.1	0.8	0.1
mmu-miR-23a-5p	99	220	46	73	17.0	50.6	8.1	20.7	0.3	0.4	2.1
mmu-miR-23b-3p	1335	2140	2685	704	229.0	491.9	473.2	199.3	0.5	2.4	0.5
mmu-miR-23b-3p. mmu-miR-23a-3p	55	70	62	48	9.4	16.1	10.9	13.6	0.6	0.8	0.9
mmu-miR-23b-5p	37	6	34	1	6.3	1.4	6.0	0.3	4.6	21.2	1.1
mmu-miR-24-2-5p	23	188	107	98	3.9	43.2	18.9	27.7	0.1	0.7	0.2
mmu-miR-24-3p	79633	63764	35380	22890	13658.4	14656.7	6235.2	6480.0	0.9	1.0	2.2
mmu-miR-25-3p	7574	2340	6973	3387	1299.1	537.9	1228.9	958.8	2.4	1.3	1.1
mmu-miR-26a-5p	37732	56419	46042	32426	6471.7	12968.4	8114.2	9179.6	0.5	0.9	0.8
mmu-miR-26b-5p	2609	3259	2876	2422	447.5	749.1	506.9	685.7	0.6	0.7	0.9
mmu-miR-27a-3p	395	484	1573	706	67.7	111.3	277.2	199.9	0.6	1.4	0.2
mmu-miR-27a-5p	1434	3977	1250	1185	246.0	914.1	220.3	335.5	0.3	0.7	1.1
mmu-miR-27b-3p	49262	64316	44226	29530	8449.2	14783.6	7794.2	8359.8	0.6	0.9	1.1
mmu-miR-27b-3p. mmu-miR-27a-3p	1179	923	865	613	202.2	212.2	152.4	173.5	1.0	0.9	1.3
mmu-miR-27b-5p	1077	523	487	204	184.7	120.2	85.8	57.8	1.5	1.5	2.2
mmu-miR-28a-3p	1042	560	1020	599	178.7	128.7	179.8	169.6	1.4	1.1	1.0
mmu-miR-296-3p	64	38	170	65	11.0	8.7	30.0	18.4	1.3	1.6	0.4
mmu-miR-299a-3p. mmu-miR-299b-3p			45	3	0.0	0.0	7.9	0.8	----	9.3	0.0
mmu-miR-29a-3p	824	938	896	353	141.3	215.6	157.9	99.9	0.7	1.6	0.9
mmu-miR-29b-3p		98	90	5	0.0	22.5	15.9	1.4	0.0	11.2	0.0
mmu-miR-29c-3p	160	159	232	157	27.4	36.5	40.9	44.4	0.8	0.9	0.7
mmu-miR-3057-5p	36	31	57	41	6.2	7.1	10.0	11.6	0.9	0.9	0.6
mmu-miR-3081-3p			32	12	0.0	0.0	5.6	3.4	----	1.7	0.0
mmu-miR-30a-3p	24968	17428	12271	6662	4282.4	4006.0	2162.6	1886.0	1.1	1.1	2.0
mmu-miR-30a-5p	1E+06	985651	704816	275942	181617.0	226560.6	124213.2	78117.8	0.8	1.6	1.5
mmu-miR-30b-3p	153	19	26	8	26.2	4.4	4.6	2.3	6.0	2.0	5.7

miRNA	Total reads of miRNA sequences				fraction of miRNA reads in rpm				Ratio		
	podocytes (WT)	podocytes (Lmx1b KO)	red cells (WT)	red cells (Lmx1b KO)	podocytes (WT) rpm	podocytes (Lmx1b KO) rpm	red cells (WT) rpm	red cells (Lmx1b KO) rpm	Podocytes WT/KO	red cells WT/KO	PodocytesWT/ red cells WT
mmu-miR-30b-5p	294	1194	925	475	50.4	274.5	163.0	134.5	0.2	1.2	0.3
mmu-miR-30c-1-3p	140	54	55	43	24.0	12.4	9.7	12.2	1.9	0.8	2.5
mmu-miR-30c-2-3p	75956	72243	67658	22258	13027.7	16605.7	11923.7	6301.1	0.8	1.9	1.1
mmu-miR-30c-5p	1473	3334	3033	1627	252.6	766.3	534.5	460.6	0.3	1.2	0.5
mmu-miR-30d-3p	79	119	55	62	13.5	27.4	9.7	17.6	0.5	0.6	1.4
mmu-miR-30d-5p	184118	113915	80361	34082	31579.2	26184.4	14162.4	9648.4	1.2	1.5	2.2
mmu-miR-30e-3p	207	126	100	58	35.5	29.0	17.6	16.4	1.2	1.1	2.0
mmu-miR-30e-5p	13281	11000	10167	4326	2277.9	2528.4	1791.8	1224.7	0.9	1.5	1.3
mmu-miR-31-5p	23		62	24	3.9	0.0	10.9	6.8	----	1.6	0.4
mmu-miR-3102-3p	5	93	19	34	0.9	21.4	3.3	9.6	0.0	0.3	0.3
mmu-miR-3102-5p		54	6	2	0.0	12.4	1.1	0.6	0.0	1.9	0.0
mmu-miR-320-3p	5329	5182	5645	5825	914.0	1191.1	994.8	1649.0	0.8	0.6	0.9
mmu-miR-322-3p	6689	9903	2402	1668	1147.3	2276.3	423.3	472.2	0.5	0.9	2.7
mmu-miR-322-5p	31	74	46	41	5.3	17.0	8.1	11.6	0.3	0.7	0.7
mmu-miR-324-5p		2	37	6	0.0	0.5	6.5	1.7	0.0	3.8	0.0
mmu-miR-326-3p	119	157	163	54	20.4	36.1	28.7	15.3	0.6	1.9	0.7
mmu-miR-328-3p	1100	602	983	332	188.7	138.4	173.2	94.0	1.4	1.8	1.1
mmu-miR-329-5p			209		0.0	0.0	36.8	0.0	----	----	0.0
mmu-miR-330-3p	69	19	49	19	11.8	4.4	8.6	5.4	2.7	1.6	1.4
mmu-miR-330-5p	63	24	8		10.8	5.5	1.4	0.0	2.0	----	7.7
mmu-miR-331-3p		34	50	31	0.0	7.8	8.8	8.8	0.0	1.0	0.0
mmu-miR-338-3p			103	164	0.0	0.0	18.2	46.4	----	0.4	0.0
mmu-miR-339-5p	131	100	231	120	22.5	23.0	40.7	34.0	1.0	1.2	0.6
mmu-miR-340-5p	316	493	145	121	54.2	113.3	25.6	34.3	0.5	0.7	2.1
mmu-miR-341-3p		4	63		0.0	0.9	11.1	0.0	0.0	----	0.0
mmu-miR-345-3p	51	5	42	12	8.7	1.1	7.4	3.4	7.6	2.2	1.2
mmu-miR-3470b	29	11	23	23	5.0	2.5	4.1	6.5	2.0	0.6	1.2
mmu-miR-3473b	1	23	42	27	0.2	5.3	7.4	7.6	0.0	1.0	0.0
mmu-miR-3473b. mmu-miR-3473e	5	44	72	42	0.9	10.1	12.7	11.9	0.1	1.1	0.1
mmu-miR-3474	192	66	22	9	32.9	15.2	3.9	2.5	2.2	1.5	8.5
mmu-miR-34a-5p	58	206	98	99	9.9	47.4	17.3	28.0	0.2	0.6	0.6
mmu-miR-350-5p	194	56	177	83	33.3	12.9	31.2	23.5	2.6	1.3	1.1
mmu-miR-351-3p	143	165	94	17	24.5	37.9	16.6	4.8	0.6	3.4	1.5
mmu-miR-351-5p	18841	12745	8202	3121	3231.5	2929.6	1445.5	883.5	1.1	1.6	2.2
mmu-miR-3535	390	110	186	103	66.9	25.3	32.8	29.2	2.6	1.1	2.0
mmu-miR-361-3p	192	315	302	246	32.9	72.4	53.2	69.6	0.5	0.8	0.6
mmu-miR-361-5p	112	32	50	55	19.2	7.4	8.8	15.6	2.6	0.6	2.2
mmu-miR-362-3p		18	18	41	0.0	4.1	3.2	11.6	0.0	0.3	0.0

miRNA	Total reads of miRNA sequences				fraction of miRNA reads in rpm				Ratio		
	podocytes (WT)	podocytes (Lmx1b KO)	red cells (WT)	red cells (Lmx1b KO)	podocytes (WT) rpm	podocytes (Lmx1b KO) rpm	red cells (WT) rpm	red cells (Lmx1b KO) rpm	Podocytes WT/KO	red cells WT/KO	PodocytesWT/ red cells WT
mmu-miR-374b-5p			37		0.0	0.0	6.5	0.0	----	----	0.0
mmu-miR-375-3p	32	1	136	93	5.5	0.2	24.0	26.3	23.9	0.9	0.2
mmu-miR-378a-3p	26708	29234	18541	8896	4580.9	6719.7	3267.6	2518.4	0.7	1.3	1.4
mmu-miR-378a-3p. mmu-miR-378b. mmu-miR-378c	37	36	81	18	6.3	8.3	14.3	5.1	0.8	2.8	0.4
mmu-miR-378a-3p. mmu-miR-378c	1353	2601	1607	993	232.1	597.9	283.2	281.1	0.4	1.0	0.8
mmu-miR-378a-5p	107	91	101	33	18.4	20.9	17.8	9.3	0.9	1.9	1.0
mmu-miR-378b	120	91	96	74	20.6	20.9	16.9	20.9	1.0	0.8	1.2
mmu-miR-379-5p			453	11	0.0	0.0	79.8	3.1	----	25.6	0.0
mmu-miR-381-3p			31	4	0.0	0.0	5.5	1.1	----	4.8	0.0
mmu-miR-382-5p	128		2929	39	22.0	0.0	516.2	11.0	----	46.8	0.0
mmu-miR-383-5p			125	52	0.0	0.0	22.0	14.7	----	1.5	0.0
mmu-miR-409-3p	25		236		4.3	0.0	41.6	0.0	----	----	0.1
mmu-miR-411-5p			60		0.0	0.0	10.6	0.0	----	----	0.0
mmu-miR-423-3p	160	84	193	92	27.4	19.3	34.0	26.0	1.4	1.3	0.8
mmu-miR-423-5p	1541	1540	2464	1590	264.3	354.0	434.2	450.1	0.7	1.0	0.6
mmu-miR-425-3p	24	48	30	33	4.1	11.0	5.3	9.3	0.4	0.6	0.8
mmu-miR-425-5p	134	39	48	40	23.0	9.0	8.5	11.3	2.6	0.7	2.7
mmu-miR-434-3p			36	3	0.0	0.0	6.3	0.8	----	7.5	0.0
mmu-miR-434-5p			100		0.0	0.0	17.6	0.0	----	----	0.0
mmu-miR-450a-5p	74	27	71	11	12.7	6.2	12.5	3.1	2.0	4.0	1.0
mmu-miR-450b-3p	29	10	14	10	5.0	2.3	2.5	2.8	2.2	0.9	2.0
mmu-miR-484	185	168	212	145	31.7	38.6	37.4	41.0	0.8	0.9	0.8
mmu-miR-486-3p. mmu-miR-3107-3p		53		7	0.0	12.2	0.0	2.0	0.0	0.0	-----
mmu-miR-486-5p. mmu-miR-3107-5p	3091	7577	1616	681	530.2	1741.6	284.8	192.8	0.3	1.5	1.9
mmu-miR-488-3p			64	23	0.0	0.0	11.3	6.5	----	1.7	0.0
mmu-miR-497-5p			28	24	0.0	0.0	4.9	6.8	----	0.7	0.0
mmu-miR-503-3p	199	173	69	23	34.1	39.8	12.2	6.5	0.9	1.9	2.8
mmu-miR-503-5p	1395	792	638	227	239.3	182.0	112.4	64.3	1.3	1.7	2.1
mmu-miR-5099	780	164	448	343	133.8	37.7	79.0	97.1	3.5	0.8	1.7
mmu-miR-5114	35		26	10	6.0	0.0	4.6	2.8	----	1.6	1.3
mmu-miR-532-5p	687	854	972	584	117.8	196.3	171.3	165.3	0.6	1.0	0.7
mmu-miR-540-3p			82		0.0	0.0	14.5	0.0	----	----	0.0
mmu-miR-541-5p	1		529	9	0.2	0.0	93.2	2.5	----	36.6	0.0
mmu-miR-542-3p	659	2535	662	643	113.0	582.7	116.7	182.0	0.2	0.6	1.0
mmu-miR-542-5p	43	42	52	5	7.4	9.7	9.2	1.4	0.8	6.5	0.8
mmu-miR-574-3p	1058	772	1296	840	181.5	177.5	228.4	237.8	1.0	1.0	0.8
mmu-miR-574-5p	861	376	593	200	147.7	86.4	104.5	56.6	1.7	1.8	1.4
mmu-miR-582-3p	55	17	37	74	9.4	3.9	6.5	20.9	2.4	0.3	1.4

miRNA	Total reads of miRNA sequences				fraction of miRNA reads in rpm				Ratio		
	podocytes (WT)	podocytes (Lmx1b KO)	red cells (WT)	red cells (Lmx1b KO)	podocytes (WT) rpm	podocytes (Lmx1b KO) rpm	red cells (WT) rpm	red cells (Lmx1b KO) rpm	Podocytes WT/KO	red cells WT/KO	PodocytesWT/ red cells WT
mmu-miR-598-3p	16	13	22	12	2.7	3.0	3.9	3.4	0.9	1.1	0.7
mmu-miR-615-3p	348	120	89	24	59.7	27.6	15.7	6.8	2.2	2.3	3.8
mmu-miR-615-5p	364	202	82	22	62.4	46.4	14.5	6.2	1.3	2.3	4.3
mmu-miR-652-3p	353	192	292	117	60.5	44.1	51.5	33.1	1.4	1.6	1.2
mmu-miR-6538		18	33	12	0.0	4.1	5.8	3.4	0.0	1.7	0.0
mmu-miR-6539	34	10	10	4	5.8	2.3	1.8	1.1	2.5	1.6	3.3
mmu-miR-664-5p	1163	894	655	226	199.5	205.5	115.4	64.0	1.0	1.8	1.7
mmu-miR-669c-5p	60	27	33	11	10.3	6.2	5.8	3.1	1.7	1.9	1.8
mmu-miR-671-3p	855	489	476	180	146.6	112.4	83.9	51.0	1.3	1.6	1.7
mmu-miR-671-5p	36	38	74	42	6.2	8.7	13.0	11.9	0.7	1.1	0.5
mmu-miR-672-5p	367	756	279	195	62.9	173.8	49.2	55.2	0.4	0.9	1.3
mmu-miR-674-3p		20		23	0.0	4.6	0.0	6.5	0.0	0.0	----
mmu-miR-676-3p	4418	4956	3342	1135	757.8	1139.2	589.0	321.3	0.7	1.8	1.3
mmu-miR-7068-3p	38				6.5	0.0	0.0	0.0	----	----	-----
mmu-miR-708-3p		24	34	20	0.0	5.5	6.0	5.7	0.0	1.1	0.0
mmu-miR-709	65	214	134	124	11.1	49.2	23.6	35.1	0.2	0.7	0.5
mmu-miR-744-3p		30	7	4	0.0	6.9	1.2	1.1	0.0	1.1	0.0
mmu-miR-744-5p	905	348	559	234	155.2	80.0	98.5	66.2	1.9	1.5	1.6
mmu-miR-760-3p	34		7	11	5.8	0.0	1.2	3.1	----	0.4	4.7
mmu-miR-7a-5p	20	72	8	46	3.4	16.5	1.4	13.0	0.2	0.1	2.4
mmu-miR-8103	21	7	33	4	3.6	1.6	5.8	1.1	2.2	5.1	0.6
mmu-miR-872-3p		11	30	3	0.0	2.5	5.3	0.8	0.0	6.2	0.0
mmu-miR-872-5p	117	158	100	105	20.1	36.3	17.6	29.7	0.6	0.6	1.1
mmu-miR-873a-5p	77	266	428	117	13.2	61.1	75.4	33.1	0.2	2.3	0.2
mmu-miR-874-3p	53	10	42	14	9.1	2.3	7.4	4.0	4.0	1.9	1.2
mmu-miR-877-5p	2	10	21	22	0.3	2.3	3.7	6.2	0.1	0.6	0.1
mmu-miR-9-5p	90	68	651	330	15.4	15.6	114.7	93.4	1.0	1.2	0.1
mmu-miR-92a-1-5p		23	30	54	0.0	5.3	5.3	15.3	0.0	0.3	0.0
mmu-miR-92a-3p	20677	5785	19990	12820	3546.4	1329.7	3522.9	3629.3	2.7	1.0	1.0
mmu-miR-92b-5p	72	22		4	12.3	5.1	0.0	1.1	2.4	0.0	----
mmu-miR-93-5p	4224	5757	4643	4156	724.5	1323.3	818.3	1176.5	0.5	0.7	0.9
mmu-miR-98-5p	2516	6938	5505	3851	431.5	1594.8	970.2	1090.2	0.3	0.9	0.4
mmu-miR-99a-3p	87	52	56	8	14.9	12.0	9.9	2.3	1.2	4.4	1.5
mmu-miR-99a-5p	279	283	293	75	47.9	65.1	51.6	21.2	0.7	2.4	0.9
mmu-miR-99b-3p	1258	1040	1038	464	215.8	239.1	182.9	131.4	0.9	1.4	1.2
mmu-miR-99b-5p	11609	14926	15608	9133	1991.1	3430.9	2750.7	2585.5	0.6	1.1	0.7

Tab. 10.7: Human genomic organization of podocyte miRNAs

miRNAs	Genomic coordinates of the precursor mirna in human	Genomic organization in human (UCSC. ensembl)	clustered miRNAs (<10kb) human
hsa-let-7e-3p	chr19: 51,692,786-51,692,864 [+]	antisense to lncRNA SPACA6P-AS. upstream of SPACA6P	hsa-mir-99b. hsa-let-7e. hsa-mir-125a
hsa-miR-107-3p	chr10: 89,592,747-89,592,827 [-]	intron of Pank1 (pantothenate kinase 1)	
hsa-miR-125b-2-3p	chr21: 16,590,237-16,590,325 [+]	locus 2: intron of lincRNA MIR99AHG (mir-99a host gene)	
hsa-miR-125b-5p	locus 1: chr11: 122,099,757-122,099,844 [-] locus 2: chr21: 16,590,237-16,590,325 [+]	locus 1: intron sense overlapping gene RP11-166D19.1. intron of lncRNA MIR100HG (mir-100 host gene) locus 2: intron of lincRNA MIR99AHG (mir-99a host gene)	
hsa-miR-130a-3p	chr11: 57,641,198-57,641,286 [+]	intron of AP000662 (sense overlapping to CLP1)	
hsa-miR-146b-5p	chr10: 102,436,512-102,436,584 [+]	intergenic	
hsa-miR-148a-3p	chr7: 25,949,919-25,949,986 [-]	intergenic	
hsa-miR-149-5p	chr2: 240,456,001-240,456,089 [+]	intron of GPC1 (glypican1)	
hsa-miR-196b-5p	chr7: 27,169,480-27,169,563 [-]	intron of Hoxa9. Hoxa10; exon of Hoxa10-as	
hsa-miR-210-3p	chr11: 568,089-568,198 [-]	intron of lncRNA MIR210HG (mir-210 host gene)	
hsa-miR-23b-3p	chr9: 95,085,208-95,085,304 [+]	intron of C9orf3 (chromosome9 open reading frame 3. protein coding). clustered with mir-27b. mir-24??? mir-3074(antisense!!!)	hsa-mir-23b hsa-mir-27b hsa-mir-3074 (antisense) hsa-mir-24-1
hsa-miR-24-1-5p	chr9: 95,086,021-95,086,088 [+]		hsa-mir-23b hsa-mir-27b hsa-mir-3074 (antisense) hsa-mir-24-1
hsa-miR-27b-5p	chr9: 95,085,445-95,085,541 [+]		hsa-mir-23b hsa-mir-27b hsa-mir-3074 (antisense) hsa-mir-24-1
hsa-miR-30a-3p	chr6: 71,403,551-71,403,621 [-]	intron of lncRNA RP3-331H24.5 together with mir-30c-2	hsa-mir-30a. hsa-mir-30c-2
hsa-miR-30a-5p	chr6: 71,403,551-71,403,621 [-]	intron of lncRNA RP3-331H24.5 together with mir-30c-2	
hsa-miR-30b-3p	chr8: 134,800,520-134,800,607 [-]	intergenic	hsa-mir-30d hsa-mir-30b
hsa-miR-30b-5p	chr8: 134,800,520-134,800,607 [-]	intergenic	
hsa-miR-30c-2-3p	chr6: 71,376,960-71,377,031 [-]		
hsa-miR-30c-5p	Locus 1: chr1: 40,757,284-40,757,372 [+] Locus 2: chr6: 71,376,960-71,377,031 [-]	locus 1: intron of NFYC (nuclear transcription factor Y. gamma) locus 2: intron of lncRNA RP3-331H24.5 together with mir-30a	locus 1: hsa-mir-30e hsa-mir-30c-1
hsa-miR-30d-3p	chr8: 134,804,876-134,804,945 [-]	integenic	hsa-mir-30d. hsa-mir-30b
hsa-miR-30d-5p	chr8: 134,804,876-134,804,945 [-]	intergenic	hsa-mir-30d. hsa-mir-30b
hsa-miR-322-3p	chrX: 134,546,614-134,546,711 [-]		hsa-mir-424 hsa-mir-503 hsa-mir-542 hsa-mir-450a-2 hsa-mir-450a-1

			hsa-mir-450b
hsa-miR-330-3p	chr19: 45,638,994-45,639,087 [-]	intron of EML2 (echinoderm microtubule associated protein like 2)	
hsa-miR-330-5p	chr19: 45,638,994-45,639,087 [-]	intron of EML2 (echinoderm microtubule associated protein like 2)	
hsa-miR-340-5p	chr5: 180,015,303-180,015,397 [-]	intron of RNF130 (ring finger protein 130)	
hsa-miR-351-3p	------	------	
hsa-miR-351-5p	------	------	
hsa-miR-450a-5p	Locus 1: chrX: 134,540,341-134,540,431 [-] Locus 2: chrX: 134,540,508-134,540,607 [-]	intergenic	
hsa-miR-450b-5p	chrX: 134,540,185-134,540,262 [-]	intergenic	
hsa-miR-503-3p	chrX: 134,546,328-134,546,398 [-]	Intron of lncRNA MIR503HG (mir-503 host gene)	
hsa-miR-503-5p	chrX: 134,546,328-134,546,398 [-]	Intron of lncRNA MIR503HG (mir-503 host gene)	
hsa-miR-542-3p	chrX: 134,541,341-134,541,437 [-]	intergenic	
hsa-miR-574-3p	chr4: 38,868,032-38,868,127 [+]	intron of Fam114a1 (family with sequence similarity 114. member A1);	
hsa-miR-615-3p	chr12: 54,033,950-54,034,045 [+]	intron of Hoxc4 (homeobox C4) and Hoxc5 (homeobox C5)	
hsa-miR-652-3p	chrX: 110,055,329-110,055,426 [+]	intron of Tmem164 (transmembrane protein 164)	
hsa-miR-873a-5p	chr9: 28,888,879-28,888,955 [-]	intron of Lingo2 (leucine rich repeat and Ig domain containing 2)	
hsa-miR-99a-3p	chr21: 16,539,089-16,539,169 [+]	intron of lincRNA MIR99AHG together with mir-let-7c and mir-125b-2	hsa-mir-99a. hsa-let-7c
hsa-miR-99a-5p	chr21: 16,539,089-16,539,169 [+]	intron of lincRNA MIR99AHG together with mir-let-7c and mir-125b-2	

11 ACKNOWLEDGEMENTS

At the end of my thesis, I would like to thank all the people who supported and encouraged me on my way towards this thesis.

Foremost, I want to thank Prof. Dr. Ralph Witzgall for giving me the opportunity to work on the very interesting miRNA-podocyte project, for trusting me in my switch from the chemical to the biological field and for all his support and advice throughout the thesis.

I am very grateful to my mentor, Prof. Dr. Gunter Meister, for all his support in the miRNA-podocyte project, all his ideas, advice and his valuable input from the miRNA side.

I would like to thank my mentor, Prof. Dr. Joachim Wegener, for evaluation of my work and for his valuable advice and his view from the outside.

Very special thanks to Dr. Melanie Zaparty, who started and took care of the miRNA-podocyte project. Without all your help and support, your energy and your ideas, none of this would have been possible.

I want to thank Dr. Gertrud Knoll, Marion Kubitza and Olga Maier for all their help and support in the laboratory work. Thanks to Gertrud, for helping me to get started in a biological lab and all her help, to Marion for her help in the podocyte isolation and all the guidance she gave me through the lab and to Olga for her help in the podocyte isolation and all her work in the miRNA project, Спасибі!

I would like to thank Dr. Anne Dueck and Norbert Eichner for performing the *deep sequencing* analyses and annotations of miRNAs. Special thanks to Anne for all her help and valuable advice.

I am very grateful to Prof. Dr. Frank Schweda and Dr. Andrea Schreiber for performing the Vivo-Morpholino injections in mice, enabling the Vivo-Morpholino project.

I would like to thank Dr. Karin Babinger for all her valuable advice in the everyday laboratory work and Dr. Tillmann Burghardt for his help and support in the LMX1B project.

Thanks to Denise Schmied, Dr. Natalya Stepanova, Ben Salecker, Jenny Flechsler, Vroni Heinz, Dr. Thomas Heimerl, Markus Setzer, Markus Dietz, Nenja Sowa, Florian Hochapfel, Gudrun Mendl and Dr. Giada Dogliotti for creating a great atmosphere and lifting my spirit many times. Special thanks to Denise for teaching me everything about mice.

I want to thank all students that helped to advance the miRNA-podocyte project through their energetic work: Martina Billmeier, Charlotte Blessing, Kevin Heizler, Markus Herrmann, Lucas Hübner, Christian Iffelsberger, Dorina Janicek and Michael Lemberger.

My gratitude is also extended to all current and former members of Professor Witzgall's group for the wonderful atmosphere at work: Prof. Dr. Reinhard Rachel, Dr. Melanie Grosch, Anita Hecht, Kerstin Herrmann, Dr. Anya Krefft, Edeltraud Lautenschlager, Ton Maurer, Christine Meese, Carina Mirbeth, Conny Niemann, Larissa Osten, Helga Othmen, Karin Schadendorf, Dr. Kerstin Schmidt, Ludwig Utz, Cäcilia Vitzthum, Uwe de Vries, Marina Wuttke, Yulia Zaytseva and Antje Zenker.

Special thanks go to Alfred Stegmüller, a great science teacher who helped me to start my “chemical career” in 2000. I guess I am able to ride a bike now :).

Last but not least, I want to thank my parents, Angelika and Manfred Baumgarten, and my brother, Ulrich Baumgarten, for all their help and support throughout the years.

EIDESSTATTLICHE ERKLÄRUNG

Ich erkläre hiermit an Eides statt, dass ich die vorliegende Arbeit ohne unzulässige Hilfe Dritter und ohne Benutzung anderer als der angegebenen Hilfsmittel angefertigt habe. Die aus anderen Quellen direkt oder indirekt übernommenen Daten und Konzepte sind unter Angabe des Literaturzitats gekennzeichnet.

Bei der Auswahl und Auswertung folgenden Materials haben mir die in der Arbeit genannten Personen in der jeweils beschriebenen Weise unentgeltlich geholfen.

Weitere Personen waren an der inhaltlich-materiellen Herstellung der vorliegenden Arbeit nicht beteiligt. Insbesondere habe ich hierfür nicht die entgeltliche Hilfe eines Promotionsberaters oder anderer Personen in Anspruch genommen. Niemand hat von mir weder unmittelbar noch mittelbar geldwerte Leistungen für Arbeiten erhalten, die im Zusammenhang mit dem Inhalt der vorgelegten Dissertation stehen.

Die Arbeit wurde bisher weder im In- noch im Ausland in gleicher oder ähnlicher Form einer anderen Prüfungsbehörde vorgelegt.

Ich versichere an Eides statt, dass ich nach bestem Wissen die reine Wahrheit gesagt und nichts verschwiegen habe.

.....

Susanne Baumgarten